Functional analysis of chloroplast signal recognition particle (cpSRP) in chlorophyll biosynthesis

DISSERTATION

zur Erlangung des akademischen Grades
Doctor rerum naturalium
(Dr. rer. nat.)
im Fach Biologie

eingereicht an der
Lebenswissenschaftlichen Fakultät
der Humboldt-Universität zu Berlin

von
M.Sc. Shuiling Ji

Präsident der Humboldt-Universität zu Berlin (kommissarisch)
Prof. Dr. Peter Frensch
Dekan der Lebenswissenschaftlichen Fakultät
Prof. Dr. Dr. Christian Ulrichs

Gutachter/in: 1. Prof. Dr. Christian Schmitz-Linneweber

2. Prof. Dr. Bernhard Grimm

3. Prof. Dr. Danja Schünemann

Datum der Promotion: 16.06.2022

Table of contents

Abstract

The assembly of light-harvesting chlorophyll (Chl)-binding proteins (LHCPs) is coordinated with Chl biosynthesis during chloroplast development. The chloroplast signal recognition particle 43 (cpSRP43) mediates the post-translational LHCP targeting to the thylakoid membrane and is also involved in tetrapyrrole biosynthesis (TBS). However, it is still unknown how cpSRP43 allocates its function in the two pathways. In the first part of this study, I showed that the chaperone activity of cpSRP43 is essential for the stability of the three critical TBS proteins: glutamyl-tRNA reductase (GluTR), the H subunit of magnesium chelatase (CHLH), and GENOMES UNCOUPLED 4 (GUN4). cpSRP43 efficiently protects these TBS clients from heat-induced aggregation and enhances their thermostability during heat shock. Although the substrate-binding domain (SBD) of cpSRP43 is sufficient for the interaction with LHCPs, the stabilization of TBS clients requires the additional chromodomain 2 (CD2). cpSRP54, which activates the chaperone activity of cpSRP43 on LHCPs, was surprisingly found to antagonize this chaperone activity on TBS proteins. The elevated temperature alleviates the binding of cpSRP43 to cpSRP54 but enhances its interaction with GluTR, CHLH and GUN4, resulting in enhanced protection of cpSRP43 to these proteins under heat shock conditions. My study suggests a working model that the temperature sensitivity of the cpSRP43-cpSRP54 complex enables cpSRP43 to serve as an autonomous chaperone for the thermoprotection of TBS proteins.

Protochlorophyllide oxidoreductase (POR) catalyzes the NADPH- and light-dependent protochlorophyllide (Pchlide) reduction to Chlorophyllide (Chlide). Since the enzymatic step is light dependent, the reaction is blocked in the dark and the Pchlide accumulates. However, Pchlide over-accumulation triggers ROS formation after re-illumination and causes cell death. Therefore, Chl synthesis needs to be tightly controlled at this step to avoid the excessive accumulation of Pchlide. In the second part of this study, PORB (one of the three POR isoforms) was found to be a new target of cpSRP43. It was revealed that cpSRP43 as a chaperone protects PORB from heat and oxidation-induced aggregation, thereby enhancing the stability of PORB. The cpSRP43-SBD domain is sufficient for PORB protection. In contrast to the antagonistic effect of cpSRP54 on cpSRP43, cpSRP54 is also involved in protecting and stabilizing PORB. The membrane-associated PORB was significantly reduced in the cpSRP54 knockout mutant (*ffc*), suggesting that cpSRP54 is perhaps involved in the association of PORB to the thylakoid membrane rather than in chaperoning PORB to avoid its denaturation. In conclusion, my study revealed a potential mechanism of PORB by concerted actions of cpSRP43 and cpSRP54: (1) cpSRP43 acts as a molecular chaperone to protect PORB from aggregation, thereby preserving the stability of PORB. (2) cpSRP54 assists PORB in attachment to the thylakoid membrane, avoids the degradation of PORB and, thus, improves the stability of PORB or enables access to the catalytic substrate.

There are two aggregation-prone regions (APRs) at the N-terminus of GluTR, which are related to the GluTR aggregation. cpSRP43 was thought to cover the N-terminus APR to protect GluTR from aggregation. However, it remains unknown whether APR triggers the GluTR aggregation

in vivo, and whether the removal of APR affects GluTR aggregation and stability, and consequently the ALA synthesis rate. In the third part of this study, I initially found that the deletion of APR negatively affects the stability and activity of GluTR. A similar observation was made in another approach with a V→P substitution mutation in the APRs of GluTR. In contrast, the V→T mutation slightly reduces the GluTR aggregation by 18-30% in vitro, which corresponded to a slight increase in the stability of GluTR (27% compared to the wild type) in an in vivo experiment. These experiments indicate that the stability but not the activity of GluTR can be improved by the point mutation in the APRs.

In summary, this thesis contributes to the extended knowledge about the interdependent chaperone function of cpSRP43 and cpSRP54 in coordination of Chl synthesis and LHCP biogenesis.

Keywords: cpSRP43, cpSRP54, chaperone, LHCP, GluTR, CHLH, GUN4, PORB, APR

Zusammenfassung

Der Zusammenbau der lichtsammelnden und chlorophyllbindenden Proteine (LHCPs) wird während der Chloroplastenentwicklung mit der Chlorophyllbiosynthese koordiniert. Das Protein chloroplastidärer Signalerkennungspartikel 43 (cpSRP43) vermittelt das posttranslationale LHCP-Targeting zur Thylakoidmembran und ist auch an der Tetrapyrrolbiosynthese (TBS) beteiligt. Es ist jedoch noch unbekannt, wie die Beteiligung von cpSRP43 in beiden Prozessen im Chloroplasten reguliert ist. Im ersten Teil dieser Studie habe ich gezeigt, dass die Chaperonaktivität von cpSRP43 für die Stabilität der drei essenziellen TBS-Proteine Glutamyl-tRNA-Reduktase (GluTR), der H-Untereinheit der Magnesium-Chelatase (CHLH) und von Genomes Uncoupled 4 (GUN4) wichtig ist. cpSRP43 schützt diese TBS-Proteine effizient vor hitzeinduzierter Aggregatbildung und verbessert ihre Thermostabilität während eines Hitzeschocks. Während die substratbindende Domäne (SBD) von cpSRP43 für die Interaktion mit LHCPs ausreicht, erfordert die Stabilisierung der TBS-Proteine die zusätzliche cpSRP43-Chromodomäne 2 (CD2). Es wurde überraschend gefunden, dass cpSRP54 die Chaperonaktivität von cpSRP43 für LHCPs aktiviert, während es sie für TBS-Proteine vermindern kann. Aber erhöhte Temperatur kann die Bindung von cpSRP43 mit cpSRP54 lösen, aber seine Wechselwirkung mit GluTR, CHLH und GUN4 verstärken, was zu einem verstärkten Schutz von cpSRP43 gegenüber diesen Proteinen unter Hitzeschockbedingungen führt. Meine Studien legen ein Arbeitsmodell nahe, dass wegen der Temperaturempfindlichkeit des cpSRP43-cpSRP54-Komplexes dem cpSRP43 Protein ermöglicht, als autonomes Chaperon für den Thermoschutz der TBS-Proteinen zu sorgen.

Protochlorophyllid-Oxidoreduktase (POR) katalysiert die NADPH- und lichtabhängige Reduktion von Protochlorophyllid (Pchlid) zu Chlorophyllid (Chlid). Da der enzymatische Schritt lichtabhängig ist, wird im Dunkeln die Reaktion blockiert und das Substrat Pchlid reichert sich an. Die Überakkumulation von Pchlid löst jedoch die ROS-Bildung nach der erneuter Belichtung aus und verursacht den Zelltod. Daher muss die Chlorophyllsynthese in diesem Schritt streng kontrolliert werden, um die übermäßige Akkumulation von Pchlid zu vermeiden. Im zweiten Teil dieser Studie wurde festgestellt, dass PORB (eines der drei POR Isoformen) ein weiteres Ziel von cpSRP43 ist. Es zeigte sich, dass cpSRP43 als Chaperon PORB vor hitze- und oxidationsinduzierter Aggregation schützt und dadurch die Stabilität von PORB erhöht. Die cpSRP43-SBD-Domäne ist für den Schutz der POR ausreichend. Im Gegensatz zur antagonistischen Wirkung von cpSRP54 auf cpSRP43 ist cpSRP54 auch am Schutz und an der Stabilisierung von PORB beteiligt. Das membranassoziierte PORB war in der cpSRP54-Knockout-Mutante (*ffc*) signifikant reduziert, was darauf hindeutet, dass cpSRP54 möglicherweise eher an der Assoziation des PORB mit der Thylakoidmembran als an der Bewahrung von PORB vor der Denaturierung beteiligt ist. Zusammenfassend haben meine Studien einen möglichen Mechanismus von PORB durch konzertierte Aktionen von cpSRP43 und cpSRP54 aufgezeigt. (1) cpSRP43 wirkt als molekulares Chaperon, um PORB vor der Aggregation zu schützen, wodurch die Stabilität des PORB bewahrt wird. (2) cpSRP54 kann PORB bei der Anlagerung an die Thylakoidmembran unterstützen, was vermutlich den Abbau

von PORB vermeidet und die Stabilität von PORB verbessert oder den Zugang zum katalytischen Substrat ermöglicht.

Es gibt zwei aggregationsanfällige Regionen (APRs) am N-Terminus von GluTR, die eine wesentliche Rolle bei der GluTR-Aggregation spielen können. Es wurde angenommen, dass cpSRP43 die APRs am N-Terminus des GluTR abdeckt, um GluTR vor Aggregation zu schützen. Es bleibt jedoch unbekannt, ob APRs die GluTR-Aggregation in vivo auslösen kann und ob die Eliminierung von APRs die GluTR-Aggregation reduzieren würde und seine Stabilität fördert, sodass höhere ALA-Syntheseraten erreicht werden können. Im dritten Teil dieser Studie fand ich heraus, dass die Deletion von APRs die Stabilität und Aktivität von GluTR vollständig verändert. Ein ähnliches Ergebnis ergab sich für die V→P-Substitution in der APR der GluTR. Im Gegensatz dazu reduzierte die V→T-Mutation im APR die GluTR-Aggregation leicht um 18–30 % in vitro, was einer leichten Erhöhung der Stabilität von GluTR (27 % im Vergleich zum Wildtyp) in einem in vivo-Experiment entsprach. Damit konnten erste Hinweise gegeben werden, dass die Stabilität, aber nicht die Aktivität von GluTR durch die Punktmutation verbessert werden kann.

Zusammenfassend trägt diese Arbeit zum erweiterten Wissen über die voneinander abhängige Chaperonfunktion der beiden Proteine cpSRP43 und cpSRP54 bei der Koordination von Chlorophyllsynthese und LHCP-Biogenese bei.

Schlüsselwörter: cpSRP43, cpSRP54, Chaperon, LHCP, GluTR, CHLH, GUN4, PORB, APR

List of abbreviations

ALAD	ALA dehydratase
ALA	5-aminolevulinic acid
Alb3	Albino 3
Ank	Ankyrin
APR	Aggregation-prone region
BCA	Bicinchoninic acid
BiFC	Bimolecular Fluorescence Complementation
BN PAGE	Blue native polyacrylamide gel electrophoresis
BSA	Bovine serum albumin
CBPs	Chl-binding proteins
CD	Chromodomain
Chl	Chlorophyll
CHLH	H subunit of magnesium chelatase
Chlide	Chlorophyllide
CHLM	Mg-protoporphyrin IX methyltransferase
Co-IP	Co-immunoprecipitation
Col-0	Columbia
cpFtsY	cpSRP receptor
CPO	Coproporphyrinogen III Oxidase
cpSRP	Chloroplast signal recognition particle
Cytb6f	Cytochrome b6f
DDM	n-Dodecyl-β-D-Maltopyranosid
DMSO	Dimethyl sulfoxide
DTT	Dithiothreitol
DW	Dry weight
FLU	Fluorescent in blue light
FW	Fresh weight
GBP	GluTR binding protein
GluTR	Glutamyl-tRNA reductase
GSAAT	Glutamate-1-Semialdehyde Aminotransferase
GUN4	GENOMES UNCOUPLED 4
H_2O_2	Hydrogen peroxide

HPLC	High-performance liquid chromatography
IPTG	Isopropyl-β-d-thiogalactoside
LD	Long day
Ler-0	Landsberg erecta
LHCP	Light-harvesting chlorophyll-binding proteins
MgCh	Magnesium chelatase
MgP	Mg protoporphyrin IX
MgMME	MgP monomethylester
MST	Microscale thermophoresis
NF	Norflurazon
NPQ	Non-photochemical quenching
OEC	Oxygen-evolving complex
Pchlide	Protochlorophyllide
PhANGs	Photosynthesis-associated nuclear genes
PLB	Prolamellar body
PORB	Protochlorophyllide oxidoreductase B
PPO	Protoporphyrinogen IX Oxidase
Proto IX	Protoporphyrin IX
PSI	Photosynthesis I
PSII	Photosynthesis II
qPCR	quantitative PCR
RED	Regulatory domain
ROS	Reactive oxygen species
RT	Room temperature
SBD	Substrate-binding domain
TBS	Tetrapyrrole biosynthesis
TMD	Transmembrane domain
TPR	Tetratricopeptide repeat
VIGS	Virus-induced gene silencing
YFP	Yellow Fluorescence Protein

1 Introduction

1.1 Overview of Chl in higher plants

Chl is the sole biomolecule on our planet that can be seen from space. As a green pigment, it absorbs photons of the red and blue wavelengths of the solar spectrum, while green wavelengths (about 550 nm) are reflected (Taiz et al., 2015). In plants, Chl is the most abundant tetrapyrrole and functions in photosynthesis. The Chl molecule consists of a chlorin ring structure with a central chelated magnesium ion (Mg^{2+}) and a long hydrocarbon tail, making it hydrophobic (Buchanan et al., 2015). Different Chl molecules have different substituent groups around the porphyrin ring. Chl *a* possesses a methyl group in pyrrole ring II, while Chl *b* contains a formyl group (Marquez and Sinnecker, 2007). Chl *a* is found in the reaction center and antenna complexes of the two photosystems of oxygenic phototrophs, whereas Chl *b* is only found in proteins of the peripheral antenna complex.

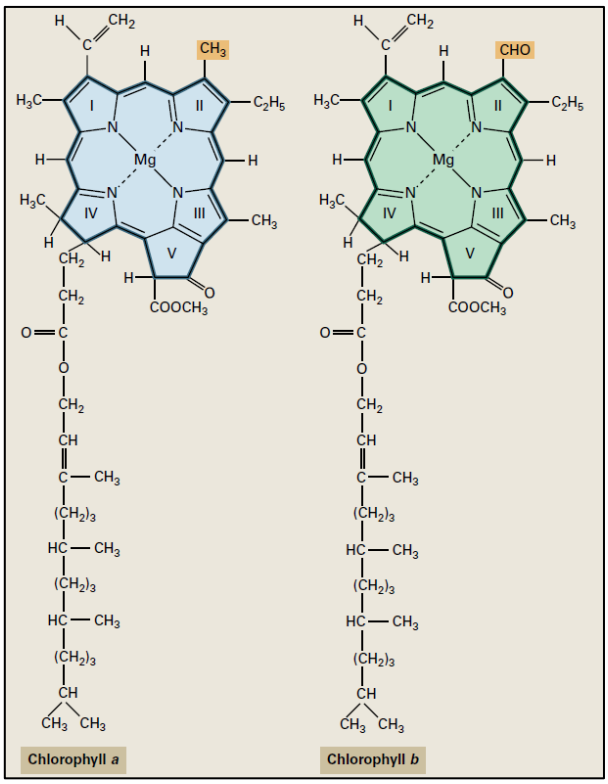

Figure 1.1 Structure of Chl *a* and *b*. In Chl *a*, a methyl group is present, whereas a formyl group is present at the same position in Chl *b* (Buchanan et al., 2015).

1.1.1 Significance of Chl in photosynthesis

Photosynthesis is the elementary biological process of converting solar energy into chemical energy, which is the energy source for all life on the earth (Xiong and Bauer, 2002). Chl has three functions in Chl-binding proteins (CBPs): light absorption, transfer of excitation energy, and photo-oxidation by charge separation in the reaction center of the photosynthetic complexes (Wang and Grimm, 2021). Specifically, Chl associated with the light-harvest Chl *a*/*b*-binding proteins (LHCPs) of the outer antenna complexes functions in capturing solar energy and

transmitting excitation energy. Chl in the photosynthetic reaction center (RC) acts as electron donor and acceptor by feeding electrons into the photosynthetic electron chain and receiving electrons from either water or plastocyanin for reduction of Chl in the special pair of photosystem II (PSII) and photosystem I (PSI), respectively.

1.1.2 Chl biosynthesis pathway in higher plants

The Chl biosynthesis pathway can be divided into four sections: (1) the synthesis of the precursor molecule 5-aminolevulinic acid (ALA), (2) synthesis of Proto IX, (3) insertion of the central Mg^{2+} into Proto IX in the Chl branch, (4) the final conversion between Chl(ide) *a* and Chl(ide) *b* in the Chl cycle.

1.1.2.1 ALA formation

Chl biosynthesis shares the first multiple steps of the ALA formation, called the C5 pathway, with the pathways to other tetrapyrroles (Oborník and Green, 2005). In the first reaction, glutamate (Glu) is esterified with the $tRNA^{Glu}$ by glutamyl-tRNA synthetase (GluRS) depending on ATP and Mg^{2+} to form glutamyl-$tRNA^{Glu}$ (Marklew, 2012). Next, glutamyl-tRNA reductase (GluTR) reduces glutamyl-$tRNA^{Glu}$ to glutamate-1-semialdehyde (GSA). GluTR is the first enzyme exclusively involved in the tetrapyrrole biosynthesis (TBS) pathway. It is also the rate-limiting step of this pathway (Wang et al., 2018). In the final step of ALA synthesis, glutamate-1-semialdehyde aminotransferase (GSAT) catalyzes the isomerization of GSA to form ALA through the intramolecular transfer of an amino group (Grimm, 1990; Hennig et al., 1997).

1.1.2.2 The porphyrin synthesis

After the formation of ALA, two ALA molecules are fused by ALA dehydratase (ALAD) to form the monopyrrole porphobilinogen (PBG) (Wittmann et al., 2018). Four PBG molecules are polymerized to hydroxymethylbilane (HMB) by the HMB synthase (HMBS). Since HMB is very unstable, the D-ring is inverted and the ring is ultimately closed by uroporphyrinogen III synthase (UROS), producing the first macrocycle uroporphyrinogen III (Uro III) (Bogorad, 1958). Uro III decarboxylase (UROD) sequentially decarboxylates the acetate residues of the four original PBG molecules, producing coproporphyrinogen III (CoPro III). The subsequent oxidative decarboxylation of two propionate side chains of rings A and B, which are catalyzed by CoPro III oxidase (CPO), results in the production of protoporphyrinogen IX (Protogen IX) (Hsu and Miller, 1970; Santana et al., 2002). In the last step, Protogen IX is oxidized by protoporphyrinogen IX oxidase (PPO) to form the Proto IX. FAD acts as a cofactor (Koch et al., 2004). The production of Proto IX marks the transition from a non-fluorescent product to a fluorescent product, which is easily photo-oxidized. Two PPO isoforms have been found in *Arabidopsis* (PPO1 and PPO2) (Lermontova and Grimm, 2006). The deficiency of PPO1 is lethal (Zhang et al., 2014), indicating PPO1 is the dominant isoform in photosynthetically active tissue (Kobayashi et al., 2014). Interestingly, PPO1 is also involved in the regulation of plastid RNA editing through interaction with and modulation of the stability of multiple organellar

RNA editing factors (Zhang et al., 2014).

1.1.2.3 The Chl branch

In the first step of the Chl branch, the magnesium chelatase (MgCh, EC 6.6.1.1) inserts Mg^{2+} as a central ion into the porphyrin ring using ATP hydrolysis and leads to the production of Mg protoporphyrin IX (MgP). MgCh is a multiprotein complex composed of three essential subunits (CHLI, CHLH and CHLD) (Adams et al., 2020). CHLH is the catalytic subunit, while CHLI and CHLD are AAA^+ subunits that hydrolyze ATP required for the reaction (Adams and Reid, 2012). In addition to the three essential subunits, GENOMES UNCOUPLED 4 (GUN4) can stimulate MgCh activity by binding to Proto IX and MgP, as well as CHLH (Larkin et al., 2003).

In the following step, MgP is esterified by the MgP methyltransferase (MgPMT/CHLM) to Mg-protoporphyrin IX monomethyl ester (MgMME) (Shepherd et al., 2003). This intermediate is then oxygenated by a cyclase to divinyl-protochlorophyllide (DV-Pchlide) (Bollivar and Beale, 1996). The cyclase consists of one soluble and two membrane-bound subunits, two of which have already been characterized (CHL27, (Rzeznicka et al., 2005) and LCAA/YCF54 (Bollivar et al., 2014)). In angiosperms, DV-Pchlide is exclusively converted to DV-chlorophyllide (DV-Chlide) in a light-dependent reaction by Pchlide oxidoreductase (LPOR) (Masuda and Takamiya, 2004). However, in gymnosperms, algae and cyanobacteria, Pchlide can also be converted to Chlide by a light-independent POR (DPOR) (Reinbothe et al., 2010).

Arabidopsis uses three LPOR isoforms: PORA, PORB and PORC. While PORA is only detected in etiolated seedlings, PORB is found in both etioplasts and chloroplasts (Holtorf et al., 1995; Runge et al., 1995). PORC expression is different from that of *PORA* and *PORB,* showing light induction at the beginning of illumination while increasing at higher light intensity (Su et al., 2001). In the etioplasts, the LPOR, NADPH and Pchlide participate the formation of the paracrystalline network of membrane tubules called the prolamellar body (PLB). This indicates the role of LPOR in coordinating Chl synthesis and photosynthetic membrane biogenesis in plants (Floris and Kuhlbrandt, 2021; Nguyen et al., 2021). In the following step, the 8-vinyl group of 3, 8-DV-Chlide is reduced by the DV-reductase (DVR) to monovinyl-Chlide a, which is then esterified by Chl synthase (CHLG) with phytyl pyrophosphate to form Chl *a*.

1.1.2.4 The Chl *a*/*b* cycle

The Chl *a* oxygenase (CAO) converts Chl *a* to Chl *b* by oxidizing the 7-methyl group (Tanaka et al., 1998). CAO has a broad substrate spectrum and can catalyze Chlide *a* to form Chlide *b* (Wang et al., 2013). Chl *b* reductase (CBR) is responsible for the conversion of Chl *b* to hydroxymethyl Chl *a,* which is then catalyzed by hydroxymethyl Chl *a* reductase (HCAR) to form Chl *a* (Meguro et al., 2011). Only recently, the Chl dephytylase (CLD1) was identified, which dephytylates both Chl *a* and Chl *b* to form Chlide *a*/*b* (Lin et al., 2016). A deficiency of CLD1 in Arabidopsis seedlings leads to increased thermal sensitivity, which is associated with

reduced PSII efficiency under heat stress (Lin et al., 2016).

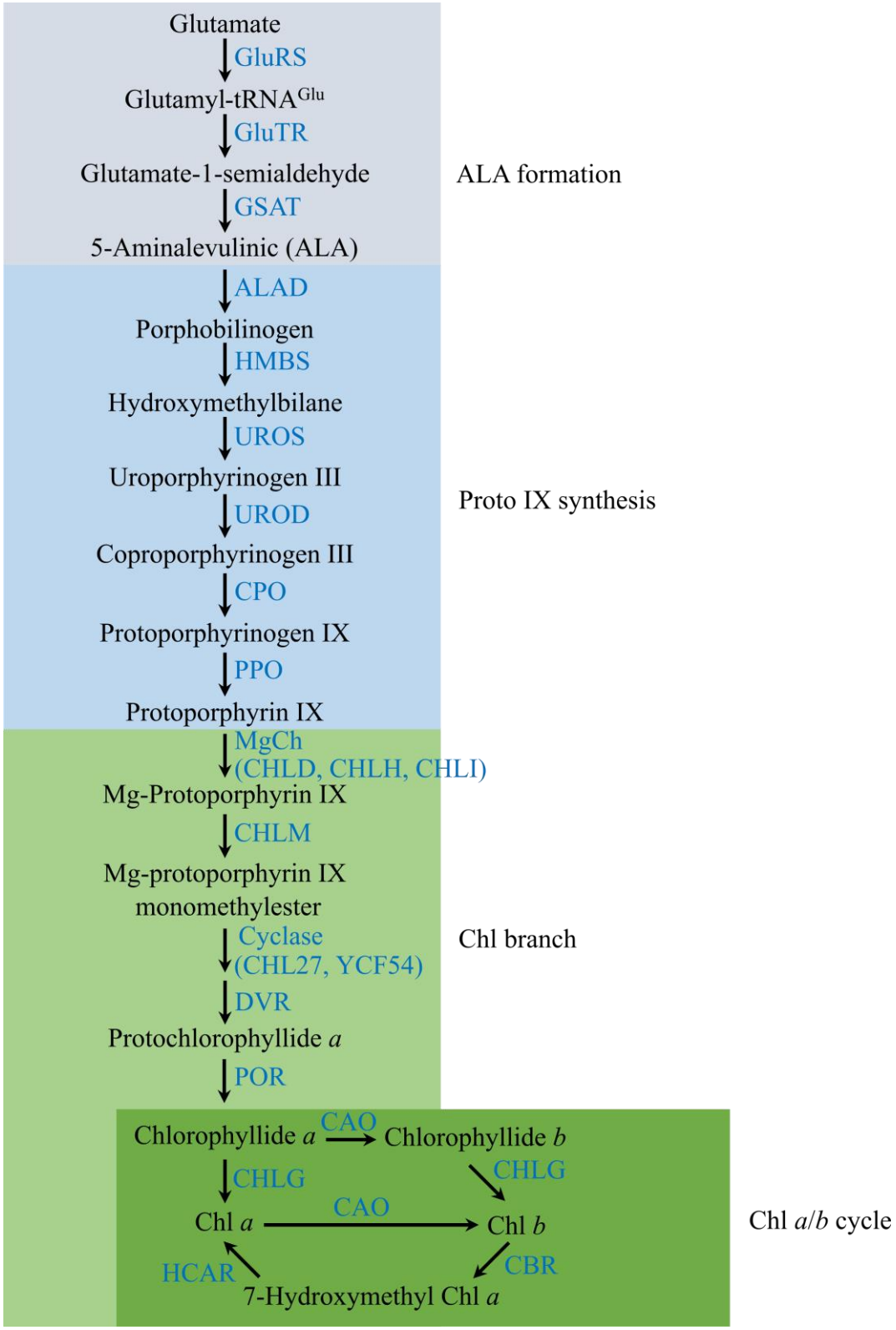

Figure 1. 2 Overview of Chl *a*/*b* biosynthesis pathway in higher plants. The pathway is divided into four parts: (I) ALA formation; (II) Proto IX formation; (III) the Chl branch and (IV) the Chl cycle. GluRS: glutamyl-tRNA synthetase; GluTR: glutamyl-tRNA reductase; GSAT: glutamate-1-semialdehyde aminotransferase; ALAD: 5-aminolevulinic acid

dehydratase; HMBS: HMB-synthase/PBG deaminase; UROS: uroporphyrinogen III synthase; UROD: uroporphyrinogen III decarboxylase; CPO: coproporphyrinogen III oxidase; PPO: protoporphyrinogen IX oxidase; MgCh: Mg-chelatase; CHLM: Mg-Proto IX methyltransferase; POR: Pchlide reductase; DVR: 3,8-divinyl Chlide reductase; CHLG: Chl synthase; CAO: Chl/ide *a* oxidase; CBR: Chl *b* reductase; HCAR: 7-hydroxymethyl Chl *a* reductase.

1.1.3 Subcellular localization of Chl biosynthesis enzymes

In higher plants, all of the enzymes in the Chl biosynthesis pathway are present in chloroplasts. An important point in the effective catalysis of intermediates is the spatial organization of enzymes involved. Except for GluTR, the trunk pathway to protoporphyrinogen is located in the stroma (Joyard et al., 2009). GluTR could be detected in both the soluble and membrane-associated fractions of plastids, and the amount of soluble GluTR correlates with the ALA activity (Schmied et al., 2018). From protoporphyrinogen oxidase to POR, all enzymes are associated with both the envelope and thylakoid membranes. The case for MgCh is quite complicated since the association of MgCh with the envelope membrane was reported to be affected by Mg^{2+} concentration (Guo et al., 1998; Nakayama et al., 1998). This complex localization manner is probably due to the localization of respective subunits. CHLI was always identified in the stroma (Joyard et al., 2009) and CHLD was predominantly found in the stromal fraction (Guo et al., 1998). However, recent proteomics data have suggested its addition in thylakoid membranes. In contrast, CHLH and GUN4 are located in both envelope membrane and stroma (Nakayama et al., 1998; Joyard et al., 2009). There is a similar uncertainty for the final steps of Chl biosynthesis, given that Chl synthase (CHLG) is present only in the thylakoid membranes (Joyard et al., 2009). In contrast, CAO has been suggested to be localized in the envelope membrane (Eggink et al., 2004).

1.1.4 Post-translational regulation of Chl biosynthesis

1.1.4.1 Post-translational control on ALA

In the last few decades, different post-translational regulatory mechanisms have been identified that influence the stability, localization and activity of GluTR: (1) Stabilization by the GluTR binding protein (GBP). (2) Feedback inhibition by heme. (3) Feedback inhibition by the FLU (Fluorescent in blue light) inactivation complex. (4) Controlling aggregation by chloroplast signal recognition particle 43 (cpSRP43). (5) Degradation by the caseinolytic protease (Clp).

1.1.4.1.1 Stabilization by GBP

The targeted search for further GluTR interaction partners resulted in GBP identification using a cDNA-based yeast two-hybrid approach (Czarnecki et al., 2011). The protein encoded in the nucleus has no transmembrane domain but is present in both the stroma and the thylakoid membrane (Czarnecki et al., 2011; Schmied et al., 2018). GBP is not a component of the FLU inactivation complex and is therefore probably anchored to the membrane by an unknown factor (Czarnecki et al., 2011). The *gbp* point mutant is characterized by a reduced heme content, which correlates with the destabilization of GluTR (Czarnecki et al., 2011). Especially in

extended dark periods, GluTR in a *gbp* mutant is subjected to an increased degradation. This observation implies that GBP protects GluTR from ClpC-dependent degradation (Apitz et al., 2016). The crystal structure of the GluTR-GBP complex showed that GBP binds directly to the cleft of the V-shaped GluTR dimer. An in vitro enzyme assay of ALA synthesis also confirmed that the presence of GBP increases the activity of GluTR about three-fold (Zhao et al., 2014; Zhao and Han, 2018).

1.1.4.1.2 Feedback inhibition by heme

It was previously reported that mutants with impaired heme degradation show a reduced Pchlide content as a result of a lower ALA synthesis (Terry and Kendrick, 1999). A 31-34 amino acids long region at the N-terminus of GluTR, which is strongly conserved in plants, was suggested to be responsible for heme binding and called the heme-binding domain (HBD) (Vothknecht et al., 1996). In accordance with this, the absence of HBD leads to a reduced inhibitory effect of heme on GluTR activity in vitro enzymatic assay in barley (Vothknecht et al., 1998). However, it was also demonstrated that Arabidopsis GluTR does not directly bind heme, so it was suggested to rename the HBD to the regulatory domain (RED) (Richter et al., 2019). RED of GluTR was justified because of its binding capacity to other proteins. The heme-induced inhibition of ALA activity was proposed to be mediated by GBP. Specifically, the binding of heme to GBP attenuates the interaction between GBP and GluTR. Thus, upon accumulation, heme competes with GluTR for binding to GBP. Ultimately, the free RED of GluTR is accessible for binding of the ClpF, ClpS or ClpC, the subunits of the Clp protease, so that the GluTR degradation can be triggered by the Clp proteasome (Richter et al., 2019).

1.1.4.1.3 Feedback inhibition by the FLU inactivation complex

In angiosperms, the Chl biosynthesis is inhibited in the dark in order to avoid an excessive accumulation of Pchlide and the associated production of ROS during re-illumination. In the *flu* mutant produced by ethyl methanesulfonate (EMS), the lack of FLU does not promote the inactivation of ALA synthesis. As a result, Pchlide massively accumulates in the dark (Meskauskiene et al., 2001) and leads after the onset of light to increased ROS accumulation and, consequently, to programmed cell death. Accordingly, the *flu* line can only survive under continuous light conditions (Meskauskiene et al., 2001).

FLU is a tetratricopeptide repeat (TPR) protein anchored in the thylakoid membrane (Kauss et al., 2012; Zhang et al., 2015). Co-immunoprecipitation (Co-IP) assays showed FLU's interaction with CHL27, PORB, and PORC. Moreover, using the blue native gel confirmed that GluTR co-migrates with these proteins, suggesting a FLU-dependent inactivation complex consisting of CHL27, PORB, PORC and FLU, which suppresses the ALA synthesis (Kauss et al., 2012). As the ALA synthesis rate was inversely correlated to the level of photoactive Pchlide (Richter et al., 2010) and as FLU was also found to co-immunoprecipitate with GluTR (Kauss et al., 2012), a feedback inhibition of ALA synthesis was proposed to depend on an interaction between FLU and GluTR, and to be steered by the binding of Pchlide to POR (Kauss et al., 2012). It was reported that stroma-localized GluTR correlates with ALA synthesis rate

and therefore, FLU was proposed to suppress the ALA synthesis by anchoring GluTR to the membrane (Schmied et al., 2018).

The crystal structure of a FLU-GluTR complex revealed that two FLU molecules assemble at the concave side of the GluTR dimer. It was suggested that FLU shields the positively charged residues of GluTR, so that binding of the negatively charged tRNA with GluTR is prevented by steric hindrance (Zhang et al., 2015). In addition to suppressing GluTR activity in darkness, FLU also has a crucial role in adjusting the ALA synthesis rate under changing light conditions (Hou et al., 2019). FLU has three structural domains, the transmembrane (TM), coiled-coil domain and tetratricopeptide repeat (TPR) domain. In vivo functional studies of these domains imply that they all are required for the appropriate inhibition of ALA synthesis. It is hypothesized that only an intact FLU protein can ensure the constitution of a membrane-bound ternary complex that is composed at least of FLU, GluTR, and POR to repress ALA synthesis. (Hou et al., 2021).

1.1.4.1.4 GluTR degradation by Clp protease

The ATP-dependent Clp protease is the most abundant proteolytic system in plastids with a large number of target proteins. The plastid-localized Arabidopsis Clp protease consists of the chaperones ClpC1/2, ClpD, and the selector proteins ClpS1 and ClpF1 (Nishimura and van Wijk, 2015). Using recombinant ClpS1 and affinity purification approach identified GluTR as a target protein of the Clp protease in *A. thaliana* (Nishimura et al., 2013). ClpS1 binds to GluTR in the HBD region and delivers it to the Clp complex. Then, GluTR interacts with the ClpC1 subunit, which is unfolded and translocated into the core complex of the Clp proteasome before it is finally proteolytically degraded (Apitz et al., 2016). Thus, in addition to FLU, the degradation of GluTR by the Clp proteasome is responsible for a loss of GluTR function in ALA synthesis.

1.1.4.1.5 Prevention of aggregation by cpSRP43

It was found that the overexpression of GluTR in *Arabidopsis* and tobacco did not lead to an increased ALA synthesis rate but triggered the formation of necrosis in tobacco, which could be attributed to the formation of insoluble, inactive GluTR aggregates (Schmied et al., 2011). Therefore, it is reasonable to suggest that the folding of active GluTR requires a chaperone function. Upon excessive accumulation of GluTR, either its precise folding cannot be accomplished due to limited chaperone function, or the resulting aggregates are a regulatory mechanism to avoid excessive ALA synthesis, which would lead to photodynamic damage of cells as a result of accumulating porphyrins and Pchlide.

The cpSRP machinery consists of two components, cpSRP43 and cpSRP54, due to the molecular weight of these proteins (Li et al., 1995; Schünemann et al., 1998). The cpSRP43 and cpSRP54 proteins are responsible for the translocation of the imported LHCPs to the thylakoid membrane. In addition, cpSRP43 was also reported to act as a chaperone to stabilize GluTR by preventing it from aggregation (Wang et al., 2018). Two aggregation-prone regions

(APRs) of GluTR were considered the reason for the spontaneous tendency of GluTR to aggregate. Therefore, it was proposed that cpSRP43 binds to the exposed APRs, masks these motifs and ensures the correct folding through its intrinsic chaperone activity (Wang et al., 2018). Interestingly, the dual role of cpSRP43 in targeting LHCP into the thylakoid membrane and regulating the amount of active GluTR represents a connection between Chl biosynthesis and cpSRP-dependent translocation of LHCP (Wang et al., 2018).

1.1.4.2 Function, structure, activity and control of MgCh activity

MgCh is the first unique enzyme of the Chl biosynthesis pathway and inserts Mg^{2+} into Proto IX. It is a huge multisubunit complex composed of three subunits, CHLH, CHLI and CHLD, and requires ATP for Mg^{2+} chelation. CHLH is the catalytic subunit binding the substrate Proto IX, whereas CHLD and CHLI are AAA^{+} subunits for ATP hydrolysis. A model for the MgCh mechanism was proposed that CHLI and CHLD form the CHLI/CHLD motor complex (Adams and Reid, 2013; Adams et al., 2016), which transiently interacts with the CHLH via the integrin domain of CHLD (Farmer et al., 2019) and then hydrolyses ATP. ATP hydrolysis drives a conformational transition in the CHLH-porphyrin complex, promoting the Mg^{2+} insertion into the Proto IX ring (Reid and Hunter, 2002).

The crystal structure of CHLH from *Synechocystis* (Chen et al., 2015) suggests that CHLH is composed of three major domains, named head, neck and body of the protein (Qian et al., 2012; Adams et al., 2014). The body is cage-like, with several subdomains surrounding an internal cavity supposed as the substrate-binding site (Chen et al., 2015). Two linked domains, the body I and body II, in an open conformation of CHLH bond Proto IX, and the arrangement of several loops cover the substrate and forms an active site cavity. The glutamate (E660) of CHLH was proposed to be the critical catalytic subunit for Mg^{2+} insertion, as it is positioned in close proximity to the porphyrin substrate (Adams et al., 2020). There are two proteins, GUN4 and the BALANCE OF CHLOROPHYLL METABOLISM 1 (BCM1) can stimulate the MgCh activity.

1.1.4.2.1 GUN4 stimulates MgCh activity

GUN4 was identified in a mutants screen with impaired communication between the nucleus and the chloroplast (retrograde signaling) (Susek et al., 1993). It is apparent that the function of GUN4 is not only specified to plastid-derived signaling but also functions as a positive regulator of the Chl biosynthesis. Although GUN4 is not a required component of the MgCh complex, it can directly bind to the CHLH, Proto IX and MgP (Larkin et al., 2003; Peter and Grimm, 2009; Adhikari et al., 2011). The existence of GUN4 markedly enhances the MgCh activity in vitro by improving the substrate-binding affinity of CHLH for Proto IX, especially with the low Mg^{2+} concentration (Larkin et al., 2003; Verdecia et al., 2005). As in the *gun4* knock-out mutant, there is no significant accumulation of Proto IX and MgP, suggesting that GUN4 is involved in the post-translational feedback regulation on ALA synthesis in response to the alteration of enzymes activities in the Chl branch (Peter and Grimm, 2009). In addition, it was shown that Arabidopsis GUN4 is phosphorylated at Ser 264. Since GUN4 was found preferentially

phosphorylated in darkness and the phosphorylation of GUN4 impaired the stimulatory influence on MgCh activity, GUN4 was proposed to attenuate the metabolic flow through the Mg branch in darkness by phosphorylation (Richter et al., 2016). It is supposed that the phosphorylation-dependent control of MgCh activity corresponds to the strict dark-inactivation of LPOR and suppresses the ALA synthesis in angiosperms. When a reduction in MgCh activity triggers the decline in ALA synthesis, the metabolic flow into the Chl branch can be limited, and the risk of excessive Pchlide-induced ROS accumulation is avoided (Richter et al., 2016).

1.1.4.2.2 BCM1 stimulates MgCh activity

Recent studies have shown that BCM1 and BCM2 can promote the Chl biosynthesis and attenuate the Chl breakdown in post-translational regulation (Wang et al., 2020). The two isoforms BCM1 and BCM2 share 87% and 75% sequence similarity and identity, respectively. The mutation of both BCM isoforms in *Arabidopsis* leads to pale leaves in seedlings and premature leaf senescence in adult plants (Wang et al., 2020; Zhang et al., 2020). Protein interaction studies and MgCh activity assays revealed that BCM1 can stimulate MgCh activity through interaction with GUN4. Meanwhile, BCM1 can interact with and destabilizes the magnesium dechelatase isoform SGR1 (STAY-GREEN 1), which dechelatases the central Mg^{2+} from Chl *a* to produce pheophytin a (Shimoda et al., 2016). In addition, at the beginning of leaf senescence, BCM2 is upregulated and can attenuate the degradation of Chl. These dual functions enable the BCM isoforms to post-translationally coordinate Chl biosynthesis and breakdown during leaf development (Wang et al., 2020).

1.1.4.3 Function, structure, activity and control of POR

In *Arabidopsis*, POR is the strictly light-dependent enzyme that catalyzes the reduction of the Pchlide to Chlide using NADPH as an electron donor. The structural basis for POR photocatalysis has been revealed recently in *Thermosynechococcus elongatus* and *Synechocystis sp* (Zhang et al., 2019). POR-NADPH crystal structure revealeds that apart from the conserved loop regions, Asn90, Tyr193 and Lys197 are directly bound to the NADPH through hydrogen bonding (Zhang et al., 2019). A simulated model of the POR-Pchlide-NADPH ternary complex shows interactions of Lys197, Thr145 and Tyr223 with Pchlide to provide a lot of hydrogen-bonding possibilities and to position Pchlide in a direction that is consistent with the desired stereochemistry of hydride and proton transfer during Pchlide reduction (Zhang et al., 2019). The property of light-triggered activity of POR makes its substrate Pchlide accumulate in the darkness, which leads to cell death after illumination (Czarnecki and Grimm, 2012). Due to this crucial enzymatic step, POR is controlled and supported by several interacting factors, such as LIGHT HARVESTING LIKE 3 (LIL3), CHAPERONE OF POR-PROTEIN 1 (CPP1), DE-ETIOLATION IN THE DARK AND YELLOWING IN THE LIGHT (DAY) and FLOWERING CONTROL LOCUS A (FCA).

1.1.4.3.1 LIL3 protein

LIL3 is a vital interaction partner for all three POR isoforms present in *Arabidopsis* (Hey et al., 2017). It belongs to the LHCP superfamily and has two transmembrane helices, which consist of the LHCP-characteristic Chl binding motif. In *Arabidopsis*, the two LIL3 isoforms (LIL3.1 and LIL3.2) have partially redundant functions (Lohscheider et al., 2015). The lack of both LIL3 isoforms, as in the *lil3.1*/*lil3.2* double mutant or by virus-induced gene silencing (VIGS) of the *LIL3.1 and 3.2* genes, leads to a drastic reduction of the POR levels and Chl synthesis, indicating the LIL3 stabilizing effect on POR (Tanaka et al., 2010; Hey et al., 2017; Mork-Jansson and Eichacker, 2018). In addition, as LIL3 binds Pchlide, it was suggested that the delivery of Pchlide by LIL3 prevents the accumulation of this unbound Chl precursor (Hey et al., 2017). It is not excluded that the transmembrane Chl binding motif of LIL3 binds Chls (Hey et al., 2017). Moreover, LIL3 also acts as a membrane anchor and interaction partner for geranylgeranyl reductase (CHLP) and thus ensures the functionality of this enzyme (Tanaka et al., 2010; Takahashi et al., 2014). Since both POR and CHLP provide the substrates for CHLG, it is proposed that the interaction with LIL3 regulates the flow of the intermediates and the synthesis of Chl (Hey et al., 2017).

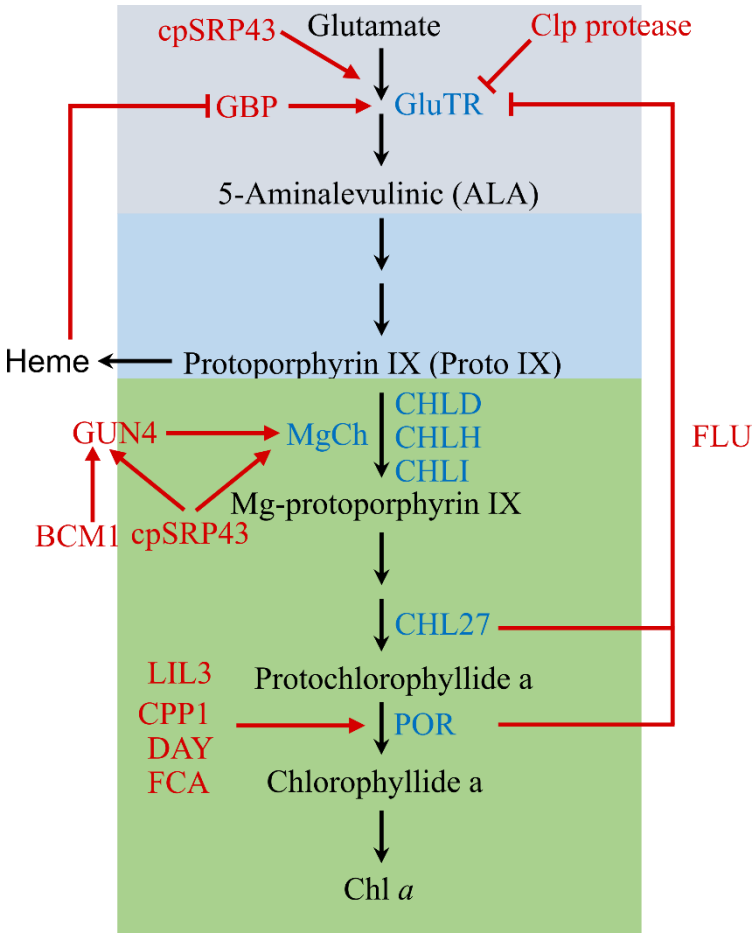

Figure 1. 3 Scheme shows post-translational control on Chl biosynthesis. (1) cpSRP43 protects GluTR from aggregation; (2) Clp protease degrades GluTR; (3) GBP protects GluTR from Clp protease involved degradation; (4) heme competes with GBP to inhibit GBP's

protection to GluTR; (5) PORB, CHL27 and FLU constitute the inactivation complex to suppress ALA activity; (6) GUN4 stimulates MgCh activity, and BCM1 interacts with GUN4 to stimulate MgCh activity; (7) LIL3, CPP1, DAY and FCA proteins stabilize POR. Arrows mean positive regulation, and flat ends mean negative regulation.

1.1.4.3.2 CPP1 protein

CPP1 belongs to the family of DnaJ-like proteins, which often act as co-chaperones (Pulido and Leister, 2018). The knock-out of *CPP1* in *Arabidopsis* inhibits embryonic development from the globular stage and prevents the formation of viable seedlings (Kawai-Yamada et al., 2014). Because of the embryo-lethal phenotype, the function of CPP1 in adult tissue was characterized by means of various gene-silencing approaches in *Arabidopsis thaliana* and *Nicotiana benthamiana*. In both organisms, the reduction of the CPP1 content triggers the formation of leaf necrosis, which was suggested to be caused by lower content of POR due to the lower stability of this protein (Lee et al., 2013). Further interaction studies verified that CPP1 interacts directly with PORA and PORB and protects these enzymes from aggregation, especially under high oxidative stress conditions (Lee et al., 2013; Liu et al., 2016)

1.1.4.3.3 DAY protein

DAY protein is a membrane-bound protein possessing a DnaJ-like domain. It functions not only in Chl biosynthesis by protecting PORC but also in photomorphogenesis by stabilizing the BR receptor, BRI1 (Lee et al., 2021). The DAY protein was studied to interact with CPP1 and PORC by BiFC and in vitro pull-down, and a holdase activity was reported that could prevent heat-induced aggregation of proteins in vitro (Lee et al., 2021). Therefore, it was suggested that DAY and CPP1 work together in chloroplasts to facilitate the Chl biosynthesis by stabilizing POR via its holdase activity (Lee et al., 2021). However, our Plant Physiology group could not reproduce the interaction between DAY and POR, which makes a holdase activity of DAY doubtful.

1.1.4.3.4 FCA protein

FCA is a notable protein that activates the autonomous flowering pathway (Macknight et al., 1997; Liu et al., 2010). It was reported that FCA is involved in the thermostabilization of POR to maintain the conversion of PChlide to Chlide in developing seedlings under heat stress (Ha et al., 2017). FCA also upregulates the *POR* genes at high ambient temperature since FCA mediates histone acetylation in PORs loci to recruit RNA polymerases to the gene promoters at high temperature (Ha et al., 2017). Altogether, FCA acts bifunctional in transcriptional and post-translational control and, thus, ensures enhanced stability of POR proteins at high temperatures. Growing seedlings encounter high temperatures as they move through the topsoil, because under natural conditions, soil temperatures often exceed air temperatures (DeVay et al., 1991). Hence, FCA was proposed to induce *POR* gene expression and suppress POR degradation, and thus, serves in Chl biosynthesis, particularly during the period of transition from hetero- to autotrophic growth (Ha et al., 2017).

1.2 Light-harvesting complex (LHC) family in higher plants

In higher plants, the peripheral antennae of the PSI and PSII consist of components of the family of pigment-binding proteins of the light-harvesting complex (LHC). The intrinsic membrane protein LHCI is attached to the PSI core and comprises two heterodimers complexes, Lhca1-Lhca4 and Lhca2-Lhca3, to form the peripheral antenna complex of PSI (Qin et al., 2015), while the LHCII surrounds the PSII core consisting of monomer CP29 (Lhcb4), CP26 (Lhcb5), CP24 (Lhcb6) and trimer Lhcb1/Lhcb2/Lhcb3 to form the peripheral antenna complex of PSII (Wei et al., 2016). Each LHC protein binds approximately a dozen Chl molecules and three to four different carotenoids for light-harvesting and energy transfer. Then excitation energy is transferred through the core antenna to the photosynthetic reaction center of the PSI and PSII, leading in PSII to water oxidation, electrons transferring along the photosynthetic electron chain, protons through the membrane from stoma to the lumen as well as in PSI subsequently to $NADP^+$ reduction. In addition, LHC proteins can also dissipate the heat caused by excess excitation energy to avoid photo-oxidative damage (Betterle et al., 2009; Ruban et al., 2012). Thus, the nuclear-encoded LHCP in the peripheral antenna complex plays an essential role in photosynthesis and photoprotection. Once synthesized as precursor proteins in the cytoplasm, they are imported into the chloroplasts through the TOC/TIC translocons in the outer and inner envelope membrane. When LHCPs are transferred through the TIC and released by LTD (Ouyang et al., 2011), their trafficking through the stroma to the thylakoid membranes is managed by the cpSRP subunits (Schünemann et al., 1998).

1.2.1 The light-harvesting complex of PSII

In plants and green algae, the light-harvesting complex LHCII is associated with the dimeric core of PSII containing three holoproteins (Lhcb1, Lhcb2 and Lhcb3) that form Lhcb1/Lhcb2/Lhcb3 heterotrimers (Jackowski et al., 2001). In addition to the trimeric LHCII, three monomeric Lhcbs are bound to the PSII core and called CP29 (Lhcb4), CP26 (Lhcb5) and CP24 (Lhcb6) based on the molecular weight of their apoproteins (Camm and Green, 2004). The trimeric LHCII can be classified into three types depending on their affinities with the PSII core (C) complex: strong association (S), moderate association (M) and loose association (L) (Boekema et al., 1999). The size of antenna complexes can change with the light intensity (Kouřil et al., 2013; Bielczynski et al., 2016). Under high light conditions, the PSII-LHCII supercomplex is mainly the C2S2 and C2S types consisting of S-LHCII, CP29 and CP26, while under low light conditions, the C2S2M2 and C2S2M complexes, which binding to the S-LHCII, M-LHCII and all minor antennae, are accumulated (Kouřil et al., 2013; Albanese et al., 2016). An important organizational feature of thylakoids is that PSI lies primarily in the unstacked and stroma membranes, whereas PSII is found mainly in the grana membranes. Phosphorylation of LHCII controls energy distribution between PSI and PSII. Excess excitation of PSII relative to PSI activates the phosphorylation of LHCII, which enables phosphorylated LHCII to migrate to the unstacked membrane region and associate with PSI. In contrast, the excessive light absorption of the PSI complex activates the dephosphorylation of LHCII, allowing it to migrate back to the stacked membrane region. This mechanism enabling adjustment of the energy

distribution between PSI and PSII is called state transition (Galka et al., 2012; Goldschmidt-Clermont and Bassi, 2015).

Chl *a* and *b* are the primary light-harvesting pigments in plant LHCI and LHCII. Every Lhcb1/Lhcb2/Lhcb3 protein possesses 8 Chl-binding sites (5 Chl *a,* 3 Chl *b*) on the stromal side and 6 (3 Chl *a* and Chl *b*) on the luminal side. Carotenoids are essential supplementary for light-harvesting molecules and are involved in the NPQ (non-photochemical quenching) process (Niyogi et al., 1997). The crystal structures of LHCII from spinach and pea have revealed that the Lhcb1/Lhcb2/Lhcb3 monomer consists of four carotenoid-binding sites, named L1, L2, N1, and V1 according to the types of carotenoids: lutein (L), neoxanthin (N), and violaxanthin (V) (Liu et al., 2004; Standfuss et al., 2005).

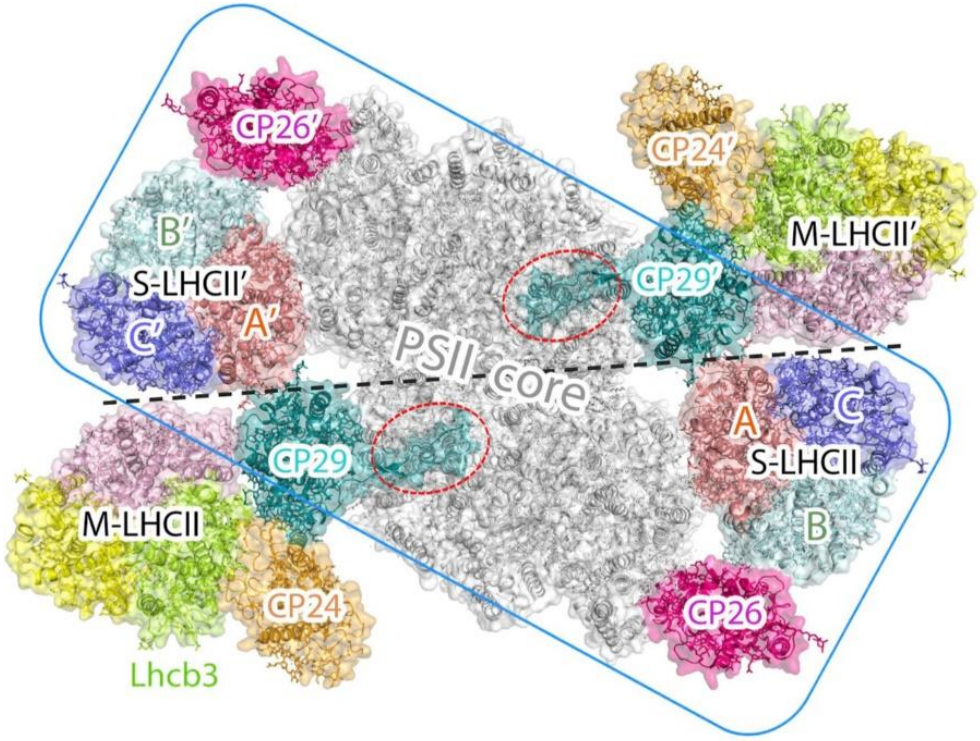

Figure 1.4 The pea C2S2M2 type PSII-LHCII supercomplex (PDB ID: 5XNL). The black-dashed line separates PSII-LHCII to the monomer. The blue box circles the C2S2 part. The apoproteins and cofactors are shown in cartoons. The peripheral LHCs are colorful while the core complexes are shown in white (Pan et al., 2020).

1.2.2 Light-harvesting complex of PSI in plant

The PSI core complex of plants is a monomer assembled with different LHC isoforms to form a PSI-LHCI supercomplex. (Nelson and Junge, 2015; Suga et al., 2016). The architecture of PSI-LHCI complexes was described: four LHCI subunits associate with the PSI core and connect to the flanks of PsaF/PsaJ to form a hemispherical belt. The four LHCI proteins are arranged to form heterodimers such as Lhca1-Lhca4 and Lhca2-Lhca3, and Lhca3, Lhca1 at the two edges closely interact with the core subunits PsaK/PsaA and PsaG/PsaB, respectively. The pea PSI-LHCI crystal structure shows that Lhca2 and Lhca4 are more distant from the core subunit, while in the maize PSI-LHCI-LHCII structure, Lhca2 contacts the core subunit PsaN

at the lumen surface. (Pan et al., 2018).

The plant LHCI proteins bind 13-15 Chls including Chl *a* and *b* (Croce et al., 2002). However, Chl *b* was only identified in the crystal structures of pea PSI-LHCI (Mazor et al., 2015; Qin et al., 2015). Plant LHCI contains 3-4 carotenoid species (Croce et al., 2002), and each binds to the conserved carotenoid-binding sites L1, L2 and N1. Three Lhca proteins (Lhca2-4) contain only three conserved carotenoids, whereas Lhca1 binds an additional Lut at the L3 site (Qin et al., 2015), which is located in the interface region between Lhca1 and Lhca4 and facing the PSI core.

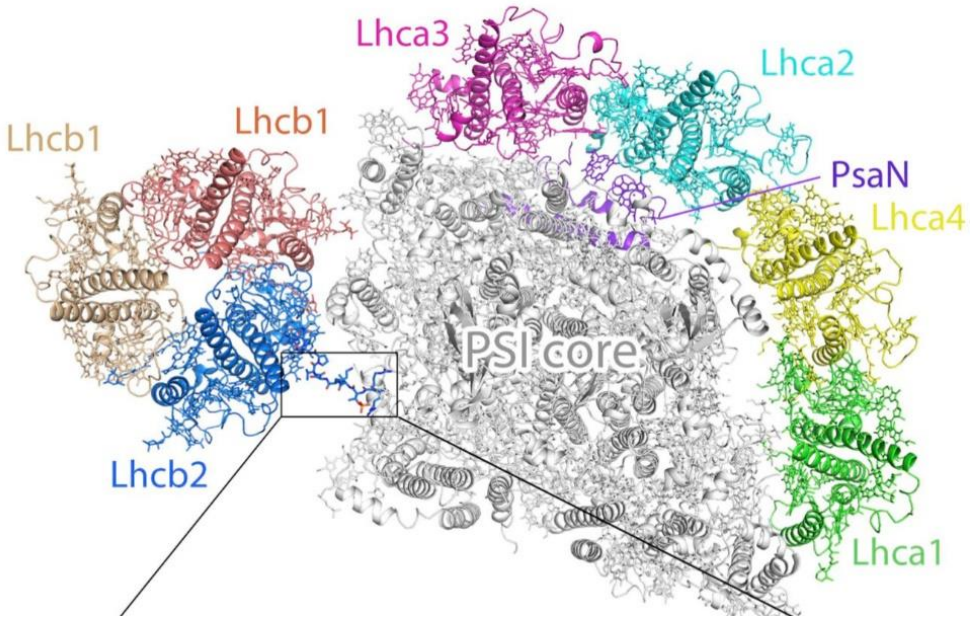

Figure 1.5 Overall structure of maize PSI-LHCI-LHCII supercomplex (PDB ID: 5ZJI). The apoproteins and cofactors are shown in cartoon and stick modes, respectively. The peripheral LHCs are colorful, while the core complexes are white, except for PsaN, which is shown in purple (Pan et al., 2020).

1.2.3 Overview of LHCP transport to the thylakoid membrane

The transport of LHCP to the thylakoid membrane is completed by the cpSRP machinery, which comprises (1) the heterodimer cpSRP43/cpSRP54 (Dünschede et al., 2015); (2) the thylakoid membrane-bound cpSRP receptor cpFtsY (Kogata et al., 1999; Tu et al., 1999); (3) GTPase of cpSRP54 and cpFtsY (Richter et al., 2010; Akopian et al., 2013), and (4) thylakoid membrane translocase Alb3 (Moore et al., 2000; Klostermann et al., 2002).

1.2.3.1 The cpSRP43/54 heterodimer

cpSRP43 three chromodomains (CD1, CD2, CD3) and four ankyrin repeats (Ank1-Ank4) (Klimyuk et al., 1999; Goforth et al., 2004; Stengel et al., 2008). cpSRP54 consists of an N-terminal domain, a central G domain with GTPase activity and a methionine-rich M domain at the C-terminus (Franklin and Hoffman, 1993; Ziehe et al., 2018). The complex formation of cpSRP43 and cpSRP54 is essential for the LHCP transport, mainly achieved by the interaction

of CD2 of cpSRP43 with the ARRKR motif of cpSRP54 (Ziehe et al., 2018). Further studies indicated that the RRKRp10 peptide attaches at the interface between CD2 and Ank4 so that both domains are more closely connected in this complex with cpSRP54 than the free cpSRP43 (Holdermann et al., 2012).

1.2.3.2 cpSRP and LHCP to form the transit complex

Since LHCP is highly hydrophobic, its transfer across the aqueous stroma requires binding to the water-soluble cpSRP43/cpSRP54 dimer. The binding is achieved by the L18 motif (VDPLYPGGSFDPLGLADD) between the second and third transmembrane of LHCP, enabling interaction with cpSRP43 (Tu et al., 2000; Groves et al., 2001; Jonas-Straube et al., 2001). It has been shown that the cpSRP54 absence or mutation of the M domain impairs the formation of the cpSRP/LHCP transit complex (Dünschede et al., 2015; Henderson, 2016). The cpSRP54 M domain was reported to drive cpSRP43 to the active conformation for protecting LHCP (Liang et al., 2016).

1.2.3.3 LHCP translocation to the thylakoid membrane

The cpSRP receptor cpFtsY is assembled to the thylakoid membrane, and biochemical and genetic data provided insight that cpFtsY is required for LHCP insertion into the membrane (Tu et al., 1999; Marty, 2009). Like the cpSRP54 structure, cpFtsY contains an NG domain required for GTP binding and hydrolysis. cpFtsY binds to cpSRP54 when the complex is formed by the interaction between both proteins' two homologous NG domains of both proteins (Wild, 2016; Ziehe et al., 2018). In addition to cpFtsY, the thylakoid membrane protein Albino 3 (Alb3), a holdase/insertase, is finally involved in LHCP insertion (Klostermann et al., 2002). Several studies have reported a direct interaction between cpSRP43 and Alb3 (Bals et al., 2010; Liang et al., 2016). Data from crystal structure revealed that the motif IV of Alb3 binds to the CD3 of cpSRP43 (Horn et al., 2015). The biochemical data point to an interaction between motif II and cpSRP43 CD1-Ank4 (Liang et al., 2016). These data conclude that the transit complex is recruited to Alb3 through the cpSRP43/Alb3 interaction.

1.2.4 cpSRP43 acts as a chaperone to protect LHCP from aggregation

cpSRP43 not only transports LHCP to the thylakoid membrane but also simultaneously prevents aggregation of the hydrophobic LHCP (Falk and Sinning, 2010; Jaru-Ampornpan et al., 2010). The substrate-binding domain (SBD) consists of chromodomain 1 (CD1), four ankyrin-repeat motifs (Ank1-Ank4) and a 20-amino-acid bridging helix is essential and sufficient to protect LHCPs from aggregation (Jonas-Straube et al., 2001; Liang et al., 2016). In contrast to the ATP-dependent chaperone activity of Hsp70 (Zhuravleva et al., 2012) and GroEL (Fenton and Horwich, 1997), cpSRP43 is ATP-independent and also can dissolve aggregates of LHCPs (Falk and Sinning, 2010). cpSRP54, as another component of cpSRP cannot chaperone LHCP, but stimulates cpSRP43's chaperone activity towards LHCP (Liang et al., 2016; Ziehe et al., 2017). A proposed mechanism for cpSRP54's stimulation to the chaperone activity of cpSRP43 points to the stabilized interaction between cpSRP43 and

cpSRP54 M-domain in a closed conformation, in which the Ankyrin repeat domain is more stably folded (Siegel et al., 2020). The high chaperone activity of cpSRP43 is emphasized by the formation of contiguous contact surfaces of the cpSRP43-SBD with the TMDs of LHCP (Siegel et al., 2020).

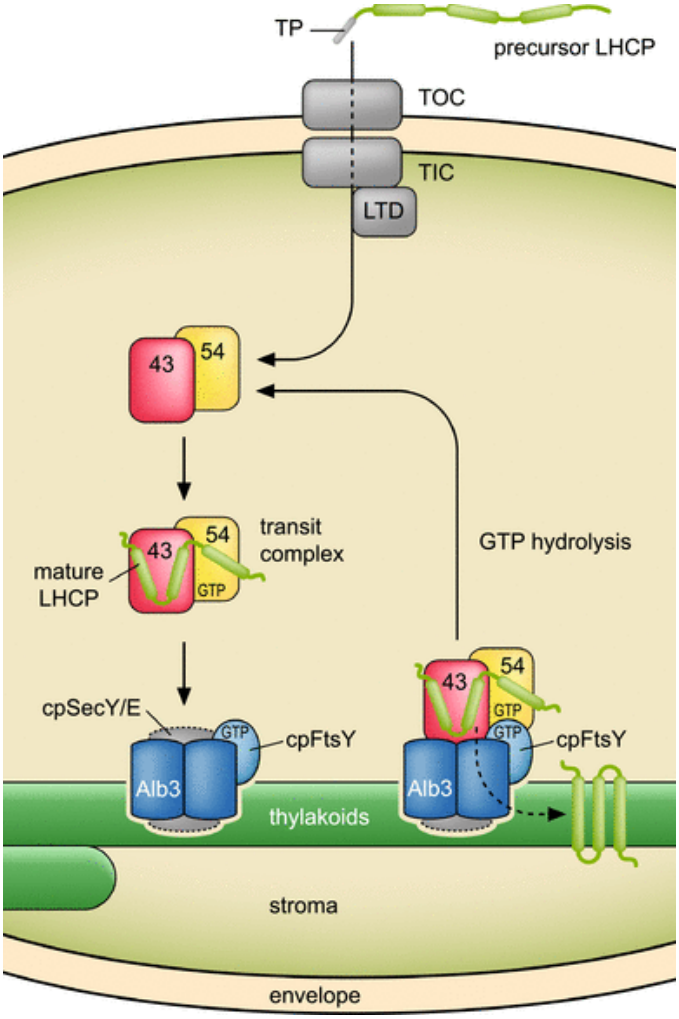

Figure 1.6 LHCP translocation to the thylakoid membrane via the cpSRP-dependent pathway. LHCPs are imported into chloroplasts via the TOC/TIC translocon machinery. Then the transit peptide is cleaved off and the LHCPs are delivered to the cpSRP43/54 complex by LTD. cpSRP43 and cpSRP54 form the transit complex for LHCP and dock to the thylakoid membrane via interaction with cpFtsY and Alb3. The SRP GTPase of cpSRP54 and cpFtsY hydrolyze the GTP to drive the dissociation of protein components for a new cycle of LHCP trafficking (Ziehe et al., 2018).

1.3 Effects of heat stress on the photosynthesis

Growth at elevated temperatures above the standard growth conditions is termed as heat stress. Since global warming is becoming a severe issue, studies regarding the growth conditions under heat stress are becoming more urgent. It is well known that higher temperatures will affect the activity of proteins and membrane integrity and can ultimately lead to cellular damage and cell death (Hemantaranjan, 2014). As a sessile organism, the plant is constantly exposed to changing stress conditions, such as temperature and other abiotic factors, and cannot escape from rapidly

changing adverse conditions. It is pronounced that heat stress can be enormously destructive (Nouri et al., 2015). In this line, photosynthesis is highly sensitive to high temperatures as the photochemical reactions and carbon metabolism are most affected (Wise et al., 2004; Wang et al., 2018). Heat stress could directly damage the photosynthetic apparatus, such as PSI and PSII, the cytochrome b6f (Cytb6f) complex and the Chl biosynthesis (Havaux, 1993; Wise et al., 2004; Hu et al., 2020), leading to the inhibition of various metabolic reactions (Mathur et al., 2014).

1.3.1 Effects of heat stress on the PSII

In photosystems, PSII is most sensitive to heat stress, in particular, photosynthetic electron chain and ATP synthesis are susceptible to the adverse effects of heat stress (Wang et al., 2018). Due to the increased fluidity of the thylakoid membrane at high temperatures, the PSII antenna complex could disassemble in the thylakoid membrane, which impairs light absorption and transmission. The oxygen-evolving complex (OEC) in PSII is dissociated by heat stress, inhibiting the electron transport from OEC to the acceptor side of PSII (Allakhverdiev et al., 2008). To prevent PSII from heat-induced damage, in parallel to excessive irradiation, Xanthophyll-dependent NPQ can reduce the excitation energy pressure in the PSII reaction center by converting excess light energy into thermal energy. Moreover, heat stress is usually accompanied by the generation of oxidative stress (Lord-Fontaine and Averill-Bates, 2002). Then, singlet oxygen ($^1O_2$) produced can damage proteins, for example, D1 in the PSII reaction center, and induce the PSII repair cycle (Dogra and Kim, 2019).

1.3.2 Effects of heat stress on the Chl biosynthesis

Chl is the most important pigment for converting light energy into chemical energy during photosynthesis. It has been reported that Chl biosynthesis is inhibited when plants are under heat stress conditions, which may be caused by the destruction of several enzymes in chlorophyll biosynthesis (Efeoglu and Ekmekci; Masoudi-Sadaghiani et al., 2011), such as ALAD, POR and CHLI. The activity of ALAD, the first enzyme of the TBS pathway, was found to be decreased under high-temperature regimes (Kumar Tewari and Charan Tripathy, 1998; Mohanty et al., 2006). A previous study showed that the abundance of POR was declined in heat-stressed *fca* mutant (*FCA* knock-out) associated with the reduced accumulation of Chl (Ha et al., 2017). The MgCh subunit CHLI-2 identified in *V. vinifera* leaves was repressed after heat stress (Liu et al., 2014). Wang et al. reported that high temperature and humidity stress decrease the content of the MgCh subunit while increasing the amount of ribulose bisphosphate carboxylase/oxygenase proteins reflect a reduction in Chl biosynthesis and an increase in photorespiration (Wang et al., 2012).

Heat stress also affects gene expression in Chl biosynthesis. To understand how heat stress modulates the Chl biosynthesis, Mohanty, et al. examined the transcript levels of many enzymatic steps of Chl biosynthesis in wheat and cucumber at 42°C for 24h (Mohanty et al., 2006). It was found that the expression of *HEMA1* was downregulated in heat-stressed seedlings in cucumber only. The transcripts of *GSA* and *UroD* were increased in illuminated heat-stressed

seedlings in both wheat and cucumber. In wheat, *CHLl* expression was almost similar in control and heat stress, while in cucumber the expression was downregulated during heat stress. The *ChlP* transcript was reduced by high temperatures in both wheat and cucumber (Mohanty et al., 2006).

1.3.3 Heat-shock proteins (HSPs) involved in the protection against heat stress

To respond to heat stress, plants have evolved strategies to overcome the damage caused by heat stress. The different families of HSPs are responsible for either protein folding, assembly, translocation or degradation in many normal cellular processes. They can also contribute to more stability of proteins and membranes, and assist in protein refolding under stress conditions. These activities of HSPs always depend on the respective protein family (LI et al., 2016). They play a crucial role in protecting plants against stress by re-establishing normal protein conformation, and cellular homeostasis (von Koskull-Döring et al., 2007; Schramm et al., 2008). The HSPs are generally divided into five major families: the HSP70 (DnaK) family, the HSP60 (GroEL) family, the HSP90 family, the HSP100 (Clp) family, and the small HSP (sHSP) family (Wang et al., 2004). HSP70 prevents the aggregation of proteins and aids in refolding non-native proteins under normal and stress conditions (Hartl, 1996; Frydman, 2001). Overexpression of the *HSP70* gene positively correlates with the acquired thermotolerance of plants (Lee and Schöffl, 1996) and enhances the tolerance to salty water and high-temperature stress (Ono et al., 2001; Sung and Guy, 2003). HSP 60 plays a critical role in correctly folding the wide range of newly synthesized and newly translocated target proteins (Bukau and Horwich, 1998; Frydman, 2001). HSP90 in plastids and mitochondria is important for folding of imported proteins (Willmund and Schroda, 2005; Schroda and Mühlhaus, 2009), maintenance of protein activity (Young et al., 2001), and inhibition of protein aggregation (Fellerer et al., 2011; Kindgren et al., 2012). The HSP100/Clp family is a member of the large AAA^{+}-ATPase superfamily and plays a role in protein disaggregation and degradation (Schirmer et al., 1996; Neuwald et al., 1999; Agarwal et al., 2001). The sHSP cannot refold the non-native proteins. They can only stabilize and protect the non-native protein from aggregation and then facilitate the subsequent refolding of the non-native protein by ATP-dependent chaperones, such as the DnaK system or ClpB/DnaK (Lee et al., 1997; Lee and Vierling, 2000; Mogk et al., 2003).

1.4 Introduction to protein aggregation

1.4.1 Protein aggregation pathway

The correct three-dimensional structure of each protein is a prerequisite for its adequate function. However, each protein is just synthesized as a linear polypeptide chain during translation at the ribosome. Therefore, proteins need to be folded into the three-dimensional structure. In this process, unfolded, partial or misfolded proteins can convert into aggregates. The resulting aggregates typically depend on noncovalent forces, such as hydrophobic attraction, hydrogen bonds and Van-der-Waals forces (Sahin et al., 2011; Roberts, 2014; O'Brien et al., 2016). Several aggregation pathways or mechanisms are summarized in Figure

1.7 (Meric et al., 2017). Step 1 represents a state, in which protein monomers (F) may form a partially or completely unfolded or misfolded monomer (I or U, respectively). Step 2 describes the process of how a monomer forms reversible oligomers by self-association. Step 3 indicates a conformational change of an oligomer when a part of the amino acid sequence is unintendedly exposed to adjacent proteins and initiates a strong stabilizing contact that results in the formation of a minimum unit of an irreversible aggregate (Fink, 1998; Uversky and Fink, 2004; Weiss IV et al., 2009). Subsequently, aggregates may grow through several different pathways in step 4 to form irreversible protein aggregations (Chiti and Dobson, 2006; Andrews and Roberts, 2007; Roberts et al., 2011; Roberts, 2014). The portion of sequences of the amino acid residues in step 3 is usually a hydrophobic polypeptide motif, originally hidden in the core of the protein. This peptide motif is also known as an aggregation-prone region (APR), because, when it is exposed to the protein surface in an aqueous solution, it tends to be masked by strong interdependent contacts, such as β-sheet structures, which will lead to protein aggregation.

1.4.2 Algorithms applied for the APRs prediction

In view of the fact that the presence of APRs will promote protein aggregation, elimination of the APRs of proteins could be a good strategy to engineer proteins and improve their functionality. How to predict the APRs of proteins? Many algorithms have been developed to predict the APRs of proteins, such as FoldX (Schymkowitz et al., 2005), RosettaDesign (Liu and Kuhlman, 2006), PyRosetta (Chaudhury et al., 2010) and TANGO (Fernandez-Escamilla et al., 2004). In my doctoral study, I used the TANGO algorithm, which is briefly introduced. The TANGO algorithm is applied to predict β-aggregation-prone regions in the sequence of the following conformations: α-helix, β-sheet, β-aggregate or helix aggregate. The prediction of the tendency of proteins to aggregate is based on the aggregate regions that were typically completely buried in β-aggregates. Using TANGO, sequences of a length of at least five amino acid residues and a β-aggregation occupancy rate of at least 5% are usually predicted as potential sites (Meric et al., 2017).

1.4.3 APRs in GluTR

Since APRs lead to protein aggregation, it was reported that APRs could be exploited to inactivate proteins functions in plants (Betti et al., 2016) . The overexpression of small peptides with the APRs of a targeted protein will posttranslationally generate highly specific protein knockdowns in different plant species (Betti et al., 2016) . Because chaperones are dedicated to protecting their clients from aggregation, the APR is generally considered the binding site with the chaperone. Therefore, a non-substrate protein can be converted to a substrate protein for GroEL by mutating the APR. Then GroEL assists in the folding of the client protein (Kumar et al., 2012). Recent studies have shown that large insoluble aggregates can act as a protective mechanism against cellular oxidative stress, as aggregated species distributed in the cytosol and cannot merge into large protein inclusions causes the highest levels of oxidative damage. (Carija et al., 2017).

The Arabidopsis GluTR functions as a very importantve rate-limiting enzyme in TBS and has been reported to possess two APRs at the N-terminus of the GluTR protein (Wang et al., 2018). It was proposed that overexpression of GluTR in *Nicotiana tabacum* or *Arabidopsis thaliana* does not exhibit a corresponding increase in ALA synthesis capacity, because excess GluTR tends to form oligomers or aggregated complexes (Schmied et al., 2011). The solubility of an N-terminal-truncated recombinant GluTR with the deletion of the two APRs was significantly enhanced in vitro (Wang et al., 2018), implying that APRs are responsible for GluTR aggregation in vitro, and cpSRP43 was proposed to interact with the APRs and prevent its aggregation. However, the functions of APRs in vivo are still unknown. Whether APRs in planta is also the reason for GluTR aggregation, still needs to be studied.

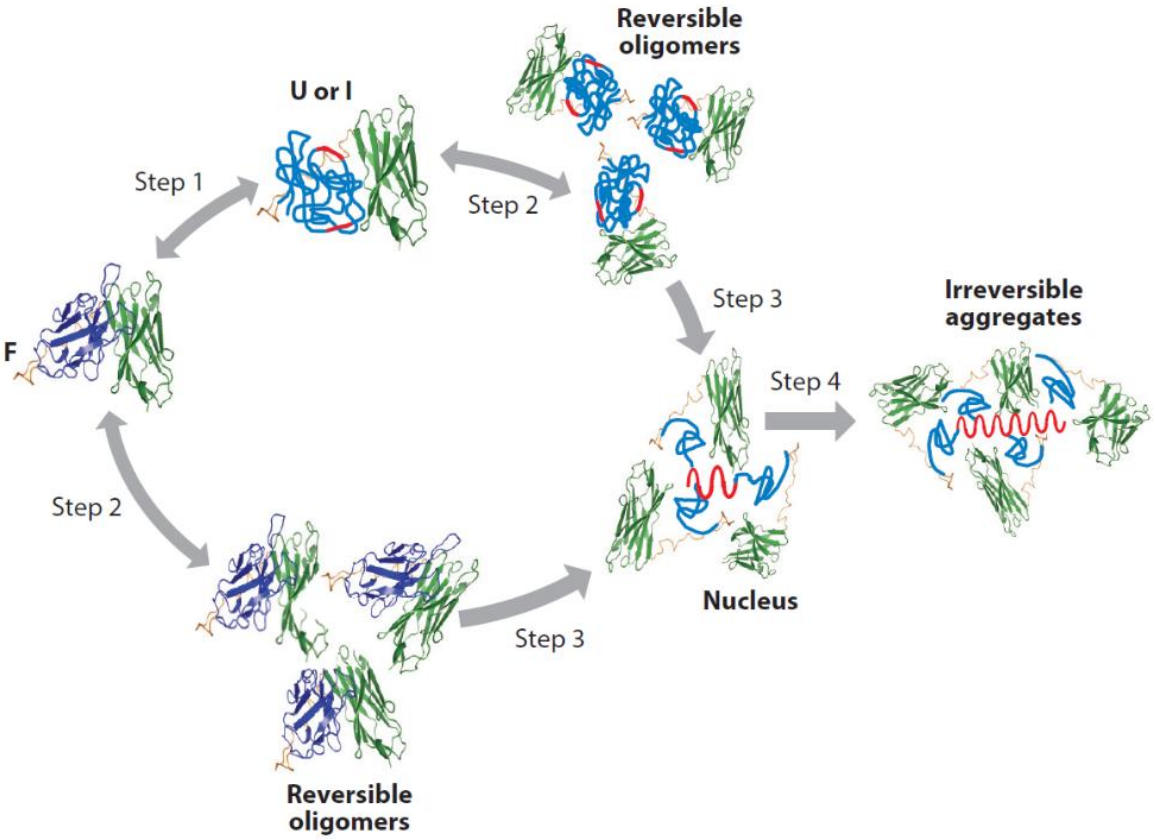

Figure 1.7 Overview of protein aggregation pathways. Step 1: partial or complete unfolding or misfolding of a natively folded protein monomer (F), leading to the exposure of aggregation-prone regions (red). Step 2: reversible self-association of protein monomers. Step 3: minimal irreversible species are generated by intermolecular noncovalent contacts between aggregation-prone regions. Step 4: growth of aggregates. Double arrows indicate reversible steps; single arrows represent irreversible steps (Meric et al., 2017).

1.5 Aims of the project

It has been reported that cpSRP43 acts as a chaperone to protect GluTR from denaturation, thereby coordinating the Chl biosynthesis and LHCP trafficking to the thylakoid membrane. However, besides GluTR, there are at least two other tightly controlled enzymes, MgCh and POR, in the Chl biosynthesis pathway. MgCh is localized at the branch point for Chl and heme synthesis. Many factors have been reported to be involved in its regulation, such as GUN4 and BCM1. The enzymatic step catalyzed by POR is NADPH- and light-dependent. Thus, the phototoxic intermediate Pchlide will accumulate in the dark until ALA synthesis is sufficiently suppressed. POR was reported to be involved in an inactivation complex of GluTR in the dark to suppress the supply of ALA for Chl synthesis. Some factors such as LIL3, CPP1, and FCA regulate the stability of PORB. However, whether cpSRP43 or even cpSRP54 can regulate these TBS enzymes is still unknown. Hence, the aims of my project are: (1) To investigate whether cpSRP43 and cpSRP54 also affect the stability of MgCh and POR. It is intended to assay the protein contents of POR and MgCh subunits, such as CHLH, CHLD, CHLI, as well as its activator GUN4 in *cpSRP43* knock-out mutant *chaos* and *cpSRP54* knock-out mutant *ffc* in comparison with wild-type control. (2) Using BiFC, Pull-down, Co-IP for the protein-protein interaction studies. It is aimed to explore the interactions of these TBS proteins with the cpSRP components. (3) Enzyme assays are planned to investigate if cpSRP43 and cpSRP54 affect the activity of GluTR, MgCh, and POR. (4) Chaperone activity assay to explore if cpSRP43 can protect its TBS clients from denaturation. (5) Applying some stress conditions, such as heat shock or dark treatment, to study the function of cpSRP components on TBS proteins in response to changing environments. (6) Separating the soluble or membrane-bound TBS proteins. It is intended to perform a functional analysis of cpSRP54 to verify its membrane binding capacity to TBS proteins.

APRs of GluTR are thought to be the regions that initiate the GluTR aggregation, and cpSRP43 was speculated to cover these regions to avoid the aggregation. In a previous study, the in vitro aggregation-prone property of APR was verified by scattering assay. However, in vivo function of APR is still unknown. Therefore, this subproject aims (1) Removal of the APR by deletion or amino acids substitution to investigate the roles of APR in planta. (2) Studies of the potential increase of GluTR accumulation, ALA synthesis, and even Chl biosynthesis by modification of the APRs of GluTR.

2 Materials and methods

2.1 Plant materials and growth conditions

2.1.1 *Arabidopsis thaliana*

Arabidopsis thaliana plants were cultivated on a soil (GS-90)-vermiculite mixture at 22 °C in a long day (LD, 16 h light/ 8 h dark). The plants were exposed to a light intensity of 100 µmol photons $m^{-2}s^{-1}$. After sowing, the seeds were vernalization for two days at 4 °C. Heat shock treatment was applied by transferring 14-18 days old seedlings from standard LD conditions to constant light (CL, 100 µmol photons $m^{-2}s^{-1}$) at a temperature of 42 °C for the indicated time. Dark treatment was applied by transferring 14-18 days old seedlings from standard LD conditions to the darkness for the stated time. Unless otherwise stated, the standard growth condition in this study is LD at 22 °C with a light intensity of 100 µmol photons $m^{-2}s^{-1}$.

The sterile cultivation of Arabidopsis plants was placed on Petri dishes with Murashige and Skoog medium (MS, with vitamins) mixed with plant cultivation agar (4.43 g/l MS, 0.5 g/l MES, 8 g/l agar, pH 5.7 with NaOH). About 50 µl seeds were incubated for 10 min in 1 ml of sterilization solution (70% ethanol (v/v), 0.05% (v/v) Triton X-100). The sterilization solution was then removed, and the seeds were washed in 70% ethanol (v/v) twice. After settling, the seeds were washed with 100% ethanol (v/v) twice, then the ethanol was removed, and the seeds were dried on a clean bench. The sterilized seeds were either applied dry or mixed with sterile water. To analyze the retrograde signaling pathway (Susek et al., 1993), Arabidopsis seeds were grown on the sterilized MS plates in the presence of 5 µM norflurazon (NF, 5 mM in DMSO as stock), an inhibitor of carotenoid biosynthesis (Breitenbach et al., 2001), vernalization for 2 days then grown in continuous light for 5-6 days.

Unless otherwise stated, all physiological experiments such as analyses of transcripts, proteins, and intermediates of the tetrapyrrole metabolism were performed with 14-18 days old seedlings. A large number of individual materials (50-100 mg) were harvested per sample. As a rule, at least three replicates were harvested and analyzed, and all experiments were repeated at least twice. After harvesting, the samples were frozen in liquid nitrogen and stored at -80 °C until processed. The information on the Arabidopsis lines used in this study was listed in Table 2.1.

Table 2.1 Genotypes used and analyzed in this study

Line	Gene ID	Gene	Description	Source
Col-0	-	-	Arabidopsis Columbia Wild type (WT)	-

Ler-0	-	-	Arabidopsis Landsberg erecta (WT)	-
chaos	AT2G47450	*cpSRP43*	*cpSRP43* knock-out mutant	(Klimyuk et al., 1999)
ffc	AT1G15310	*cpSRP54*	*cpSRP54* knock-out mutant	(Amin et al., 1999)
chaos/ffc	AT2G47450/ AT1G15310	*cpSRP43/ cpSRP54*	Double mutant of *cpSRP43* and *cpSRP54*	(Amin et al., 1999)
cpftsy	AT2G45770	*cpFTSY*	Chloroplast SRP receptor *cpFtsY* knock-out mutant	(Tzvetkova-Chevolleau et al., 2007)
cpSRP43-OX	AT2G47450	*cpSRP43*	*chaos* complementation line expressing cpSRP43	(Wang et al., 2018)
cpSRP43-SBD-OX	AT2G47450	*cpSRP43*	*chaos* complementation line expressing SBD of cpSRP43	This study
cpSRP43ΔCD1-OX	AT2G47450	*cpSRP43*	*chaos* complementation line expressing cpSRP43 without CD1	(Wang et al., 2018)
cpSRP43ΔAnk-OX	AT2G47450	*cpSRP43*	*chaos* complementation line expressing cpSRP43 without Ank	(Wang et al., 2018)
cpSRP43ΔCD2-OX	AT2G47450	*cpSRP43*	*chaos* complementation line expressing cpSRP43 without CD2	(Wang et al., 2018)
cpSRP43ΔCD3-OX	AT2G47450	*cpSRP43*	*chaos* complementation line expressing cpSRP43 without CD3	(Wang et al., 2018)
gun4-1	AT3G59400	*GUN4*	L88→F88 mutation in GUN4	(Larkin et al., 2003)

HEMA1(V99P/V151P)	AT1G58290	*HEMA1*	*hema1* complementation line expressing GluTR (V99P/V151P)	This study
HEMA1(V99T/V151T)	AT1G58290	*HEMA1*	*hema1* complementation line expressing GluTR (V99T/V151T)	This study
HEMA1/hema1	AT1G58290	*HEMA1*	*hema1* heterozygous	(Apitz et al., 2014)
hema1	AT1G58290	*HEMA1*	*HEMA1* knock-out mutant	(Apitz et al., 2014)

2.1.2 *Nicotiana benthamiana*

The *Nicotiana benthamiana* plant used for the transient transformation was grown in the LD at 30 °C in the greenhouse on soil (type T)-vermiculite mixture.

2.2 Bacteria and growth conditions

2.2.1 *Escherichia coli*

The medium for cultivation of the *Escherichia coli* (DH5α, BL21 and Rosette) is LB (10 g/l tryptone, 5 g/l yeast extract, 10 g/l NaCl, pH 7.0) or 2YT (15 g/l tryptone, 10 g/l yeast extract, 5 g/l NaCl, pH 7.0) at 37 °C with specific selection markers (Table 2.3). The 2YT medium is specially used for the prokaryotic overexpression of recombinant proteins. The solid medium is added with additional 15 g/l agar. Bacterial strains used in this study are listed in Table 2.2.

2.2.2 *Agrobacterium tumefaciens*

Agrobacterium tumefaciens (GV2260) was cultivated in YEB medium (5 g/l tryptone, 1 g/l yeast extract, 5 g/l sucrose, 0.5 g/l $MgSO_4 \cdot 7\ H_2O$, pH 7.2) which contained 100 µM rifampicin and the vector-specific antibiotics (Table 2.3). Liquid cultures were generally grown overnight at 30 °C in the shaker (250 rpm). The cultivation on a solid medium took place on a YEB agar (15 g/l) plate with antibiotics and incubated for 2 days at 30 °C.

Table 2.2 Bacterial strains used in this study

Strain	Resistance	Usage	Source
DH5α	-	Cloning	Invitrogen
BL21 (DE3)	-	Recombinant protein expression	Invitrogen
Rosetta (DE3)	Chloramphenicol	Recombinant protein expression	Novagen
PRIL (BL21)	Chloramphenicol	Recombinant protein expression	
GV2260	Rifampicin and Ampicillin	Plant transformation	

Table 2.3 Antibiotics used in this study

Antibiotic	Final concentration	Stock solution
Ampicillin (Ap)	100 µg/ml	100 mg/ml in 50% Ethanol
Kanamycin (Km)	50 µg/ml	50 mg/ml in ddH_2O
Gentamycin (Gen)	25 µg/ml	25 mg/ml in ddH_2O
Rifampicin (Rif)	50 µg/ml	50 mg/ml in DMSO
Spectinomycin (Sp)	50 µg/ml	50 mg/ml in ddH_2O
Chloramphenicol (ChlorA)	25 µg/ml	25 mg/ml in 100% Ethanol

2.3 Transformation of organisms

This section describes the methods for growing and transforming bacteria, as well as the protocols for the transient (in *Nicotiana benthamiana*) and stable (in *Arabidopsis thaliana*) transformation of plants. Bacterial strains used in this study are listed in Table 2.2.

2.3.1 Chemical transformation of *E. coli*

E. coli strain is transformed using heat shock. An aliquot (usually 50 µl) of competent *E. coli* was thawed on ice and mixed with a different volume of plasmid or ligation mixture (usually 1-5 µl). The transformation mixture was incubated at 42 °C for 90 seconds and then put on ice for 2 min. After adding 500-800 µl liquid LB medium, the transformation mixture was incubated for one hour at 37 °C in a shaker (250 rpm). Then a portion was applied to LB plates with specific antibiotics. Colonies were further cultivated overnight in a warm cabinet.

2.3.2 Transformation of *Agrobacterium tumefaciens*

10 µl of electrically competent agrobacteria were mixed with 1 µl of purified plasmid and transferred to a cooled electroporation cuvette (plate spacing 1 mm). The transformation occurred with an electrical pulse (Bio-Rad MikroPulser: 2.3 kV, pulse duration: 1-4 ms). The cells were then mixed with 500 µl of liquid YEB and incubated for 2-3 h at 30 °C in a shaker (250 rpm), and then a portion was plated onto a YEB solid medium.

2.3.3 Transient transformation of *Nicotiana benthamiana*

For the transient expression of proteins in *Nicotiana benthamiana* leaves, an overnight grown agrobacterium was harvested (10 min, 4,500 g, RT) and resuspended in an infiltration medium (10 mM $MgCl_2$, 10 mM MES, 100 µM acetosyringone, pH 5.7). The OD_{600} was adjusted to 0.8-1.0, and the bacterial suspension was infiltrated into the underside of the tobacco leaves using a syringe. The infiltrated plants were incubated in the dark for 2-3 days and analyzed according to the experimental requirements.

2.3.4 Stable transformation of *Arabidopsis thaliana*

Stable transformants of *Arabidopsis* are generated using the modified "floral dip" method (Clough and Bent, 1998). For this purpose, an agrobacteria culture that had grown overnight was harvested (10 min, 4,500 g, RT) and resuspended in inoculation medium (0.5% (w/v) MS, 0.05% (w/v) MES, 5% (w/v) sucrose, 0.05% (v/v), Silwet L-77, pH 5.7). The bacterial solution was diluted to the OD_{600}= 0.8 and dripped onto the top of newly unopened inflorescences of Arabidopsis plants. Transformed plants should grow under dim light for 1-2 days, and the transformation should be repeated 3-4 times at intervals of 2-3 days. The primary transformants were selected using a suitable selection marker (e.g., sprayed with BASTA) from 14 days after germination.

2.4 Nucleic acids analyses

2.4.1 Rapid extraction of genomic DNA

Arabidopsis leaves were homogenized then added 200 µl DNA extraction buffer (200 mM Tris-HCl, 150 mM NaCl, 25 mM EDTA, 0.5% SDS (w/v), pH 7.5). After a centrifugation step at RT (14,000 *g*, 5 min), the supernatant was mixed with an equal volume of isopropanol, and the DNA was precipitated in the centrifuge for 5 min (RT, 14,000 *g*). The pellet was washed with

500 µl 70% ethanol (v/v) and then dried at RT. The DNA was finally dissolved in 100 µl of ddH_2O.

2.4.2 Polymerase chain reaction (PCR)

Two different PCR strategies amplify DNA fragments: Dream-Taq polymerase is used for genotyping or test PCR (such as colony PCR). Proofreading polymerase (Phusion) is used to clone the target gene. The composition of PCR reaction and program for PCR running are shown in Tables 2.4 and 2.5. The analysis of PCR products was carried out in 1.0 % agarose gels in 1xTAE buffer (50xTAE stock solution (1 l): 242 g Tris-HCl, 100 ml 0.5 M EDTA (pH 8.0), 57.1 ml acetic acid (anhydrous)). If not already present in the polymerase buffer system, loading buffer (5x: 100 mM EDTA, 50% glycerol (v/v), 0.1% bromophenol blue (w/v)) had to be added to the PCR batches before analysis in the agarose gel. To stain the DNA fragments, ethidium bromide (3 µl/ 100 ml gel) was added to the melted agarose.

Table 2.4 Compositions of PCR reaction applied in this study

Composition	Volume (µl)
10x DreamTaq- / 5x Phusion buffer	2 / 4
10 mM dNTPs	0.8
10 µM forward primer	0.4
10 µM reverse primer	0.4
DNA template	variable
Dream Taq/ Phusion	0.1
ddH_2O	to 20

Table 2.5 Standard PCR program applied in this study

Step	Temperature (°C)	Time
1	95	2 min

2	95	30 s
3	56-60 (primer specific)	30 s
4	72	variable, usually 15-30 s/ 1 kb amplicon length
	Cycles (step 2-4): up to 40x	
5	72	5 min
6	4	pause

2.4.3 Genotyping PCR

The genotyping of Arabidopsis plants is carried out using genomic DNA and specific primers (Table Appendix I). One pair of primers is used to amplify the WT allele (LP + RP primer), and the second pair of primers is used to amplify a possible T-DNA (LB + RP primer). The LP and RP primers span the T-DNA insertion site. With the LB (T-DNA specific) and RP combination, part of the T-DNA is amplified together with part of the gene sequence. In the case of a WT plant, only one amplicon is detected for the WT allele. A heterozygous mutant (one allele carries a T-DNA) is distinguished by amplification for both primer pairs. A mutant with a homozygous insertion of a T-DNA into both alleles, on the other hand, is characterized by the absence of amplification for the WT allele.

2.4.4 Introduction of mutations into DNA fragments by PCR

Two PCR techniques are used to introduce point mutations into a protein-encoding sequence. Both methods are based on the usage of mutated primers, which bring the desired base substitution and thus the mutation of the encoded amino acids. The first approach is that the mutated fragment is amplified with mutated primers, containing the corresponding base substitution and restriction site for further cloning (see chapter 2.4.5). This method is used to construct the plasmids for the generation of transgenic lines *HEMA1 (V99T/V151T)*, *HEMA1 (V99P/V151P)* (see chapter 3.3.4). The second approach directly amplified the whole already cloned vector with mutated primers (Laible and Boonrod, 2009). After successful PCR, the template vector, which originates from a bacterial extraction and consequently has DNA methylations, was digested with a methylation-specific restriction enzyme DpnI. The remaining linear PCR products, which contain the mutated site, were then transformed into *E. coli* cells (see chapter 2.3.1). The PCR program used differs from that shown in Table 2.3 in the following points: the annealing temperature was set at 55 °C and the elongation time at 1 min/ 1 kb. The number of cycles was reduced to 20-25. This method is applied to construct the plasmids for

the prokaryotic expression of recombinant protein GluTR (V99T/V151T) (see chapter 3.3.4.3).

2.4.5 Cloning

2.4.5.1 Cloning of PCR fragments

PCR fragments were purified from the agarose gel using a gel extraction kit (Invisorb Spin DNA Extraction Kit) and ligated with the initial vector pJET 1.2 (Table 2.6). The ligation mixture was transformed into 50 µl DH5α cells by heat shock and applied to antibiotic-containing LB plates. The colonies grown overnight were checked for the presence of the vector by means of colony PCR (Table 2.5, 30 cycles), and positively selected colonies were inoculated into 3 ml of liquid LB medium and grown overnight.

Table 2.6 pJET 1.2 Ligation

Composition	Volume (µl)
2x pJET 1.2 ligation buffer	5
pJET 1.2 blunt vector	0.5
1 ng fragment	max. 4
T4 DNA ligase	0.5

2.4.5.2 Plasmid DNA extraction

2 ml of *E. coli* culture grown overnight were centrifuged (RT, 2 min, 6,000 *g*), and the pellet was resuspended in 300 µl buffer P1 (50 mM Tris-HCl, 10 mM EDTA, 100 µg/ ml RNaseA, pH 8.0 with HCl). Then 300 µl of P2 (200 mM NaOH, 1% SDS (w/ v)) were added and slightly inverted 10 times. After adding 300 µl of P3 (3 M potassium acetate, pH 5.5), the mixture was vortex and then centrifuged for 10 min (RT, 14,000 *g*). 0.7 volume (560 µl) of isopropanol was added to 800 µl of the supernatant and precipitated on ice for 10 min. Then centrifuged again (14,000 *g*, 10 min, 4 °C), and the pellet obtained was washed with 75% ethanol. After centrifugation, the pellet was air-dried for 5-10 min, and the final plasmid DNA was dissolved in 30 µl ddH_2O.

2.4.5.3 Sequencing

To check the correctness of cloned sequences, 1 µg of the plasmid DNA to be examined was made up to a total volume of 12 µl, including 5 µl of the 10 µM pJET 1.2 Forward primer. The sequencing was done by LGC-Genomics, and the generated sequence was evaluated using Vector NTI (Thermo Scientific).

2.4.5.4 DNA digestion by restriction enzymes

Once the sequence was checked, the target fragment and the target vector were digested with the two restriction enzymes of choice. The approach used for this is shown in Table 2.7. The digestion was incubated for 2 h at the optimal temperature for the restriction enzymes. After the time had elapsed, 1.5 µl of 6x DNA loading buffer was added to the reaction mixture, and it was electrophoretically separated (see chapter 2.4.2). The target fragment was cut from the gel (gel extraction kit, Invisorb).

Table 2.7 Two-restriction enzymes digestion

Composition	Volume (µl)
1 µg extracted plasmid	max. 8
10× digestion buffer	1
Restriction enzyme 1	0.5
Restriction enzyme 2	0.5
ddH_2O	to 10

2.4.5.5 Ligation into the target vector

The previously digested fragments (see above) were used in a molar ratio of 3:1 (insert: vector) to ligate the target gene into the final vector. The ligation approach based on this was summarized in Table 2.8. The ligation took place at RT for 1 h. The T4 DNA ligase was then inactivated at 65 °C for 10 min. The ligation mixture was transformed into DH5α cells and plated onto an LB agar medium containing the vector-specific selection marker. Selection took place overnight at 37 °C. The following day, the correct insertion of the target gene was verified by means of colony PCR. Transformants that tested positive were inoculated into 3 ml of LB and grown overnight at 37 °C. The plasmid was then extracted and kept for the following application.

Table 2.8 T4 DNA ligation

Composition	Volume (µl)
10× T4 ligase buffer	1
Target vector	1
DNA fragment	4
T4 DNA ligase	0.5
ddH_2O	to 10

2.4.5.6 Plasmids generated and used in this work

Plasmids constructed and used in this study are listed in Table 2.9. The plasmids used to express recombinant protein are listed in Table 2.15.

Table 2.9 Plasmids constructed and used in this work

Plasmids	Resistances	Genes	Purpose
PJA1-HEMA1ΔAPR1	Km/BASTA	*HEMA1*	For generation of transgenic lines
PJA1-HEMA1ΔAPR2	Km/BASTA	*HEMA1*	
PJA1-HEMA1ΔAPR1/2	Km/BASTA	*HEMA1*	
PJA1-HEMA1(V99P/V151P)	Km/BASTA	*HEMA1*	
PJA1-HEMA1(V99T/V151T)	Km/BASTA	*HEMA1*	
pSPYNE-cpSRP43	Km/Rif	*cpSRP43*	For BiFC experiments
pSPYNE-cpSRP54	Km/Rif	*cpSRP54*	

pSPYNE-GUN4	Km/Rif	*HEMA1*	
pSPYCE-GluTR	Km/Rif	*HEMA1*	
pSPYCE-CHLH	Km/Rif	*CHLH*	
pSPYCE-GUN4	Km/Rif	*GUN4*	
pSPYCE-CHLM	Km/Rif	*CHLM*	
pSPYCE-PORA	Km/Rif	*PORA*	
pSPYCE-PORB	Km/Rif	*PORB*	
pSPYCE-PORC	Km/Rif	*PORC*	
pSPYCE-CPP1	Km/Rif	*CPP1*	
pGL1-cpSRP43(SBD)	Ap/BASTA	*cpSRP43*	For generation of *cpSRP43(SBD)-OX*

2.4.6 Isolation of RNA from leaf tissue

The isolation of RNA from leaf tissue of Arabidopsis leaves was carried out according to the protocol (Oñate-Sánchez and Vicente-Carbajosa, 2008). For this purpose, 50-100 mg of leaf material was homogenized in a vibrating mill in liquid nitrogen. After adding 300 µl lysis buffer (2% SDS, 68 mM sodium citrate, 132 mM citric acid, 1 mM EDTA), the homogenate was mixed and incubated at RT until thawed completely. After centrifugation of 14,000 *g* at RT for 10 min, the suspension was transferred to a new tube and then treated with 100 µl protein-DNA precipitation buffer (4 M NaCl, 16 mM sodium citrate, 32 mM citric acid) and incubated in ice for 10 min. After subsequent centrifugation (10 min, 4 °C, 14,000 *g*), the supernatant was transferred to a new reaction tube and centrifuged again. 300 µl of the supernatant was mixed with 300 µl isopropanol, and the RNA was precipitated for 10 min (4 °C, 14,000 *g*). The RNA pellet was washed with 500 µl of 70% ethanol (v/v), centrifuged, dried at RT, and dissolved in 25-30 µl ddH_2O. The RNA solution was warmed for 10 min at 65 °C in the heating block and then centrifuged for 5 min (4 °C, 14,000 *g*). The RNA concentration was determined on the Nano-Drop (Thermo Scientific).

2.4.7 RNA qualification and DNaseI treatment

As a rule, 2 µg RNA was diluted in 8 µl ddH_2O. 4 µl of the RNA dilution was mixed with 4 µl

of 2x RNA loading buffer and placed on a 1.2 % agarose gel in 0.5x TBE (5xTBE (1 l): 54 g Tris-HCl, 27.5 boric acids, 20 ml of 0.5 M EDTA, pH 8.0) separated at 80 V. After qualitative and quantitative control of the isolated RNA on a UV table, the remaining RNA solution (4 µl) was mixed with 0.5 µl 10x DNase buffer and 0.5 µl DNase I (Table 2.10) and incubated at 37 °C for 30 min. Then 0.5 µl of 50 mM EDTA was added, and DNase I was inactivated for 10 min at 65 °C. According to the following section, the RNA was reversely transcribed into cDNA (Table 2.11). All incubations steps were carried out according to the protocol from Table 2.12 in a thermal cycler.

Table 2.10 DNase I digestion

Composition	Volume (µl)
Extracted RNA (1-2 µg)	4
10× DNase buffer	0.5
DNase I	0.5
EDTA (50 mM)	0.5

2.4.8 cDNA synthesis

The reverse transcription of the RNA into cDNA was carried out by means of reverse transcriptase using oligo-dT (18) primers. The composition of the reaction mixture is shown in Table 2.11. The thermal cycler program used is shown in Table 2.12. Following the reverse transcription, the cDNA was diluted 1: 5 with ddH_2O.

Table 2.11 Reverse transcription

Composition	Volume (µl)
DNase treated RNA	5.5
oligo-dT primer (100 µM)	0.5
5x RT buffer	2
10 mM dNTPs	1

RiboLock RNase-Inhibitor	0.25
Reverse Transcriptase RevAid	0.5
dd H_2O	0.25

Table 2.12 Thermo-cycler program for cDNA synthesis

Step	Temperature (°C)	Time (min)
	37	pause
DNase I treatment	37	30
	37	pause
Inactivation of DNase I	65	10
	42	pause
Reverse transcription	42	60
	70	10
Inactivation RT	4	pause

2.4.9 Quantitative PCR

The gene expression was analyzed using quantitative PCR (qPCR) in a CFX96-C1000 (Bio-Rad) thermal cycler in 96-well plates. The amplification of the target cDNA was monitored using SYBR green, which is embedded into DNA double strands. The composition of a qPCR reaction is shown in Table 2.13, and the thermal cycler program used is shown in Table 2.14. The primer pairs used to analyze the gene expression are listed in Appendix I. The gene expression was evaluated with the CFX-Manager software 1.6 (Bio-Rad) and the method implemented in it for the relative quantification of gene expression using the ΔΔC (t) method (Pfaffl, 2001). The relative expression of the target gene in a sample "X" (e.g., mutant) is then related to the relative expression of the target gene in a control sample (e.g., wild type)

(ΔΔC (t)).

Table 2.13 Composition of a qPCR reaction mixture

Composition	Volume (µl)
cDNA	1
ddH_2O	1.7
10 µM forward primer	0.15
10 µM reverse primer	0.15
2× SYBR green Mix	3

Table 2.14 Running program for quantitative PCR

Step	Temperature (°C)	Time (s)
1	95	30
2	95	10
3	60	30
Cycles (Step 1-3): 40x		
4	95	15
Melting curve	60-95	5 s/ 0.5 °C

2.5 Expression and purification of recombinant protein in *E. coli*

2.5.1 Expression of recombinant proteins

The expression of recombinant proteins took place in strains of *E. coli*. The most important modifications in the derivatives of the DE3 strain are the deletion of protease genes *LON* (*lon*-) and *OMP-T* (*omp-t*-) protease, which can degrade heterologous proteins due to their proteolytic

activity. Since the eu- and prokaryotic translations have different codon preferences, the Rosetta strain was constructed for expressing tRNA that is rarely used in *E. coli*. The expression protocol can be summarized: An expression strain was inoculated 1:500 (v/v) to a larger volume of 2× YT medium. The culture was then incubated in a shaker (250 rpm) at 37 °C until an OD_{600} of 0.8-1.0 (usually 2.5-3 h) was reached. The transgene expression was then induced by adding isopropyl-β-D-thiogalactopyranoside (IPTG, usually 1 mM). This lactose analog induces the lactose operon (lac operon) by binding the lac repressor, which is inactivated and can no longer bind to promoters. As a result, transcriptional factors and RNA polymerases can bind to the promoter region, and the corresponding mRNA is transcribed, then the recombinant protein is translated. After adding the IPTG, the cultures were incubated at different times and temperatures. Then the cultures were harvested by centrifugation, and the cell pellets were stored at -20 °C. The expression conditions used in this work for the respective proteins are listed in Table 2.15.

Table 2.15 Expression conditions of recombinant proteins

Protein	Vector	Strain	Antibiotic	Induction temperature (°C)	Induction time
His-*At*GUN4	pQE-80L	Rosetta	Ap/ ChlorA	30	3 h
His-*Os*CHLH	pET-28a	Rosetta	Km/ ChlorA	18	Overnight
His-*Os*CHLD	pET-28a	Rosetta	Km/ ChlorA	18	Overnight
His-*Os*CHLI	pET-28a	BL21	Km	30	3-4 h
His-cpSRP43	pET-28a	PRIL	Km/ ChlorA	37	3-4 h
His-cpSRP43-SBD	pET-28a	PRIL	Km/ ChlorA	37	3-4 h
His-cpSRP43ΔSBD	pET-28a	PRIL	Km/ ChlorA	37	3-4 h
His-cpSRP43ΔCD2	pET-28a	PRIL	Km/ ChlorA	37	3-4 h
His-cpSRP43ΔCD3	pET-28a	PRIL	Km/ ChlorA	37	3-4 h

His-cpSRP54	pET-28a	Rosetta	Km/ ChlorA	37	3-4 h
His-cpSRP54M	pET-28a	Rosetta	Km/ ChlorA	37	3-4 h
His-PORA	pET-15b	PRIL	Ap/ ChlorA	22	3-4 h
His-PORB	pET-15b	PRIL	Ap/ ChlorA	22	3-4 h
His-PORC	pET-15b	PRIL	Ap/ ChlorA	22	3-4 h
His-GluTR	pQE-80L	BL21	Ap	18	Overnight
GST	pGEX-4T-1	PRIL	Ap/ ChlorA	37	3-4 h
GST-cpSRP43	pGEX-4T-1	PRIL	Ap/ ChlorA	37	3-4 h

2.5.2 Purification of recombinant proteins from *E. coli*

The protocol for the purification of the His-tagged recombinant proteins was essentially based on the information in the manual "The QIAexpressionist ™" (Qiagen). The bacterial pellet was resuspended with 10 ml lysis buffer (50 mM NaH_2PO_4, 300 mM NaCl, 10 mM imidazole, pH 8.0) in the first step. The suspension was then treated with ultrasonication (Sonoplus-Bandelin: 2 min,3 cycles, level 5, frequency 36%) and centrifuged for 30 min at maximum speed (4 °C). The supernatant was mixed with 0.25 ml Ni-NTA agarose and incubated on a rotary incubator for 1 h at 4 °C. An Amicon Ultra-4 Centrifugal Filter Unit (Merck- Millipore) filled with the suspension was opened, and the flow-through was collected. The matrix was washed with 4 ml washing buffer (50 mM NaH_2PO_4, 300 mM NaCl, 20 mM imidazole, pH 8.0) for 4 times, and then the bound proteins were eluted with 1 ml of elution buffer (50 mM NaH_2PO_4, 300 mM NaCl, 250 mM imidazole, pH 8.0) for 3 times. All steps were carried out on the ice. Since imidazole itself can negatively influence the stability and folding of proteins, it should be removed from the protein solution by suitable further processing (see following section 2.5.3).

The protocol for the purification of the GST tagged recombinant proteins was essentially based on the information in the manual "Glutathione Sepharose 4B" (GE Healthcare). In the first step, the bacterial pellet was resuspended with 10 ml binding buffer (140 mM NaCl, 2.7 mM KCl, 10 mM Na_2HPO_4, 1.8 mM KH_2PO_4, pH 7.3). The suspension was then treated with ultrasonication (Sonoplus-Bandelin: 2 min,3 cycles, level 5, frequency 36%) and centrifuged for 30 min at maximum speed (4 °C). The supernatant was mixed with 50 µl Glutathione Sepharose 4B agarose and incubated on a rotary incubator for 1 h at 4 °C. An Amicon Ultra-4

Centrifugal Filter Unit (Merck- Millipore) filled with the suspension was opened, and the flow-through was collected. The matrix was washed with 4 ml binding buffer 4 times, and then the bound proteins were eluted with 1 ml of elution buffer (50 mM Tris-HCl, 10 mM reduced glutathione, pH 8.0) for 3 times. All steps were carried out on the ice. Since reduced glutathione itself can negatively influence the stability and folding of proteins, it should be removed from the protein solution by suitable further processing (see following section 2.5.3).

2.5.3 Dialysis, concentration, buffer exchange, and storage

All the purified proteins in this work were concentrated after elution using centrifugation concentrators (Amicon® Ultra Centrifugal Filters, Merck Millipore). The eluate was concentrated to a small volume (~ 200 µl) and diluted with 4 ml PBS buffer (137 mM NaCl, 2.7 mM KCl, 10 mM Na_2HPO_4, 2 mM KH_2PO_4, pH 7.5). This step was repeated three times to dilute the imidazole or reduce glutathione about 1,000-fold. About 10% glycerol was added to the final protein, and aliquots were fast frozen in liquid nitrogen and stored in a -80 °C freezer. The qualitative and quantitative control of the recombinant proteins was carried out using SDS-PAGE after denatured at 95 °C for 5 min in an SDS loading buffer (50 mM Tris-HCl, 10% glycerol (v/v), 2% SDS (w/v), 100 mM DTT, 0.05% bromophenol blue (w/v), pH 6.8) (see chapter 2.6.3.1).

2.6 Analysis of protein extracts from plant

2.6.1 Protein extraction from leaf tissue

Whole 14- to 18-day-old rosette seedlings were harvested from each genotype from three to six individual plants. When plants had been grown under standard growth conditions or shortly after dark treatment, the freshly harvested leaves were ground in liquid nitrogen. Total leaf proteins were extracted from the powder using 2× Laemmli buffer (100 mM Tris-HCl, pH 6.8, 4% (w/v) SDS, 20% (v/v) glycerol, 200 mM DTT and 0.01% Bromophenol Blue) and incubated at 95 °C for 10 min. Protein concentrations were determined and are expressed relative to leaf FW (fresh weight). For the heat shock experiment, rosette leaves were harvested before or after heat treatment and ground in liquid nitrogen. Total leaf protein was extracted from the frozen plant material into PEB buffer (2% (w/v) SDS, 56 mM $NaCO_3$, 12% (w/v) sucrose, and 2 mM EDTA) by heating the samples for 20 min at 70 °C. Protein concentrations were determined using the Pierce BCA Protein Assay Kit (Thermo Fisher Scientific). All samples in PEB buffer were diluted to the same protein concentration, supplemented with 56 mM DTT, and incubated at 70 °C for 5 min.

2.6.2 Determination of the protein concentration

For proteins extracted with 2× Laemmli buffer, protein concentrations were determined relative to leaf FW. Protein concentrations were determined using the Pierce BCA Protein Assay Kit for proteins extracted with PEB buffer. For purified recombinant proteins in PBS buffer, the concentrations were determined by Bradford reagent and SDS-PAGE.

2.6.2.1 Determination of the protein concentration with Bradford reagent

The SDS- and DTT-free protein extract was mixed with 1 ml Bradford reagent (100 mg Coomassie Blue G-250 dissolved in 50 ml 95% ethanol (v/v) and 100 ml of 85% H_3PO_4 (w/v), added ddH_2O to 1 l, filtered), incubated for 5 min at RT and then measured the absorption at 595 nm.

2.6.2.2 Determination of the protein concentration with BCA reagent

The protein content was determined using a BCA reagent (Thermo Scientific) following the User Guide: Pierce BCA Protein Assay Kit. The absorption of the color complex was determined at 562 nm.

2.6.2.3 Determination of the protein concentration with SDS-PAGE

The examined protein and different concentrations of standard BSA protein were loaded on the SDS-PAGE. After the Coomassie brilliant blue (CBB) staining of the gel, the Image J software (NIH) was applied to analyze the intensity of the protein blots. BSA protein concentrations are plotted on the standard curve against the intensity of blots then the concentration of examined protein can be calculated according to the standard curve.

2.6.3 Western blot analyses

2.6.3.1 SDS polyacrylamide gel electrophoresis (SDS-PAGE)

Denatured protein samples were separated electrophoretically on a polyacrylamide gel (10% or 12% separating gel and 5% stacking gel, Table 2.16). In the case of vegetable protein extracts, 10-20 µg total protein was applied per lane. The electrophoretic separation took place in an electrophoresis chamber filled with 1× running buffer (25 mM Tris, 192 mM glycine, 0.1% SDS (w/v)). A voltage of 80 V was initially applied, followed by a 120-140 V voltage for the subsequent separation.

Table 2.16 Recipe for SDS-PAGE gel

Solution	Separation gel (ml)		Stacking gel (ml)
	10% (5 ml)	12% (5 ml)	5% (2 ml)
ddH_2O	1.9	1.6	1.4
30% Acrylamide (29:1)	1.7	2	0.33
1.5 M Tris-HCl pH 8.8	1.3	1.3	-

0.5 M Tris-HCl pH 6.8	-	-	0.25
10% SDS	0.05	0.05	0.02
10% APS	0.05	0.05	0.02
TEMED	0.002	0.002	0.002

2.6.3.2 Protein blot transfer

After the proteins had been separated in the polyacrylamide gel, the gels were transferred to a Semi-dry blotting apparatus (Bio-Rad). The membrane and filter papers were pre-wetted in transfer buffer (20% methanol (v/v), 25mM Tris, 92 mM glycine) for 5 min. The structure for transfer consisted of (from bottom to top): 3x filter paper, 1x Nitrocellulose membrane (GE Healthcare), polyacrylamide gel, and 3x filter paper. The protein transfer took place with 50 mA per gel area in the transfer buffer. After 1.5 h, the membrane was stained in Ponceau solution (0.1% Ponceau S (w/v), 5% acetic acid (v/v)) and then decolored with water.

2.6.3.3 Immunoblotting assay

The detection of specific proteins in a protein extract was carried out using antibody detection. Initially, the unspecific proteins were blocked in 4% milk in TBS (20 mM Tris-HCl, 150 mM NaCl, pH 7.4) at RT for one hour. The membranes were then washed 1x for 5 min with TBST (20 mM Tris-HCl, 150 mM NaCl, 0.1% (v/v) Tween-20, pH 7.4) and then 2x for 5 min with TBS. The incubation with the primary antibody specific for the target protein (Table 2.17) (2% milk in TBS) was carried out for 2 h at RT or overnight at 4 °C. The membranes were then rewashed (1x for 5 min with TBST and then 2x for 5 min with TBS) and incubated with the secondary antibody specific for the primary antibody (IgG, peroxidase coupled, 2% milk in TBS). After washing again (1x for 5 min TBST, 4x for 5 min TBS), the membranes were incubated with the ClarityTM Western ECL Blotting Substrate (Bio-Rad), and Immunoblotting signals were detected with the ChemoStar Touch Imager (v.0.5.61, Intas Biopharmaceuticals).

Table 2.17 Antibodies used in this study

Antibodies	Description	Dilution	Source
α-GluTR	Rabbit IgG against *At*GluTR1	1:1,000	(Hedtke et al., 2007)
α-GSAT	Rabbit IgG against *At*GSAT	1:2,000	(Grimm et al., 1989)
α-GUN4	Rabbit IgG against *At*GUN4	1:2,000	(Peter and Grimm, 2009)

α-PORB	Rabbit IgG against *At*PORB	1:1,000	this lab
α-PORC	Rabbit IgG against *At*PORC	1:1,000	
α-CHLM	Rabbit IgG against *At*CHLM	1:500	(Richter et al., 2016)
α-POR	Rabbit IgG against *At*PORA/B	1:5,000	Agrisera
α-CHL27	Rabbit IgG against *At*CHL27	1:1,000	Agrisera
α-LHCa1	Rabbit IgG against *At*LHCa1	1:2,500	Agrisera
α-LHCb1	Rabbit IgG against *At*LHCb1	1:2,500	Agrisera
α-cpSRP43	Rabbit IgG against *At*cpSRP43	1:2,500	(Schünemann et al., 1998)
α-cpSRP54	Rabbit IgG against AtcpSRP54	1:2,500	(Schünemann et al., 1998)
α-CHLH	Rabbit IgG against *At*CHLH	1:1,000	D.-P. Zhang (Tsinghua University)
α-CHLI	Rabbit IgG against *pea*GSAT	1:5,000	From Meizhong Luo's lab (Zhou et al., 2012)
α-6xHIS	Mouse IgG coupled to peroxidase against 6x histidine polypeptide	1:2-4,000	Sigma
α-GST	Mouse IgG coupled to peroxidase against GST tag	1:1,000	Sigma
α-GFP	Mouse IgG coupled to peroxidase directed against Green Fluorescence Protein	1:2,000	Sigma
α- mouse	-	1:5,000	Agrisera
α- rabbit	-	1:5,000	Agrisera

2.7 Blue native polyacrylamide gel electrophoresis (BN-PAGE)

Blue native PAGE (BN-PAGE) was used to study the protein complexes in the chloroplast. Here, 4-12.5% gradient gels were used, and the composition of the solutions required for this is listed in Table 2.15. Intact chloroplast with Chl content of 1 µg/µl was suspended in BTHG buffer (25 mM BisTris-HCl pH 7.0, 30 % Glycerin (v/v)). To solubilize the thylakoid membrane-associated proteins, 0.8% n-dodecyl-β-D-maltopyranoside (DDM) was added and incubated on ice for 10 min. After the undissolved membrane fraction had been removed by centrifugation (10 min, 14,000 *g*, 4 °C.), 0.1 volume of 10× BN buffer (100 mM BisTris-HCl, 0.5 M 6-aminocaproic acid, 30% glycerin, 0.05% Coomassie Brilliant Blue G250, pH 7.0) was added to the supernatant and loaded onto the gradient gel. The 1x cathode buffer (10x cathode buffer: 0.5 M Tricine, 150 mM BisTris-HCl, pH 7.0) and the 1x anode buffer (5x anode buffer: 0.25 M BisTris-HCl, pH 7.0) were used for running this electrophoresis. At the beginning of the electrophoresis, a cathode buffer with 0.01% Coomassie Blue G250 was used, which was exchanged for a cathode buffer without Coomassie Blue G250 about halfway through the electrophoresis. To separate the complexes, the initial voltage of 50 V was increased by 25 V every 30 min until a maximum voltage of 200 V was reached. The photosynthetic complexes were separated at 200 V until the migration front reached the bottom of the gel. The banding pattern was then recorded photographically. If the protein complexes were also to be separated in the second dimension, the gel was incubated in 1x SDS sample buffer (50 mM Tris-HCl pH 6.8, 10% (v/v) glycerin, 2% (w/v) SDS, 50 mM DTT, 0.002% bromophenol blue) for 30 min and then loaded onto a 12% SDS gel. The second dimension was separated as usual (chapter 2.6.3.1).

Table 2.18 Composition of the solutions for 4-12.5% gradient gel

Solution	Separation gel (ml)		Stacking gel (ml)
	4%	12.5%	4%
ddH_2O	1.257	0.125	1.72
40% Acrylamide	0.25	0.781	0.3
3x Gel buffer	0.833	0.833	1
75% Glycerol	0.15	0.75	-
10% APS	0.0075	0.0075	0.016
TEMED	0.003	0.003	0.006

3x Gel buffer: 150 mM BisTris-HCl, 1.5 M 6-aminocaproic acid, pH 7.0

2.8 Extraction and analysis of intermediates and end products of TBS

2.8.1 Extraction

The intermediates ProtoIX, MgP, MgMME, Pchlide, Chlide, and end products Chl *a*, Chl *b*, and heme of TBS were isolated sequentially from a sample. About 50-100 mg of plant material was harvested, ground in a steel ball mill (Retsch mill, 1.5 min, 27 Hz) in liquid nitrogen, and directly weighted to determine the FW. For deciding the DW (dry weight), samples were lyophilized overnight (at least 12 h) and then weighted with a balance (Sartorius).

TBS intermediates and end-products were extracted from frozen or lyophilized leaf powders in 400 µl cold alkaline acetone (acetone: 0.2 M NH_4OH, 9:1, v/v) at -20 °C for at least 1 h, vortex three times during the extraction. After centrifugation (14,000 *g*, 20 min, 4 °C), the supernatant was subjected to HPLC. After removing the supernatant, non-covalently bound heme was extracted from the pellet using AHD buffer (acetone: hydrochloric acid: dimethylsulfoxide, 10:0.5:2, v/v/v) for at least 20 min at RT and then centrifuged at 14,000 *g* for 20 min at RT. The supernatant obtained was then subjected to HPLC analyses.

2.8.2 HPLC analyses

As part of this work, many intermediates and end products of the tetrapyrrole metabolic pathway were analyzed using HPLC, which was conducted using the Agilent 1100 or 1290 HPLC system equipped with a diode array and fluorescence detectors (Agilent Technologies). The Agilent ChemStation for liquid chromatography system (product no. G2170BA) was used in the HPLC analyses. The HPLC programs and parameters specific to each molecule are shown in Appendix II for clarity.

2.8.3 Measurement of Chl *a*/*b* by spectrophotometer

As an alternative to HPLC, Chl content was determined using a spectrophotometer. For this purpose, the pigments were isolated with alkaline acetone (acetone: 0.2 M NH_4OH, 9:1, v/v) from plant material or chloroplast or thylakoid preparations. The determination was carried out according to (Lightenthaler, 1987). Table 2.19 shows the calculation formula.

Table 2.19 Spectrophotometric determination of Chl.

Pigments	Formula for calculation (µg/ ml)
Chl *a*	12.25 x ($A663_{nm}$ - $A720_{nm}$) - 2.79 x ($A646_{nm}$ - $A720_{nm}$)

Chl *b*	21.50 x ($A646_{nm}$ - $A720_{nm}$) - 5.10 x ($A663_{nm}$ - $A720_{nm}$)

2.9 Chloroplast isolation

Arabidopsis plants were grown on soil for a short day at 100 µmol photons m^{-2} s^{-1} for four weeks to isolate intact chloroplasts. Plants of a dish were mixed with 500 ml homogenization buffer (450 mM sorbitol, 20 mM tricine, 10 mM EDTA, 10 mM $NaHCO_3$, 0.1% BSA (w/v), pH 8.4 with KOH) in a modified Waring Blender (2x 4s lowest level). The homogenate was filtered through a layer of Miracloth (Merck) into a centrifuge beaker, and the chloroplasts were pelleted at 500 g for 8 min at 4 °C (acceleration: maximum, brake: maximum). The pellet was taken up in 1-2 ml 1x resuspension buffer (RB buffer: 300 mM sorbitol, 20 mM tricine, 2.5 mM EDTA, 5 mM $MgCl_2$, pH 8.4 with KOH) and placed on a Percoll with a cut tip. The step gradient consisted of a pillow of 13 ml 80% Percoll (v/v) (for 30 ml: 24 ml Percoll, 6 ml 5x RB), which was filled with 12 ml 40% Percoll (v/v) (for 30 ml: 12 ml Percoll, 6 ml 5x RB, 12 ml H_2O). The loaded gradient was centrifuged for 30 min at 6,500 *g* in a swingout rotor at 4 °C. (acceleration: minimum and no brake). After centrifugation, the chloroplasts collected at the interface between 80% and 40% Percoll, while the thylakoids/ defective chloroplasts could not penetrate the gradient. The band of thylakoids was discarded, the intact chloroplasts were transferred to 20 ml 1x RB, carefully swirled, and then centrifuged again (6 min, 3,800 *g*, swing-out rotor, 4 °C, acceleration: minimum, no brake). After centrifugation, the supernatant was discarded, and the chloroplast pellet was taken up in 500-1000 µl 1x RB. Alternatively, the chloroplasts were lysed in RB buffer without sorbitol or taken up in a buffer specific for the subsequent experiment. All work was carried out quickly in the cold room or on ice.

2.10 Protein-protein interaction studies

2.10.1 Microscale thermophoresis (MST)

All MST reagents and consumables were purchased from NanoTemper Technologies. His-GUN4 and His-GluTR were labeled using the Protein Labeling Kit RED-NHS. The labeling reaction was performed according to the manufacturer's instructions in the supplied labeling buffer by applying a concentration of 20 µM protein (ratio of molar dye to protein, ~3:1) at 4 °C for 30 min. Unreacted dye was removed with the supplied dye removal column equilibrated with PBS buffer (137 mM NaCl, 2.7 mM KCl, 10 mM Na_2HPO_4, and 2 mM KH_2PO_4, pH 7.5).

The degree of labeling was determined using UV spectrophotometry at 650 nm and 280 nm and was typically 0.75. The labeled His-GUN4 was adjusted to 40 nM with MST buffer (50 mM Tris-HCl, pH 7.8, 150 mM NaCl, and 10 mM $MgCl_2$) supplemented with 0.05% Tween 20. The ligand-protein cpSRP43 and its truncated proteins were dissolved in PBS buffer, and a series of 16 1:1dilutions was prepared using the same buffer, producing ligand concentrations ranging from 6.1 nM to 200 µM. For the measurement, each ligand dilution was mixed with one volume of labeled His-GUN4, which led to a final concentration of His-GUN4 of 20 nM and final ligand concentrations ranging from 3.05 nM to 100 µM. After 10 min of incubation followed by

centrifugation at 14,000 *g* for 5 min at 4 °C, the samples were loaded into Premium Monolith NT.115 Capillaries. MST was measured using a Monolith NT.115 instrument (NanoTemper Technologies) at a constant temperature of 30 °C. The instrument parameters were adjusted to 60% LED power and medium MST power. Data from three independently pipetted measurements were analyzed (MO. AffinityAnalysis software v.2.1.3, NanoTemper Technologies) using the signal from an MST-on time of 2.5 s. Plot fitting and Kd estimation were achieved using nonlinear regression analysis in GraphPad Prism v.9.1.2 (226). Specifically, the equation Biphasic, X is log (concentration) was used to fit cpSRP43-FL and SBD+CD3, and the equation Agonist versus response (three parameters) was used for the fitting of the other truncated cpSRP43 proteins.

2.10.2 In vitro and in vitro pull-down assays

In vitro GST pull-down analysis was performed as described previously (Wang et al., 2018) with the following modifications. Purified recombinant GST and GST-cpSRP43 were used as baits and incubated with purified His-GUN4 or His-CHLH at 4 °C overnight in a binding buffer (25 mM Tris-HCl, pH 7.8, 150 mM NaCl, 5 mM $MgCl_2$, 10% (v/v) glycerol and the cOmplete protease inhibitor cocktail). A 10 µl aliquot of an equilibrated 50% (v/v) slurry of Glutathione 4B Agarose (GE Healthcare) was added to each tube and incubated for 1 h at 80 rpm at 4 °C. The agarose was collected by centrifugation (2,800 *g*, 30 s, 4 °C) and washed three or four times with a binding buffer. The proteins bound to GST-cpSRP43 or GST were eluted with a binding buffer containing 10 mM reduced glutathione, denatured in 2× Laemmli buffer, and finally subjected to SDS-PAGE immunoblot analyses.

For in vitro His pull-down analysis, purified His-GluTR, His-CHLH, and His-GUN4 proteins were used as baits and first incubated with 50 µl of an equilibrated 50% (v/v) slurry of Ni-NTA in the binding buffer (300 mM NaCl, 2.7 mM KCl, 10 mM Na_2HPO_4, 1.8 mM KH_2PO_4, 20 mM imidazole and 2 mM DTT, pH 7.3) for 1 h at 80 rpm at 4 °C. Then, the purified GST or GST-cpSRP43 was added and incubated at 15 °C or 30 °C for 1 h. The Ni-NTA agarose was collected by centrifugation (2,800 *g*, 30 s, 4 °C) and washed three or four times using wash buffer (50 mM NaH_2PO_4, 20 mM imidazole, and 300 mM NaCl, pH 8.0). Finally, His-tagged proteins and their potential interaction proteins were eluted with elution buffer (50 mM NaH_2PO_4, 250 mM imidazole, and 300 mM NaCl, pH 8.0). The eluted proteins were denatured in 2× Laemmli buffer and separated on a 12% SDS-PAGE gel. The proteins bound to His-tagged GluTR, CHLH, and GUN4 were analyzed by immunoblotting using the indicated antibodies.

In vivo, His pull-down analysis was performed as described previously (Wang et al., 2018) with the following modifications. Purified His-cpSRP43 protein (50 µg) was used as bait and incubated with total chloroplast extracts (100 µg of Chl), which had been solubilized with 1% (w/v) DDM in binding buffer (25 mM Tris-HCl, pH 7.8, 150 mM NaCl, 5 mM $MgCl_2$, 10% glycerol (v/v), cOmplete protease inhibitor) overnight at 4 °C. Solubilized total chloroplast extracts that had not been incubated with His-cpSRP43 were used as a negative control. An aliquot (50 µl) of an equilibrated 50% (v/v) slurry of Ni-NTA agarose (ThermoFisher

Scientific) was then added to each tube and incubated for 1 h at 80 rpm at 4 °C. All subsequent steps were carried out as described above.

2.10.3 BiFC assay

cDNA fragments encoding full-length cpSRP43 or GUN4 were cloned into the *pSPYNE* vector (fusing them to the N-terminal half of YFP, YFPn), whereas the full-length coding sequences of *CHLH*, *GUN4,* and *CHLM* were cloned into *pSPYCE* (fusing them to the C-terminal half of YFP, YFPc). The BiFC constructs were transiently transformed into the abaxial epidermal cells of *N. benthamiana* leaves using *Agrobacterium tumefaciens* strain GV2260. After three days in darkness, the infiltrated leaf areas were analyzed for YFP fluorescence with an LSM 800 confocal microscope (Carl Zeiss). YFP signals were detected at excitation/emission (ex/em) 514/530-555 nm, while Chl fluorescence was visualized at ex/em 514/600-700 nm. Fluorescent signals were captured by using the Leica Application Suite AF (v.2.7.9723.3).

2.10.4 Co-Immunoprecipitation of cpSRP43 from plant extracts

Intact chloroplasts (100 µg of Chl) isolated from wild type (Ler-0) or transgenic plants expressing cpSRP43-FLAG, cpSRP43ΔCD2-FLAG, or cpSRP43ΔCD3-FLAG were solubilized in binding buffer (25 mM Tris-HCl, pH 7.8, 150 mM NaCl, 5 mM $MgCl_2$, 10% (v/v) glycerol and cOmplete protease inhibitor cocktail). The Chl concentrations of the extracted chloroplasts were adjusted to 1-1.2 µg/µl. The thylakoids were then solubilized with 1% (w/v) DDM in a binding buffer for 10 min on ice. After centrifugation (14,000 *g*, 10 min, 4 °C), the supernatant was incubated at room temperature for 2 h with 10 µl of anti-FLAG affinity gel (Biotool). When analyzed the protein binding affinity after heat treatment, the incubation was performed at 4 °C for 1 h. The agarose beads were then pelleted by centrifugation (2,800 *g*, 30 s, 4 °C) and washed four times to remove non-specifically bound proteins. Finally, cpSRP43, cpSRP43ΔCD2, or cpSRP43ΔCD3-FLAG and their interaction partners were eluted from the agarose beads with 2× Laemmli buffer and subjected to SDS-PAGE and immunoblot analyses.

2.11 Enzyme activity assays

2.11.1 Measurement of ALA synthesis capacity

To determine ALA synthesis rates in seedlings of the various lines of interest, whole rosette leaves were excised from 18-day-old plants, weighed to determine FW, and incubated in 5 ml of 50 mM Tris-HCl (pH 7.2) containing 40 mM levulinic acid (Sigma-Aldrich) for 3 h under standard growth conditions. The leaf materials were then frozen and homogenized in liquid nitrogen before resuspension in 0.5 ml of 20 mM potassium phosphate buffer (pH 7.2). After centrifugation at 14,000 *g* for 5 min at 4 °C, 0.4 ml of the homogenate was mixed with 0.1 ml of ethyl acetoacetate (Sigma-Aldrich) and boiled for 10 min. The chilled samples were then mixed with 0.5 ml of Ehrlich's reagent (373 ml of acetic acid, 90 ml of 70% (v/v) perchloric acid, 1.55 g of $HgCl_2$, 9.10 g of 4-dimethylamino benzaldehyde and 500 ml of ddH_2O) and centrifuged at 14,000 *g* for 5 min at 4 °C. The absorption of the ALA pyrrole was measured at 525, 553, and 600 nm. The ALA content was calculated using a standard dilution curve of

authentic ALA solutions (Sigma-Aldrich) and normalized to the incubation time and FW of leaf material used.

2.11.2 MgCh activity assay

The MgCh assay was performed as described previously (Zhou et al., 2012) using 150 µl of a mixture containing 2.5 µM CHLH, 1 µM CHLD, 1 µM CHLI, and 2.5 µM GUN4 in assay buffer (50 mM Tricine-KOH, pH 8.0, 15 mM $MgCl_2$, 0.2 mM DTT, 1 mM ATP, and 10 µM Proto). His-tagged cpSRP43, cpSRP43ΔSBD, CHLH, GUN4, and Proto in MgCh assay buffer (overall 100 µl) were pre-incubated in darkness for 30 min on ice, while CHLD and CHLI were separately pre-incubated in 50 µl of MgCh assay buffer. The two mixtures were then warmed for 5 min at 30 °C and combined in the 96-well plate to start the assay. MgP formation was continuously monitored by spectrofluorometry using a 96-well plate reader mounted on a Hitachi F7000 fluorescence photometer. Excitation and emission wavelengths were set to 416 nm and 595 nm, respectively, with slit widths of 5 nm (ex) and 10 nm (em). The delay time for each scan was 5 min, and the whole scan time was indicated in the figure legend. The absolute amounts of MgP formed were calculated from a standard curve. A 30 µl sample of the reaction solution was boiled in 2× Laemmli buffer (100 mM Tris-HCl, pH 6.8, 4% SDS, 20% glycerol, 200 mM DTT, and 0.01% Bromophenol Blue) and applied to a 12% SDS-PAGE to determine the protein levels at the end of the reaction.

2.11.3 POR activity assay at room temperature

2.11.3.1 Pchlide extraction for POR activity assay

The barley seeds were sown on GS-90 medium with some water. Then they were transferred to a cold room for 2 daysand then exposed to light for 2 h. Put in a dark room for about 6 daysafterward, cut and collected the seedlings, and put them on a plate. Feed the seedlings with 1 mM ALA (pH 7.5) in the darkness overnight. Ground the seedlings in liquid nitrogen with mortar. When it became powder, 25 ml extraction buffer (Acetone: 0.1 N NH_4OH (9:1)) was added and then transferred to a 50 ml falcon tube. 8,000 *g*, 4 °C, 5 min centrifugation before transferring the supernatant to a new tube. Then washed the supernatant with 1:1 n-Hexane. The below fraction (light green) should be kept and repeated to be washed 2 times. The final below fraction was kept as the Pchlide and the concentration of Pchlide was determined by HPLC.

2.11.3.2 POR activity assay

POR activity was examined at ambient temperature in PBS buffer containing 5mM DTT, 0.05 mM NADPH. The reaction was performed in a fluorescence cuvette (1×1 cm cuvette, for a sample volume of 2 ml) placed in the fluorometer's sample holder (Perkin Elmer LS-50B). Fluorescence emission spectra were usually recorded from 600 nm to 720 nm with a 240 mm/ min scanning speed. The excitation wavelength was 440 nm. Excitation and emission slits were 5 nm. The first two emission spectrums were recorded immediately after the mixture of Pchlide (about 2 µM) and NADPH. POR activity was measured as soon as possible after adding 0.05

μM POR. The spectral curves were automatically collected one after another for several min, with stirring of the sample. The fluorescence intensity at 680 nm indicates the concentration of product Chlide.

2.12 Measurement of Chaperone Activity

To investigate cpSRP43 and cpSRP54's chaperone activity towards PORB, 2 μM His-PORB was incubated in PBS buffer at 42 °C with various concentrations of cpSRP43, cpSRP54M and cpSRP43ΔSBD. Aggregation of His-PORB (2 μM) in response to 5-10 mM H_2O_2 was examined for 20 min at 30 °C with different amounts of cpSRP43 and cpSRP54M. Aggregation of His-PORB induced by heat or H_2O_2 was determined by monitoring the turbidity arising (A_{340nm}) at 2-min intervals by using a temperature-controlled spectrophotometer (SPECTRA max M2; Molecular Devices). To investigate the consequence of aggregation caused by point mutation, 2 μM His-GluTR and His-GluTR (V99T/V151T) in PBS buffer were subjected to a 42 °C heat treatment. The heat-induced aggregation of GluTR was also determined by monitoring the turbidity arising (A_{340nm}) at 2-min intervals.

2.13 Rapid separation of soluble and membrane-bound proteins

Leaf material (20 mg) was harvested and homogenized in liquid nitrogen. Samples were dissolved in 200 μl PBS buffer (20 mM sodium phosphate buffer and 150 mM NaCl, pH 7.4). Then, 120 μl of the remaining sample was centrifuged at 14,000 *g* for 30 min. One volume of the supernatant was added to 1 volume of 4x Laemmli buffer and served as the soluble fraction. Pellets (membrane fraction) were dissolved in 120 μl PBS buffer and added to 120 μl 4×Laemmli buffer. Equal volumes of each extract were loaded on a 12% SDS-polyacrylamide gel. Proteins were separated and analyzed by immunoblotting.

2.14 Image processing and graphic evaluation

Image files (Western blots, protein gels, photographs, etc.) were processed with Photoshop CS3 (Adobe) and Inkscape (https://inkscape.org/). Blot signals of proteins were quantified densitometrically with the Image J software (NIH). Graph Pad Prism 8.0 (www.graphpad.com) showed the graphical representation of measurement results. The protein's crystal structure was analyzed with pyMOL (Educational edition).

3 Results

3.1 Chloroplast SRP43 autonomously protects Chl biosynthesis proteins against heat shock

3.1.1 cpSRP43 deficiency impairs the metabolic flow of Chl biosynthesis

To identify TBS clients for cpSRP43, the metabolic flow through the TBS pathway was re-examined in seedlings of wild type (Landsberg erecta, Ler-0), *cpSRP43* knockout mutant (*chaos*) (Klimyuk et al., 1999), and *cpSRP43-OX* (constitutive expression of *cpSRP43* driven by the CaMV 35S promoter in the background of *chaos*). The *chaos* mutant showed a retarded growth and pale-green leaf phenotype, fully recovered by overexpressing *cpSRP43* (Figure 3.1A). The ALA synthesis rate in *chaos* was strongly reduced and correlated with reduced Chl levels (Figure 3.1B-C). In contrast, the amount of non-covalently bound heme was not altered in *chaos* and *cpSRP43-OX* compared to wild-type seedlings (Figure 3.1D). These results strongly suggest that cpSRP43 is specifically required for Chl synthesis. Consistent with the lower ALA synthesis rate and Chl levels in *chaos*, the levels of the Chl precursors Proto IX, MgP, MgPMME, and Pchlide were also drastically decreased in *chaos* (Figure 3.1E). The decreased ALA synthesis capacity and lower levels of Chl precursors in *chaos* were rescued by constitutive expression of *cpSRP43*, pointing to a specific requirement for cpSRP43 to maintain efficient Chl synthesis.

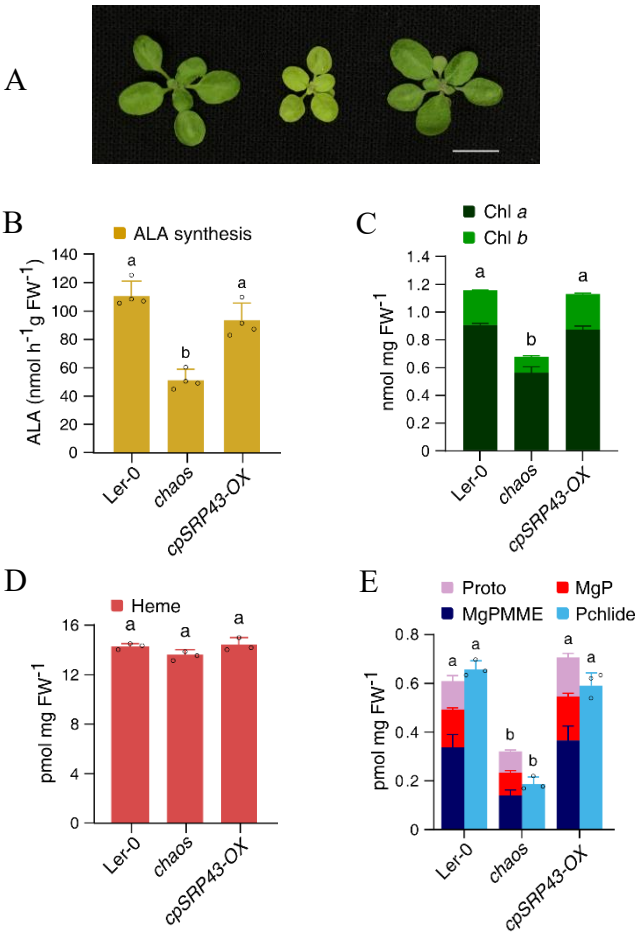

Figure 3.1 cpSRP43 is required to maintain efficient Chl synthesis. A, A representative image of 18-day-old *chaos*, *cpSRP43-OX*, and wild-type (Ler-0) plants grown under standard conditions (16 h light/8 h dark, 100 µmol photons m^{-2} s^{-1}). Scale bar, 1 cm. **B-E**, ALA synthesis rates (**B**) and levels of Chl *a*/*b* (**C**), Heme (**D**), and TBS metabolic intermediates ProtoIX, MgP, MgMME, Pchlide (**E**) in 18-day-old Ler-0, *chaos* and *cpSRP43-OX* grown under standard conditions. FW, fresh weight. All values are plotted as means ± s.d. ($n = 4$ independent samples for ALA synthesis rate and $n = 3$ independent samples for the others). The small open circles represent the individual data points. The letters above the histograms indicate significant differences, as determined by one-way analysis of variance (ANOVA) with Tukey's test ($P < 0.05$).

3.1.2 cpSRP43 deficiency reduces steady-state levels of GluTR, CHLH and GUN4

The steady-state levels of TBS proteins in *chaos* were compared with those in *cpSRP43-OX* and Ler-0 (Figure 3.2A). In agreement with previous observations, amounts of GluTR were reduced by approximately 25% in *chaos*, while levels of MgP methyltransferase (CHLM) and MgPMME oxidative cyclase (CHL27) were unaltered (Wang et al., 2018). Similar to GluTR, the steady-state levels of CHLH and GUN4 were significantly decreased in *chaos* compared with Ler-0 and were restored to wild-type levels in *cpSRP43-OX*. Although the contents of GluTR, CHLH, and GUN4 were slightly reduced in *chaos* compared to wild type, these data were statistically and significantly different (Figure 3.2B). The positions of GluTR, CHLH, and GUN4 in the TBS pathway were indicated in the scheme (Figure 3.2C). Taken together, cpSRP43 contributes to the control of the TBS pathway by regulating the stability of two key enzymes, GluTR and MgCh, in the TBS pathway.

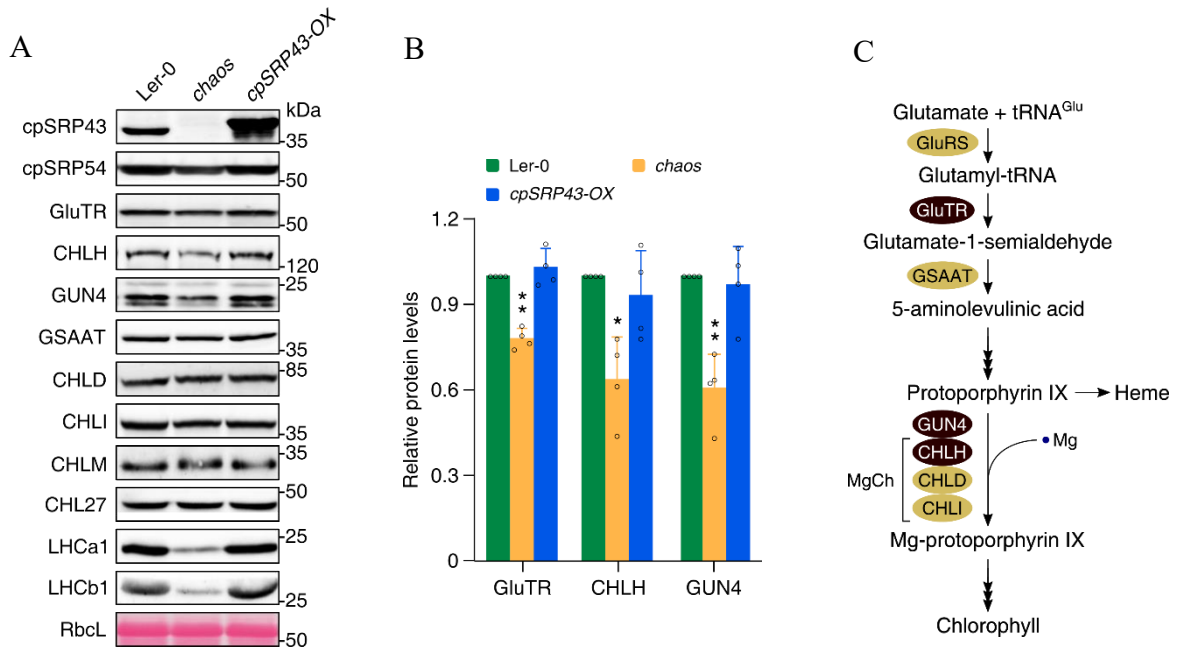

Figure 3.2 Steady-state levels of GluTR, CHLH and GUN4 in Ler-0, *chaos* and *cpSRP43-OX*. A. Steady-state levels of TBS proteins in 18-day-old Ler-0, *chaos*, and *cpSRP43-OX* under standard growth conditions were quantified by immunoblotting using the indicated antibodies. The Ponceau S-stained large subunit of RuBisCO (RbcL) is shown as a loading control. **B**, Semiquantitative analysis of the immunoblots with Image J software (NIH) in **A**. The relative

amounts of GluTR, CHLH, and GUN4 in *chaos* and *cpSRP43-OX* were normalized to the levels in Ler-0. The data are plotted as means ± s.d. (n = 4 independent biological repeats). The small open circles represent the individual data points. The statistical analysis was performed using two-tailed Student's *t*-tests. The asterisks indicate significant differences compared with protein levels in Ler-0: **P* < 0.05, ***P* < 0.01. **C**. Scheme of the TBS pathway in plants. The key enzymes regulated by cpSRP43 are highlighted in reddish-brown. GluRS, glutamyl-tRNA synthetase.

3.1.3 Post-translational regulation of cpSRP43 stabilizes GluTR, CHLH and GUN4

The two constituents, cpSRP43 and cpSRP54, contribute to the cpSRP pathway. Thus, I assumed whether the cpSRP54 deficiency could also lead to the decreased levels of GluTR, CHLH and GUN4. Therefore, the steady-state levels of these TBS proteins in the *cpSRP54*-deficient mutant *ffc* (Pilgrim et al., 1998) were compared to those in the wild type (Col-0). Although *ffc* also showed a pale-green and retarded growth phenotype (Figure 3.3A), the similar levels of GluTR, CHLH, and GUN4 in *ffc* and wild type (Figure 3.3B-C) imply that cpSRP54 does not directly regulate the steady-state levels of these TBS proteins. Thus, cpSRP43 is the sole component of the cpSRP complex, which acts on the stability of the TBS proteins.

In order to know whether the reduced GluTR, CHLH, and GUN4 levels in *chaos* correspond to compromised gene expressions, the transcriptional levels of *HEMA1*(gene encoding GluTR), *CHLH*, and *GUN4* were quantified by using qRT-PCR analysis. The mRNA levels of these three genes were not altered in both *chaos* and *cpSRP43-OX* compared with these in wild type (Figure 3.3D), indicating that the reduced levels of GluTR, CHLH, and GUN4 in response to cpSRP43 deficiency are not due to the down-regulation of their corresponding genes, but likely to a post-translational response. All in all, these observations also suggest a cpSRP43 function in addition to GluTR (Wang et al., 2018) in the post-translational control of CHLH and GUN4.

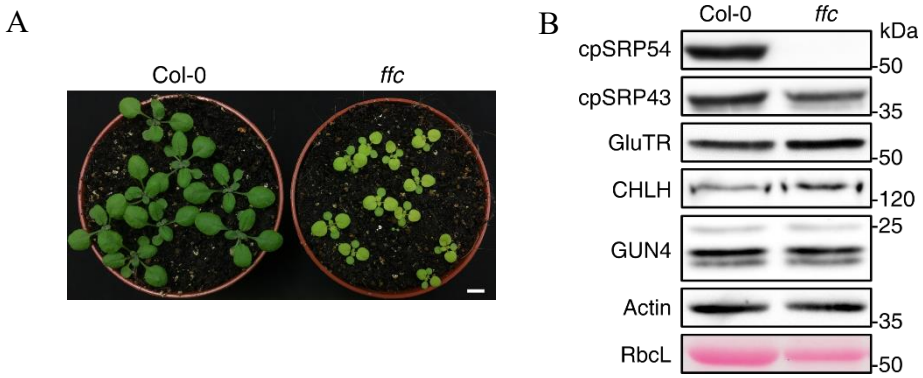

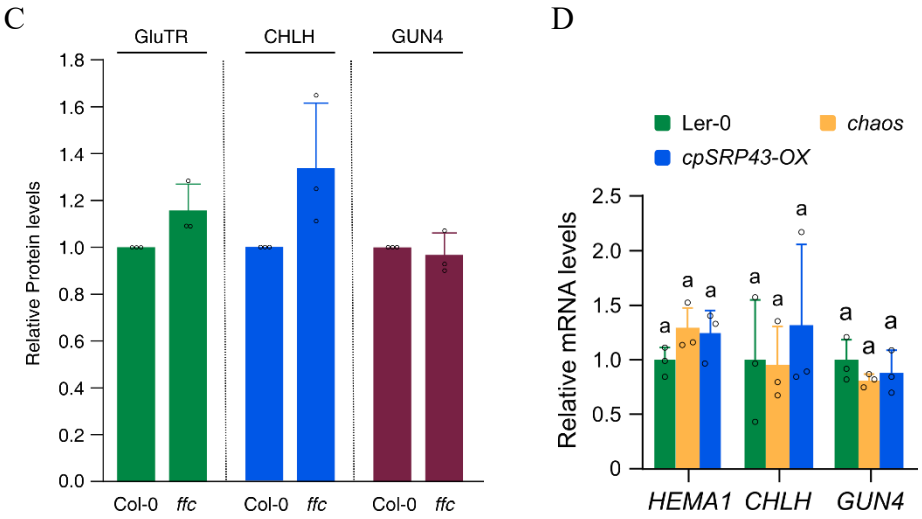

Figure 3.3 cpSRP43 stabilizes GluTR, CHLH and GUN4 in post-translational control. A, Phenotype of the 18-day-old *cpSRP54* knock-out mutant (*ffc*) and wild type (Col-0) in long-day (18 h light/ 6 h dark). Scale bar, 1 cm. **B**, Steady-state levels of TBS proteins in the wild type and *ffc* were detected by immunoblotting using the indicated antibodies. The Actin and ponceau-stained RbcL are shown as loading controls. **C**, Semiquantitative analysis with Image J software (NIH) of the immunoblots in **B**. The relative amounts of GluTR, CHLH and GUN4 in *ffc* were normalized to the levels in Col-0. The data are plotted as means ± s.d. (n = 3 independent biological replicates). The small open circles represent the individual data points. The statistical analysis was performed using two-tailed Student's *t*-tests. No asterisk indicates no significant differences compared to protein levels in Ler-0: * $P < 0.05$, ** $P < 0.01$. **D**, Relative quantities of mRNA from *HEMA1*, *CHLH* and *GUN4* genes in 18-day-old Ler-0, *chaos* and *cpSRP43-OX* grown under standard growth conditions. The gene expression levels were calculated relative to that in Ler-0, using *SAND* as the reference gene. All values are plotted as means ± s.d. (n = 3 independent samples). The small open circles represent the individual data points. The letters above the histograms indicate significant differences, as determined by one-way analysis of variance (ANOVA) with Tukey's test ($P < 0.05$).

3.1.4 cpSRP43 interacts directly with GluTR, CHLH and GUN4

As cpSRP43 deficiency causes a reduction of the steady-state levels of GluTR, CHLH and GUN4, it is interesting to find out the molecular mechanism of this protein instability. GluTR has already been examined by bimolecular fluorescence complementation (BiFC) to interact directly with cpSRP43 (Wang et al., 2018). Therefore, the BiFC assay was also performed with CHLH and GUN4. Gene constructs encoding the N-terminal half of the split yellow fluorescent protein (YFPn) fused with the cpSRP43 and the C-terminal half (YFPc) with CHLH, GUN4 or CHLM (as negative control) were generated in binary vectors, which were used for the transient leaf transformation of *Nicotiana benthamiana.* The co-expressions of the fusion gene products were analyzed in epidermal and parenchyma cells. Co-expressions of cpSRP43 with GluTR (for confirmation and positive control) and with CHLH and GUN4 reconstituted YFP fluorescence in chloroplasts for the first time. As a negative control, cpSRP43-YFPn co-expressed with CHLM-YFPc did not result in a YFP signal, indicating a specificity of the interaction of cpSRP43 with GluTR, CHLH and GUN4 (Figure 3.4A).

To verify these interactions, an in vitro pull-down assay was carried out. In this approach, 5 µM of purified recombinant GST or GST-cpSRP43 was used as bait and incubated with His-tagged CHLH and GUN4 (10 µM). The proteins bound to GST-cpSRP43 and GST were eluted with buffer containing 10 mM reduced glutathione. Aliquots of the input and elution fractions were probed with the indicated antibodies. CHLH and GUN4 were immunologically detectable in the eluate after incubation with GST-cpSRP43, but not with GST and agarose beads (Figure 3.4B-C). Taken together, two different approaches for analyzing protein-protein interaction verified the physical interaction of cpSRP43 with GluTR, CHLH and GUN4 and confirmed a direct impact of cpSRP43 deficiency on the stability of these enzymes.

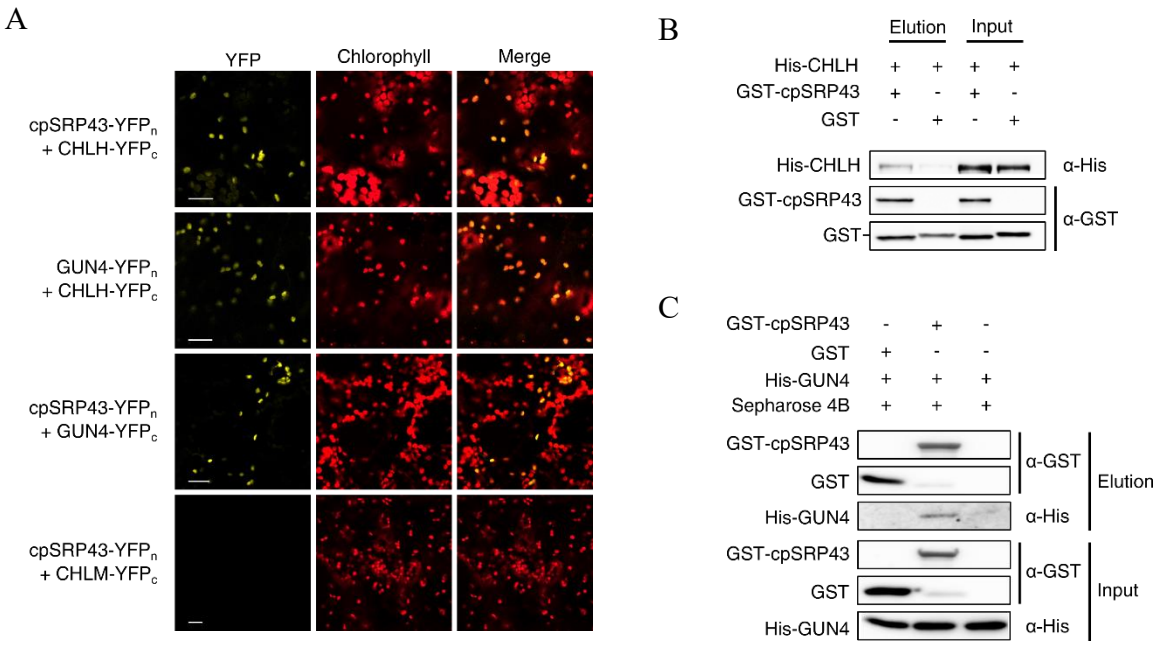

Figure 3.4 Physical interactions of cpSRP43 with CHLH and GUN4. A, BiFC demonstrates that cpSRP43 interacts with CHLH and GUN4. The co-expression of cpSRP43-YFPn with CHLM-YFPc served as the negative control, and that of GUN4-YFPn with CHLH-YFPc served as the positive control. Scale bars, 20 µm. **B-C**, CHLH (**B**) and GUN4 (**C**) bound to cpSRP43 were detected by in vitro GST pull-down assays. Recombinant purified GST-cpSRP43 (5 µM) was used as bait and incubated with His-tagged CHLH or GUN4 (10 µM). The proteins bound to GST-cpSRP43, or GST were eluted with buffer containing 10 mM reduced glutathione. The input and elution fractions were analyzed by immunoblot using the indicated antibodies.

3.1.5 cpSRP43 does not affect the MgCh activity

Since cpSRP43 stabilizes CHLH and GUN4 by physical interaction, I wondered whether cpSRP43 also affects the enzymatic activity of MgCh. Therefore, MgCh enzyme assays were conducted with and without cpSRP43 to identify the impact of cpSRP43 on MgCh activity. Since the SBD domain is essential for cpSRP43 to interact with its clients such as LHCP and GluTR (Liang et al., 2016; Wang et al., 2018), here the cpSRP43ΔSBD is regarded as the negative control for the assay. The supply of cpSRP43 did not alter the catalytic activity of MgCh regardless of the presence or absence of GUN4 (Figure 3.5A-B). Similar results were obtained when cpSRP43ΔSBD was supplied, indicating that cpSRP43 does not modulate the

MgCh activity.

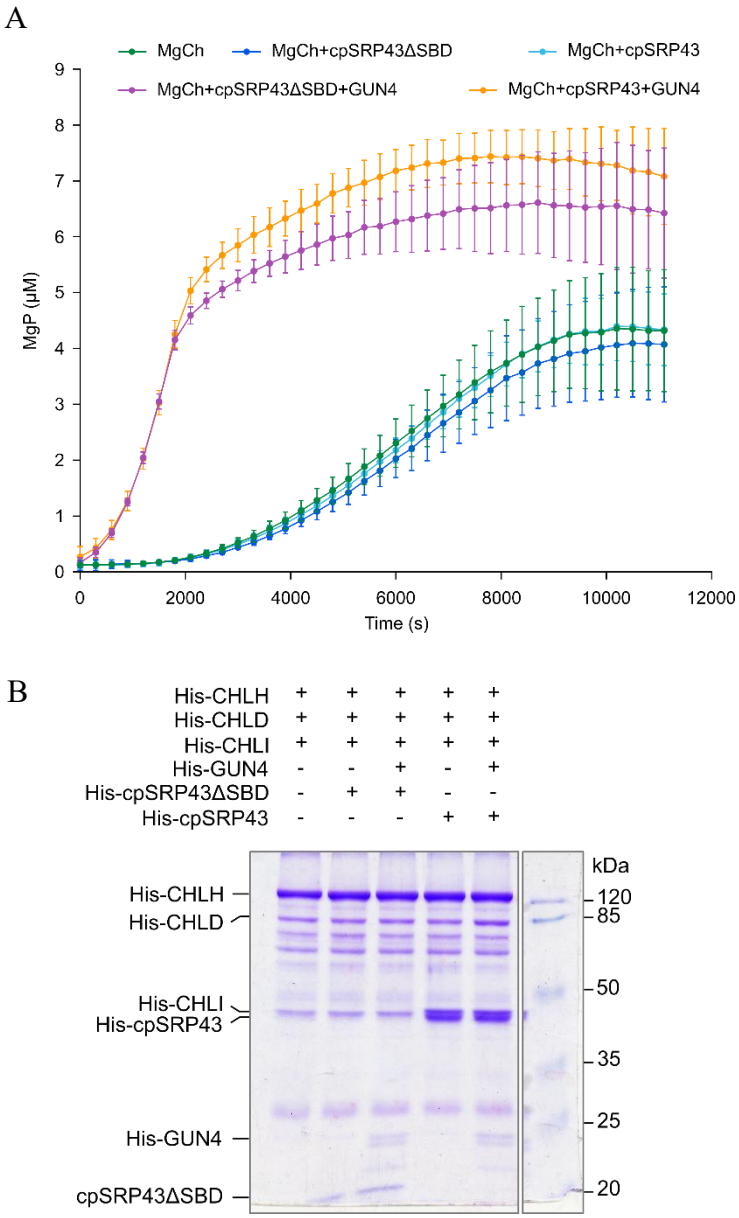

Figure 3.5. In vitro enzyme assays of MgCh. A, Time course curves of the MgCh enzyme assay with fluorescence detection of MgP (Ex 416 nm/Em 595 nm). The data are plotted as mean ± s.d. (n = 3 independent experiments). **B**, Recombinant proteins used in the assay were stained by Coomassie Brilliant Blue.

3.1.6 cpSRP43 is not involved in the retrograde singling pathway

Communication between cellular compartments is vital for development and environmental adaptation. Signals emanating from organelles, which are also designated retrograde signals, coordinate nuclear gene expression during plant development and in response to the functional status of the organelle (Wu and Bock, 2021). In the course of plastid development, nuclear-encoded *PHOTOSYNTHESIS-ASSOCIATED NUCLEAR GENES* (*PhANGs*), such as *LIGHT HARVESTING CHLOROPHYLL-BINDING PROTEINS* (*LHCPs*), *RuBisCO SMALL SUBUNIT* (*RBCS*), *PLASTOCYANIN* (*PC*), *CHLOROPLAST PROTEIN 12* (*CP12*) and

CARBONIC ANHYDRASE1 (*CA1*), are also controlled by these plastid-derived signals.

However, when plastid biogenesis is disturbed, *PhANGs* are repressed (Susek et al., 1993; Hess et al., 1994; Ruckle et al., 2007). Important knowledge about biogenic plastid-to-nucleus signaling was obtained by analysis of a set of *genomes uncoupled (gun)* mutants which shows impaired retrograde signaling (Susek et al., 1993; Mochizuki et al., 2001; Larkin et al., 2003; Koussevitzky et al., 2007; Woodson and Chory, 2008). For example, genetic perturbation of MgCh, a key enzyme of plastid-localized Chl biosynthesis, leads to the uncoupling of *PhANGs* expression from the developmental state of plastids. Mutation of the *GUN4* gene, *GUN5* (Larkin et al., 2003; Peter and Grimm, 2009) and *CHLI*, *CHLD* of MgCh showed a *gun* phenotype, i.e., reduced repression of *PhANGs* when chloroplast development is perturbed in *Arabidopsis* and barley (Gadjieva et al., 2005; Huang and Li, 2009). Since CHLH and GUN4 are involved in the retrograde singling pathway, it was intended to examine whether cpSRP43 is also involved in the retrograde singling by interacting with CHLH and GUN4. For this purpose, the expressions of *PhANGs* (*LHCB*, *RBCS, PC*, *CP12* and *CA1*) were analyzed in *gun4-1* and *chaos* in comparison to Col-0 and Ler-0, respectively, under standard (in DMSO) and NF (norflurazon) treatment. As a control, all *PhANGs* of both wild type and mutant exhibited comparable expression levels in DMSO under continuous light for 6 days (Figure 3.6A-E). As expected, when NF was applied, the expression of *PhANGs* in *gun4-1* was much higher than those in Col-0, while *chaos* showed comparable expression levels of *PhANGs* to those of Ler-0 (Figure 3.6F-J), indicating that cpSRP43 is not involved in retrograde singling in contrast to GUN4.

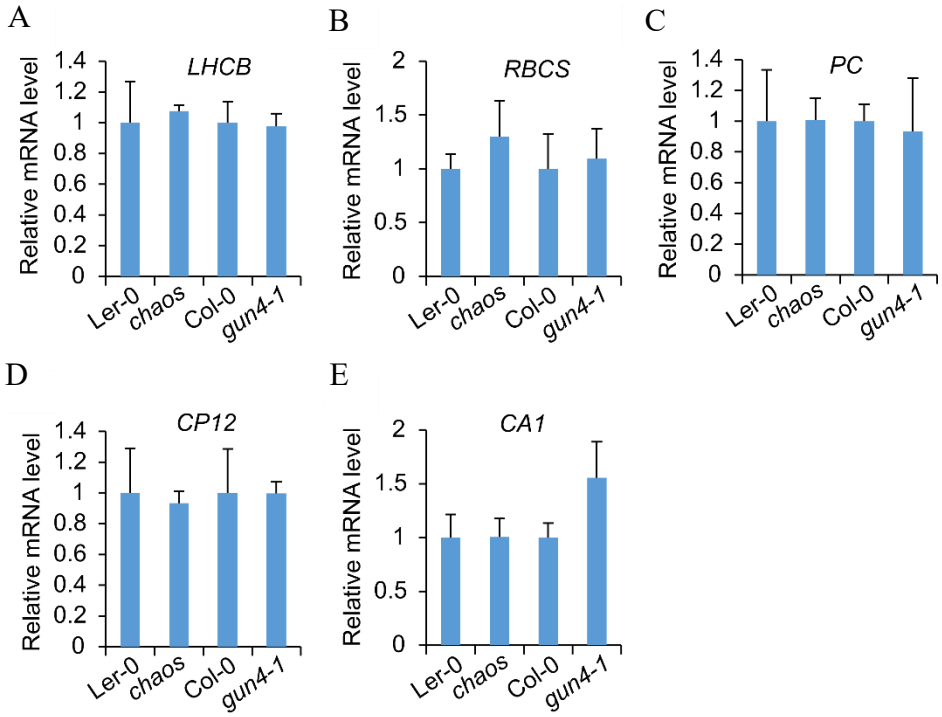

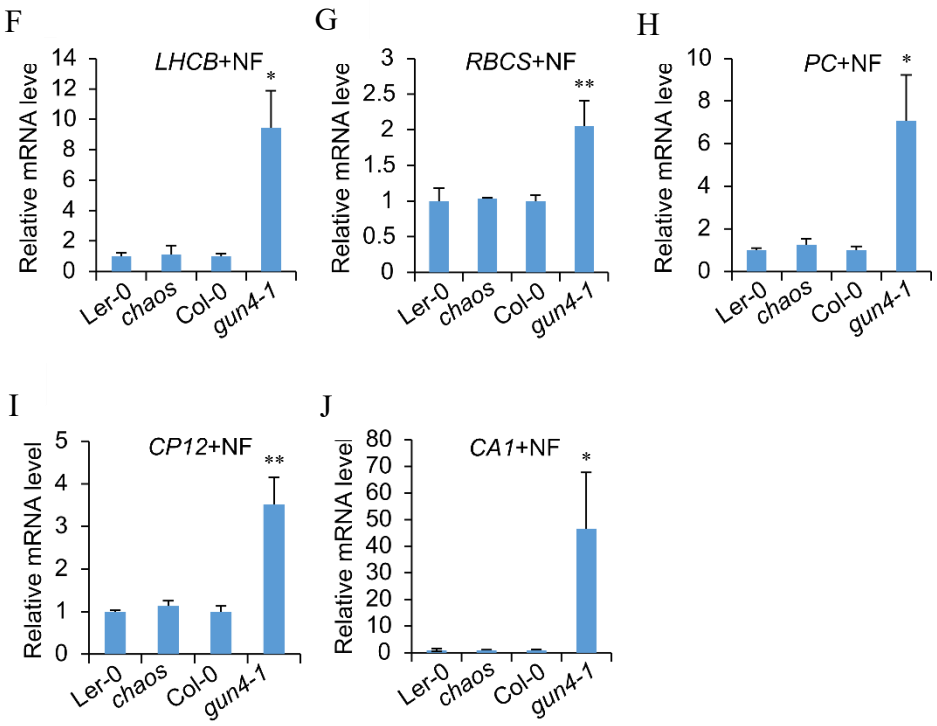

Figure 3.6. *PhANGs* expression in seedlings of Col-0, *gun4-1*, Ler-0 and *chaos* grown for 6 days in continuous light with or without 5 µM NF treatment. A-E, qRT-PCR analysis of *PhANGs* (*LHCB*, *PC*, *CA1*, *RBCS*, *CP12*) in DMSO. **F-I**, qRT-PCR analysis of *PhANGs* (*LHCB*, *PC*, *CA1*, *RBCS*, *CP12*) in 5 µM NF. Data are given as mean ± s.d. (n = 3). The statistical analysis was performed using two-tailed Student's t-tests. The asterisks indicate significant differences compared with the transcript levels in the wild type (*chaos* versus Ler-0, *gun4-1* versus Col-0): *P < 0.05, **P < 0.01.

3.1.6 cpSRP43 can effectively chaperone TBS proteins

3.1.6.1 cpSRP43 stabilizes TBS proteins against heat shock

To maintain the levels of TBS proteins, cpSRP43 could protect unfolded client proteins when they are just translocated into the chloroplast. This action of cpSRP was established for LHCP after its plastid import (Schünemann et al., 1998). Alternatively, cpSRP43 could prevent misfolding of mature enzymes in the stroma (Falk and Sinning, 2010). Given the fact that cpSRP43 act as a chaperone to protect GluTR from aggregation (Wang et al., 2018), I asked whether cpSRP43 also protects the TBS proteins in response to heat shock in planta. To answer this question, the steady-state levels of TBS proteins were compared in wild type, *chaos*, and *cpSRP43-OX* seedlings under standard growth (22 °C) and heat shock (42 °C) conditions. After several preliminary experiments, a 2 h heat treatment was chosen for a comparative analysis of the steady-state levels of TBS proteins with those under standard growth conditions (0 h).

The immunoblot analysis showed that the protein levels of cpSRP43 and cpSRP54 were not altered after a 2 h heat treatment at 42 °C (Figure 3.7A). In contrast, the heat treatment approximately diminished by 20–40% the levels of GluTR, CHLH and GUN4 in *chaos*, whereas the levels of these proteins were not diminished by heat treatment in the wild type and *cpSRP43-OX* seedlings (Figure 3.7A-B). Although cpSRP43 has been proven to interact with

PORC (see chapter 3.2.2, Figure 3.19), the unaltered protein level of PORC in *chaos* even under heat shock indicates that PORC does not require cpSRP43 action after heat treatment and consequently is not a potential vulnerable client of the protective action of cpSRP43.

To exclude that reduced protein levels in *chaos* can be explained by compromised transcript levels of the corresponding genes, qRT-PCR analysis was conducted to determine the transcript levels of *HEMA1*, *CHLH* and *GUN4* before and after heat shock. Unaltered transcript levels after 2 h heat shock indicate that the reduced protein levels in *chaos* were due to the lack of the protective role of cpSRP43 for the TBS proteins after heat shock treatment (Figure 3.7C). In addition, qRT-PCR and immunoblot analysis indicate that neither cpSRP transcripts nor levels of cpSRP43 and cpSRP54 were altered after a 2 h heat treatment at 42 °C (Figure 3.7A and 3.7C), excluding increased cpSRP43 expression or degradation of cpSRP54 to be involved in thermotolerance. These results suggest that cpSRP43 plays a key role in protecting certain TBS proteins against denaturation during heat shock.

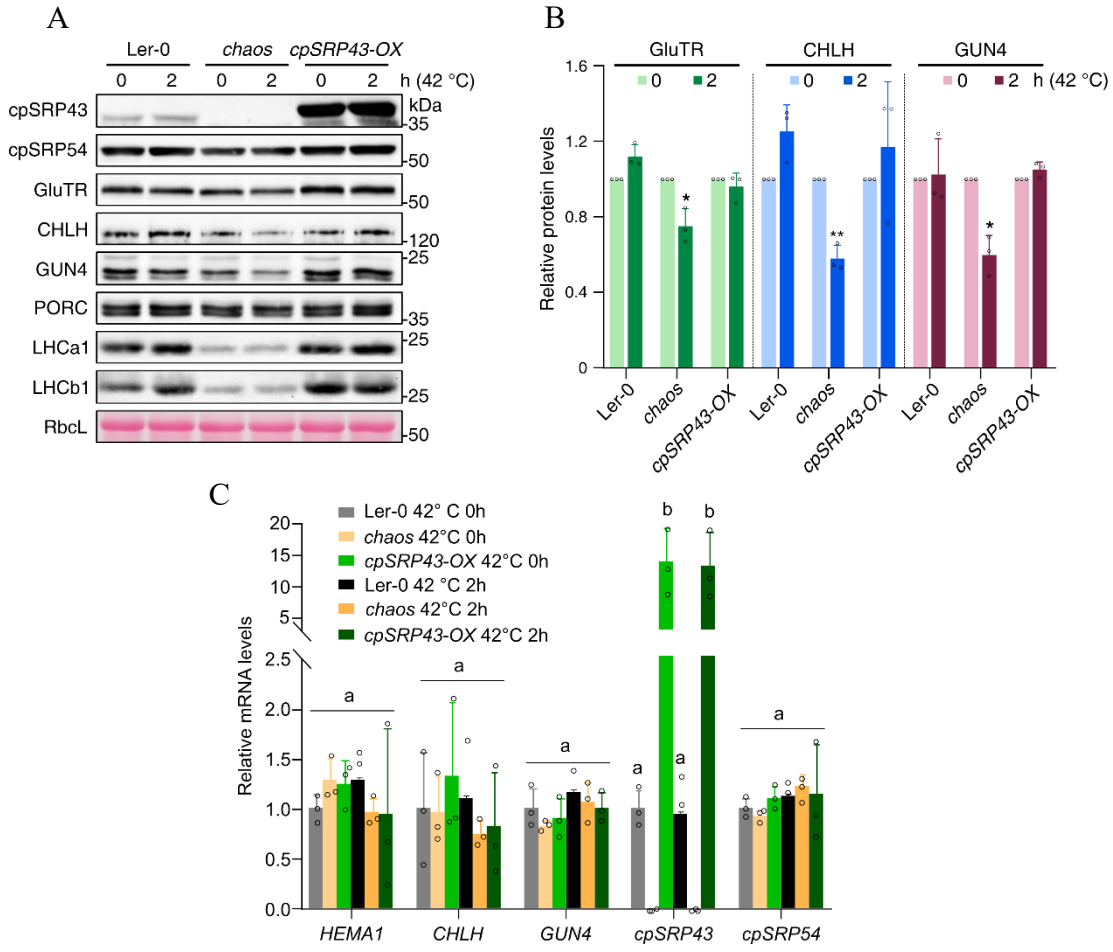

Figure 3.7 cpSRP43 protects GluTR, CHLH and GUN4 against heat shock in planta. A, Steady-state levels of the indicated proteins in Ler-0, *chaos* and *cpSRP43-OX* seedlings before and after 2 h of heat treatment at 42 °C were quantified by immunoblotting using the indicated antibodies. The Ponceau S-stained RbcL is shown as a loading control. **B**, Semiquantitative analysis with Image J software (NIH) of the immunoblots from **A**. The relative amounts of GluTR, CHLH and GUN4 in Ler-0, *chaos* and *cpSRP43-OX* were normalized to their levels before heat treatment (0 h). The data are plotted as means ± s.d. (n = 3 independent biological

repeats). The small open circles represent the individual data points. The statistical analysis was performed using two-tailed Student's t-tests. The asterisks indicate significant differences compared with protein levels before heat treatment: *P < 0.05, **P < 0.01. **C**, Relative amounts of mRNA of indicated genes in 18-day-old Ler-0, *chaos* and *cpSRP43-OX* were measured before and after 2 h heat treatment at 42 °C. Gene expression was calculated relative to the wild-type level of the reference gene *SAND*. The data are plotted as mean ± s.d. (n = 3 independent biological repeats). The small open circles represent the individual data points. The letters above histograms indicate significant differences as determined by two-way ANOVA with Tukey test ($P < 0.05$).

3.1.6.2 cpSRP43 preserves the Chl biosynthesis under heat shock

Because cpSRP43 protects the TBS proteins against heat shock, it was supposed that cpSRP43 also protects the metabolic flow of Chl biosynthesis under heat shock. HPLC analysis thereby was performed to measure the contents of the intermediates and Chl in Ler-0, *chaos* and *cpSRP43-OX* before and after 2 h heat shock. Although the results showed only slightly elevated Chl levels in Ler-0 and *cpSRP43-OX* but not in *chaos* seedlings after 2 h heat treatment (Figure 3.8A), the heat treatment greatly led to the significantly increased accumulation of Chl precursors, such as MgP, MgPMME, and Pchlide in wild type and *cpSRP43-OX* but not in *chaos* seedlings (Figure 3.8B-C). However, this elevated metabolic flow was only observed in the Chl synthesis pathway prior to the Chlide production, as Chlide levels were unaltered in these three plants after heat shock treatment (Figure 3.8D). This could exclude the possibility

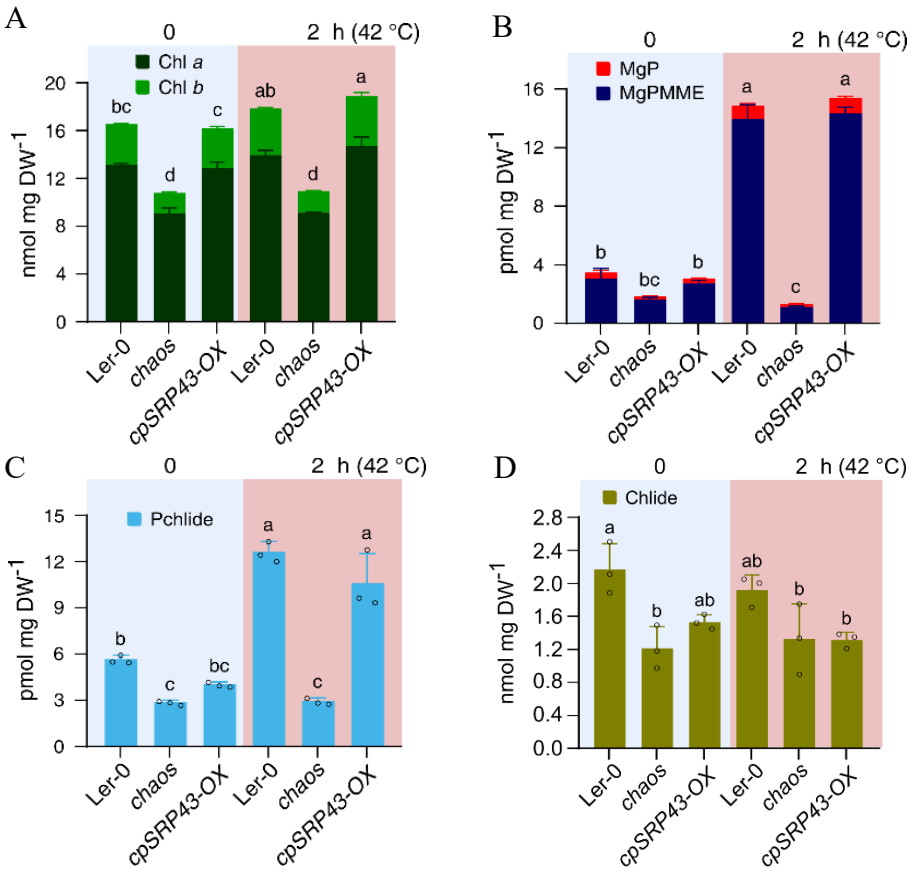

Figure 3.8 cpSRP43 effectively preserves the metabolic flow of Chl biosynthesis. A-D, Levels of Chl (**A**), MgP and MgPMME (**B**), Pchlide (**C**) and Chlide (**D**) in Ler-0, *chaos* and

cpSRP43-OX before and after heat treatment were detected by HPLC. DW, dry weight. The data are plotted as means ± s.d. (n = 3 independent biological repeats). The small open circles represent the individual data points. The letters above the histograms indicate significant differences as determined by two-way ANOVA with Tukey's test ($P < 0.05$).

that the accumulation of the Chl precursors is due to the inactivation of POR activity under heat shock because the inactive POR could lead to the reduced Chlide level. Therefore, it is likely that the enhanced stability or activity of some enzymes prior to POR results in the elevated Chl precursors, and cpSRP43 is apparently to be involved in this enhancement. Moreover, I suppose that the short-term accumulation of Chl precursors is likely to be a quick response by plants to activate some other pathways against the heat shock stress. Taken together, these results suggest that cpSRP43 plays a key role in adjusting the metabolic flow through the Chl biosynthesis pathway by protecting TBS proteins against denaturation during heat shock.

3.1.7 The peptide domains of cpSRP43 and their function in the thermostability of TBS clients.

3.1.7.1 The SBD domain is essential for cpSRP43 to protect Chl biosynthesis in planta

cpSRP43 contains three chromodomains (CD1, CD2 and CD3) and four ankyrin repeats (Ank1-Ank4) (Klimyuk et al., 1999; Goforth et al., 2004; Stengel et al., 2008). CD1, Ank1-Ank4, and a 20-aa Bridging Helix (BH) located between Ank4 and CD2 form a substrate-binding domain (SBD) (Figure 3.9A). Given the novel protective role of cpSRP43 for folded TBS proteins, I aimed to explore which domains and motifs of cpSRP43 are essential for the protection of TBS proteins. Previous work established the central importance of the cpSRP43-SBD to prevent LHCP aggregation (Richter et al., 2010; Akopian et al., 2013; Liang et al., 2016). Our research group previously showed that GluTR and LHCP bind to different sites within the SBD of cpSRP43 and that the three proteins can form a ternary complex (Wang et al., 2018). Additionally, expression of truncated cpSRP43 lacking either CD1 or the Ankyrin repeat domain of the SBD reduced the content of both GluTR and LHCP in transgenic lines (Wang et al., 2018), underlining the essential role of the SBD in the stability of the two client proteins. To test the role of each functional domain of cpSRP43 for the stability of the newly identified client proteins, I used the same series of *chaos* complementation lines that constitutively express wild-type cpSRP43 or truncated cpSRP43 variants as previously described (Wang et al., 2018). Expression of truncated cpSRP43 without either CD1 or the Ankyrin repeat domain in the SBD did not complement the pale-green leaf phenotype of *chaos* and the corresponding steady-state levels of GluTR, CHLH, and GUN4 were also decreased compared to those in Ler-0. In contrast, expression of either cpSRP43ΔCD2 or cpSRP43ΔCD3 completely rescued the pale-green phenotype of *chaos* and the corresponding steady-state levels of GluTR, CHLH, and GUN4 were also comparable to those in Ler-0 (Figure 3.9B-C). These results point to the significance of the SBD domain of cpSRP43 for the stability of GluTR, CHLH and GUN4. The dramatically reduced levels of Chl and Chl precursors in transgenic lines expressing cpSRP43 without the CD1 or Ankyrin repeat domain correlated with the lower steady-state levels of TBS proteins in these lines (Figure 3.9D-F). These observations suggest that SBD of cpSRP43 is

required for the stability of TBS proteins, thereby the metabolic flow of Chl biosynthesis is retained.

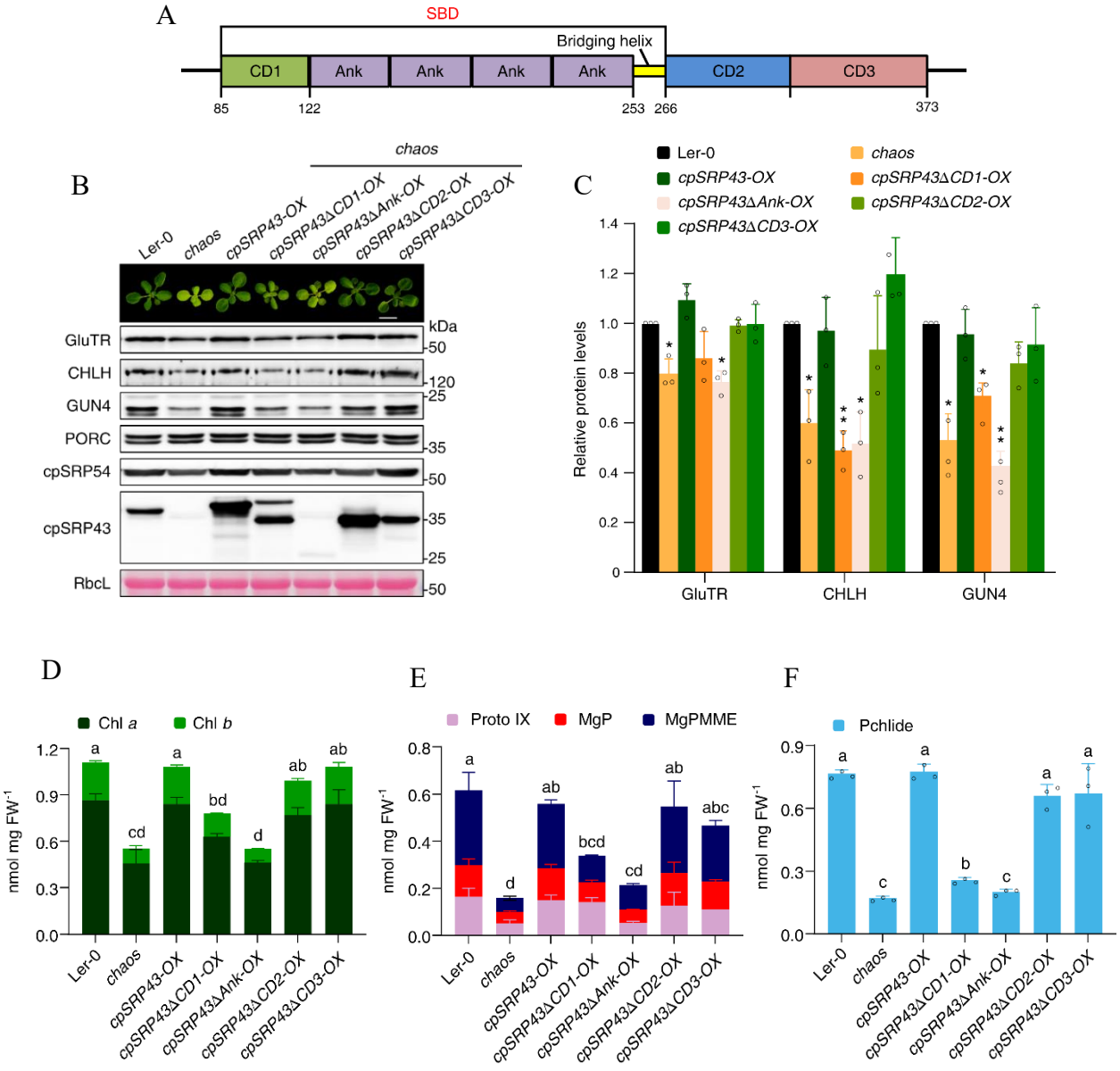

Figure 3.9 SBD is required for cpSRP43 to protect GluTR, CHLH and GUN4. A, Schematic overview of cpSRP43 domains. **B**, A representative image (top panel) and steady-state levels of the indicated cpSRP43, cpSRP54 and TBS proteins (lower panels) in 18-day-old Ler-0, *chaos* and the indicated *chaos* complementation lines under standard conditions (16 h light/8 h dark, 100 µmol photons m^{-2} s^{-1}). RbcL is shown as a loading control. **C**, Semiquantitative analysis with Image J software (NIH) of the immunoblots in **B**. The relative amounts of GluTR, CHLH and GUN4 in *chaos* and various *chaos* complementation lines were normalized to the levels in Ler-0. The data are plotted as means ± s.d. (n = 3 independent biological repeats). The small open circles represent the individual data points. The statistical analysis was performed using two-tailed Student's *t*-tests. The asterisks indicate significant differences compared with protein levels in Ler-0: *P < 0.05, **P < 0.01. HPLC analyses of Chl (**D**), Proto, MgP and MgPMME (**E**) and Pchlide (**F**) in the seedlings of 18-day-old Ler, *chaos* and a set of *chaos* complementation lines. FW, fresh weight. The data are plotted as mean ± s.d. (n = 3 independent biological repeats). The small open circles represent the individual

data points. Letters above histograms indicate significant differences as determined by one-way ANOVA with Tukey test ($P < 0.05$).

3.1.7.2 The CD2 or CD3 domain is required for interactions between cpSRP43 and TBS proteins in vitro

Given that the cpSRP43-SBD is required for the stability of TBS proteins (Figure 3.9B-3.9C) and the Ank3 of SBD recognizes an L18 motif of LHCP (DeLille et al., 2000; Stengel et al., 2008; Jaru-Ampornpan et al., 2013), I speculate whether SBD is also sufficient to recognize and bind TBS proteins. Therefore, I performed the Microscale Thermophoresis (MST) assay to identify the binding sites of cpSRP43 to the TBS proteins. It was found that the deletion of the SBD (a truncated cpSRP43 with a remaining CD2 and CD3 fragment) completely abolished the binding affinity of cpSRP43 with GluTR and GUN4 (Figure 3.10E, 3.10F), suggesting a critical role of the SBD for the interaction with TBS proteins. Surprisingly, cpSRP43-SBD alone could not mimic the binding affinities of full-length cpSRP43 with GluTR, and GUN4 (Figure 3.10A-B,3.10G-H), In contrast, SBD in combination with CD2 (cpSRP43-SBD+CD2) or CD3 (cpSRP43-SBD+CD3) could mimic the binding affinity of FL cpSRP43 with GluTR and GUN4 (Figure 3.10A, 3.10C-D, 3.10G, 3.10I-J), suggesting in addition to SBD that CD2 or CD3 of cpSRP43 are also required for stabilizing interaction between cpSRP43 and TBS proteins. In other words, the MST assay proved that both SBD and chromodomain 2 or 3 of cpSRP43 are required to recognize the TBS proteins.

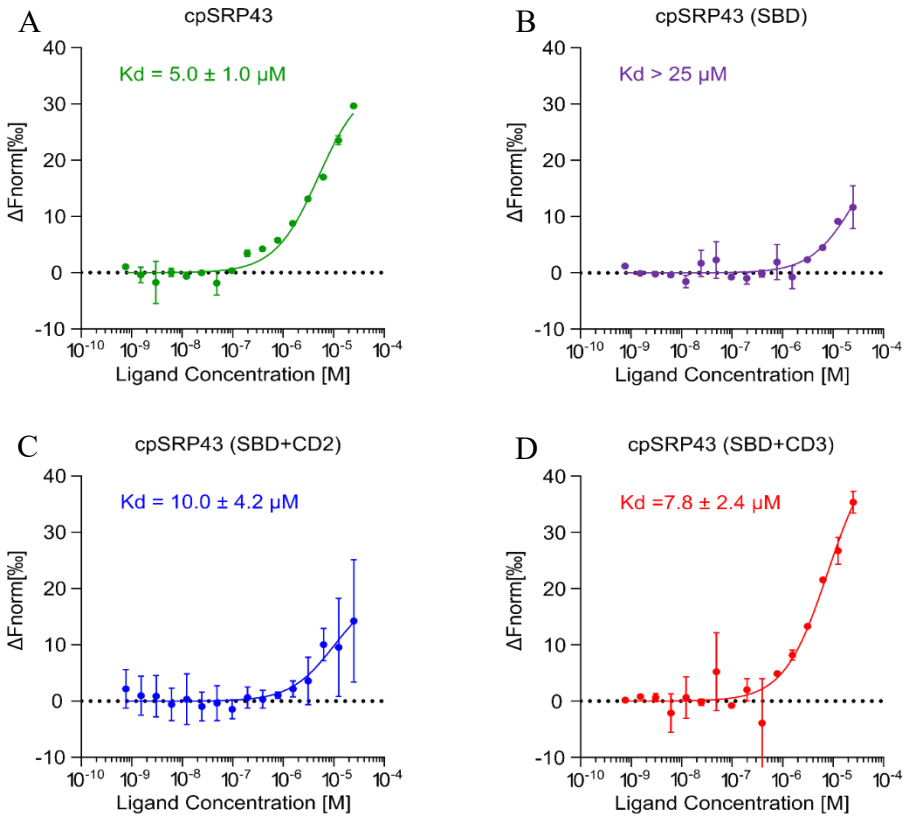

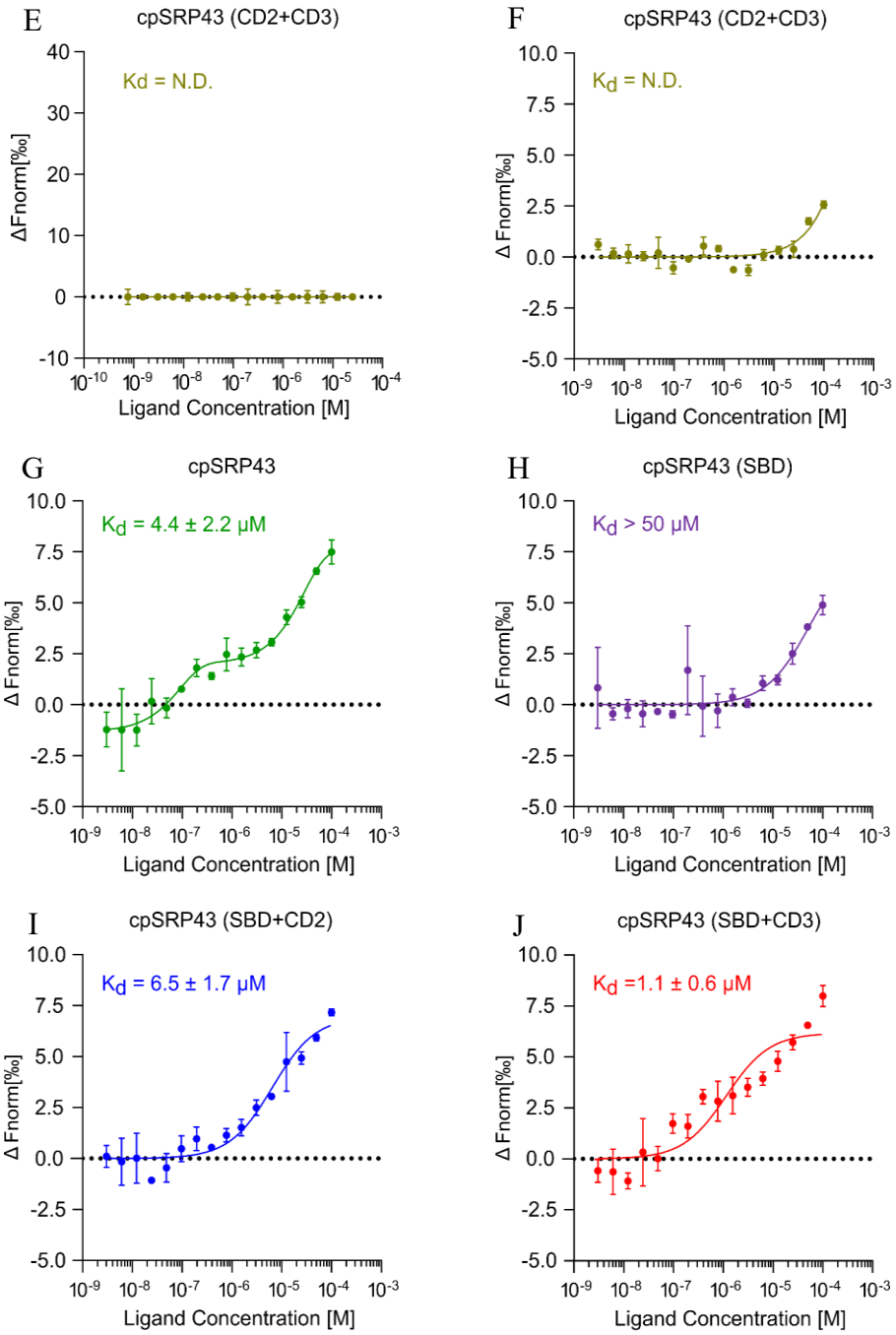

Figure 3.10 Measurement of the binding affinity of cpSRP43 with GluTR and GUN4 using Microscale Thermophoresis (MST). The fluorophore-labeled GluTR (Figure 3.10**A-E**) and GUN4 (Figure 3.10**F-J**) were used at a constant concentration (20 nM), while the concentration of the non-labeled wild-type or truncated cpSRP43 varied between 3.05 nM and 100 µM. N.D., not detectable. The data are plotted as mean ± s.d. (n = 3 independent experiments).

3.1.7.3 The CD2 domain is required for cpSRP43 to interact with TBS proteins in planta

Besides the CD1 in SBD domain, cpSRP43 contains two other chromodomains, CD2 and CD3, at the C-terminal end. To determine the functional indispensability of the CD2 and CD3 domains of cpSRP43 for the preserved stability of TBS proteins, I conducted a Co-IP assay to assess the binding capacity of truncated cpSRP43 (with CD2 or CD3 deletion) to TBS proteins

in vivo. The assays were performed by using the chloroplast extracts from seedlings of wild type, *cpSRP43-OX*, *cpSRP43ΔCD2-OX*, and *cpSRP43ΔCD3-OX* lines, which expressed the cpSRP43, cpSRP43-FLAG, cpSRP43ΔCD2-FLAG and cpSRP43ΔCD3-FLAG, respectively. The wild-type sample was regarded as a negative control to exclude any unspecific binding of proteins with anti-FLAG affinity agarose. As a result, cpSRP43ΔCD2 does not interact with detectable amounts of GluTR, whereas wild-type cpSRP43 and cpSRP43ΔCD3 showed similar binding affinity to GluTR (Figure 3.11), suggesting that CD3 may substitute for CD2 in the interaction with GluTR in vitro, while CD2 is essential and irreplaceable for interactions with TBS clients in vivo.

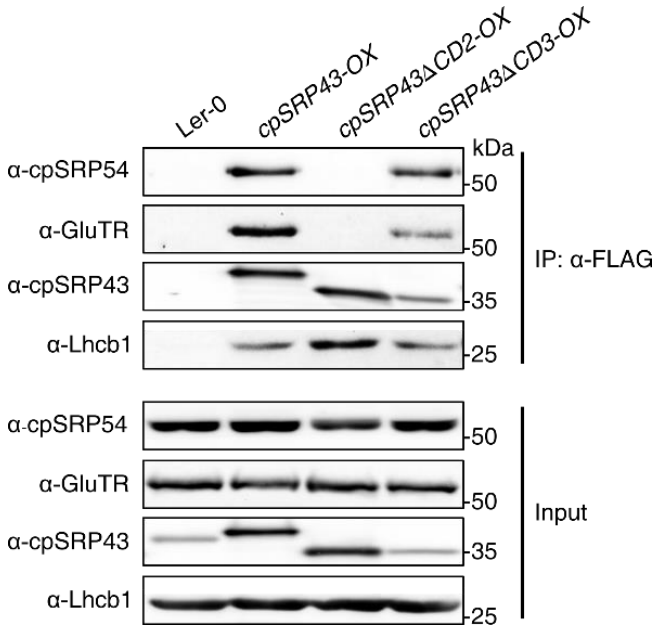

Figure 3.11 The CD2 domain of cpSRP43 is indispensable for the binding with TBS proteins in planta. The co-immunoprecipitation (Co-IP) assay demonstrates the abolished in vivo binding affinity of cpSRP43ΔCD2 for GluTR and cpSRP54. Total chloroplast extracts from Arabidopsis transgenic lines overexpressing cpSRP43-FLAG (*cpSRP43-OX*), truncated FLAG-tagged cpSRP43 without CD2 (*cpSRP43ΔCD2-OX*), FLAG-tagged cpSRP43 without CD3 (*cpSRP43ΔCD3-OX*) and wild type (Ler-0, used as a negative control) were incubated with the anti-FLAG affinity gels. The cpSRP43 interaction partners were identified by immunoblotting using the indicated antibodies.

3.1.7.4 The CD2 structure is essential for cpSRP43 to protect TBS proteins against heat shock in planta

As CD2 is essential for the interaction capacity of cpSRP43 with TBS proteins, I explored the contributions of CD2 and CD3 for the thermoprotective action of cpSRP43 on TBS proteins in vivo during an extended heat shock treatment. The immunoblotting analyses showed that after a heat treatment at 42 °C for 2 or 4 h, the steady-state levels of GluTR, CHLH and GUN4 were decreased in *cpSRP43ΔCD2-OX* seedlings compared with the results obtained from wild type, and *cpSRP43-OX* seedlings (Figure 3.12A-B). In contrast, the steady-state levels of GluTR, CHLH and GUN4 in *cpSRP43ΔCD3-OX* were comparable with those in wild type or *cpSRP43-OX*, indicating that CD2 is essential for the protective interaction of cpSRP43 with TBS

proteins. This result was also supported by the data obtained from analysis of the metabolic flow in Chl biosynthesis. HPLC analyses revealed the levels of Chl precursors in *cpSRP43ΔCD2-OX*, including MgP, MgPMME and Pchlide, which were significantly lower than those in the control seedlings during the heat treatment. In contrast, the contents of Chl precursors in *cpSRP43ΔCD3-OX* resembled those in wild type or *cpSRP43-OX* (Figure 3.12C-E). Taken together, these results demonstrate the key roles of SBD and CD2 of cpSRP43 for the stabilization of TBS clients under heat shock conditions.

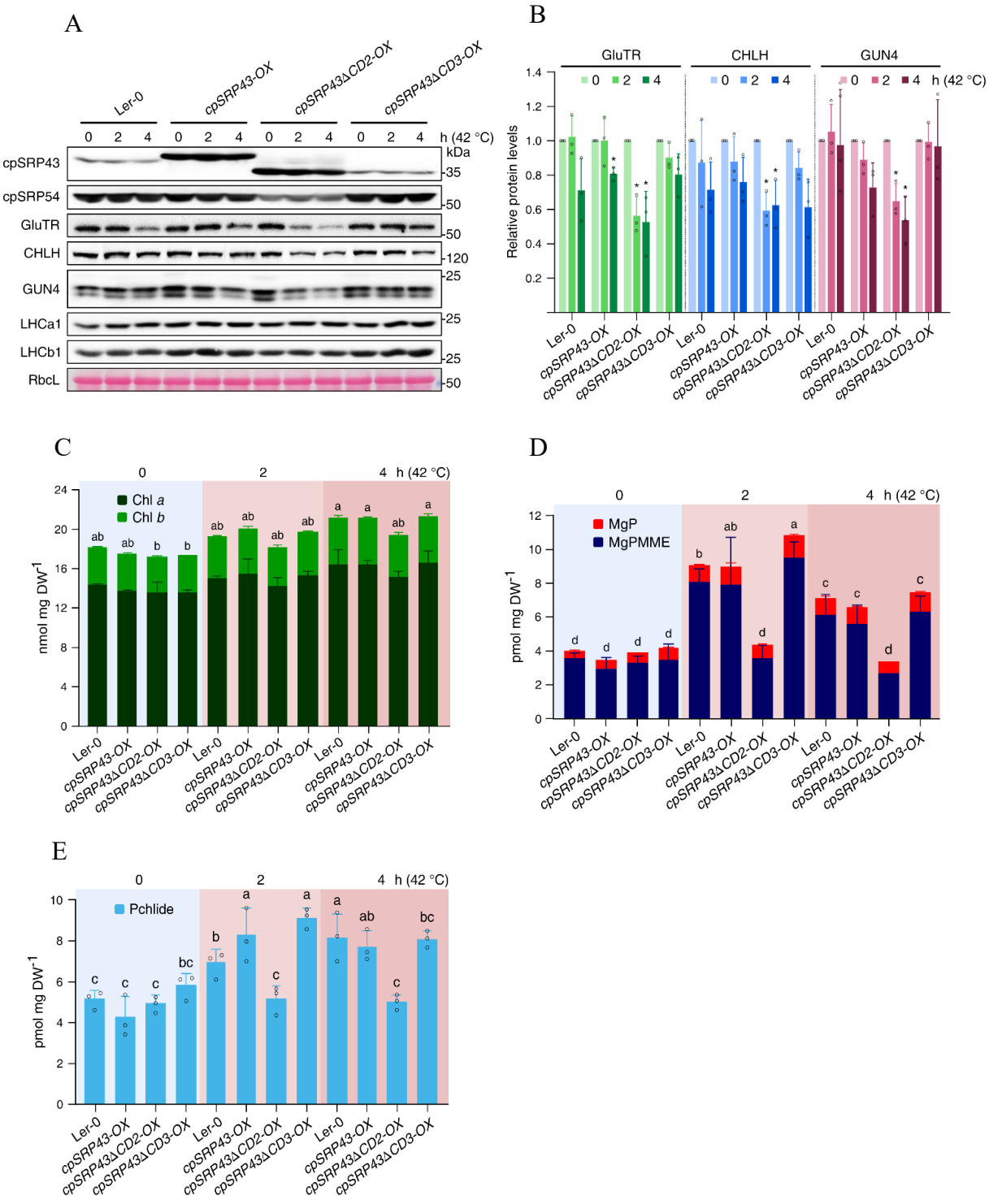

Figure 3.12 The CD2 domain of cpSRP43 is indispensable for the stability of TBS proteins in planta. A, Steady-state levels of cpSRP43, cpSRP54, TBS proteins and LHCPs in 18-day-old Ler-0, *cpSRP43-OX*, *cpSRP43ΔCD2-OX* and *cpSRP43ΔCD3-OX* before (0 h at 42 °C) or after 2–4 h of heat treatment (2 or 4 h at 42 °C) were detected by immunoblotting using the indicated antibodies. The Ponceau S-stained RbcL is shown as a loading control. **B**, Semiquantitative analysis with Image J software (NIH) of the immunoblots in **A**. The relative amount of GluTR, CHLH and GUN4 was normalized to their levels prior to exposure of the seedlings to the elevated temperature (0 h at 42 °C). The data are plotted as means ± s.d. (n = 3 independent biological repeats). The small open circles represent the individual data points. The statistical analysis was performed by using two-tailed Student's t-tests. The asterisks indicate significant differences relative to each ecotype before heat treatment (0 h at 42 °C): *P < 0.05. **C-E**, Levels of Chl (**C**), MgP and MgPMME (**D**), and Pchlide (**E**) in Ler-0, *cpSRP43-OX*, *cpSRP43ΔCD2-OX* and *cpSRP43ΔCD3-OX* before and after 2–4 h of heat treatment were determined by HPLC. DW, dry weight. The data are plotted as means ± s.d. (n = 3 independent biological repeats). The small open circles represent the individual data points. The letters above the histograms indicate significant differences as determined by two-way ANOVA with Tukey's test (P < 0.05).

3.1.8 cpSRP54 inhibits the chaperone function of cpSRP43 for TBS proteins

3.1.8.1 In vivo cpSRP54 deficiency increases the thermostabilities of TBS proteins under heat shock

It was already known that the chaperone activity of cpSRP43 for LHCPs is stimulated by allosteric regulation by cpSRP54 (Liang et al., 2016; Siegel et al., 2020). The RRKRp10 segment of cpSRP54 (hereafter designated cpSRP54M peptide) sufficiently binds to CD2 of cpSRP43 and triggers a conformational change of the protein, which promotes the chaperone activity towards LHCP by 6-fold (Liang et al., 2016; Siegel et al., 2020). Considering the new finding of chaperone activity of cpSRP43 on GluTR, CHLH and GUN4 of the TBS pathway, it became very interesting to determine the potential interference of cpSRP54 on the chaperone activity of cpSRP43 towards these TBS proteins. In order to validate the effect of cpSRP54 on cpSRP43 by an experimental in planta approach, the steady-state levels of TBS proteins in wild type (Col-0) and cpSRP54-deficient (*ffc*) seedlings were compared during heat shock and under standard growth conditions. The immunoblot analysis showed firstly that the contents of GluTR, CHLH and GUN4 were always increased in all samples of *ffc* before and during the heat treatment than in the equivalent samples of wild type and secondly that the GluTR, CHLH and GUN4 content in Col-0 was faster degraded than that in *ffc* during a 2–4 h heat shock treatment (Figure 3.13A-B). These data indicate enhanced stability of GluTR, CHLH and GUN4 in *ffc* relative to wild type and are in favor of a negative role of cpSRP54 in respect to the maintenance of a stable content of TBS proteins during heat shock.

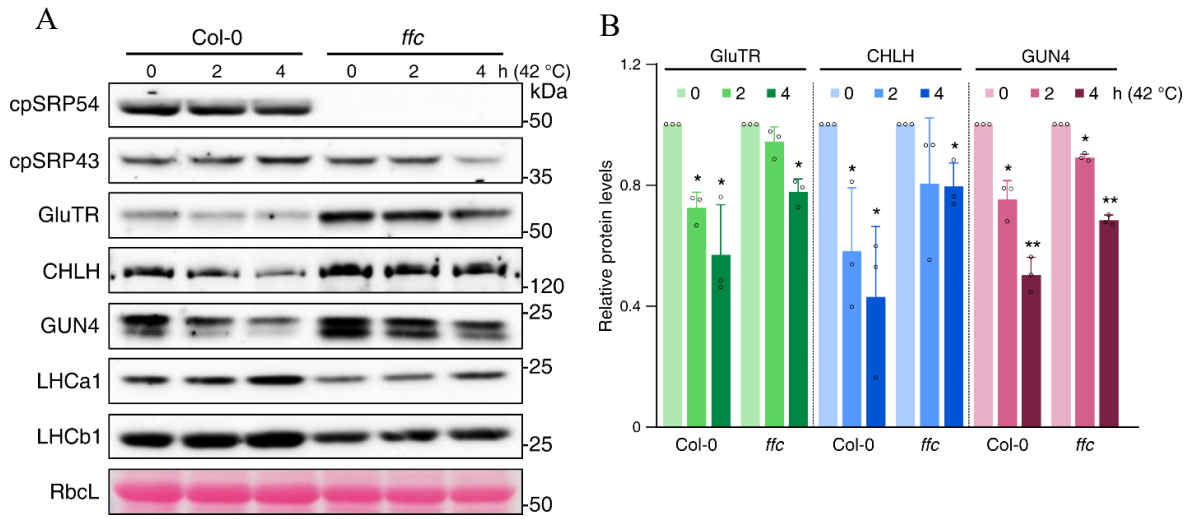

Figure 3.13 Steady-state levels of TBS proteins in Col-0 and *ffc*. A, Steady-state levels of the indicated proteins in 18-day-old ecotype Columbia-0 (Col-0) and the *ffc* mutant seedlings before and after 2–4 h of heat treatment at 42 °C were quantified by immunoblotting using the indicated antibodies. The Ponceau S-stained RbcL is shown as a loading control. **B**, Semiquantitative analysis with Image J software (NIH) of the immunoblots in **A**. The relative amounts of GluTR, CHLH and GUN4 in Col-0 and *ffc* were normalized to their levels before the exposure of plants to elevated temperature. The data are plotted as means ± s.d. (n = 3 independent biological repeats). The small open circles represent the individual data points. The statistical analysis was performed by using two-tailed Student's t-tests. The asterisks indicate significant differences relative to protein levels in each ecotype before heat treatment: *P < 0.05, **P < 0.01.

3.1.8.2 cpSRP54 deficiency leads to a more effectively preserved Chl biosynthesis during heat shock treatment

The next open question regards the impact of cpSRP54 on the flow of metabolites in Chl synthesis. Therefore, I intended to examine whether the lack of cpSRP54 causes a better preservation of Chl biosynthesis during heat shock. HPLC analyses was performed to measure the contents of Chl and Chl precursors in Col-0 and *ffc* during heat shock treatment. The Chl contents remained stable in wild-type and *ffc* seedlings during heat shock although the Chl content in *ffc* was lower than in wild type before the heat treatment. The levels of Chl precursors including MgP, MgMME and Pchlide remained stable in *ffc* during heat shock, while the higher steady-state levels of the tetrapyrrole intermediates in Col-0 decreased down to the *ffc* values after heat stress treatment (Figure 3.14A-C). These results suggest that missing cpSRP54 preserves the Chl biosynthesis during the heat shock treatment. Considering that cpSRP54 inhibits the chaperone activity of cpSRP43 towards TBS clients in vitro, it was proposed that also a negative effect of cpSRP54 can be expected in planta on the stability of TBS proteins subjected to a short-term heat stress.

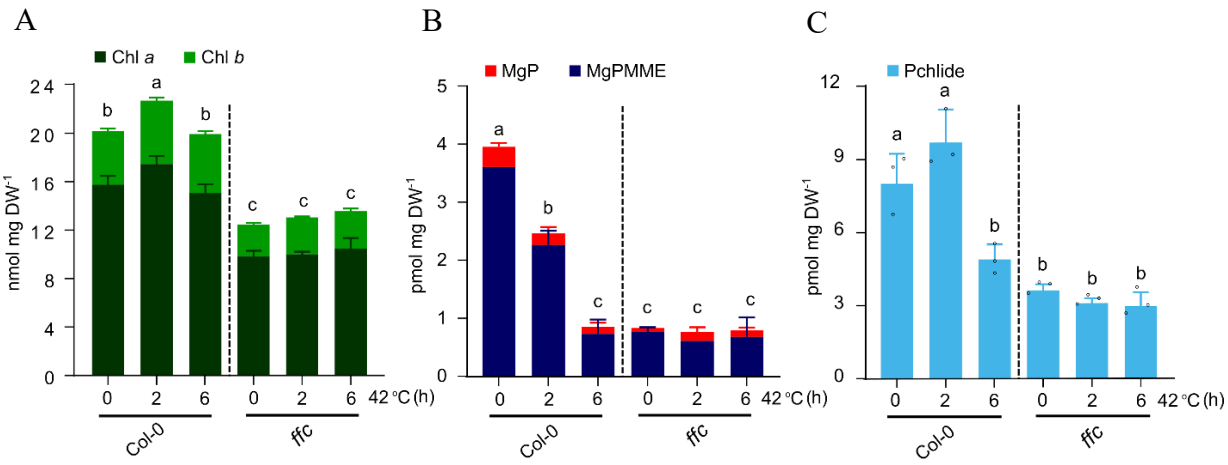

Figure 3.14 cpSRP54 deficiency does not compromise Chl biosynthesis during heat treatment. HPLC analyses of Chl (**A**), MgP and MgPMME (**B**) and Pchlide (**C**) in 18-day-old Col-0 and *ffc* prior to and after 2 or 6 h heat treatment at 42 °C. DW, dry weight. The data are plotted as mean ± s.d. (n = 3 independent biological repeats). The small open circles represent the individual data points. Letters above histograms indicate significant differences as determined by two-way ANOVA with Tukey test (P< 0.05).

3.1.9 How does cpSRP43 cooperate with cpSRP54 to protect TBS proteins?

3.1.9.1 Heat treatment compromises the interaction of cpSRP43 with cpSRP54

As shown in the previous chapter (see 3.1.1), cpSRP43 chaperones and, consequently, stabilize certain TBS enzymes under standard conditions (Figure 3.2A-B). While heat stress could induce the protein aggregation, which likely induces the protein degradation (Del Vesco et al., 2015), the chaperone activity of cpSRP43 reinforces the structure of TBS enzymes, leads to elevated content of stabilized TBS enzymes. Therefore, given that the chaperone function of cpSRP43 stabilizes Chl biosynthesis under heat shock, while cpSRP54 may interfere with this chaperone function, we asked how cpSRP43 and cpSRP54 cooperatively adjust the chaperone activity of cpSRP43 towards TBS enzymes under heat shock.

My first assumption refers to possibly increased cpSRP43 content during heat shock, which could stimulate the chaperone activity of cpSRP43 on TBS proteins during heat shock. Since the qRT-PCR and immunoblot analysis showed the unaltered cpSRP43 transcript and protein level under heat shock, this idea can be excluded (Figure 3.7A, 3.7C). Secondly, it is assumed that the enhanced chaperone activity of cpSRP43 is due to a decreased level of cpSRP54 which could lower its intervening impact of cpSRP54 on the chaperone activity of cpSRP43 on TBS proteins. However, the unaltered protein level of cpSRP54 during heat shock also exclude this assumption (Figure 3.7A). The third assumption is based on the possibility that enhanced chaperone activity of cpSRP43 is triggered by an impaired interaction between cpSRP43 and cpSRP54 during elevated temperature or an enhanced interaction between cpSRP43 and TBS proteins in response to the modified endogenous and environmental cues. In order to verify this assumption, I carried out Co-IP assays with protein extracts from wild type and transgenic plants overexpressing FLAG-tagged cpSRP43 (*cpSRP43-FLAG*) before and after heat

treatment to determine the binding of cpSRP43 to TBS proteins and to cpSRP54. The anti-FLAG affinity agarose was the bait, and the wild-type sample was regarded as the negative control to exclude the unspecific binding of anti-FLAG agarose with cpSRP54 and TBS proteins.

The amount of cpSRP43 bound to the anti-FLAG agarose were normalized to allow quantification of the binding capacity of cpSRP43 with cpSRP54 and TBS proteins. Although both BiFC and pull-down assay proved the interaction of cpSRP43 with CHLH and GUN4 (Figure 3.4A-C), the interaction of cpSRP43 with these two proteins could not be detected in the Co-IP assay (Figure 3.15B). It is assumed that most likely the presence of detergent during lysis interferes with the interactions. Therefore, only GluTR as the TBS proteins was shown in the Co-IP assay (Figure 3.15A). The results demonstrated that after 2 h heat treatment at 42 °C, less cpSRP54 was bound to cpSRP43, and a corresponding increase in the amount of GluTR was detectable, which was bound via FLAG-tagged cpSRP43 to the Co-IP matrix (Figure 3.15A). These results point to the third assumption and favor a regulatory mechanism of the chaperone activity by heat-induced modulation of the binding properties of cpSRP43 to its interaction partners: heat shock impairs the interaction of cpSRP43-cpSRP54, while it enhances the binding capacity between cpSRP43 and TBS enzymes. Thus, the chaperone activity of cpSRP43 will be strengthened on TBS proteins when plants are exposed to a higher temperature.

To verify these observations in vitro, I aimed to compare the binding capacity of cpSRP43 with cpSRP54 at different temperatures by using an in vitro pull-down assay. His-tagged cpSRP54 was used as bait and incubated with GST-cpSRP43 at 15 °C or 45°C. It was observed that 1 h heat treatment at 45 °C reduced the interdependency of cpSRP43 with cpSRP54 by 22% in comparison to their interplay at 15 °C. This finding points to thermal-dependent disturbance of the cpSRP43-cpSRP54 interaction in vitro (Figure 3.15C). This result is consistent with the outcome of the in vivo Co-IP assay, showing that high temperature diminished the binding affinity of cpSRP43 with cpSRP54.

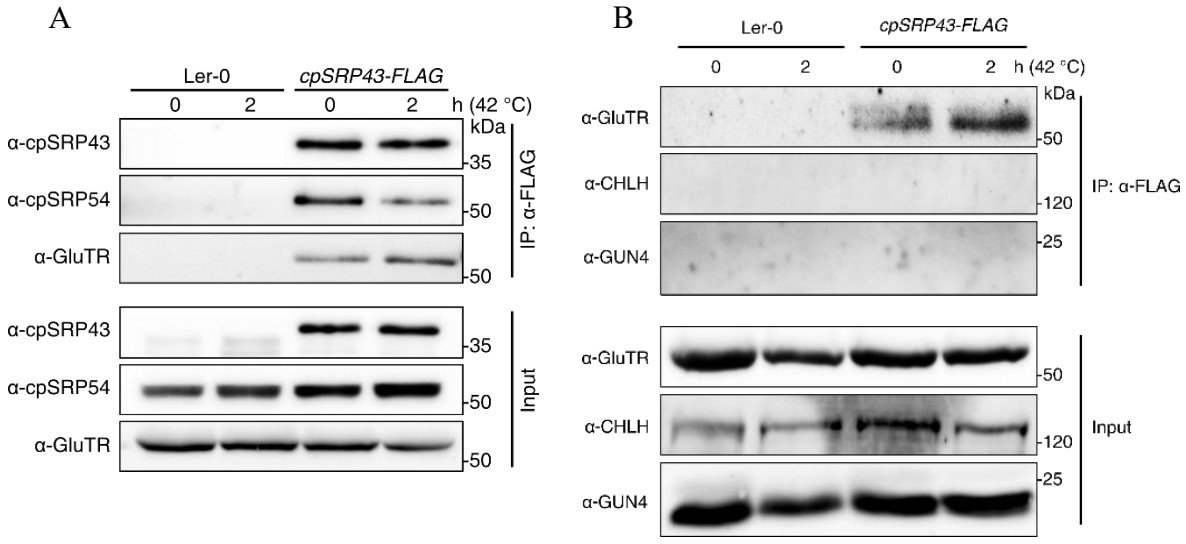

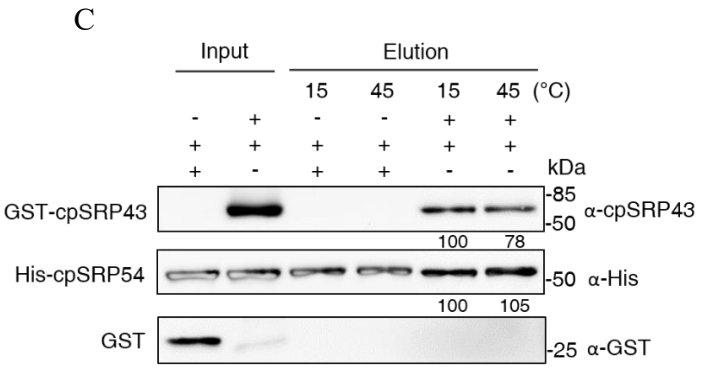

Figure 3.15 Heat treatment reduces the binding affinity of cpSRP43 with cpSRP54. A, Co-IP assay to determine the changes in the interaction of cpSRP43 with cpSRP54 or with GluTR before and after heat treatment. The interaction partners of cpSRP43 were detected by immunoblotting using the indicated antibodies. **B**, Co-IP assay to determine the changes in the interaction of cpSRP43 with GluTR, CHLH and GUN4 prior to or after heat treatment at 42 °C for 2 h. Total chloroplast extracts from wild type (Ler-0, used as negative control) and transgenic Arabidopsis lines overexpressing cpSRP43-FLAG (*cpSRP43-FLAG*) were incubated with anti-FLAG affinity agarose. cpSRP43 interaction partners were detected by immunoblotting analyses using the indicated antibodies. **C**, In vitro His pull-down assay showed the reduced binding affinity of GST-cpSRP43 with His-tagged cpSRP54 at high temperature. Recombinant purified His-tagged cpSRP54 (5 μM) was used as bait and incubated with GST or GST-cpSRP43 (5 μM) at 15 °C or 45 °C for 1 h. The proteins bound to His-tagged cpSRP54 were eluted with the elution buffer containing 250 mM imidazole. Input and elution fractions were analyzed by immunoblot analyses using the indicated antibodies. Two independent biological repeats were performed with similar results.

3.1.9.2 Heat treatment stimulates binding affinity of cpSRP43 with TBS proteins

In the previous assay described in 3.1.9.1, only GluTR was detected by the Co-IP assay (Figure 3.15B). Thus, it was not clear how the binding affinity of cpSRP43 is changed to CHLH and GUN4 after a heat treatment. In order to get more experimental insight in the thermal dependency of cpSRP43 interdependency with other TBS proteins and to support the third assumption (see chapter 3.1.9.1), I compared the binding affinities of cpSRP43 with TBS clients as the change of the temperature by in vitro pull-down assays subjected to different temperatures. It was observed that 1 h heat treatment at 30 °C enhanced the affinities of cpSRP43 with GluTR, CHLH and GUN4 compared with those at 15 °C (Figure 3.16A-C), suggesting a promoted interaction between cpSRP43 and TBS clients as a result of the elevated temperature. Considering the compromised interaction between cpSRP43 and cpSRP54 (see 3.1.9.1), my results suggest that thermostress triggers the dissociation of cpSRP43-cpSRP54 heterodimer, by which the pool of apo cpSRP43 is increased, allowing binding and protection of TBS clients during heat shock treatment.

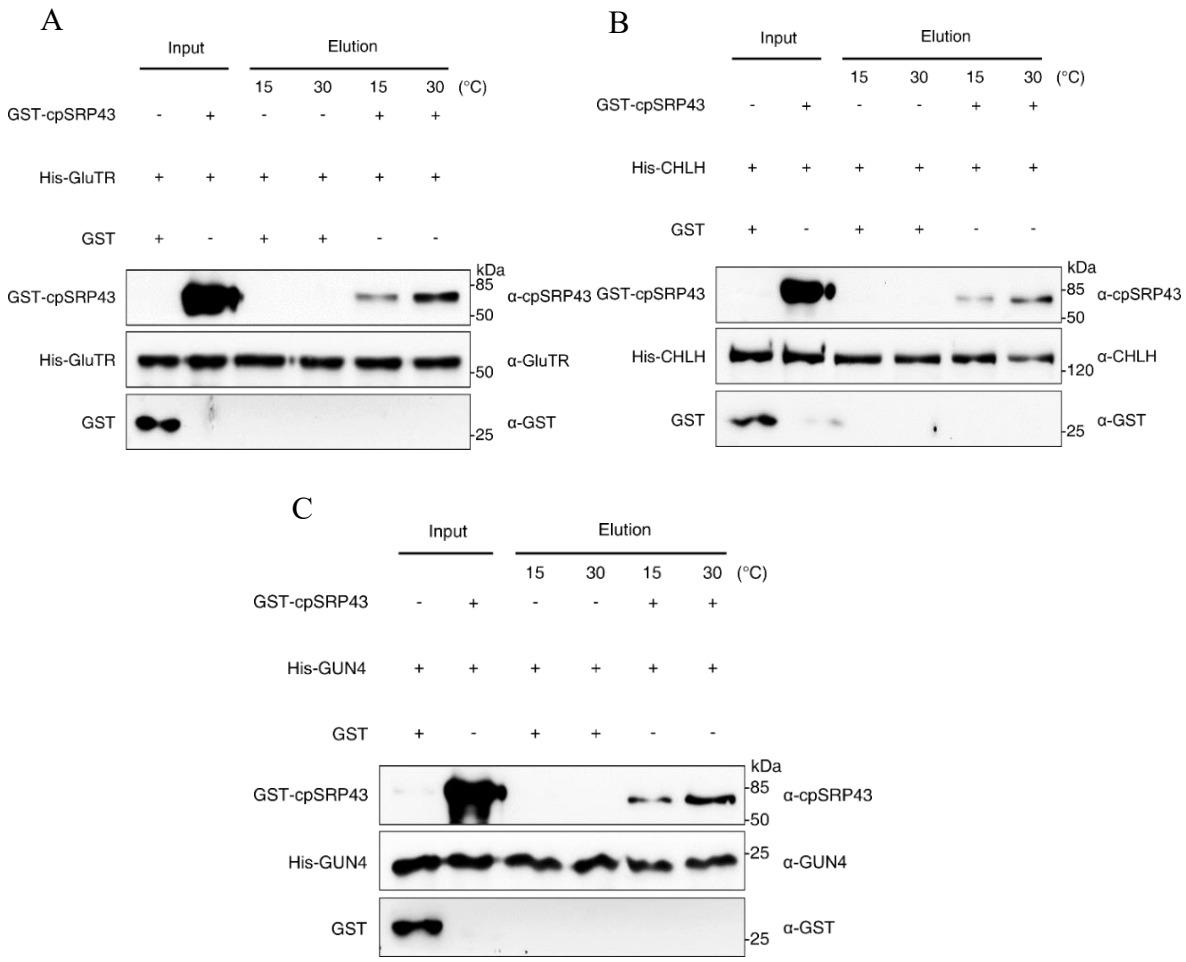

Figure 3.16 Heat treatment promotes the binding affinity of cpSRP43 with GluTR, CHLH and GUN4. A-C, In vitro His pull-down assay showing the enhanced binding affinity of GST-cpSRP43 with His-tagged GluTR (**A**), CHLH (**B**) and GUN4 (**C**) at high temperature. Recombinant purified His-tagged GluTR, CHLH and GUN4 (5 μM) were used as baits and incubated with GST or GST-cpSRP43 (5 μM) at 15 °C or 30 °C for 1 h. The proteins bound to His-tagged GluTR, CHLH and GUN4 were eluted with the elution buffer containing 250 mM imidazole. Input and elution fractions were analyzed by immunoblot analyses using the indicated antibodies. Two independent biological repeats have been performed with similar results.

3.2 Chloroplast SRP acts as a chaperone for protochlorophyllide oxidoreductase B (PORB) in *Arabidopsis thaliana*

The previous section presented data from cpSRP43 as a chaperone, which protects the TBS proteins GluTR, CHLH and GUN4 against the formation of aggregates and, thereby, stabilizes these proteins and preserved the Chl biosynthesis under both normal growth conditions and during heat shock. In the course of my studies, I found that cpSRP43 deficiency not only correlated with reduced content of GluTR, CHLH and GUN4, but also with that of another important enzyme, PORB, which is the light-operating enzyme in TBS. However, unlike the cpSRP54 suppressed protective action of cpSRP43 for GluTR, CHLH and GUN4, cpSRP54 is likely to be involved in stabilizing PORB together with cpSRP43. In this section, I describe the studies of how cpSRP43 and cpSRP54 coordinately regulate PORB, including its stability, activity and spatial distribution.

3.2.1 cpSRP43 and cpSRP54 stabilize PORB and regulate the Chl biosynthesis

3.2.1.1 cpSRP43 and cpSRP54 modulate the Chl biosynthesis

In order to study the cooperative regulation of cpSRP43 and cpSRP54 on PORB in planta, I chose the mutants *chaos* (*cpSRP43* knock-out) and *ffc* (*cpSRP54* knock-out), the *ffc*/*chaos* double mutant (Hutin et al., 2002), and the corresponding overexpression lines, *cpSRP43-OX* (*cpSRP43* overexpression line) and *cpSRP54-OX* (*cpSRP54* overexpression line) as well as the wild-type control lines Col-0 (background of *ffc* and *cpSRP54-OX*) and Ler-0 (background of *chaos*, *cpSRP43-OX* and *ffc*/*chaos*). When grown under the condition of a long day for 16 d, the seedlings of *chaos* and *ffc* showed a pale-green and growth retarded phenotype (Figure 3.17A). In the *chaos/ffc* double mutant, the mutant phenotype was enhanced, and the leaves of the seedlings remained yellow and smaller in size (Figure 3.17A). However, this phenotype of the single and double mutant could be rescued by the overexpression of the corresponding *cpSRP43* or *cpSRP54* genes (Figure 3.17A), indicating that the phenotypes of *chaos* and *ffc* are directly caused by the deficiency of cpSRP43 and cpSRP54, respectively. The contents of Chl (Figure 3.17B) and intermediates such as MgP, MgMME (Figure 3.17C), Pchlide (Figure 3.17D) analyzed by HPLC in the mutants and overexpression lines were consistent with their respective phenotypes. The metabolic flow of Chl biosynthesis was decreased in *chaos*, *ffc* and *ffc/chaos,* while it was similar in wild type and the overexpression lines, indicating that apart from cpSRP43, the dysfunction of cpSRP54 also disrupts the Chl biosynthesis. Intriguingly, a reduced content of non-covalently bound heme was found in *chaos/ffc* but not in *chaos* (Figure 3.17E), implying that cpSRP54, but not cpSRP43 may specifically affect the heme biosynthesis.

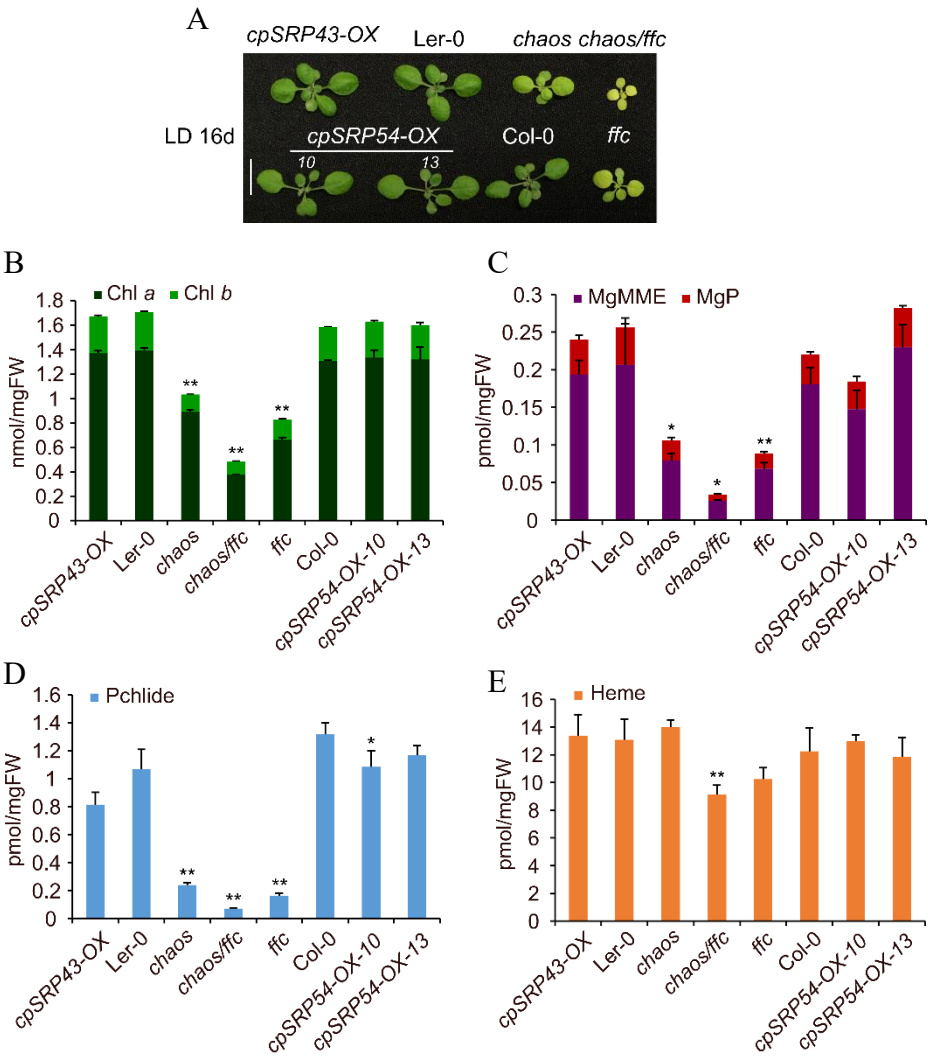

Figure 3.17 cpSRP43 and cpSRP54 deficiency impact the Chl and heme biosynthesis. A, A representative image of 16-day-old *chaos*, *ffc*, *chaos/ffc*, *cpSRP43-OX*, *cpSRP54-OX* and wild-type seedlings (Col-0 ecotype for *ffc*, *cpSRP54-OX* and Ler-0 ecotype for *chaos*, *chaos/ffc* and *cpSRP43-OX*) grown under standard conditions. Scale bar, 1 cm. **B-E**, Levels of Chl *a*/*b* (**B**), TBS metabolic intermediates MgMME, MgP (**C**), Pchlide (**D**) and heme (**E**) in 18-day-old Ler-0, *chaos*, *chaos/ffc*, *ffc*, Col-0, *cpSRP43-OX* and *cpSRP54-OX* grown under the same conditions as in **A**. FW, fresh weight. The statistical analysis was performed using two-tailed Student's t-tests. The asterisks indicate significant differences compared with protein levels in wild type: *P < 0.05, **P < 0.01.

3.2.1.2 cpSRP43 and cpSRP54 cooperatively stabilize PORB

In order to explore whether other proteins in TBS- apart from GluTR, CHLH and GUN4- would also be disadvantaged in the *chaos* and *ffc* single and double mutants, I analyzed the steady-state levels of other TBS proteins in these mutants and overexpression lines (see the chapter 3.1). The result was consistent with the previous study as the levels of GluTR, CHLH and GUN4 were significantly reduced in *chaos,* but not altered in *ffc* (Wang et al., 2018). Interestingly, I found that the PORB level was decreased in both *chaos* and *ffc*, and the reduction became more significant in *ffc/chaos* (Figure 3.18A-B). The reduced PORB level could be

rescued in the *cpSRP43-OX* and *cpSRP54-OX* and similar or excessive levels were displayed in comparison to wild type. In *cpSRP54-OX*, the PORB level was higher than that in wild type (Figure 3.18A-B), suggesting that cpSRP43 and cpSRP54 cooperatively lead to a stabilized PORB content. PORC, another isoform of POR, was only found to be significantly decreased in *ffc*/*chaos* (Figure 3.18A), suggesting that cpSRP43 and cpSRP54 probably contribute differently to the control of the PORC level than that of PORB.

In order to verify whether the reduced PORB levels in mutants correlate with down-regulated transcript levels, I analyzed the transcript levels of *PORB* of the same mutant and wild-type seedlings as in Figure 3.14A. I found that the mRNA levels of *PORB* in *chaos* and *ffc* resembled that of wild type. Although the transcript level of *PORB* in the double mutant *ffc/chaos* was decreased (46%) (Figure 3.18C), its protein level was more significantly decreased (68%) as a result of cpSRP43 and cpSRP54 deficiency (Figure 3.18A-B), suggesting that both cpSRP components could be involved in post-translational control of the PORB stability.

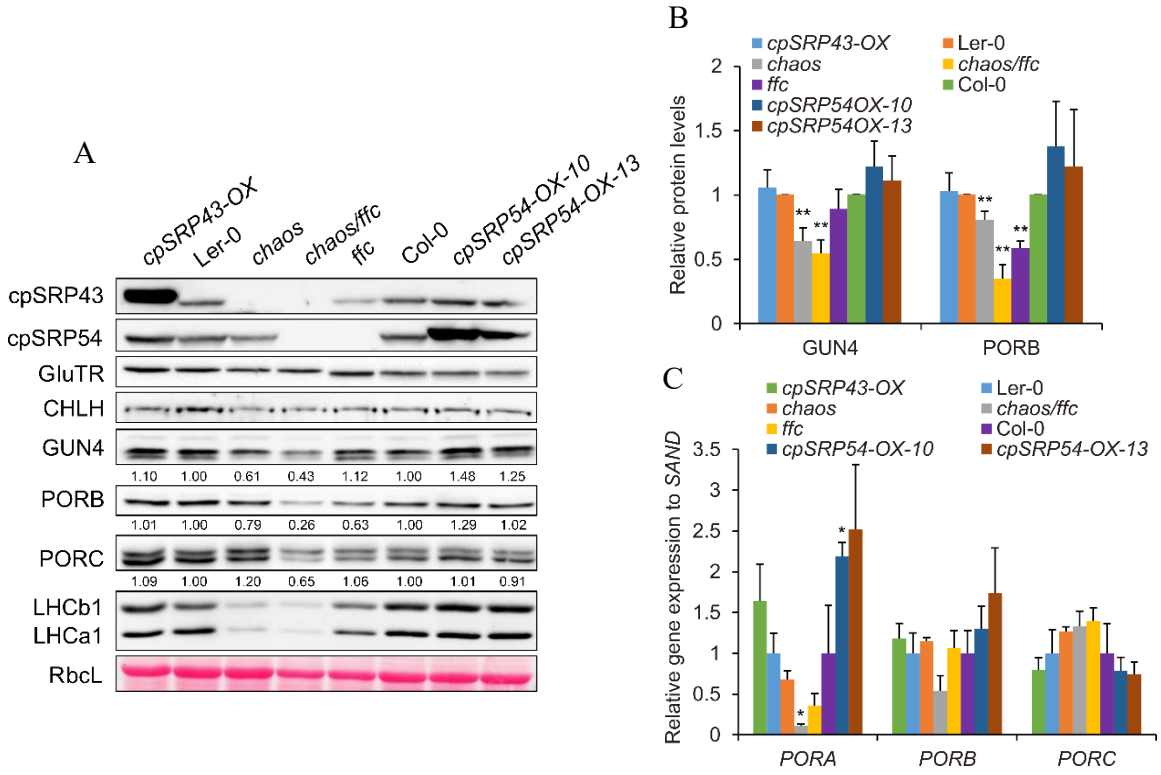

Figure 3.18 cpSRP43 and cpSRP54 are required for the stabilization of PORB. A, Steady-state levels of TBS proteins in 18-day-old Ler-0, *chaos*, *chaos/ffc*, *ffc*, Col-0, *cpSRP43-OX* and *cpSRP54-OX* grown under standard conditions (16 h light/8 h dark, 100 µmol photons m^{-2} s^{-1}) were quantified by immunoblotting using the indicated antibodies. The Ponceau S-stained RbcL nis shown as a loading control. **B**, Semiquantitative analysis with Image J software (NIH) of the immunoblots in **A**. The relative amounts of PORB and GUN4 in mutants and overexpression lines were normalized to the levels in wild type. **C**, Relative mRNA levels of *PORA*, *PORB* and *PORC* in 18-day-old Ler-0, *chaos*, *chaos/ffc*, *ffc*, Col-0, *cpSRP43-OX* and *cpSRP54-OX* grown as in **A**. The gene expression levels were calculated relative to that in Ler-0 or Col-0, using *SAND* as the reference gene. The data are plotted as means ± s.d. (n = 3 independent biological repeats). The statistical analysis was performed using two-tailed

Student's *t*-tests. The asterisks indicate significant differences compared with protein levels in wild type: *$P < 0.05$, **$P < 0.01$.

3.2.2 cpSRP43 and cpSRP54 interact directly with PORs

Arabidopsis mutants lacking either cpSRP43 or cpSRP54 show a reduced PORB content (Figure 3.19A-B). Thus, it was aimed to verify whether a direct or indirect effect of the two cpSRP factors is responsible for the lower PORB content. I conducted a BiFC assay to examine the physical interaction between the two cpSRP proteins and POR enzymes. The N-terminal half of the split yellow fluorescent protein (YFPn) was fused to cpSRP, and the C-terminus was fused to the proteins of interest: PORA, PORB, PORC, CHLM and CPP1, respectively. The two complementary gene constructs were transiently co-expressed in epidermal and parenchymal cells of *Nicotiana benthamiana* leaves. CHLM and CPP1 were regarded as a negative control for the protein-protein interaction approach. The YFP signals were observed after expression of fusion proteins containing cpSRP and PORs, but not for the combination cpSRP43 and CHLM or cpSRP54 and CPP1. As a result, the two cpSRP proteins interact with PORs (Figure 3.19A and 3.19D).

To confirm the direct interaction between cpSRP43 and PORs, I also performed the in vitro and in vivo pull-down assay. In in vitro assays, purified recombinant GST and GST-cpSRP43 (5 μM) were used as baits and incubated with 10 μM recombinant His-PORs. The proteins bound to the GST-cpSRP43, or GST were eluted with elution buffer containing 10 mM reduced glutathione. Input and elution fractions were probed with the indicated antibodies. The presence of PORs in the eluate together with GST-cpSRP43, but not with GST suggests the direct interaction between both proteins (Figure 3.19B). The in vivo pull-down assay was repeated with purified recombinant proteins GST and GST-cpSRP43 (10 μM) as baits, which were incubated with purified intact chloroplasts. Proteins bound to cpSRP43 were eluted with elution buffer containing 10 mM reduced glutathione and detected by immunoblotting using the indicated antibodies. In *Arabidopsis*, among the three isoforms of PORs , PORB is the dominant isoform in green tissue (Runge et al., 1995). PORB was selected to represent all POR isoforms and CHLM acted as a negative control. The presence of PORB and the absence of CHLM in the eluate fraction confirm the direct interaction between cpSRP43 and PORB (Figure 3.19C). However, due to the time limitation, in vitro experimental evidence for the direct interaction between cpSRP54 and PORs are still lacking, which will be conducted in the future. Taken together, the BiFC and the pull-down assays reveal the direct interaction between cpSRP and PORs and further corroborate the direct impact of missing cpSRP in *chaos* and *ffc* against PORB.

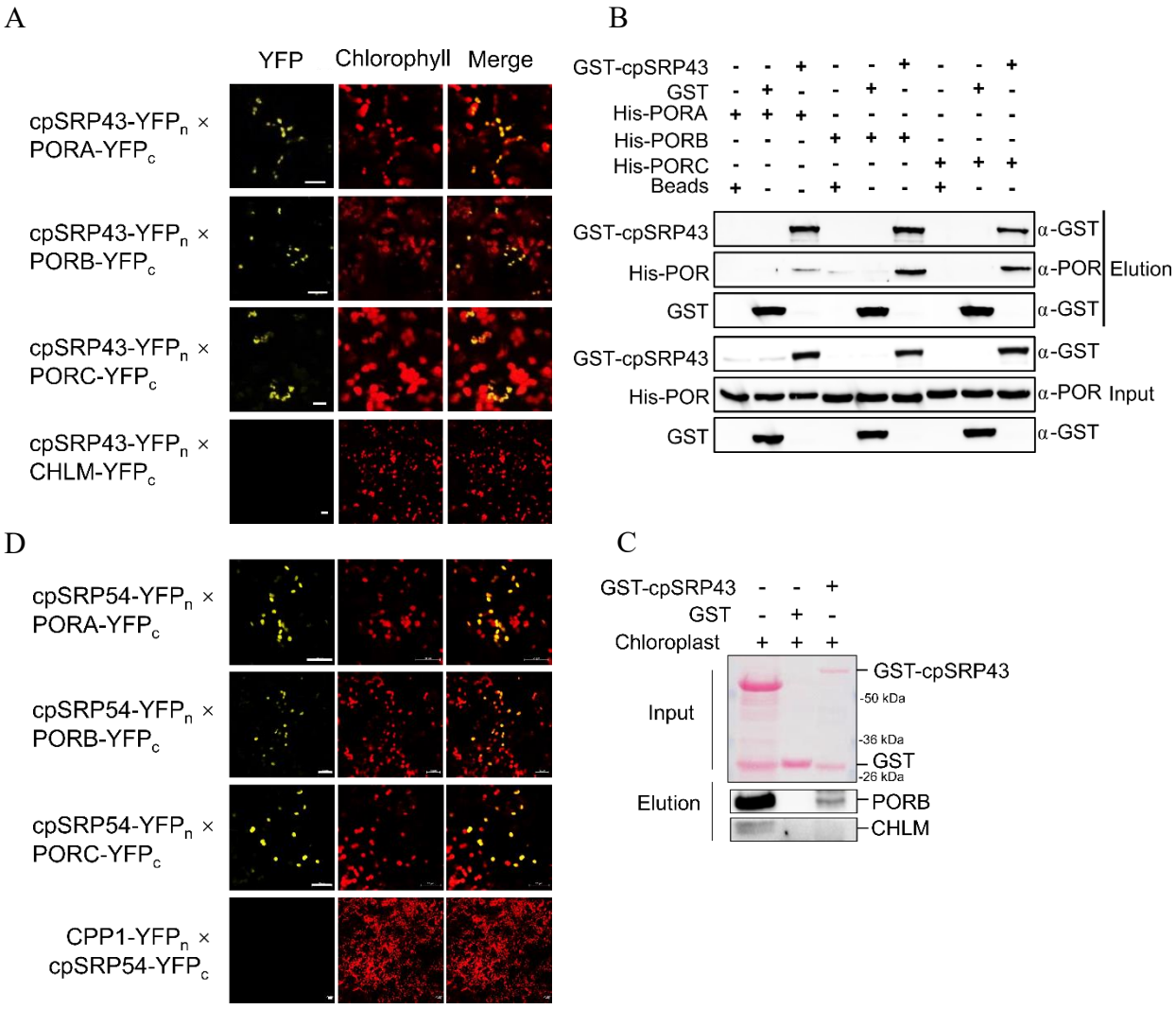

Figure 3.19 Physical interaction of cpSRP components with PORs. A, The BiFC assay demonstrates that cpSRP43 and cpSRP54 both interact with PORs. The co-expression of cpSRP43-YFPn with CHLM-YFPc served as the negative control, and that of PORA/PORB/PORC-YFPc with cpSRP43-YFPn served as the positive control. Scale bars, 20 μm. **B,** PORs bound to cpSRP43 were detected by in vitro GST pull-down assay. Recombinant purified GST-cpSRP43 (5 μM) was used as bait and incubated with His-tagged PORs (10 μM). The proteins bound to GST-cpSRP43, or GST were eluted with buffer containing 10 mM reduced glutathione. The input and elution fractions were analyzed by immunoblot using the indicated antibodies. **C**, The in vivo pull-down assay. 10 μM GST-cpSRP43 was used as bait and incubated with isolated intact chloroplast extracts. Proteins bound to cpSRP43 were detected by immunoblotting using the indicated antibodies. The intact chloroplast extract and elution fractions were visualized by staining of nitrocellulose membranes with Ponceau S. CHLM acts as a negative control. **D**. BiFC demonstrates that cpSRP54 interacts with the three POR isoforms. The co-expression of cpSRP54-YFPn with CPP1-YFPc served as the negative control. Scale bars, 20 μm.

3.2.3 cpSRP43 does not affect the enzymatic activity of PORs

In angiosperms, POR isoforms are strictly light-dependent enzymes that catalyze the reduction of Pchlide to Chlide by means of NADPH as electron donor (Masuda and Takamiya, 2004).

Since cpSRP43 has already been proved to physiologically interact with all PORs, I planned to examine whether the cpSRP43-POR interaction affects the enzymatic activity of POR. Therefore, I overproduced and purified recombinant POR and constituted in vitro the POR/ NADPH/ Pchlide ternary complex to assess the potential effects of additional factors on the Pchlide reduction. The results demonstrated that the enzymatic activity of PORs was not altered significantly independent of the absence or presence of cpSRP43 (Fig. 3.20A-C). It is proposed that cpSRP43 does not modulate the enzymatic activities of the POR isoforms in vitro.

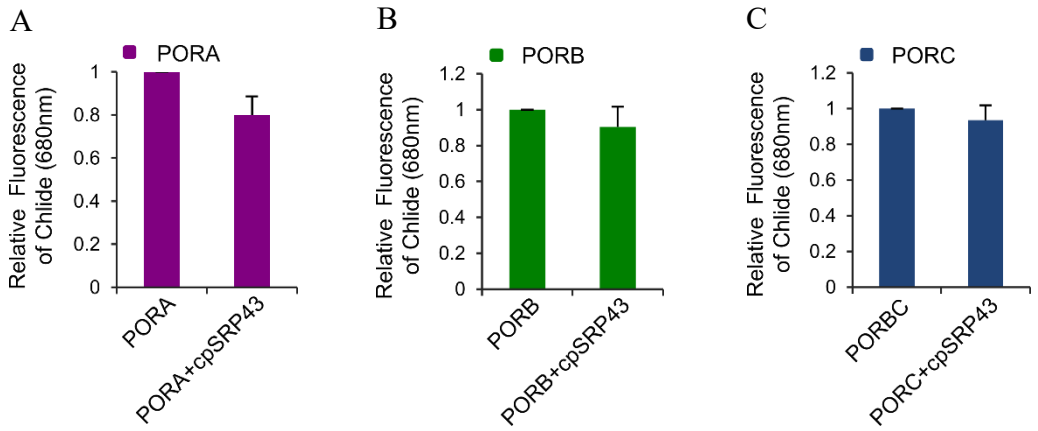

Figure 3.20 In vitro enzymatic activity assays of PORs. After pre-incubation of Pchlide (2 µM) and NADPH (100 µM) in assay buffer, the fluorescence intensity of emission at 680 nm (Chlide) was immediately recorded as the zero-time point. The subsequently recorded fluorescence intensity at 680 nm once PORs (1 µM) or pre-incubated PORs-cpSPR43 (1 µM for each) were present in the assay buffer represents the enzyme activity. Excitation wavelength: 440 nm, scan range for emission fluorescence is 600-720 nm with scan speed of 240 nm/min. **A**, Relative PORA activity. **B**, Relative PORB activity. **C**, Relative PORC activity. The data are plotted as means ± s.d. (n = 3 independent biological repeats). The statistical analysis was performed using two-tailed Student's t-tests. No asterisks here indicate no significant effects on the enzyme activity.

3.2.4 In vitro chaperone activity of cpSRP43 and cpSRP54 on PORB

3.2.4.1 cpSRP43 protects PORB from heat-induced aggregation

cpSRP43 has been reported acts as a chaperone to prevent LHCP(Falk and Sinning, 2010; Jaru-Ampornpan et al., 2010) and GluTR(Wang et al., 2018) from aggregation in vitro scattering assy. In the previous chapter (see chapter 3.1), it was also shown that cpSRP43 can stabilizes GluTR, CHLH and GUN4 for maintaining Chl biosynthesis under heat shock conditions in vivo planta experiments. Based on the ability of cpSRP to interact with PORB, I was wondering whether cpSRP also protects PORB against heat-induced aggregation. Therefore, I applied a light scattering approach to study the chaperone activity of cpSRP towards 2 µM PORB in vitro to assess the POR aggregation. As shown in Figure 3.21A, I found that PORB alone significantly forms aggregates at 42 °C. When the concentration of applied cpSRP43 was less than that of PORB, the protein aggregation was more intensive, however, the aggregation of PORB was diminished with increasing cpSRP43 concentrations when they exceed the amount of PORB (Figure 3.21A), indicating that cpSRP43 protects PORB from heat-induced aggregation in a dose-dependent ratio. Consistently, as a negative example, the truncated

cpSRP43ΔSBD (see chapter 3.1.5) showed no protection towards PORB. On the other hand, when the protective impact of cpSRP54 was assayed for PORB stability, PORB was not relieved from the heat-induced aggregation, which was even more exacerbated with increasing amounts of cpSRP54 (Figure 3.21B). It is proposed that cpSRP54 does not protect PORB from heat-induced protein aggregation. What's more, cpSRP54 alone also forms the heat-dependent aggregates (Figure 3.21C). In summary, it is concluded that a higher concentration of cpSRP43 compared to the target protein PORB correlates with increasing chaperone activity, which can protect PORB from heat-induced aggregation.

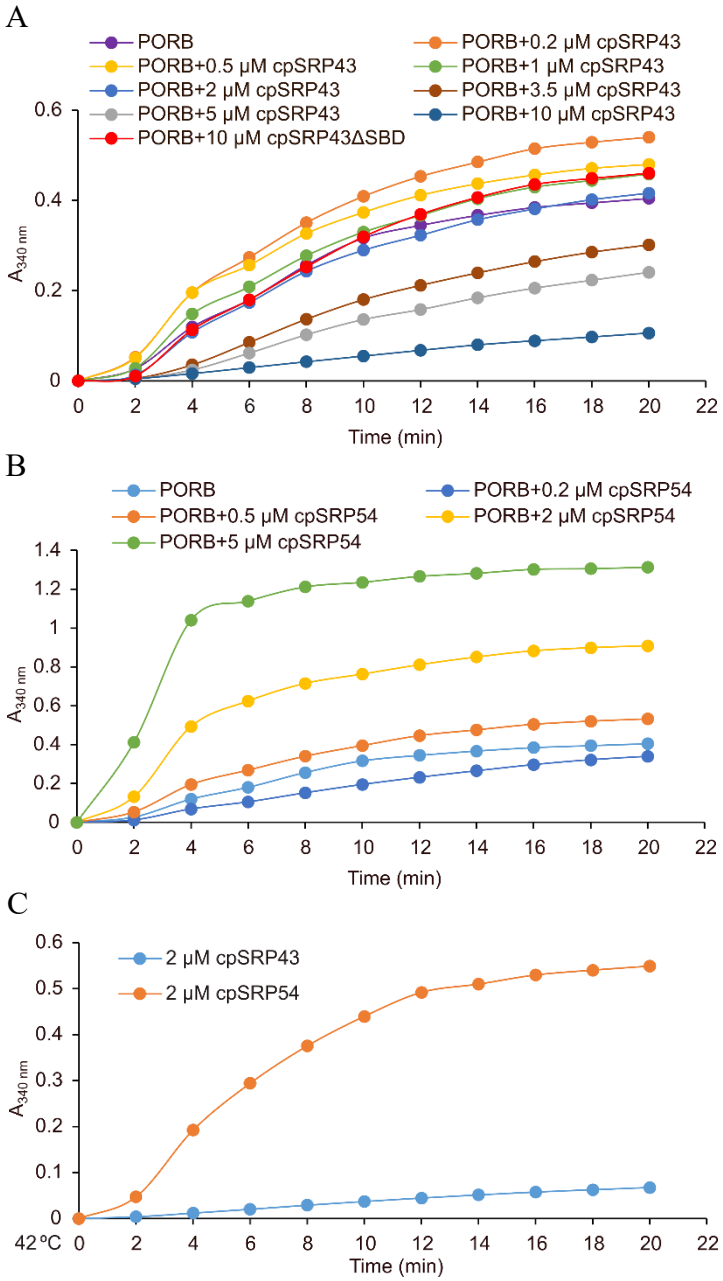

Figure 3.21 Chaperone activity of the cpSRP components against heat-induced aggregation of PORB. Absorbance at 340 nm ($A_{340\ nm}$) was measured at 2 min intervals to quantify turbidity. Thermal aggregation of His-PORB (2 µM) was examined for 20 min at 42°C with increasing amounts of His-cpSRP43 (**A**), His-cpSRP54 (**B**). In addition, indicated amounts

of separately applied cpSRP43 and cpSRP54 were also assayed for the aggregate formation at elevated temperature in the course of the assay (**C**).

3.2.4.2 cpSRP43 and cpSRP54 protect PORB from oxidation-induced aggregation

Most of the tetrapyrrole intermediates, including Pchlide, are strong photosensitizers, when they accumulate as free molecules in excess amounts and produce ROS upon photooxidation, causing oxidative damage and cell death (Ledford and Niyogi, 2005; Li et al., 2009). PORB is a light-operating enzyme which reduces Pchlide to Chlide, two chlorins that are potent photosensitizers (Reinbothe et al., 1996; Sperling et al., 1997; Buhr et al., 2008). Oxidative stress causes oxidation of the amino acid residues, in particular of Met and Cys, which leads to protein destabilization and denaturation (Berlett and Stadtman, 1997; Stadtman, 2006). It is hypothesized that PORB is carefully protected by chaperones against ROS-dependent oxidation and aggregation (Lee et al., 2013). Therefore, I intended to explore the role of the cpSRP components for the prevention of PORB from denaturation and aggregation, which are induced by oxidative stress. As shown in the Figure 3.22A-B, PORB alone forms aggregates in 5 mM or 10 mM H_2O_2. When lower or equal amounts of cpSRP43 were applied to PORB (2 µM cpSRP43), the POR aggregation was aggravated (Figure 3.22A). But its aggregation was gradually reduced with an increasing amount of cpSRP43 relative to POR content (Figure 3.22A). It is proposed that cpSRP43 protects PORB from oxidation-dependent aggregation when more cpSRP43 is available than the client POR (cpSRP43: PORB >1). The supply of cpSRP54 surprisingly reduced the tendency of POR aggregation (Figure 3.22B), suggesting that cpSRP54 could also contribute to protection of PORB against oxidation-induced aggregation, but not in a strict concentration-dependent manner.

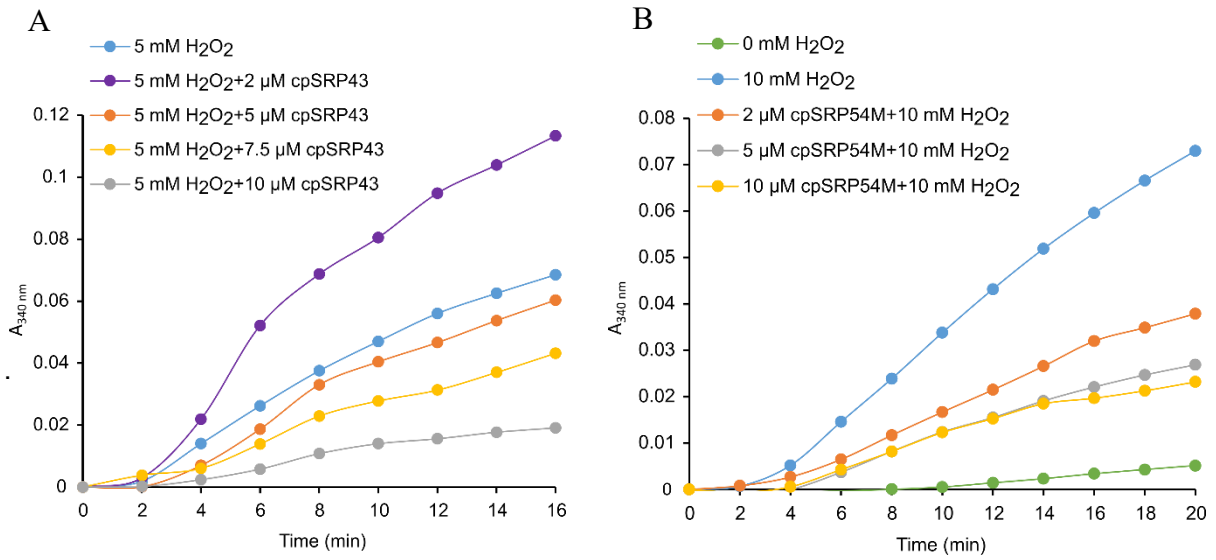

Figure 3.22 Chaperone activity of cpSRP on PORB against oxidation-dependent aggregation. $A_{340\ nm}$ was measured at 2 min intervals to quantify turbidity. Protein aggregation of His-PORB (2 µM) in 5 mM or 10 mM H_2O_2 was examined for 20 min with increasing amounts of His-cpSRP43 (**A**) or His-cpSRP54 (**B**). One representative result out of two similar results is here represented.

3.2.5 cpSRP43 protects PORB against heat shock in planta

In order to test whether cpSRP could also chaperone PORB to be preserved from heat stress in vivo, I applied a 2 h 42 °C heat shock treatment to Ler-0, *chaos*, *cpSRP434-OX*, *ffc* and Col-0. In comparison to Ler-0 and *cpSRP43-OX*, I found that the PORB level in *chaos* was significantly reduced after heat treatment (Figure 3.23A-B), while the *PORB* transcript content was unaltered in all three genotypes (Figure 3.23C). In contrast, PORB levels were unaltered in both *ffc* and wild type even after 4 h heat treatment (Figure 3.23D-E), indicating in consistency with the in vitro scattering assays that only cpSRP43 protects PORB against heat shock. In addition, PORC has apparently to use another mode of control. An unaltered PORC level after 2 h heat treatment at 42 °C indicates that PORC is likely more tolerant to heat stress than PORB (Figure 3.23A-B).

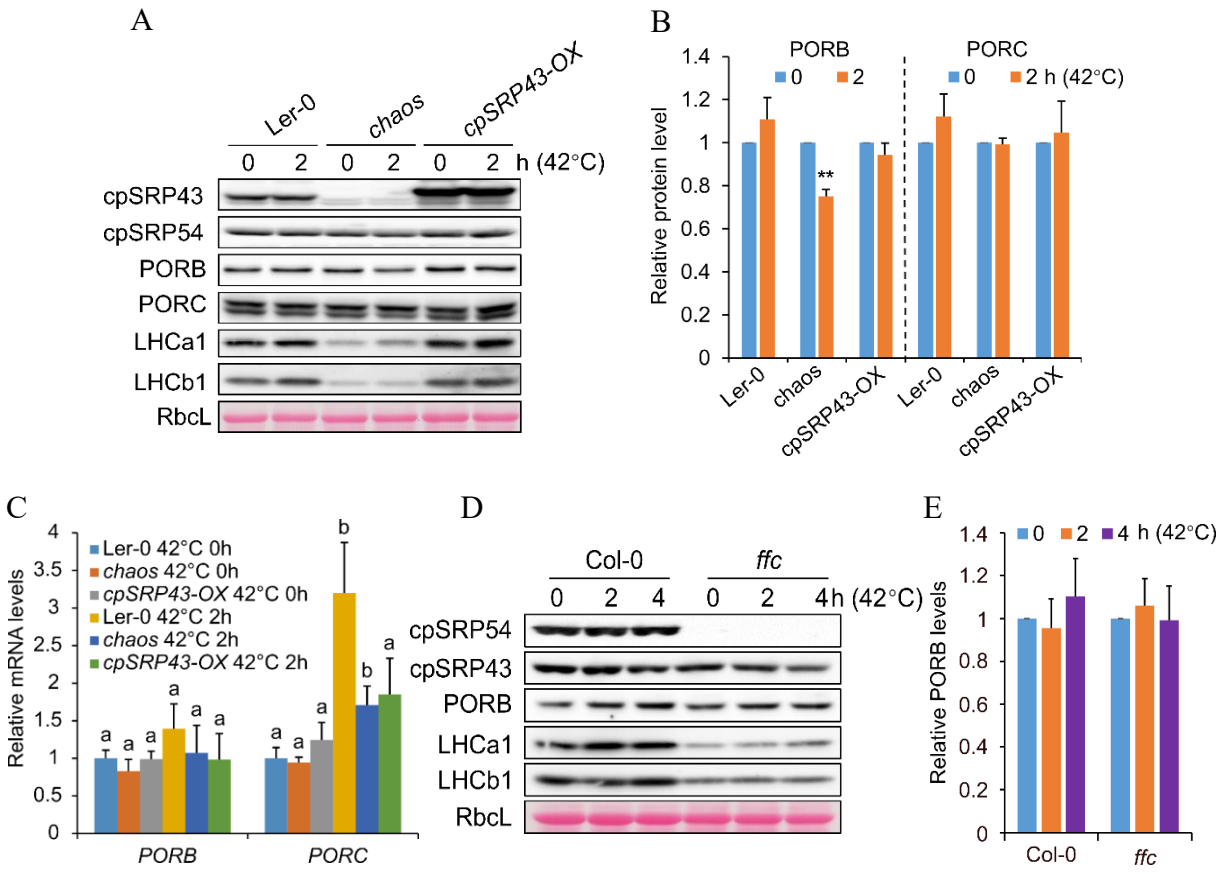

Figure 3.23 cpSRP43 improves the thermostability of PORB against heat shock. A and **D**, Steady-state levels of the indicated proteins in Ler-0, *chaos*, *cpSRP43-OX* (**A**) and in Col-0, *ffc* (**D**) seedlings before and after the indicated hours of heat treatment at 42 °C were quantified by immunoblotting using the indicated antibodies. The Ponceau S-stained RbcL is shown as a loading control. **B** and **E**, Semiquantitative analysis with Image J software (NIH) of the immunoblots from **A (B)** and **D (E)**. The relative amounts of PORB and PORC in Ler-0, *chaos* and *cpSRP43-OX* (**B**) and PORB in *ffc* and Col-0 (**D**) were normalized to their levels before heat treatment. The data are plotted as means ± s.d. ($n = 3$ independent biological repeats). The statistical analysis was performed using two-tailed Student's *t*-tests. The asterisks indicate significant differences compared with protein levels before heat treatment: $*P < 0.05$, $**P < 0.01$. **C,** Relative mRNA levels of indicated genes in 18-day-old Ler-0, *chaos* and *cpSRP43-*

OX were measured prior to and after 2 h heat treatment at 42 °C. Gene expression was calculated relative to the Ler-0 and *SAND* was used as the reference gene. The data are plotted as mean ± s.d. (n = 3 independent biological repeats). Letters above histograms indicate significant differences as determined by two-way ANOVA with Tukey test ($P < 0.05$).

3.2.6 The SBD domain is sufficient for cpSRP43 to protect PORB

SBD and CD2 are essential for cpSRP43's chaperone activities towards GluTR, CHLH and GUN4 (see chapter 3.1). I aimed to clarify whether SBD and CD2 of cpSRP43 are also required for its chaperone activity on PORB. In a genetic approach, a series of *chaos* complementation lines that constitutively express either FL-cpSRP43 or truncated cpSRP43 variants lacking one of the four cpSRP43 domains were generated to characterize the functional role of specific domains of cpSRP43 for the PORB stability. Looking at the phenotypes of these transgenic lines, it became obvious that the deletion of either CD1 or the Ank domain in the SBD of cpSRP43 did not compensate for the phenotype of *chaos* (Figure 3.24A). In contrast, expression of either the truncated cpSRP43ΔCD2 or cpSRP43ΔCD3 completely rescued the pale-green phenotype of *chaos* (Figure 3.24A). Regarding the steady-state level of PORB, deletion of the Ank domain in SBD led to a significant reduction of the PORB level in *cpSRP43ΔAnk-OX* compared to that in wild type. However, this reduced POR content was not observed, when the truncated cpSRP43ΔCD2 or cpSRP43ΔCD3 were expressed in the *chaos* background (Figure 3.24A). In addition, the complementation line *cpSRP43(SBD)-OX* shows a wild-type-like phenotype and the PORB level is comparable with that in Ler-0 (Figure 3.24B). These experimental findings directly indicate that SBD is sufficient for the protective role of cpSRP43 on PORB. However, it is still not entirely clear whether the sole SBD is sufficient for the chaperone activity of cpSRP43 on PORB during heat shock. Therefore, I applied 2–4 h of heat treatment to the *cpSRP43(SBD)-OX*, *cpSRP43ΔCD2-OX* and *cpSRP43ΔCD3-OX* and determined the alteration of PORB levels in these transgenic lines. The significantly reduced levels of GUN4 found in the *cpSRP43 (SBD)-OX* and *cpSRP43ΔCD2-OX* lines after heat shock are in agreement with the previous finding that protection of GUN4 requires the SBD and CD2 domains of cpSRP43 (Figure 3.24C-D). In contrast, after a 2–4 h heat treatment of 42 °C, PORB levels were not altered among these transgenic lines (Figure 3.24C-D), indicating unlike GUN4 that the possible protective interaction for chaperone function of cpSRP43 with PORB occurs with SBD.

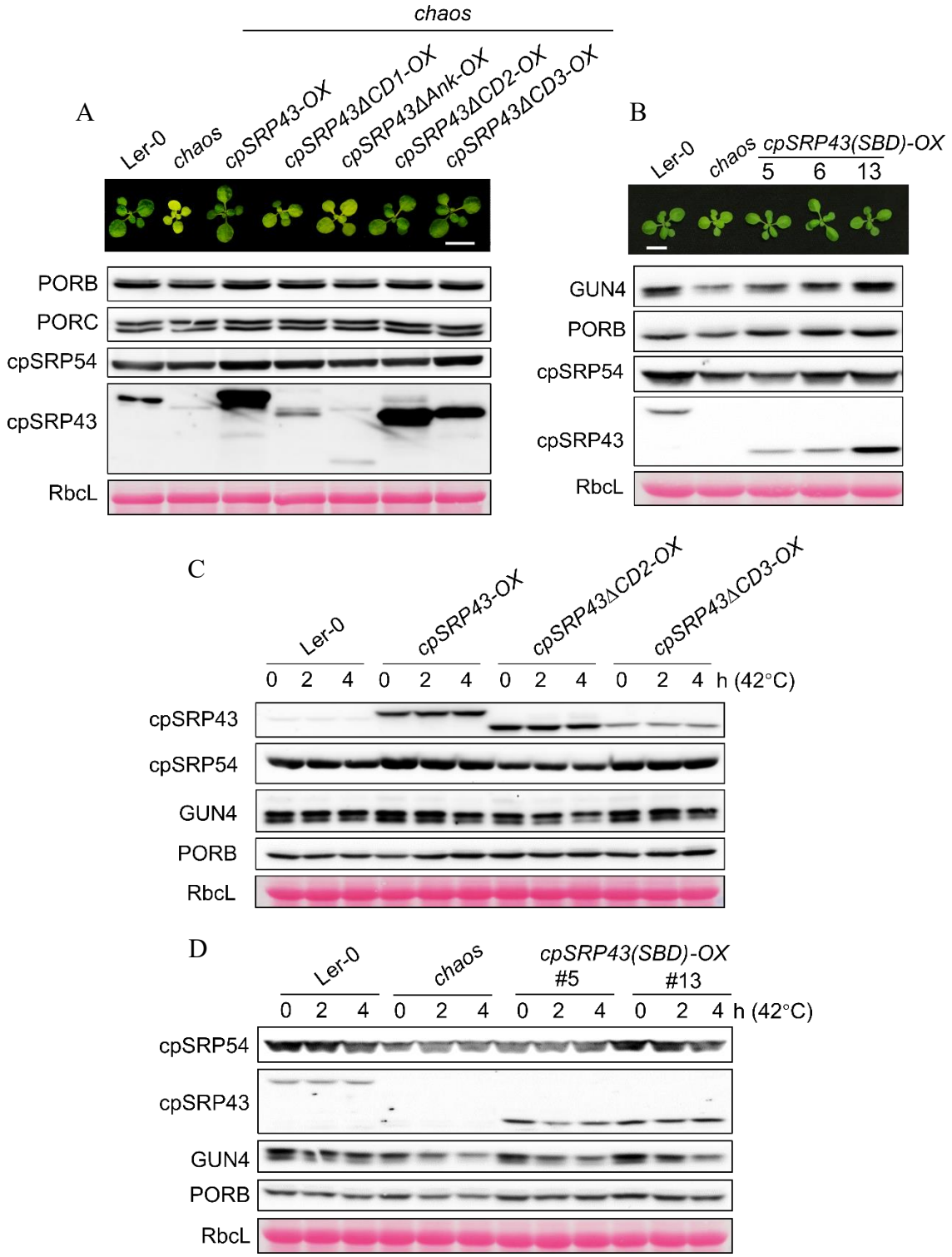

Figure 3.24 The chaperone activity of cpSRP43 on PORB requires the SBD. A, A representative image of Ler-0, *chaos* and the indicated *chaos* complementation lines (top panel) and steady-state levels of the indicated cpSRP43, cpSRP54 and TBS proteins (lower panels) in these indicated lines. **B**, A representative image Ler-0, *chaos* and *cpSRP43(SBD)-OX* seedlings (top panel) and steady-state levels of the indicated cpSRP43, cpSRP54 and TBS proteins (lower panels) in Ler-0, *chaos* and *cpSRP43(SBD)-OX*. **C**, Steady-state levels of cpSRP43, cpSRP54 and TBS proteins in Ler-0, *cpSRP43-OX*, *cpSRP43ΔCD2-OX* and *cpSRP43ΔCD3-OX* seedlings before (0 h at 42 °C) or after 2–4 h of heat treatment (2–4 h at 42 °C) were detected by immunoblotting using the indicated antibodies. **D**, Steady-state levels of cpSRP43, cpSRP54

and TBS proteins in Ler-0, *chaos* and *cpSRP43(SBD)-OX* before (0 h at 42 °C) or after 2–4 h of heat treatment (2–4 h at 42 °C) were detected by immunoblotting using the indicated antibodies. 18-day-old seedlings were harvested. The standard growth condition is 16 h light/8 h dark, 100 µmol photons m^{-2} s^{-1} and the Ponceau S-stained RbcL is shown as a loading control.

3.2.7 cpSRP54 is involved in the membrane association of PORB

As described in chapter 3.2.1.2, cpSRP54 post-translationally stabilizes PORB (Figure 3.18A-C). In order to explore how cpSRP54 stabilizes PORB, I firstly performed an in vitro scattering assay to explore if cpSRP54 also acts as a chaperone to protect PORB from protein aggregation. However, I found that cpSRP54 itself was sensitive to higher temperature during this assay because aggregation of cpSRP54 was determined (Figure 3.25C). Moreover, the deficiency of cpSRP54 in *ffc* did not affect the content of PORB in response to the heat shock treatment (Figure 3.25C). Therefore, cpSRP54 is proposed not to protect PORB from aggregation. But it remained open, how cpSRP54 stabilizes PORB.

It is accepted that cpSRP54 guides LHCP during trafficking to the thylakoid membrane by binding to the receptor protein cpFtsY. At this last step, cpSRP54 probably acts as an optimizing element that maintains the transit complex in an ideal insertion-competent state, thereby making the transport process more efficient (Ziehe et al., 2018). It was speculated that cpSRP deficiency would significantly reduce the amount of membrane-associated LHCPs. Figure 25A typically reflects the effect of cpSRP on LHCa/b translocation: LHCa/b are membrane-bound proteins as they were only found in the membrane fraction. The LHCa/b levels were significantly decreased in the single mutant *chaos* and *ffc*, and became almost undetectable in the double mutant *chaos/ffc* (Figure 3.25A), suggesting that cpSRP43 and cpSRP54 cooperatively transport LHCa/b to the thylakoid membrane.

PORB in *Arabidopsis* is a thylakoid membrane-associated protein although it does not contain a transmembrane domain, such as the L18 of LHCPs. I hypothesize that cpSRP54 is involved in the transport and targeting of PORB to the thylakoid membrane. Similar to the experiment by which the effect of cpSRP on LHCPs translocation has been verified (Schünemann et al., 1998) (Figure 3.25A), chloroplasts were separated into the membrane and soluble fraction (methods see 2.13). Aliquots of the two fractions were separated on SDS-PAGE gel. As a result, the distribution of membrane-associated and soluble PORB was achieved and presented from wild type, *chaos*, *ffc,* and *chaos/ffc* samples. I also assessed the ratio of membrane-associated versus soluble amounts of PORB. As shown in Figure 3.25B-C, the absence of cpSRP43 in *chaos* or concurrent absence of cpSRP54 in double mutant *chaos*/*ffc*, did not affect the relative quantitative ratio of membrane-bound and soluble PORB. However, in *ffc* mutant, I found that the ratio of membrane-associated PORB was significantly reduced compared to the wild type (Figure 3.25B-C), indicating that the cpSRP54 deficiency compromises the amount of membrane-associated PORB. It is proposed that cpSRP54 is involved in the trafficking and association of PORB to the membrane. In summary, the cpSRP components can act as chaperones to protect PORB against denaturation caused by high temperature and oxidative stress. cpSRP54 may assist in the attachment of PORB to thylakoids.

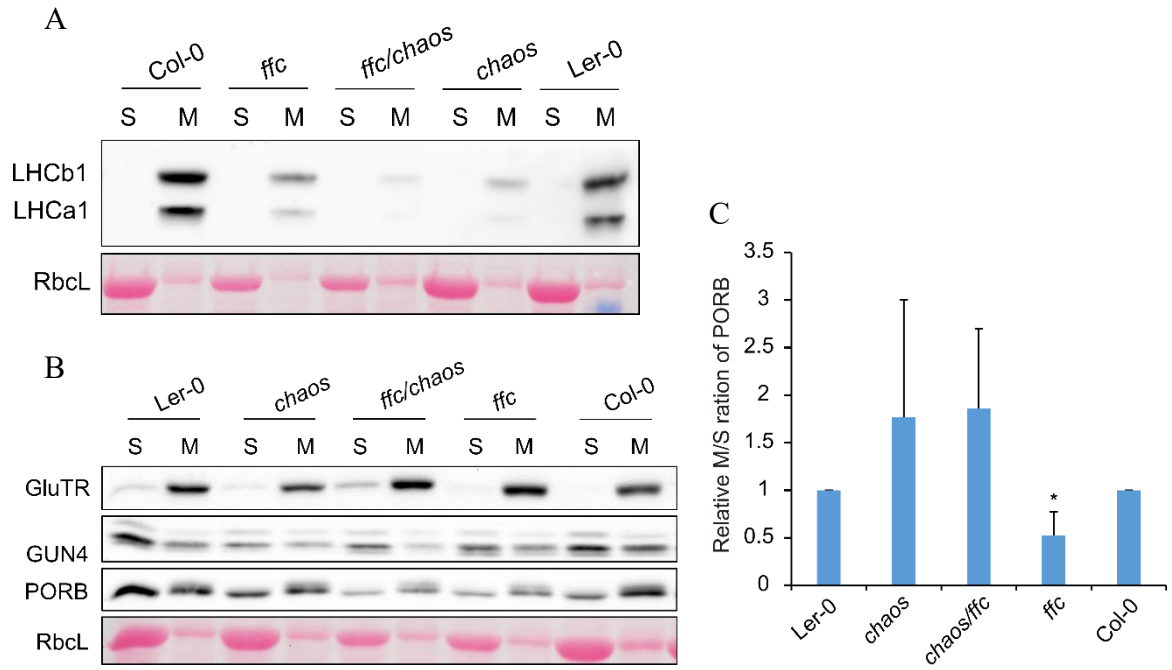

Figure 3.25 cpSRP54 is involved in the membrane association of PORB. A, Immunoblot analysis of membrane-bound (M) and soluble (S) LHCb1 and LHCa1 in Ler-0, *chaos*, *chaos/ffc*, *ffc* and Col-0 plants grown under standard conditions. **B**, M and S fractions of GluTR, GUN4 and PORB were also analyzed in these plants. The Ponceau S-stained RbcL is shown as a loading control**. C**, Relative M/S ratio of PORB in *chaos*, *chaos/ffc* and *ffc* were normalized that in wild type. The data are plotted as means ± s.d. (n = 3 independent biological repeats). The statistical analysis was performed using two-tailed Student's t-tests. The asterisks indicate significant differences compared with protein levels in wild type: *P < 0.05, **P < 0.01.

3.3 Functional analysis of the aggregation-prone region (APR) in GluTR

The aggregation-prone region (APR) is usually hidden in the core of protein in an aqueous environment since this portion of the amino acid sequence belongs to the hydrophobic polypeptide. The APR could be exposed on the surface when the protein is mis- or unfolded, which tends to form a strong intermolecular contact with the analogous sequences in a neighboring protein such as β-sheet structures, thereby leading to the protein aggregation (Meric et al., 2017).

In *Arabidopsis*, GluTR is the rate-limiting enzyme in the TBS pathway, which is encoded by the gene *HEMA1*. It has been reported that there are two APRs at the N-terminus of the GluTR. Interestingly, overexpression of *HEMA1* in *Nicotiana tabacum* or *Arabidopsis thaliana* did not display a corresponding increase in ALA synthesis rate, but instead, an increase of GluTR aggregates (Schmied et al., 2011; Wang et al., 2018). The protein aggregation of GluTR indicates that overexpression of *HEMA1* in vivo cannot accumulate GluTR as the excess GluTR will form protein aggregation and is degraded. The solubility of the truncated recombinant GluTR with deletion of the two APRs at the N-terminus was significantly improved in vitro, implying that APRs are responsible for GluTR aggregation in vitro (Wang et al., 2018). However, the functions of APRs of GluTR in vivo are still unknown. Whether APRs in planta are also responsible for the aggregation of GluTR and whether the accumulation of GluTR is achieved by modifying the APRs in planta still remains to be further studied.

3.3.1 Generation and analysis of APRs deletion mutants

Structural domains of a typical GluTR are shown in the Figure 3.26A. At the N-terminus there is a regulatory domain (RED) (Richter et al., 2019), followed by the catalytic domain, the NADPH binding domain and the dimerization domain, and finally at the C-terminus there is the FLU binding domain (FBD) (Wang et al., 2018). Algorithm analysis found that the two APRs of GluTR are both in the catalytic domain and close to the RED domain (Wang et al., 2018). In order to explore the function of APRs in GluTR, I generated APRs deletion mutants in the background of *hema1* (*HEMA1* knockout) named *HEMA1ΔAPR1*, *HEMA1ΔAPR2* and *HEMA1ΔAPR1/2*, which expressed the truncated GluTRΔAPR1, GluTRΔAPR2 and GluTRΔAPR1/2, respectively (Figure 3.26B).

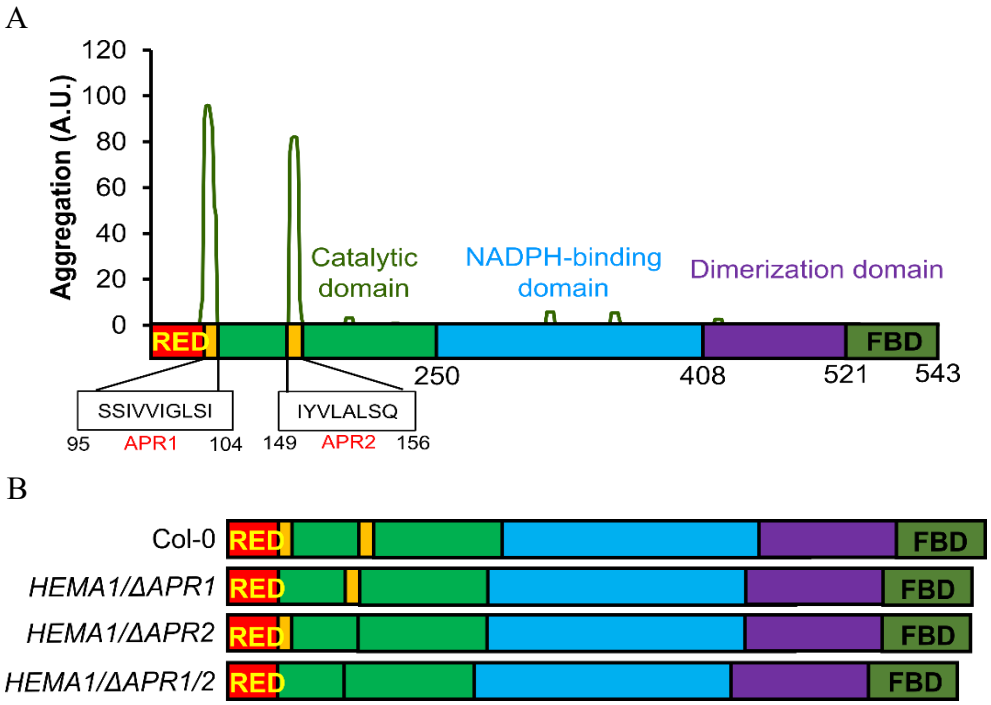

Figure 3.26 Schematic overview of GluTR and its truncated types. A, GluTR sequence was analyzed with the TANGO algorithm, which identified regions that are predicted to be prone to aggregation. The sequences of two APRs (yellow) are indicated below. **B**, Schema of the truncated GluTRΔAPR1, GluTRΔAPR2 and GluTRΔAPR1/2, which was expressed in the transgenic lines *HEMA1ΔAPR1*, *HEMA1ΔAPR2* and *HEMA1ΔAPR1/2*, respectively. RED, regulatory domain. FBD, FLU binding domain.

Genotyping showed that the T-DNA fragments were successfully amplified, while the lack of amplification of the *HEMA1* gene confirmed the homozygous background of *heam1*, and the successful amplification of the transgenes indicated that the corresponding transgenic fragments were successfully transformed into *hema1*. Taken together, this genotyping showed that the APRs deletion mutants were constructed correctly as I expected (Figure 3.27A). Phenotyping of the seedlings of all different APR deletion mutants revealed that their yellow leaves and retarded growth were similar to the properties of *hema1* (Figure 3.27B). These observations are consistent with the analyzed ALA synthesis rates and Chl contents (Figure 3.27C-D), indicating that the lack of APRs severely impaired the GluTR function and, thereby, abolished the Chl biosynthesis.

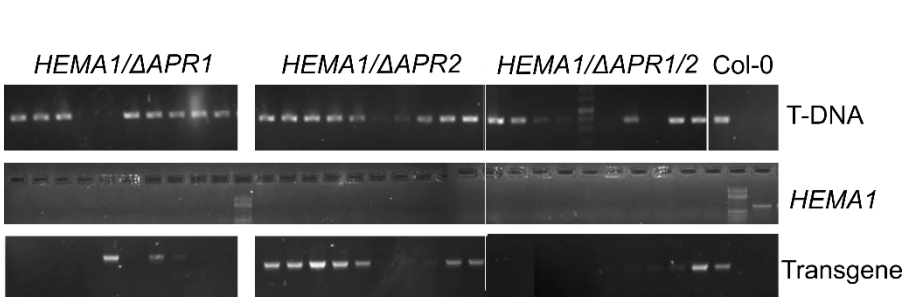

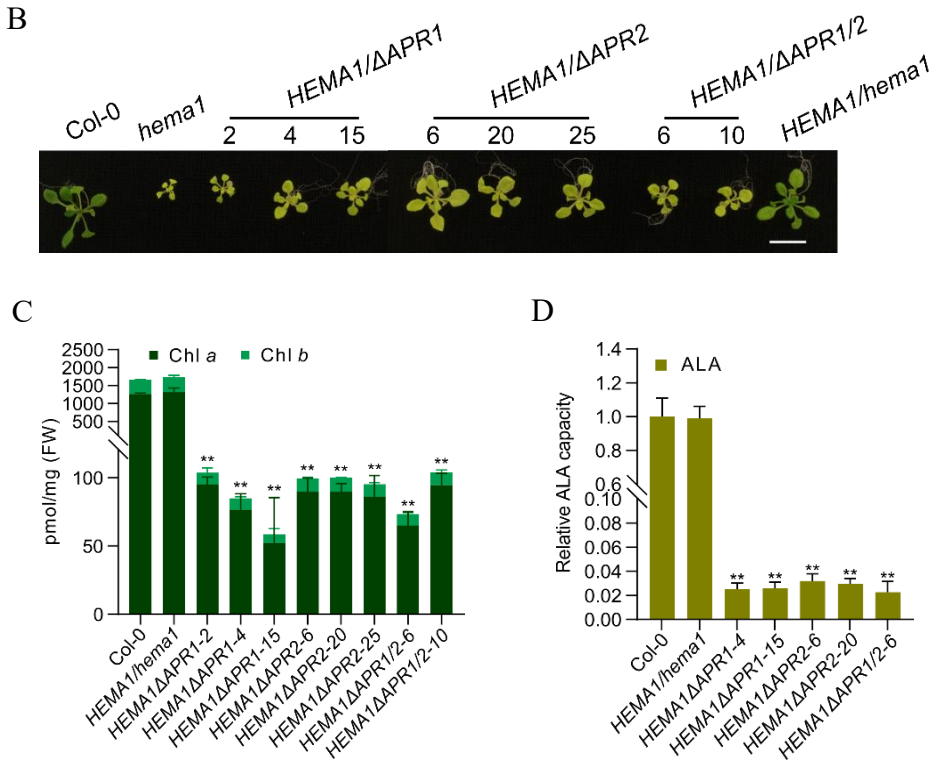

Figure 3.27 APRs deletion mutants showed severely impaired Chl biosynthesis. A, PCR analyses of genomic DNA from the Col-0, *HEMA1ΔAPR1*, *HEMA1ΔAPR2* and *HEMA1ΔAPR1/2* confirmed the correct construct of the APRs deletion mutants. **B**, An image with representatives of 16-day-old Col-0, *hema1*, *HEMA1/hema1*, *HEMA1ΔAPR1*, *HEMA1ΔAPR2* and *HEMA1ΔAPR1/2* plants grown under standard conditions (16 h light/8 h dark, 100 µmol photons m^{-2} s^{-1}). Scale bar, 1 cm. **C-D**, Chl content (**C**) and ALA synthesis rate (**D**) in 16-day-old plants grown under the same conditions as in **B**. FW, fresh weight. All values are plotted as means ± s.d. (n = 3 independent samples). The statistical analysis was performed using two-tailed Student's *t*-tests. The asterisks indicate significant differences compared with the corresponding levels in Col-0: *P < 0.05, **P < 0.01.

3.3.2 APR deletion compromises the stability and activity of GluTR

Immunoblot analysis of the GluTR levels in the APRs deletion mutants indicated that only a decreased GluTR level was detected in *HEMA1ΔAPR2*-20, while accumulation of GluTR variants in the other genotypes was not detectable (Figure 3.28A). In order to exclude that reduced or undetectable GluTR levels are due to the low transcriptional level, I performed a qRT-PCR to analyze the transcript levels of *HEMA1* in the APRs deletion mutants. The results showed that the transcript of *HEMA1* was higher in *HEMA1ΔAPR2*-20, while in other lines wild type-like transcript levels were determined (Figure 3.28B). This finding could be one explanation, why GluTR was only detectable in *HEMA1ΔAPR2*-20. Considering a barely detectable ALA synthesis rate in *HEMA1ΔAPR2*-20 (Figure 3.28D), it was concluded that the APR2 deletion abolished the activity of GluTR, while – even more important – the GluTR without APR(s) are extremely instable. Other APRs deletion mutants such as *HEMA1ΔAPR1*-4 and *HEMA1ΔAPR1/2*-6, showed more accumulation of *HEMA1* RNA expression than Col-0, although no GluTR content was detectable (Figure 3.28A-B). Taken together, the APR deletion

dramatically affects the integrity of GluTR and compromised the stability and activity of GluTR in planta. However, it should be pointed out that the two GluTR-APRs are located at the N-terminal catalytic domain. Their deletion would inevitably affect the enzyme activity and the structural integrity of GluTR. Hence, the described approach with deleted APR fragments turned out to be inappropriate to assess the function of APRs in GluTR. Therefore, I intended to continue with another strategy to unravel the function of APRs in GluTR and envisaged to substitute single amino acid residues within the APRs.

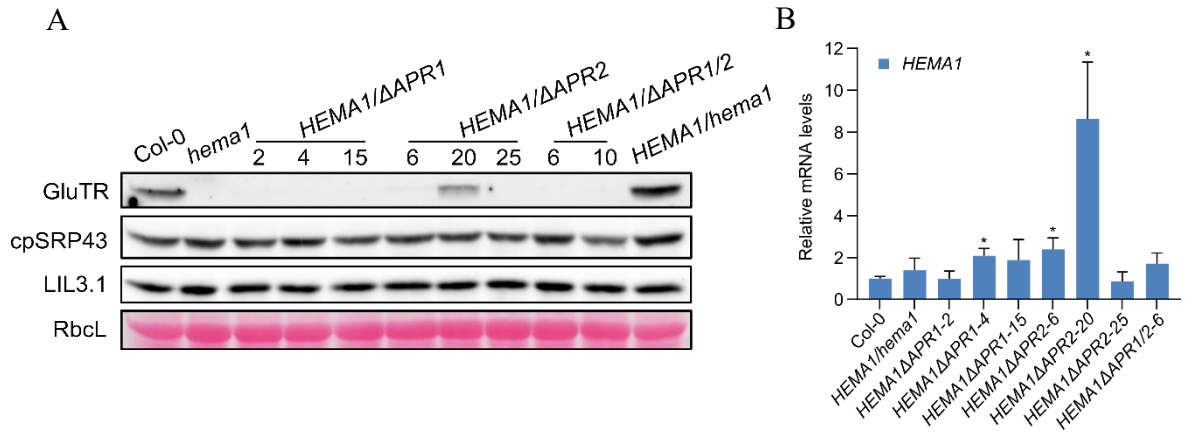

Figure 3.28 The deletion of APRs dramatically affects the integrity of GluTR. A, Steady-state levels of GluTR, cpSRP43, LIL3.1 in 16-day-old Col-0, *hema1*, *HEMA1/hema1*, *HEMA1ΔAPR1*, *HEMA1ΔAPR2* and *HEMA1ΔAPR1/2* grown under standard growth condition were quantified by immunoblotting using the indicated antibodies. The Ponceau S-stained RbcL is shown as a loading control. **B**, The relative quantities of mRNA content of *HEMA1* in different indicated genotypes. The *HEMA1* expression levels in all transgenic lines were normalized to that in Col-0 using *SAND* as the reference gene. All values are plotted as means ± s.d. (n = 3 independent s). The statistical analysis was performed using two-tailed Student's t-tests. The asterisks indicate significant differences compared to *HEMA1* mRNA levels in Col-0: *$P < 0.05$.

3.3.3 The substitution of amino acid residues in the two GluTR-APRs

It turned out that the deletion approach of APRs in the GluTR structure was too careless. In order to investigate the roles of APRs for GluTR aggregation, a strategy was intended to replace the APR with a stretch of amino acid residues, which minimizes the effects of APR, but keeps the activity and integrity of GluTR. The most straightforward approach was to exchange a single amino acid residue, making the APR a non-APR peptide motif. Therefore, the algorithm TANGO was used to evaluate the aggregation tendency of the modified APRs after a single amino acid substitution (Fernandez-Escamilla et al., 2004). As expected from the mechanism of β-aggregation, aggregating regions are strongly enriched in aliphatic hydrophobic residues Val (V), Leu (L), Ile (I), as well as in aromatic residues Phe (F), Tyr (Y) but also Trp (W) (Rousseau et al., 2006). The flanks of aggregation-prone regions are enriched with charged residues and proline (P), the so-called gatekeeper residues (Reumers et al., 2009). For the case of GluTR in this study, the Val, Leu, and Ile are enriched in the APRs. In addition, it has been reported that the substitution of Val-251 and Ile-254 by two prolines (P) that lowers the aggregation propensity (Richardson and Richardson, 2002) in the BIN2249-257 APR,

completely abolished its aggregation capacity (Betti et al., 2016). Thirdly, I replaced the single amino acid in APR with Pro one by one and predicted the aggregation tendency of the point mutated APR by TANGO. I found that the substitution of Val-99 or Val-151 by Pro completely abolished the aggregation. These suggest that Val might be a good target for amino acid substitution.

As shown in Figure 3.29B-C, I chose two kinds of amino acids to replace the Val as the approach for amino acid substitution: Val→Pro and Val→Thr substitution. Because Val and Pro are basic amino acids, and Val and Thr are different only in one group ($-CH_3$ in Val while -OH in Thr) (Figure 3.29A). By using the TANGO software, it was assessed that a replacement of Val with Pro, the aggregation tendency of both APRs is abolished. When Val was replaced by Thr, the aggregation tendency of APR1 and APR2 was reduced by 50% and 80%, respectively (Figure 3.29B-C), indicating that the two experimental approaches of amino acids substitution might be a better way to reduce the aggregation-prone tendency of APRs without disturbing the entire structure of GluTR and, consequently its activity and integrity of GluTR.

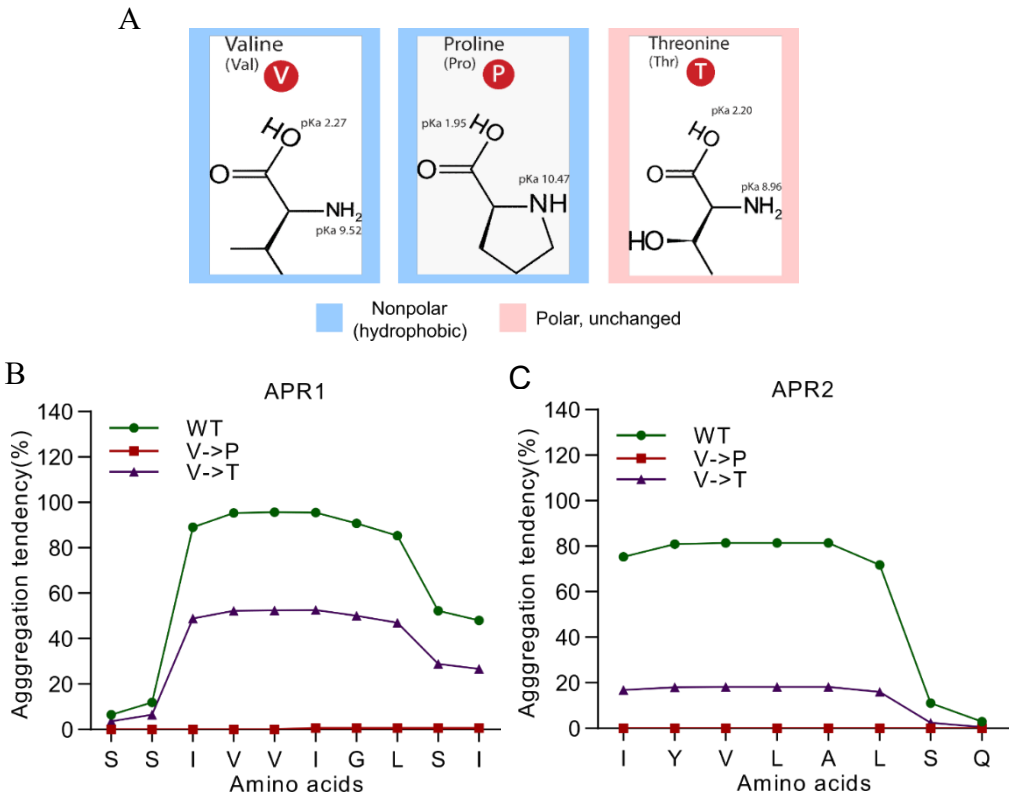

Figure 3.29 An amino acid residue substitution in APRs predictably abolishes the tendency of aggregation. A, Structural formula and a reference to the hydrophobic properties of amino acids Val (V), Pro (P) and Thr (T). **B**, the amino acid substitutions of APR1 and APR2 were analyzed with the TANGO algorithm. The original (green), V→P substituted (red) and V→T substituted (purple) APR-sequences are plotted against their aggregation tendency.

3.3.4 Generation and analysis of APRs point mutants

3.3.4.1 Phenotype of the APRs point mutants

I generated APRs point mutants, in which the point mutated *HEMA1* sequences were driven by itself *HEMA1* promoter in the background of *hema1*. The transgenic lines were named *HEMA1 (V99P/V151P)* and *HEMA1 (V99T/V151T)*, which expressed the point mutated GluTR (V99P/V151P) and GluTR (V99TV151T). Genotyping (not shown) and sequencing confirmed that the point mutants *HEMA1 (V99P/V151P)* and *HEMA1 (V99T/V151T)* were successfully generated (Figure 3.30B). Phenotypic analysis showed that the selected lines expressing *HEMA1 (V99T/V151T)* showed a wild-type like growth, while *HEMA1 (V99P/V151P)* exhibited yellow seedlings and severe growth retardation, similar to the severe phenotype of *hema1* (Figure 3.30A). The different phenotypes of lines expressing either *HEMA1 (V99P/V151P)* or *HEMA1 (V99T/V151T)* indicate that the expression of mutant GluTR corresponds to modified Chl biosynthesis, most likely by deregulation of ALA synthesis rates. It turned out that the ALA synthesis rate of *HEMA1 (V99T/V151T)* was the same as in wild type, while the ALA synthesis rate in *HEMA1 (V99P/V151P)* was drastically decreased (Figure 3.30C-D).

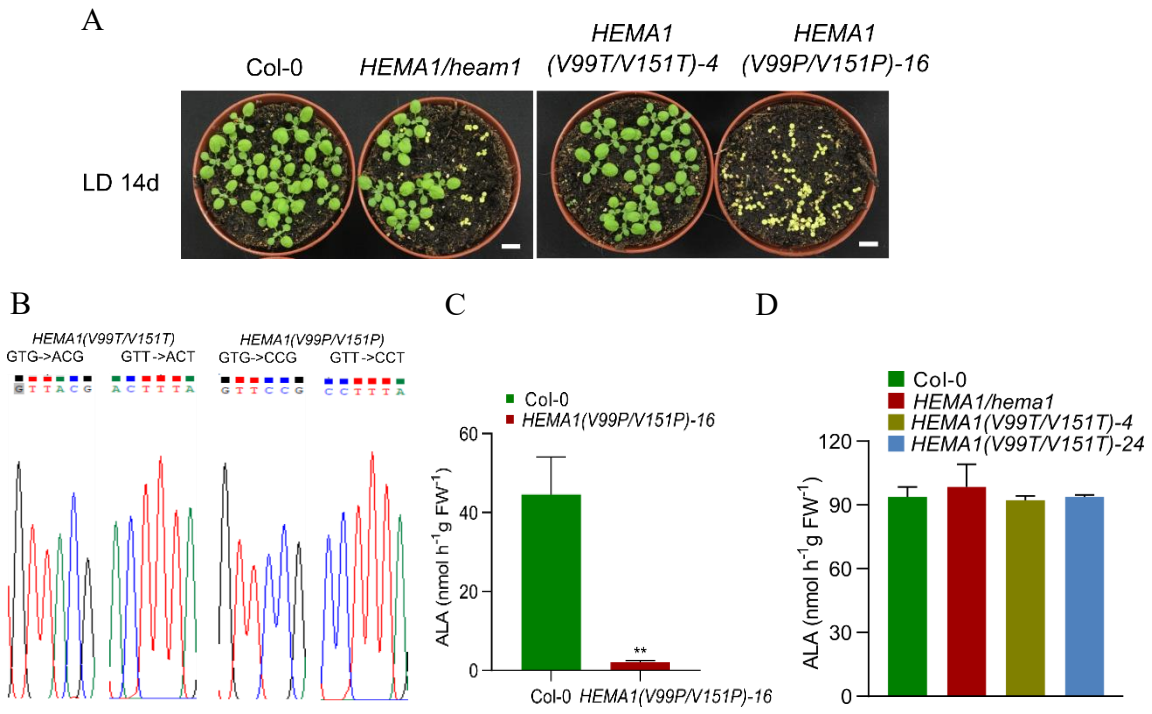

Figure 3.30 Characterization and analysis of the transgenic lines *HEMA1 (V99T/V151T)* and *HEMA1 (V99P/V151P)*. A, A representative image of 14-day-old Col-0, *HEMA1/hema1, HEMA1 (V99T/V151T)-4* and *HEMA1 (V99P/V151P)-16* plants grown under standard conditions (16 h light/8 h dark, 100 µmol photons m^{-2} s^{-1}). Scale bar, 1 cm. **B**, Sequencing confirmed the transformation of coding sequences *HEMA1 (V99T/V151T)* and *HEMA1 (V99P/V151P)* in homozygous lines *HEMA1 (V99T/V151T)* and *HEMA1 (V99P/V151P)*, respectively. **C-D**, ALA synthesis rates in *HEMA1 (V99P/V151P) -16* (**C**) and *HEMA1 (V99T/V151T)-4/24* (**D**) grown under standard growth conditions. All values are plotted as means ± s.d. (*n* = 3 independent samples). The statistical analysis was performed using two-

tailed Student's *t*-tests. The asterisks indicate significant differences compared with the corresponding levels in Col-0: *$P < 0.05$, **$P < 0.01$.

3.3.4.2 GluTR (V99T/V151T) improves the stability of GluTR

qRT-PCR and immunoblotting were applied to analyze the transcript and protein levels of GluTR in the *HEMA1 (V99P/V151P)* and *HEMA1 (V99T/V151T)* lines. The *HEMA1* transcript level in *HEMA1 (V99P/V151P)* was comparable to that in wild type, while the GluTR content was significantly reduced (Figure 3.31A-B), suggesting that V→P mutation reduces the stability of GluTR. The compromised steady-state level of GluTR (V99P/V151P) in *HEMA1 (V99P/V151P)* correlated with the almost abolished ALA synthesis rate (Figure 3.31C), suggesting that the V→P mutation also impairs the enzymatic activity of GluTR. Taken together, the V→P mutation likely caused a more negative effect on the integrity of GluTR, and therefore, the stability and activity of GluTR were compromised.

In contrast, although the transcript level of *HEMA1* in *HEMA1 (V99T/V151T)-24* was equivalent to that of wild type (Figure 3.31B), the protein level of GluTR (V99T/V151T) was slightly increased 27% (Figure 3.31D-E). In consistency with the wild-type like GluTR (V99T/V151T) content in *HEMA1 (V99T/V151T)-4*, the almost 50% reduced transcript levels suggest that the V→T mutation could slightly improve the stability of GluTR (Figure 3.31B-E). However, the ALA synthesis rates in both *HEMA1 (V99T/V151T)-4* and *HEMA1 (V99T/V151T)-24* were comparable with those in wild type (Figure 29D), suggesting that V→T mutation does not impair the ALA synthesis rate. Considering the accumulated GluTR in *(V99T/V151T)-24*, it suggests that the V→T mutation could also inactive the activity of GluTR, which can be explained by the location of APR in the N-terminal catalytic domain of GluTR. In summary, slightly increased stability of GluTR could be achieved by substitution of amino acids in APR.

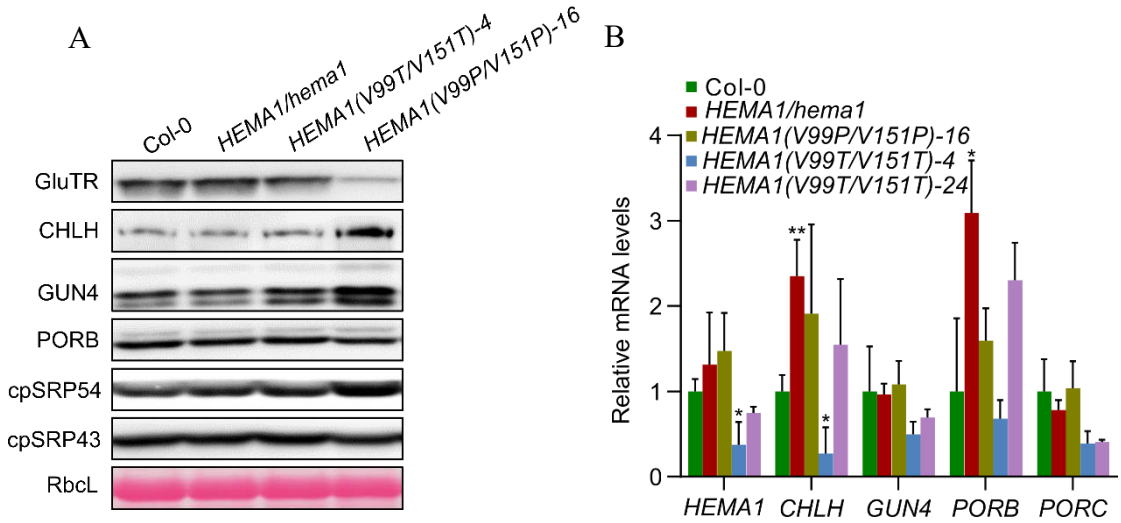

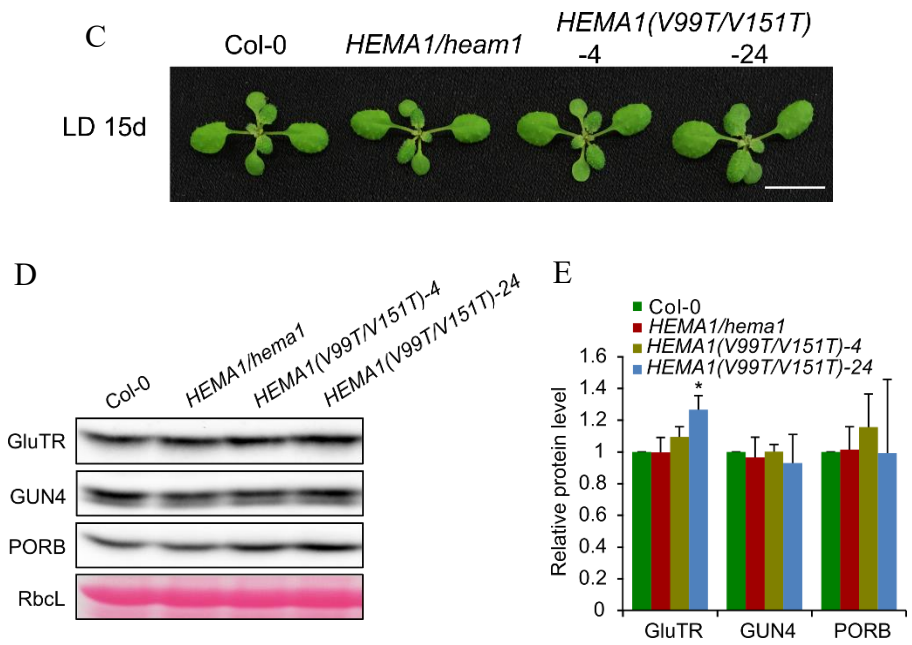

Figure 3.31 Analysis of the transcript and protein levels of GluTR in *HEMA1 (V99P/V151P)* and *HEMA1 (V99T/V151T)*. **A**, Steady-state levels of cpSRP43, cpSRP54 and TBS proteins in 14-day-old Col-0, *HEMA1/hema1*, *HEMA1 (V99T/V151T)* and *HEMA1 (V99P/V151P)* were quantified by immunoblotting using the indicated antibodies. The Ponceau S-stained RbcL is shown as a loading control. **B**, Relative mRNA levels of *HEMA1*, *CHLH, GUN4, PORB and PORC* in Col-0, *HEMA1/hema1*, *HEMA1 (V99T/V151T)* and *HEMA1 (V99P/V151P)*. The gene expression levels were calculated relative to that in Col-0, using *SAND* as the reference gene. **C**, A representative image of 15-day-old Col-0, *HEMA1/hema1, HEMA1 (V99T/V151T)-4* and *HEMA1 (V99T/V151T)-24* plants grown under standard conditions (16 h light/8 h dark, 100 µmol photons m^{-2} s^{-1}). Scale bar, 1 cm. **D**, Steady-state levels of GluTR, GUN4 and PORB in 15-day-old Col-0, *HEMA1/hema1, HEMA1 (V99T/V151T)-4* and *HEMA1 (V99T/V151T)-24* were quantified by immunoblotting using the indicated antibodies. The Ponceau S-stained RbcL is shown as a loading control. **E**, Semiquantitative analysis with Image J software (NIH) of the immunoblots in **D**. The relative amounts of GluTR, GUN4 and PORB in *HEMA1 (V99T/V151T)-4* and *HEMA1 (V99T/V151T)-24* were normalized to the levels in the Col-0. The data are plotted as means ± s.d. (n = 3 independent biological repeats). The statistical analysis was performed using two-tailed Student's t-tests. The asterisks indicate significant differences compared with protein levels in Col-0: *$P < 0.05$.

3.3.4.3 GluTR (V99T/V151T) reduces the aggregation in vitro, does not modulate the oligomerization of GluTR in planta

In order to test whether the GluTR (V99T/V151T), which possesses a predictable tendency of decreased aggregation by TANGO algorithm, can reduce the GluTR aggregation, I investigated the effects of V→T mutation on GluTR aggregation/oligomerization by in vitro and in vivo experimental approaches. In vitro, I expressed and purified the recombinant proteins GluTR (V99T/V151T) and GluTR (Figure 3.32B), and conducted the scattering assays to analyze the formation of GluTR aggregates at 42 °C. As shown in the Figure 3.32A, compared with the wild-type GluTR, the GluTR (V99T/V151T) slightly decreased the heat-induced aggregation

of GluTR by 18-30% in vitro, especially at the time point 4-6 min. This observation suggests that the V→T mutation could increase the stability of GluTR via prevention of its aggregation. In vivo, I performed a Blue Native gel electrophoresis to analyze the GluTR oligomerization in *HEMA1 (V99T/V151T)*, *HEMA1/hema1* and wild type. As shown in the Figure 3.32C-D, GluTR showed a comparable pattern of complex formation in the tested *HEMA1 (V99T/V151T)*, *HEMA1/hema1* and wild type, indicating that the GluTR (V99T/V151T) in vivo does not significantly alter the complex formation of GluTR. Based on the in vivo and in vitro assays, GluTR (V99T/V151T) is proposed to contain slightly inactivated APRs, which do not affect the oligomerization of GluTR in planta.

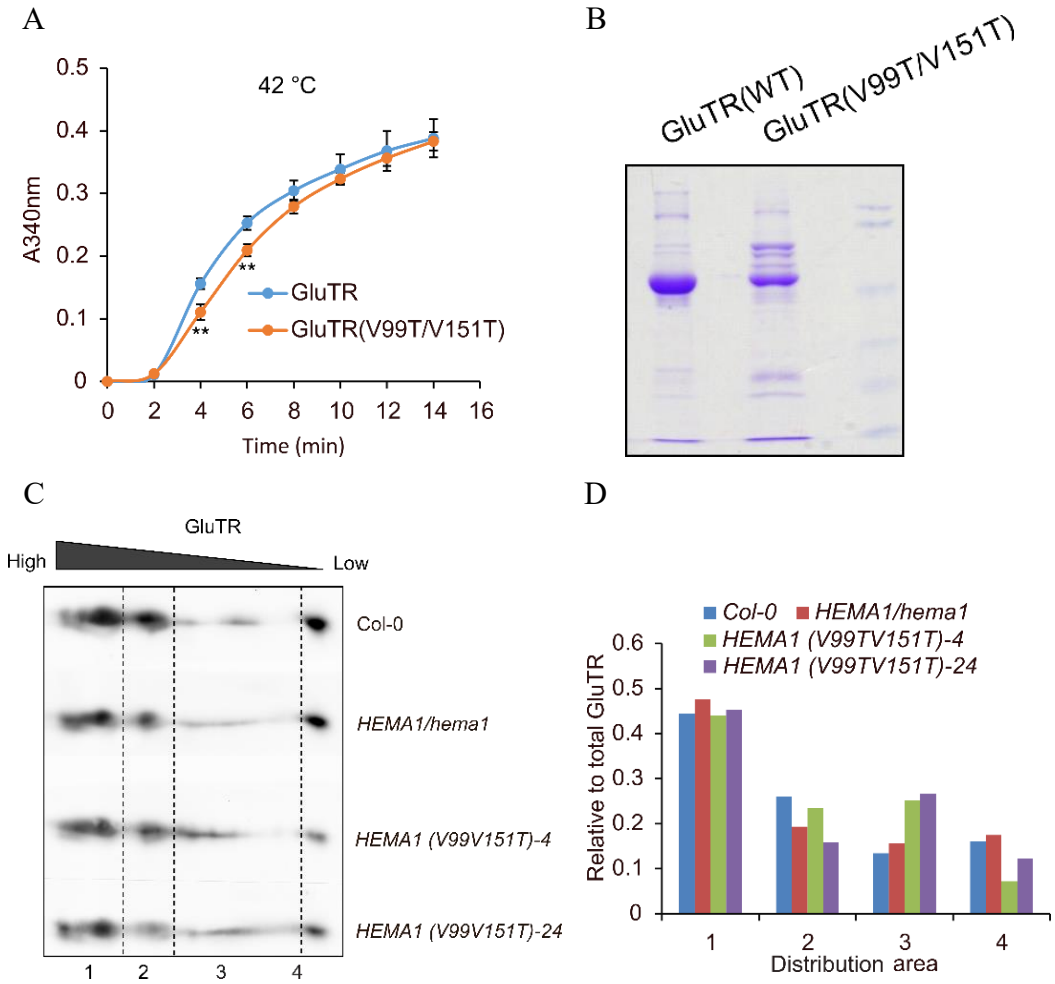

Figure 3.32 Aggregation and oligomerization analyses of GluTR (V99T/V151T). A, Scattering assays to evaluate the heat-induced aggregation of GluTR and GluTR (V99T/V151T). $A_{340\ nm}$ was measured at 2-min intervals to quantify turbidity. Thermal aggregation of His-GluTR and His- GluTR (V99T/V151T) (2 μM) was examined for 14 min at 42°C. The data are plotted as means ± s.d. ($n = 3$ independent biological repeats). The statistical analysis was performed using two-tailed Student's *t*-tests. The asterisks indicate significant differences compared with the aggregate in GluTR: $^{**}P < 0.01$. **B**, Coomassie blue-stained recombinant proteins GluTR and GluTR (V99T/V151T). **C**, Two-dimensional BN-SDS/PAGE analysis of GluTR allocation in chloroplasts isolated from Col-0, *HEMA1/hema1*, *HEMA1 (V99T/V151T)-4* and *HEMA1 (V99T/V151T)-24*. GluTR monomers and oligomers were detected by immunoblotting analysis. **D**, Semiquantitative analysis with Image J software

(NIH) of the immunoblots in **C**. The relative amounts of GluTR in the indicated allocation areas were normalized to the corresponding total GluTR of each plant.

3.3.4.4 GluTR (V99T/V151T) does not modulate the thermostability of GluTR

The APR is suggested to be the cause for the aggregation of GluTR, a heat shock treatment aggravates protein aggregation and reduces protein stability. Therefore, I was asking whether the substitution of the amino acids in the APRs would improve the thermostability of GluTR. I applied heat shock to seedlings of Col-0, *HEMA1/hema1*, *HEMA1 (V99P/V151P)* and *HEMA1 (V99T/V151T)*. The amount of GluTR was measured after 2 h and 4 h heat treatment at 42 °C, and it was found that GluTR of the *HEMA1 (V99T/V151T)* and *HEMA1 (V99P/V151P)* lines similarly degraded compared to wild-type GluTR (Figure 3.33A). Further analysis of the ALA synthesis rates under heat shock was also consistent with the unstable GluTR levels in *HEMA1 (V99P/V151P)* and *HEMA1 (V99T/V151T)* (Figure 3.33B), indicating that both the V→P and V→T mutations cannot increase the thermostability of GluTR under heat shock.

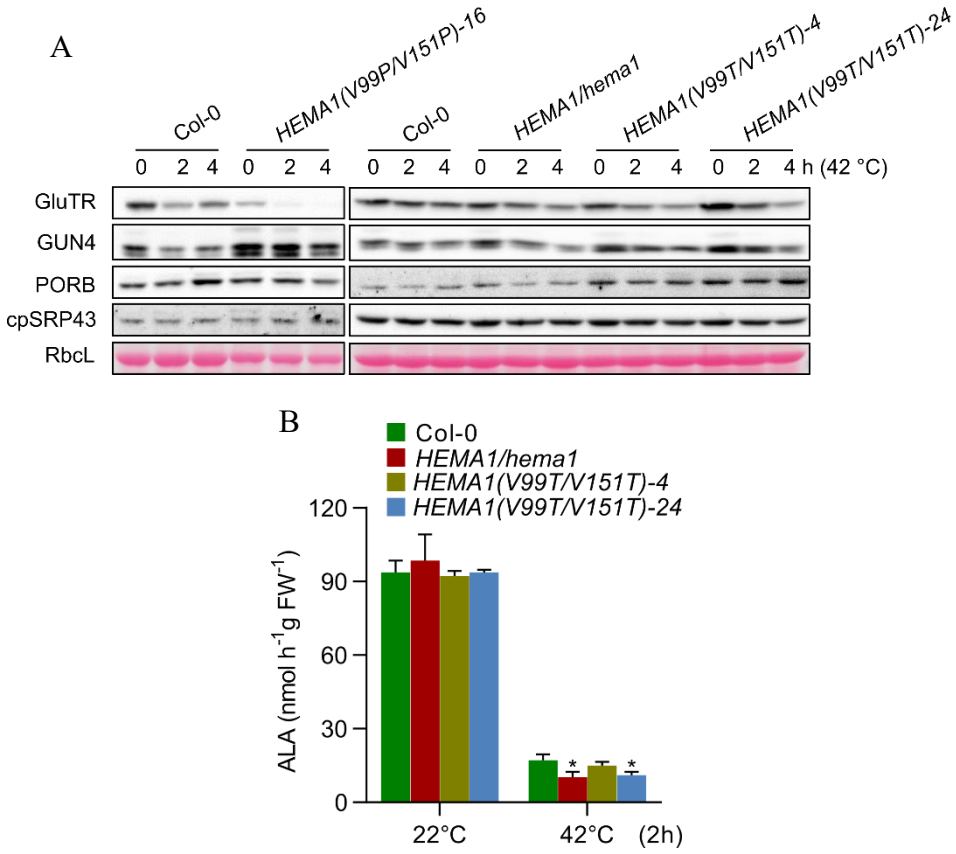

Figure 3.33 Amino acids substitution of GluTR cannot improve the thermostability of GluTR. A, Steady-state levels of GluTR, GUN4, PORB and cpSRP43 in 16-day-old Col-0, *HEMA1/hema1*, *HEMA1 (V99P/V151P)-16*, *HEMA1 (V99T/V151T)-4*, and *HEMA1 (V99T/V151T)-24* before (0 h at 42 °C) or after 2–4 h of heat treatment (2–4 h at 42 °C) were detected by immunoblotting using the indicated antibodies. The Ponceau S-stained RbcL is shown as a loading control. B, The ALA synthesis rates in Col-0, *HEMA1/hema1*, *HEMA1 (V99T/V151T)-4* and *HEMA1 (V99T/V151T)-24* were determined under standard (22°C) and heat shock conditions (42°C 2 h). The data are plotted as means ± s.d. (n = 3 independent

biological repeats). The statistical analysis was performed using two-tailed Student's t-tests. The asterisks indicate significant differences compared with protein levels in Col-0: *P < 0.05, **P < 0.01.

3.3.4.5 GluTR (V99T/V151T) enhances the stability of GluTR in darkness

Apitz et al. reported that GluTR is gradually degraded by ClpC in the dark, thereby inhibiting the ALA synthesis to avoid the accumulation of toxic intermediates in darkness (Apitz et al., 2016). Therefore, I was wondering whether the GluTR (V99T/V151T) could affect the rate of degradation of GluTR during dark incubation. I moved *HEMA1 (V99T/V151T)*, *HEMA1/hema1* and wild type to darkness for indicated time. The degradation of GluTR was determined after 16 h and 24 h dark treatment, GluTR in the *HEMA1 (V99T/V151T)* lines were degraded more slowly than that in the wild type (Figure 3.34A-B). It is assumed that the point mutation of GluTR lowered the degradation rate of GluTR. Therefore, improved the stability of GluTR in the dark can be proposed.

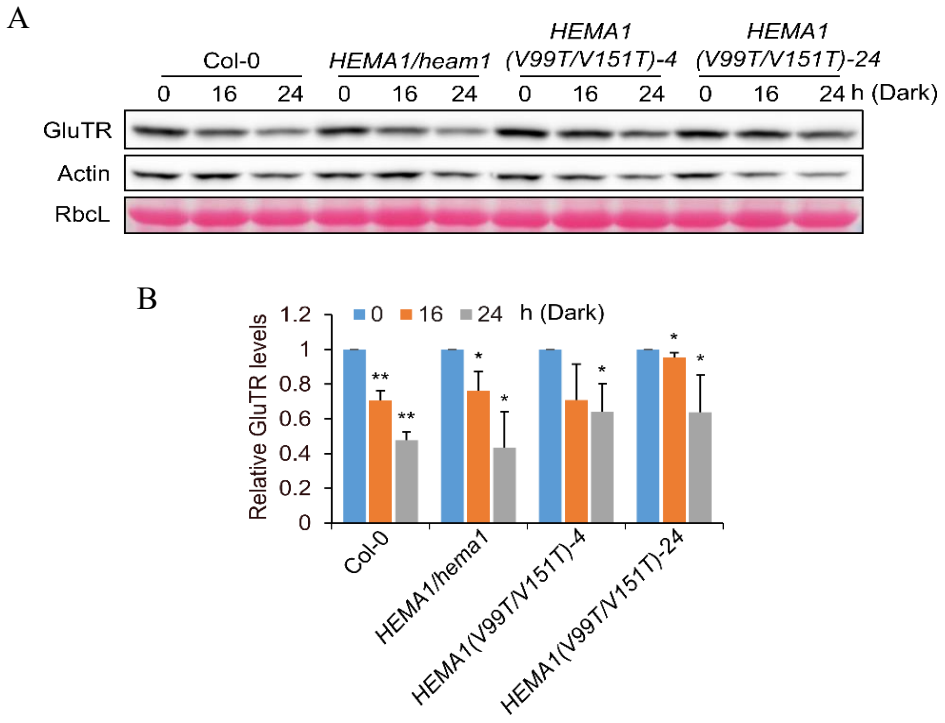

Figure 3.34 V→T mutation improves the stability of GluTR in darkness. A, Steady-state levels of GluTR in 16-day-old Col-0, *HEMA1/hema1*, *HEMA1 (V99T/V151T)-4* and *HEMA1 (V99T/V151T)-24* before (0 h dark) or after 16-24 h of dark treatment were detected by immunoblotting using the indicated antibodies. The Ponceau S-stained RbcL and Actin are shown as a loading control. **B**, Semiquantitative analysis with Image J software (NIH) of the immunoblots in **A**. The relative amounts of GluTR were normalized to their levels before being transferred to the dark treatment (0 h in dark). The data are plotted as means ± s.d. (n = 3 independent biological repeats). The statistical analysis was performed by using two-tailed Student's *t*-tests. The asterisks indicate significant differences relative to each ecotype before dark treatment (0 h dark): *P < 0.05, **P < 0.01.

In summary, my studies show that (1) the APRs contribute substantially to the 3D structure and

conformation of GluTR, which is important for the integrity of GluTR, and the APR deletion dramatically reduces the stability and activity of GluTR. (2) It was presumed that the V→P mutation of GluTR abolishes the aggregation tendency, but the experiments indicate that this replacement of amino acid residues strongly affects the integrity of GluTR, and therefore, compromises the stability and activity of GluTR. (3) The V→T mutation of GluTR was suggested to inactive the APR, which could slightly improve the stability of GluTR by preventing its aggregation. (4) V→T mutation could affect the GluTR degradation and improve the stability of GluTR in the dark. Overall, my study demonstrates that the reduced aggregation and elevated stability of GluTR can be achieved by reducing the aggregation tendency of APR. Although in the V→T mutation, the alterations of aggregation and stability of GluTR are minor, it is still possible to slightly reduce the aggregation and increase the stability of GluTR by optimizing the strategies of amino acids substitution.

4 Conclusions and discussion

4.1 Chloroplast SRP43 autonomously protects Chl biosynthesis proteins against heat shock

Chloroplast development requires coordination between Chl biosynthesis and the assembly of LHCPs (Wang and Grimm, 2021). The ATP-independent chaperone function of cpSRP43 mediates the post-translational LHCP translocation to the thylakoid membrane, but also participates in the TBS pathway (Schünemann et al., 1998; Wang et al., 2018). However, it is still not known, how cpSRP43 allocates its tasks to both pathways. Based on previous research in our group, this study intends to comprehensively and deeply explore the regulatory mechanism of cpSPR43 on the TBS pathway, including the search for new TBS clients of cpSRP43, to find out the potential general mechanism, by which cpSRP43 regulates these TBS clients, thereby unraveling the mechanism, how cpSRP43 coordinates Chl synthesis and LHCP biogenesis.

4.1.1 Autonomous chaperone activity of cpSRP43 is crucial for the stability of Chl biosynthesis proteins

Chl biosynthesis is tightly regulated in oxygenic photosynthetic organisms to avoid phototoxicity of free Chl and most of its precursors (Apel and Hirt, 2004). A set of auxiliary factors, such as chaperones, scaffold proteins, and proteases, are required for efficient Chl synthesis in light and rapid shutdown of Chl metabolic flux in the dark (Czarnecki and Grimm, 2012; Brzezowski et al., 2015). In this study, immunoblot analysis of leaf extracts from *chaos* revealed reduced accumulation of the two MgCh components CHLH and GUN4 (Figure 3.2B), while *CHLH* and *GUN4*-mRNA levels were not modified (Figure 3.3D). Thus, a post-translational degradation of these proteins was proposed in response to cpSRP43 deficiency. In line with this assumption, cpSRP43 physically interacts with GluTR, CHLH, and GUN4 (Figure 3.4), suggesting that the effect of cpSRP43 on the stability of GluTR, CHLH and GUN4 relies on direct physical interaction of cpSRP43. While cpSRP43 did not influence the enzymatic activity of MgCh (Figure 3.5), in vivo analyses of protein levels showed that a chaperone function of cpSRP43 is involved in stabilizing GluTR, CHLH and GUN4 under standard growth and heat stress conditions (Figure 3.2A, Figure 3.7A). Therefore, these data identify GluTR, CHLH and GUN4 as new cpSRP43 clients.

The SBD of cpSRP43, which is responsible for the chaperone activity on the LHCP (Liang et al., 2016; Siegel et al., 2020), is not sufficient for interaction with and protection of TBS proteins (Figure 3.9B, Figure3.10B,G). Although the C-terminal CD2 or CD3 motif are required for the stable protein interaction of cpSRP43 with TBS proteins in vitro (Figure 3.10D, C, H, I), in vivo analysis highlights the key role of the SBD+CD2 domains during physical interaction with and thermostabilization of TBS proteins (Figures 3.11 and 3.12). While cpSRP43 alone can act as an ATP-independent chaperone for unfolded LHCP through interaction with SBD of cpSRP43 (Liang et al., 2016; Siegel et al., 2020), the cpSRP43

efficiently prevents pre-folded TBS proteins through interactions with its SBD+CD2. While the reason for the strict necessity of CD2 for chaperoning TBS proteins in vivo remains to be determined, the mechanism by which cpSRP43 interacts with LHCPs is different from that of interaction with TBS proteins.

4.1.2 cpSRP54 modulates chaperone activity of cpSRP43 in a client-dependent manner

The dominant role of the LHCP-cpSRP43-cpSRP54 'transit complex' is the protection and transfer of the hydrophobic LHCPs through the aqueous stroma to the thylakoid membrane-localized Alb3 translocase (Richter et al., 2010; Dunschede et al., 2011; Akopian et al., 2013). The versatile functions evoke the question, how cpSRP43 manage to serve for the two different groups of target proteins?

My study suggests a critical role for cpSRP54 in orchestrating this coordination. cpSRP54 stimulates cpSRP43's chaperone activity on LHCPs by stabilizing the SBD domain of cpSRP43 in a closed, tightly folded conformation (Liang et al., 2016; Siegel et al., 2020). Surprisingly, my data show that cpSRP54 has the opposite effect on the activity of cpSRP43 for TBS clients (Figure 3.13). Thus, cpSRP54 deficiency improved the thermostabilities of TBS proteins and maintained the Chl metabolic flow under heat shock, compared to those in the wild type (Figure 3.13 and Figure 3.14). This finding supports the idea that free cpSRP43, rather than the cpSRP43-cpSRP54 complex, serves as the active chaperone for TBS proteins under heat stress. Given that CD2 forms the binding site for the cpSRP43-cpSRP54M interaction (Jonas-Straube et al., 2001; Holdermann et al., 2012) and is also required for cpSRP43 to provide thermoprotection for TBS proteins (Figure 3.12), I speculate that the protection of TBS proteins requires additional client contacts by means of CD2 that are antagonized by interaction with cpSRP54. The binding of cpSRP54 to cpSRP43 could occlude the binding sites of CD2 for TBS enzymes or force cpSRP43 to adopt a conformation that is incompatible with TBS interaction. Although the mechanistic details behind the cpSRP54-mediated inhibition on cpSRP43 remain to be understood, these results provide compelling evidence that cpSRP54 acts as a switch that directs cpSRP43 either to the trafficking of LHCP or to the maintenance of structural intactness of TBS clients.

4.1.3 cpSRP54-bound cpSRP43 turns to the TBS proteins in response to heat shock

Plants normally experience elevated temperatures in the early afternoon, especially during summertime. Plants have evolved strategies to cope with this daily heat shock, maintain cell integrity and preserve the integrity of crucial cellular processes (Kotak et al., 2007). My results provide evidence that cpSRP43 helps to maintain the stability of TBS clients during short-term heat treatment, thereby promoting the metabolic flow of Chl biosynthesis during maximal sunlight (Figure 3.7 and Figure 3.8). The inhibitory effect of cpSRP54 on the chaperone activity of cpSRP43 on TBS proteins further raises questions, such as how this chaperone activity is switched on during heat stress. Remarkably, Co-IP assays indicated reduced interactions of cpSRP43 with cpSRP54 and increased interaction with TBS proteins upon heat treatment (Figure 3.15A). In vitro pull-down assays further showed that the cpSRP54-cpSRP43

interaction is sensitive to increased temperature and weakened as soon as the temperature is rising (15 °C to 45 °C) (Figure 3.15C). These results support a model in which higher temperature drives the dissociation of the complex and release cpSRP43 for new functions on TBS proteins (Figure 4.1).

4.1.4 Summary: Heat-induced release of cpSRP43 from cpSRP54 maintains Chl biosynthesis during heat shock

Based on my data presented, I propose two pools of cpSRP43 which exist in *Arabidopsis* for interacting with the TBS proteins or cpSRP54 plus LHCP, respectively. Under standard growth conditions (Figure 4.1A-B), the majority of cpSRP43 functions together with cpSRP54 for transport of newly imported unfolded LHCPs within the chloroplasts. Under stress conditions such as heat shock that halts LHCP biosynthesis, the pool of cpSRP43 could be purposed as a stress-response chaperone to facilitate the rapid protection of TBS enzymes against their potential heat-induced aggregation. In this scenario, the affinity of cpSRP43 to cpSRP54 is remarkably diminished, causing the release of cpSRP43 from the cpSRP54-bound cpSRP43 pool as well as, consequently, the binding of apo cpSRP43 to TBS enzymes and protects them from heat-induced aggregation (Figure 4.1C). Since both the TBS clients and cpSRP54 interact with cpSRP43-CD2, it is hypothesized that the cpSRP43-CD2 is subjected to a thermolabile conformational change that brings TBS clients into a privileged position to interact with cpSRP43. Owing to this structural change of cpSRP43, interaction with TBS enzymes is more stable than with cpSRP54. In the future, the conformational changes of cpSRP43 and cpSRP54 during heat treatment will be studied in more detail.

.

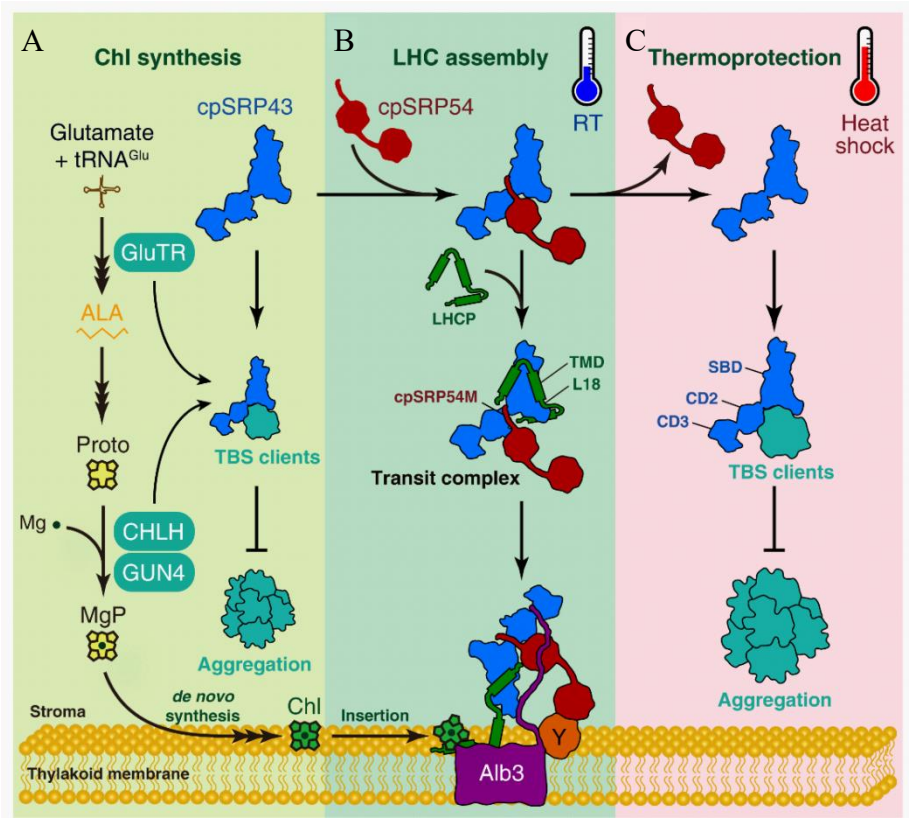

Figure 4.1 Model for a dual participation of cpSRP43 in Chl synthesis and LHCP transport in plants. cpSRP43 harbors two distinct chaperone activities: as a general chaperone for protection of TBS proteins (**A**, **C**), or as a dedicated chaperone to mediate the protection and delivery of LHCPs (**B**). The switch between these two activities is regulated by cpSRP54 binding. Under standard growth conditions, a minor portion of apo cpSRP43 optimizes Chl biosynthesis by protecting crucial and perhaps vulnerable TBS proteins, including GluTR, CHLH and GUN4, against aggregation (**A**). Meanwhile, a majority of cpSRP43 was bound to cpSRP54 with high affinity (**B**). cpSRP54 optimizes the conformation of the cpSRP43-SBD domain for interaction with and protection of LHCP (Liang et al., 2016) , while inhibition of the chaperone activity of cpSRP43 on TBS proteins is mainly excluded due to limited access of cpSRP43 to TBS proteins. At the thylakoid membrane, cpSRP54 binds to cpFtsY (Y), and the stromal domain of Alb3 interacts with cpSRP43 to trigger the release of LHCP and mediate insertion into the thylakoid membrane. The participation of cpSRP43 in both Chl synthesis and LHCP transport ensures that plants produce sufficient amounts of Chl for LHC assembly during leaf greening. In contrast, when plants experience short-term heat shock stress (**C**), the affinity of cpSRP54 for cpSRP43 becomes weaker and caused an increased pool of apo cpSRP43 which can use its SBD and CD2 domains to effectively interact with TBS proteins and prevent them from heat-induced aggregation. ALA, 5-aminolevulinic acid. L18, L18 motif of LHCP interacting with cpSRP43. RT, room temperature. TMD, transmembrane domain.

4.2 Chloroplast SRP acts as a chaperone for protochlorophyllide oxidoreductase B (PORB) in *Arabidopsis thaliana*

POR is the penultimate enzyme in the Chl biosynthesis pathway, which reduces Pchlide to Chlide. Since this catalytic step is light-dependent, the reaction is blocked and the substrate Pchlide accumulates in the dark (Gabruk and Mysliwa-Kurdziel, 2015). However, accumulating Pchlide triggers the ROS formation after illumination and causes cell death (Ledford and Niyogi, 2005; Li et al., 2009). Therefore, plant cells need to suppress the accumulation of Pchlide in the dark and POR becomes to be tightly regulated. In the previous chapter, I reported the novel regulatory mechanism of cpSRP43 on GluTR and MgCh. Since PORB is equally important as GluTR and MgCh in the Chl synthesis, in this study, I also explored the potential regulatory mechanism of cpSPR43 and cpSRP54 on PORB.

4.2.1 cpSRP43 and cpSRP54 coordinately promote the stability of PORB

Apart from GluTR, CHLH and GUN4, I also found that PORB level was significantly decreased in both *chaos* and *ffc*. This reduction was more pronounced in the double mutant *chaos/ffc* (Figure 3.18A-B), suggesting that cpSRP43 and cpSRP54 coordinately stabilize PORB. In contrast to the previous results which indicate that cpSRP54 inhibits chaperone function of cpSRP43 on GluTR, CHLH and GUN4, here I report about modified action of cpSRP54 to PORB. Transcriptional analysis ruled out that the decreased stability of PORB was due to the modified mRNA level (Figure 3.18C), implying a post-translational stability of PORB by the concerted action of cpSRP43 and cpSRP54. Further protein interaction studies using BiFC and in vitro pull-down assays confirmed that cpSRP43 can directly interact with PORB (Figure 3.19A-C). In addition, interaction between cpSRP54 and PORB was also verified by the BiFC assay (Figure 3.19D), indicating that cpSRP43 and cpSRP54 contribute to the preserved

stability of PORB through the direct physical interactions with PORB.

4.2.2 cpSRP components act as chaperones to protect PORB from aggregation

In vitro scattering assays showed that only when the cpSRP43 concentration exceeded PORB, cpSRP43 could exhibit a concentration-dependent protection of PORB against heat or oxidation-induced aggregation (Figure 3.21A, Figure 3.22A). Since cpSRP54 itself underwent aggregation at high temperature (Figure 3.21B), cpSRP54 cannot protect PORB from heat-induced aggregation. However, the presence of cpSRP54 significantly reduced the PORB aggregation induced by oxidation, although this protective effect was concentration-independent (Figure 3.22B), indicating that cpSRP54 somehow contributes to protection of PORB from oxidation-induced aggregation. As result of in vivo heat shock experiments, the PORB level in *chaos* decreased significantly after 2 h of heat shock (Figure 3.23A-B), while the PORB level in *ffc* remained comparably stable to that in wild type even after 4 h of heat shock (Figure 3.23C-D). These results suggest consistent with the in vitro scattering assays that cpSRP43 but not cpSRP54 is able to maintain intact PORB levels in response to heat shock.

Enzymatic activity of POR depends on light-activation. The substrate and product of this step are photosensitizers which generate ROS upon light exposure (Reinbothe et al., 1996; Sperling et al., 1997; Buhr et al., 2008). Excessive ROS can lead to oxidative damage and cell death, and PORB therefore requires additional chaperones to be protected against photooxidative damage (Ledford and Niyogi, 2005; Li et al., 2009). CPP1 is a plastid-localized protein that prevents POR aggregation, especially under oxidative stress, and its deficiency leads to the decreased PORB protein level and defective Chl synthesis (Lee et al., 2013). In this study, cpSRP43 and cpSRP54 were found effectively protect PORB from oxidation-induced aggregation by in vitro scattering assays (Figure 3.22), suggesting similar to CPP1 that cpSRP43 and cpSRP54 may protect PORB against oxidative stress by preventing aggregation through molecular chaperone activity.

PORB is abundant in leaves. In vitro scattering assays, cpSRP43 showed chaperone function on PORB only when the concentration of cpSRP43 exceeds that of PORB. It is not clear whether the concentration of cpSRP43 also exceeds that of PORB in vivo in order to demonstrate a protective function on PORB. However, it is difficult to tackle this question experimentally, because, firstly, previous studies found that there are two pools of cpSRP43 in the chloroplasts, one with apo cpSRP43 and the other with cpSRP54-bound cpSRP43. Only apo cpSRP43 pool is involved in the protective function of TBS proteins. Since cpSRP43 amounts in these two pools are changing and apo cpSRP43 is also involved in the protection of GluTR, CHLH and GUN4, it might be difficult to determine the cpSRP43 amounts that are available for PORB protection. Secondly, it is also difficult to determine the amount of unfolded or misfolded PORB that requires the protection of cpSRP43. It is also unclear whether the two forms of PORB in chloroplasts, stromal PORB and membrane-bound PORB, both require the protection of cpSRP43.

Nevertheless, cpSRP43 does indeed protect PORB in vivo, as shown (1) during chloroplast development, when the cpSRP43 deficiency leads to the compromised stability of PORB (Figure 3.18, chapter 3.2.1.2), (2) under heat shock, when cpSRP43 maintains the stability of PORB against heat shock (Figure 3.23, chapter 3.2.5), and (3) when the SBD domain of cpSRP43 is sufficient for interaction and protection of PORB (Figure 3.24, chapter 3.2.6). I therefore speculate that the concentration of cpSRP43 exceeds that of PORB within the local range of chloroplasts to protect PORB from aggregation.

4.2.3 cpSRP54 is involved in the attachment of PORB to the plastid membranes

It is well known that cpSRP54 directs LHCP to the thylakoid membrane by binding cpFtsY, a receptor protein at the thylakoid membrane required during the membrane targeting of LHCP (Tu et al., 1999; Ziehe et al., 2018). In addition, cpSRP54 is also responsible for the co-translational insertion of D1 protein to the thylakoid membrane by interacting with ribosomal 70S (Franklin and Hoffman, 1993; Nilsson and van Wijk, 2002; Hristou et al., 2019). Therefore, cpSRP54 is considered to play an important role in the localization of proteins on thylakoid membranes. In this study, I found the ratio of membrane-bound PORB in *ffc* was significantly decreased compared with the wild type, while the membrane-bound PORB in *chaos* was equivalent to the wild type (Figure 3.25B-C), implying that only cpSRP54 might be involved in the transfer of POR across the stroma and attachment to the thylakoid membrane. This is different from the cpSRP-mediated transport of LHCP to the thylakoid membrane. When the membrane-bound LHCP portion is significantly reduced in *chaos* and *ffc*, and moreover, cpSRP43 and cpSRP54 synergically transport LHCP into the thylakoid membrane (Figure 3.25A). However, I still cannot explain why membrane-bound PORB was unaltered in *chaos/ffc* compared with that in *ffc* (Figure 3.25B-C). More experiments are required in the future to verify the function of cpSRP54 in membrane binding of PORB.

4.2.4 cpSRP43 and cpSRP54 enhance the stability of PORB in distinct ways

These studies revealed that cpSRP43 and cpSRP54 play different roles in regulating PORB stability: (1) cpSRP43 acts as a chaperone to protect PORB from heat or oxidation-induced aggregation; (2) A portion of cpSRP54 is independent of the function of trafficking LHCP to the thylakoid membrane or mediating the cotranslational transport of plastid-encoded protein, assists in the association of PORB to the thylakoid membrane and prevents the oxidation-induced aggregation of PORB.

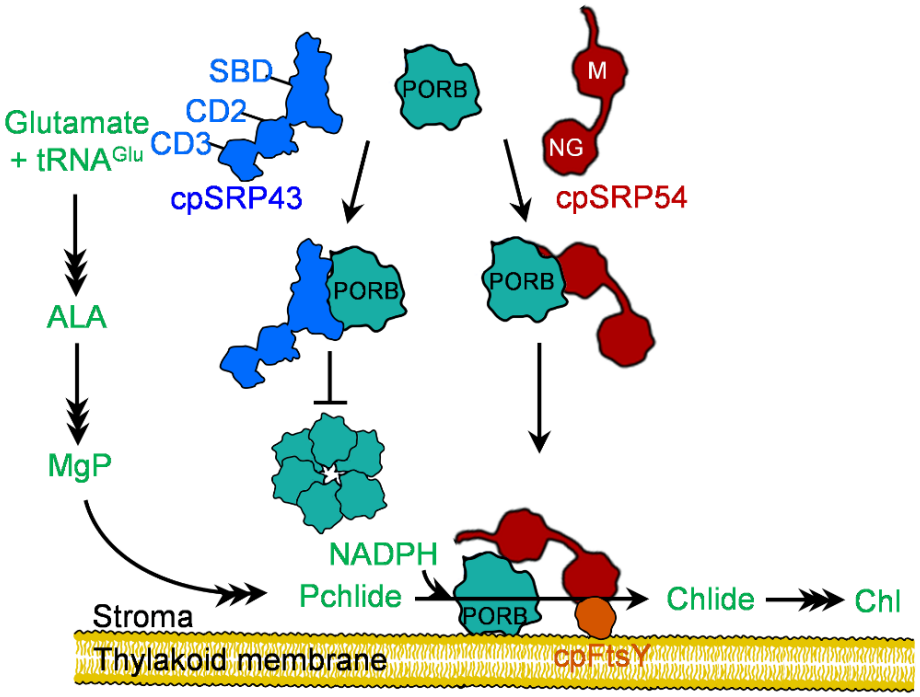

Figure 4.2 Model: cpSRP43 and cpSRP54 protect PORB in different ways. cpSRP43 protects PORB from aggregation during PORB traverses the stroma, while a portion of apo cpSRP54 protects and directs PORB binding to the thylakoid membranes, where PORB functions properly.

4.2.5 Chaperone function is essential in all organisms

Molecular chaperones are essential in various life activities. Because the molecular processes inside living cells is much more complex than the ideal in vitro conditions of low protein concentration and carefully optimized temperature. Crowded molecular activities and rapidly changing environments within cells can interfere with the folding processes of newly synthesized polypeptide chains or causing changes in the native conformation of mature proteins (Liberek et al., 2008). The native conformational change cannot only lead to the loss of protein function, but also cause other problems in cells, such as protein aggregation (Liberek et al., 2008). Cells, thus, require chaperones to (1) prevent aggregation and misfolding during the folding of newly synthesized polypeptide chains, (2) assist in the assembly of proteins and protein complexes, and (3) disassemble protein aggregates and undergo refolding (Fink, 1999).

In plants, ClpB/HSP100 proteins are critical in governing plant thermotolerance. Arabidopsis mutants with defects in ClpB/HSP100 protein expression are extremely sensitive to heat stress (Mishra and Grover, 2016). HSP90 was reported to act as chaperone to deliver precursor proteins to the chloroplast import receptor Toc64 (Qbadou et al., 2006). Heat treatment of Arabidopsis plants deficient in HSP70 experience an extremely high mortality and show that HSP70 performed an important role in plants against heat stress during normal growth (Jungkunz et al., 2011). HSP40, which was over-expressed in *Arabidopsis* could contribute to NaCl-stress tolerance (Zhichang et al., 2010). In this study, cpSRP43 acts as a chaperone not only to protect LHCP (Falk and Sinning, 2010), but also to protect GluTR, CHLH, GUN4 and

PORB against denaturation. Thus, cpSRP43 stabilizes these proteins and preserves Chl synthesis during short-term heat stress (see chapter 3.1 and 3.2).

4.2.6 The evolution of SRP pathway- from bacteria to higher plants

The SRP system is conserved from bacteria to higher plants (Akopian et al., 2013; Steinberg et al., 2018). In *E. coli*, the cytosolic SRP is a ribonucleoprotein comprising two components, an SRP RNA and a conserved protein subunit Ffh, called SRP54 in eukaryotes. The bacterial SRP pathway functions by means of co-translation, SRP binds to the ribosome nascent chain (RNC), and the SRP-RNC complex is then directed to the membrane-bound SRP receptor (FtsY) and finally translocated to the SecYEG/YidC machinery (Frain et al., 2016).

In cyanobacteria, although homologues of the SRP components, Ffh and FtsY were found in cyanobacteria (Packer and Howe, 1996), the proteins inserted into the plasma membrane were also likely to follow a pathway similar to that in bacteria (Frain et al., 2016). However, it is still known very little about it. On the other hand, the targeting of proteins in thylakoid membranes may be similar to that of proteins directed to plant thylakoid membranes, but it is only speculation.

The higher plants possess a special SRP system that includes bacterial SecY (cpSecY1), the Ffh (cpSRP54), the SRP receptor (cpFtsY), and the chloroplast homologue of YidC (Alb3), apparently differs from the cytosolic SRP in several aspects (Ziehe et al., 2017). (1) The application of SRP RNA is missing in plastids of higher plants during their evolution from cyanobacterial ancestors (Rosenblad and Samuelsson, 2004; Träger et al., 2012). (2) The chloroplast contains a post-translationally active SRP system that mediates the translocation of nuclear-encoded LHCP to the thylakoid membrane (Schünemann et al., 1998; Klimyuk et al., 1999). cpSRP54 forms a heterodimer with the plant-specific cpSRP43 protein (see 1.2.23 for the plant cpSRP pathway). (3) In addition to the pool of cpSRP54 associated with cpSRP43, the chloroplast contains a second pool of cpSRP54 associated with the ribosome (Franklin and Hoffman, 1993; Schünemann et al., 1998). The ability of cpSRP54 to interact with the nascent chains of PsbA and PetB (Nilsson et al., 1999; Nilsson and van Wijk, 2002; Piskozub et al., 2015) suggests that ribosome-associated cpSRP54 pools play a role in the co-translational targeting of some plastid-encoded proteins to the thylakoid membrane. Thus, cpSRP43 extends the functions of cpSRP54 from a co-translational translocation mechanism to a post-translational mechanism. Interestingly, both cpSRP43 and SRP RNA were present in *Physcomitrella patens*, suggesting that the cpSRP system of the moss is obviously at an intermediate position in the evolution of bacterial SRP to higher plant cpSRP systems (Träger et al., 2012).

4.2.7 LHCP and cpSRP43 are co-evolved

Post-translational targeting of membrane proteins presents a huge challenge to protein homeostasis, which requires tight links between the protein translocation and chaperone functions of the protein targeting machinery (Flores-Perez and Jarvis, 2013). The high

abundance and hydrophobicity of the LHCP family requires efficient molecular chaperones during translocation, and cpSRP43 efficiently meets these requirements. As a molecular chaperone, cpSRP43 can protect LHCP from protein aggregation in the stromal aqueous environment (Falk and Sinning, 2010), and also forms a complex with cpSRP54 to transport LHCP to the thylakoid membrane (Dünschede et al., 2015). In addition, it was reported that cpSRP43 alone might also transport LHCP to the thylakoid membrane (Tzvetkova-Chevolleau et al., 2007).

cpSRP43 is dedicated to chaperone members of the LHC protein family because: First, the efficiency of cpSRP43 to reverse LHCP aggregation is comparable to the AAA^+-ATPase assembly machinery (Doyle and Wickner, 2009). Whereas the assembly machines such as ClpB/DnaK/DnaJ/GrpE (Mogk et al., 2003) are large macromolecules over 600 kDa and depend on ATP hydrolysis, cpSRP43 does not contain an ATPase site and the minimum functional unit required for chaperone activity is only approximately 35 kDa. Second, cpSRP43 establishes a highly specific and broad interaction with LHCP, using its ankyrin repeat to contact the L18 motif of LHCP and other interactions involving its chromatin domain and the transmembrane part of LHCP (Ziehe et al., 2018). Third, the major difference between cpSRP43 and ATP-driven chaperone action could be their different substrate specificities. Most chaperones from the Clp and HSP families have evolved to bind various substrates through general hydrophobic interactions to rescue proteins from aggregation regardless of sequence identity (Tomoyasu et al., 2001; Mogk et al., 2004; Barkow et al., 2009). These chaperones likely require the synergy of numerous chaperones and power-driven by ATP hydrolysis to exert their functions. In contrast, cpSRP43 is only present in the chloroplasts of green plants, and its evolution may coincide with its substrate LHCP (Schünemann, 2004). Thus, cpSRP43 is specialized in the LHC protein family and thus establishes broad and particular binding interactions with its substrates.

4.2.8 Why does cpSRP also protect the protein in Chl biosynthesis?

It has been previously reported that cpSRP43 is dedicated to the transport and chaperone protection of LHCP (Falk and Sinning, 2010). However, in this study I also found that cpSRP43 protects the TBS enzymes GluTR, MgCh and PORB from denaturation. Additionally, cpSRP54 may also be involved in membrane binding of PORB. When cpSRP43 and LHCP co-evolved, how could did this emerge during evolution? One explanation is that the TBS pathway, especially Chl biosynthesis, should be coordinated with the LHCP targeting and insertion, as both, Chl and the apo protein, must assemble together to form the light-harvesting antenna complex for photosynthesis. This dynamic coordinated assembly is particularly important in response to the change of light intensity. Second, both LHCP and TBS proteins are translated in the cytosol and transported into the chloroplast post-translationally, so it is not surprising that cpSRP43 can bind to these TBS proteins and acts as a chaperone to protect them. Third, although cpSRP43 actually protects both LHCP and TBS proteins, they do not bind to the same site of cpSPR43. For LHCP, SBD is sufficient (Liang et al., 2016), however additional CD2 is required for GluTR, CHLH and GUN4 (see chapter 3.1.7.5), which may reflect the different

protective mechanisms of cpSRP43 for these two types of clients. In addition, it is still cannot excluded that cpSRP43 may regulate other proteins in TBS or other pathways.

4.2.9 Why not any other TBS enzymes be regulated by cpSRP?

In the TBS pathway, the accumulation of some intermediates is hazardous due to their phototoxicity. For example, free porphyrins and Pchlide can be photo-oxidized. Excessive amounts of these intermediates will cause a large amount of ROS after light illumination and lead to the programmed cell death. Thus the TBS pathway needs to be tightly regulated. However, tight regulation of each step inevitably potentially leads to a waste of resources and inefficiency. Thus, it is a most sensible choice to focus on a few key enzymatic steps. There are three enzymes in the TBS pathway at very critical positions, which are, interestingly, regulated by many factors: These are GluTR (see 1.1.4.1), MgCh (see 1.1.4.2) and PORB (see 1.1.4.3). GluTR is located at the beginning of the pathway and catalyzes the synthesis of the first precursor in TBS, ALA. The tight regulation of GluTR can ensure the supply the appropriate quantities of ALA. MgCh is located at a central site of the pathway, when TBS is branched towards Chl synthesis. Its regulation determines the synthesis of an appropriate amount of MgProto IX for Chl. PORB is located in the penultimate position of the TBS pathway, and catalyzes the synthesis of NADPH- and light-dependent Pchlide to Chlide. The regulation of PORB on the one hand is to avoid the overaccumulation of Pchlide by adjusting the stability and activity of PORB, and on the other hand to inhibit the supply of ALA in the dark through feedback control. Based on this consideration, cpSRP43 and cpSRP54 have substantial tasks in the control of TBS by regulating content of active GluTR, MgCh and PORB. Of course, I still cannot rule out the possibility that cpSRP43 or cpSRP54 regulates other TBS proteins as well. To get a complete view on the regulation of the TBS pathway by cpSRP43 and cpSRP54, several other approaches, such as Co-IP combined with mass spectrometry (MS) will be applied in the future.

4.3 Functional analysis of the aggregation-prone region (APR) in GluTR

GluTR is the rate-limiting enzyme in the TBS pathway and is regulated by multiple proteins, among which cpSRP43 can protect GluTR from aggregation. There are two APRs in the N-terminal half of GluTR, which are related to potential aggregation of GluTR (Wang et al., 2018). In vitro deletion of APR can significantly improve the solubility of GluTR and reduce the aggregation of GluTR (Wang et al., 2018). It is speculated that cpSRP43 binds to the N-terminus of GluTR, masks the two APRs at the N-terminus and reduces the outward of APRs, thereby preventing GluTR from forming interprotein connections and aggregations (Wang et al., 2018). My presented experiments of this doctoral studies intended to explore the function of GluTR-APRs in vivo, and it has been requested to demonstrate increased accumulation of functioning GluTR by eliminating APRs, with the consequence of increased ALA synthesis rates and an improved efficiency of Chl synthesis.

4.3.1 APR is critical to the integrity of GluTR

The APRs of GluTR are located in the catalytic domain at the N-terminus of GluTR and, therefore, very important for the enzymatic activity of GluTR (Figure 3.26). In this study, first APR deletion mutants were constructed, and it was found that the Chl content and ALA synthesis rate of the APR-deficient mutants were drastically diminished (Figure 3.27C-D). The transcriptional level of *HEMA1* was not decreased in the mutants, however the protein level of GluTR was immunologically detectable only in one out of 8 transgenic lines expressing GluTRΔAPR2 in *HEMA1ΔAPR2-20* (Figure 3.28), suggesting that the deletion of APR impairs the stability of GluTR. In the *HEMA1ΔAPR2-20* line, although the GluTR level decreased by half compared to wild type, the ALA synthesis rate was only 1/50 of that in the wild type (Figure 3.28A, Figure 3.27D), indicating that the deletion of APR also erased the activity of GluTR.

In the second approach, the *HEMA1 (V99P/V151P)* point mutant was obtained by a V→P substitution of APR. Phenotypic analysis revealed that the mutant had a phenotype like the *hema1* knockout mutant (Figure 3.30D). Although the transcription level of *HEMA1* in *HEMA1 (V99P/V151P)* was comparable to that in the wild type, the GluTR level was significantly decreased (Figure 3.31A-B), indicating that the V→P mutation also dramatically impaired the stability and activity of GluTR. Since APRs are located at the N-terminus of GluTR (aa 95-aa156), it is speculated that the two APRs of GluTR are very important for the structural integrity of GluTR.

4.3.2 APRs in CHLH, GUN4 and PORB

In my study, I found that GluTR, CHLH, GUN4 and PORB can form aggregates under heat shock conditions, and this aggregation of GluTR is probably caused by its two APRs. Therefore, I supposed that the other three proteins CHLH, GUN4 and PORB could also have these APRs. In order to explore the APRs in these proteins, I applied the TANGO algorithm to predict the APRs of CHLH, GUN4 and PORB. As shown in the Figure 4.3A (GluTR, see Figure 3.26), and as expected, CHLH, GUN4, and PORB have 21, 2 and 5 predicted APRs, respectively. Among them, CHLH contains 9 APRs with aggregation tendency of more than 80%, GUN4 contains only 1 APR with an aggregation tendency of 72%, while the highest aggregation tendency of APRs in PORB is only 22%, which suggests that CHLH, GUN4 may form aggregates more easily than PORB.

Sequence analyses of theses APRs indicate that their lengths are also long and short, and no similarity was found in their amino acid sequences (see Appendix III). However, it has been reported previously that the aggregation regions are strongly enriched in aliphatic hydrophobic residues Val, Ile, Leu (Rousseau et al., 2006). In my study, I also found these three amino acids are enriched in the APRs of GluTR, CHLH, UN4 and PORB (see Appendix III). In addition, I also tried to explore their similarities in the three-dimensional structure. The crystal structure of the Arabidopsis GluTR-GBP complex and that of ligand-free GUN4 has been resolved (Zhao et al., 2014; Hu et al., 2021), while the structures of CHLH, and PORB has only been resolved in cyanobacteria (Zhang et al., 2019; Adams et al., 2020). I used Phyre^2 to predict the crystal

structure of these two proteins. Figure 4.3B shows the structure of GluTR, CHLH, GUN4, PORB and all the APRs were marked in red. I found that APRs in GluTR and PORB form β-sheets and are buried in the proteins. However, due to its small molecular weight, GUN4 has no β- sheet in its crystal structure, the APR of GUN4 is therefore in the form of α-helix and exposed on the surface of the GUN4. In CHLH, APRs form an equivalent number of β-sheets and α-helices, and most of the APRs are buried in the protein. In conclusion, APRs are present in GluTR, CHLH, GUN4 and PORB, although the aggregation tendency of APRs in PORB are low. No similarity is detectable in the amino acid sequence of these APRs, but most of them are β-sheets in structure, although sometimes they also form α-helixes. They are mainly buried

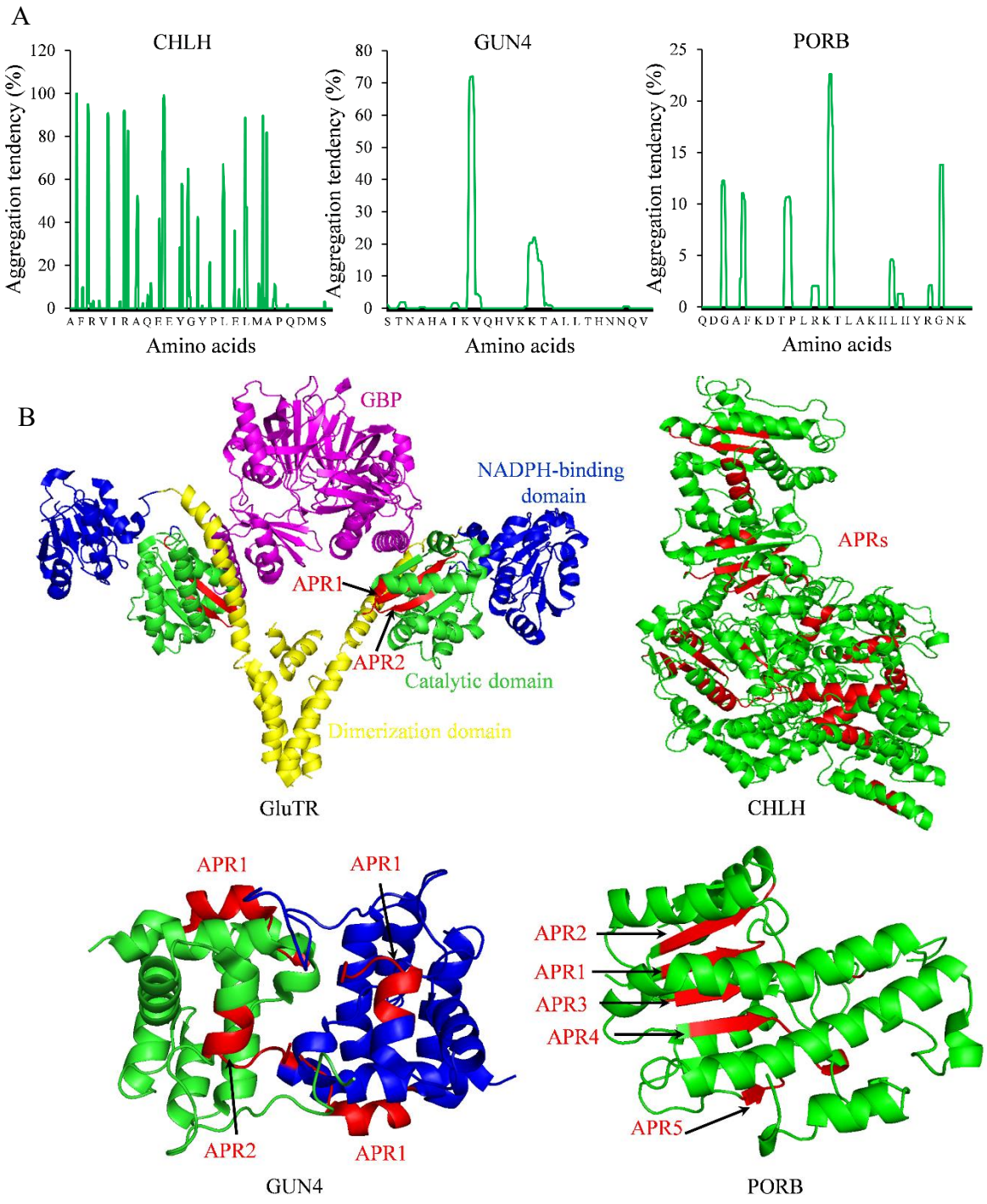

Figure 4.3 APRs are predicated by TANGO in CHLH, GUN4 and PORB. **A**, Aggregation tendency of APRs in CHLH, GUN4 and PORB. **B**, Crystal structure of APRs in GluTR, CHLH, GUN4 and PORB, the APRs are labelled in red. The PDB ID for GluTR is 4N7R, for GUN4 is 7E2R. The structures for the other proteins were predicated by algorithm Phyre2 (http://www.sbg.bio.ic.ac.uk/phyre2/html/page.cgi?id=index). Protein structures were analyzed by using the software PyMOL.

in the proteins and avoid the exposure to the surface as well as the formation of interprotein aggregates. In future, the functions of these APRs in CHLH, GUN4 and PORB can be studied, which could improve our understanding of the biochemical mechanisms of protein aggregation and disaggregation.

4.3.3 The V→T mutation slightly improves the stability of GluTR under light and dark

The algorithm TANGO was used to predict the aggregation tendency of peptides (Fernandez-Escamilla et al., 2004). By using this algorithm, it was found that the aggregation of GluTR tends to be reduced by half when in the first APR Val 99 was replaced by Thr, while the impact of APR2 on aggregation was only 20%, when Val 151 was replaced by Thr (Figure 3.29B). However, in vitro scattering assays found that the aggregation of GluTR (V99T/V151T) was only slightly decreased compared with GluTR (WT) (Figure 3.32A). As a result, the corresponding protein level of GluTR (V99T/V151T) in *HEMA1 (V99T/V151T)* was slightly increased by 27% (Figure 3.31D-E), indicating that the V→T mutation likely confers an enhanced stability of GluTR. However, the accumulating GluTR did not possess an increased ALA synthesis rate (Figure 3.30D), suggesting the inactive activity of GluTR by V→T mutation. One explanation is that the APRs are located in the catalytic domain of GluTR. Another explanation is that the accumulation of total GluTR did not increase the accumulation of soluble (non-bound to the thylakoid membrane) GluTR, since only soluble GluTR content correlates with the rate of ALA synthesis (Schmied et al., 2018; Hou et al., 2019) . In addition, the degradation rate of GluTR in the *HEMA1(V99T/V151T)* line was significantly slower than in wild type after dark treatment. After 24h in the darkness, the level of GluTR in *HEMA1(V99T/V151T)* was still significantly higher than that in the wild type (Figure 3.34), indicating that the V→T mutation can delay the degradation of GluTR and improve its stability in the dark. In conclusion, the V→T mutation apparently tend to reduce the aggregation of GluTR and improve the stability of GluTR in light and darkness.

4.3.4 Structural alignments revealed that APR structures are essential for the structural integrity of GluTR

Using Phyre[2], I also predicted the crystal structure of the APR-deleted GluTRs and compared them with the WT GluTR. As shown in Figure 4.4, the cartoons in brown indicated by the black arrows represent the altered crystal structure caused by the APR deletion. In the structural region of APR (black rectangular box), the deletion of APR changed the structure of APR. Specifically, the structure of APR was changed in two positions for the deletion of APR1 (Figure 4.4A), in five positions for the deletion of APR2 (Figure 4.4B) and six positions for the

deletion of both APR1 and APR2 (Figure 4.4C), suggesting that APR2 may be more important than APR1 in maintaining the structural integrity of GluTR. This speculation is also consistent with the previous study that the recombinant protein GluTRΔAPR2 in vitro scattering assay dramatically decreases the GluTR aggregation compared with the GluTRΔAPR1(Wang et al., 2018).

In addition to the structural region of APR, structural alterations caused by the APR deletion were also found in the NADH-binding domain (blue) and the dimerization domain (yellow). However, this may not be the reason for the disruption of the stability and the loss of activity of GluTR after APR deletion, since such a change also was modeled into the GluTR (V99T/V151T) structure (Figure 4.4E). In GluTR (V99P/V151P), the structural region of APR1 was obviously altered (black arrow) (Figure 4.4C). In contrast, the structure of the GluTR (V99T/V151T) variant was completely the same as that of the wild-type APR, suggesting that the V→T mutation does not alter the structure of APR, which may explain the unaffected integrity of GluTR in the *HEMA1 (V99T/V151T)* line. In summary, the crystal structure of GluTR with APRs deletion or APRs point mutation was predicted by Phyre^2, and it was found that the deletion of APRs, especially that of the APR2, significantly affected the overall structure of GluTR. In addition, the structure of APRs in the point mutation *HEMA1 (V99P/V151P)* line was also significantly affected. These conformational changes caused by the deletion or point mutation of APR in *HEMA1ΔAPR1*, *HEMA1ΔAPR2*, *HEMA1ΔAPR1/2* and *HEMA1 (V99P/ V151P)* might be the reasons for the disrupted stability and activity of GluTR. In contrast, the structure of APRs in GluTR (V99T/V151T) was not changed (Figure 4.4E), leading to the unaffected integrity of GluTR in *HEMA1 (V99T/V151T)*. Finally, this suggests that the spatial integrity of GluTR including the APRs is critical to maintain function of GluTR.

4.3.5 A new strategy to improve the stability of GluTR: point mutation of APR

In this study, V→T mutation in in vitro scattering assay decreases the aggregation of GluTR by only 18-30% (Figure 3.32A). This lower aggregation tendency corresponds in vivo to a 27% increased stability of GluTR (V99T/V151T) (Figure 3.31D-E), indicating that the improved GluTR stability in vivo positively correlated with the decreased aggregation of GluTR in vitro. This result on GluTR integrity points to a potential method to improve the stability of GluTR and to design a protein with optimal amino acid substitutions. However, this approach with the exchange of amino acid residues in APRs does inactive the activity of GluTR, because the GluTR APRs are located in the catalytic domain. In summary, this strategy to modify APRs includes bioinformatics to predict an optimized sequence of amino acid residues. Then the proposed mutant proteins with predicted substitutions and modified peptide motifs will be assayed as recombinant proteins by in vitro scattering assays, and these assays should be performed with the intention to strongly improve the stability of GluTR.

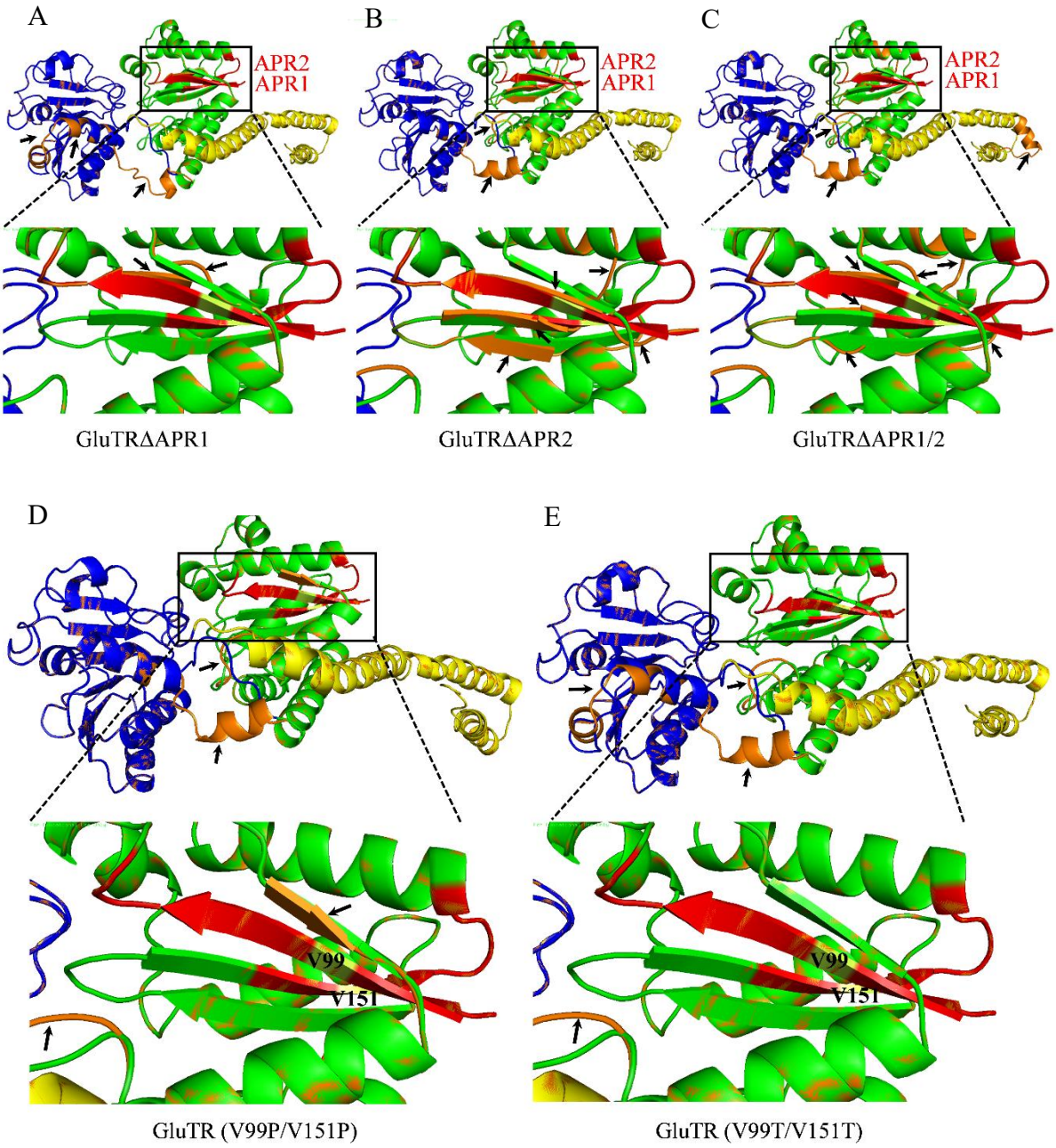

Figure 4.4 Structural angliments of the APR mutated GluTRs with GluTR (WT). Structural alignments of GluTR(WT) with GluTRΔAPR1 (**A**), GluTRΔAPR2 (**B**), GluTRΔAPR1/2 (**C**), GluTR (V99P/V151P) (**D**) and GluTR (V99T/V151T) (**E**). Black rectangles indicate the structure of APRs which was displayed in a magnification. Black arrows indicate the positions where the crystal structures were altered compared to the GluTR (WT). The upper picture always shows the entire protein structure, while the lower image in each panel shows the zoom in of the aligned area, where the APRs are positioned. APRs are labelled in red.

References

Adams NB, Brindley AA, Hunter CN, Reid JD (2016) The catalytic power of magnesium chelatase: a benchmark for the AAA+ ATP ases. FEBS letters **590(12):** 1687-1693

Adams NB, Marklew CJ, Qian P, Brindley AA, Davison PA, Bullough PA, Hunter CN (2014) Structural and functional consequences of removing the N-terminal domain from the magnesium chelatase ChlH subunit of Thermosynechococcus elongatus. Biochemical Journal **464(3):** 315-322

Adams NB, Reid JD (2012) Nonequilibrium isotope exchange reveals a catalytically significant enzyme–phosphate complex in the ATP hydrolysis pathway of the AAA+ ATPase magnesium chelatase. Biochemistry **51(10):** 2029-2031

Adams NB, Reid JD (2013) The allosteric role of the AAA+ domain of ChlD protein from the magnesium chelatase of synechocystis species PCC 6803. Journal of Biological Chemistry **288(40):** 28727-28732

Adams NBP, Bisson C, Brindley AA, Farmer DA, Davison PA, Reid JD, Hunter CN (2020) The active site of magnesium chelatase. Nature Plants **6(12):** 1491-1502

Adhikari ND, Froehlich JE, Strand DD, Buck SM, Kramer DM, Larkin RM (2011) GUN4-porphyrin complexes bind the ChlH/GUN5 subunit of Mg-Chelatase and promote chlorophyll biosynthesis in Arabidopsis. The Plant Cell **23(4):** 1449-1467

Agarwal M, Katiyar-Agarwal S, Sahi C, Gallie DR, Grover A (2001) Arabidopsis thaliana Hsp100 proteins: kith and kin. Cell stress & chaperones **6(3):** 219-224

Akopian D, Shen K, Zhang X, Shan SO (2013) Signal recognition particle: an essential protein-targeting machine. Annual review of biochemistry **82:** 693-721

Albanese P, Manfredi M, Meneghesso A, Marengo E, Saracco G, Barber J, Morosinotto T, Pagliano C (2016) Dynamic reorganization of photosystem II supercomplexes in response to variations in light intensities. Biochimica et Biophysica Acta (BBA)-Bioenergetics **1857:** 1651-1660

Allakhverdiev SI, Kreslavski VD, Klimov VV, Los DA, Carpentier R, Mohanty P (2008) Heat stress: an overview of molecular responses in photosynthesis. Photosynthesis research **98:** 541-550

Amin P, Sy DA, Pilgrim ML, Parry DH, Nussaume L, Hoffman NE (1999) Arabidopsis mutants lacking the 43-and 54-kilodalton subunits of the chloroplast signal recognition particle have distinct phenotypes. Plant physiology **121:** 61-70

Andrews JM, Roberts CJ (2007) A Lumry− Eyring nucleated polymerization model of protein aggregation kinetics: 1. Aggregation with pre-equilibrated unfolding. The Journal of Physical Chemistry B **111:** 7897-7913

Apel K, Hirt H (2004) Reactive oxygen species: metabolism, oxidative stress, and signal transduction. Annual review of plant biology **55:** 373-399

Apitz J, Nishimura K, Schmied J, Wolf A, Hedtke B, van Wijk KJ, Grimm B (2016) Posttranslational Control of ALA Synthesis Includes GluTR Degradation by Clp Protease and Stabilization by GluTR-Binding Protein. Plant Physiology **170:** 2040-2051

Apitz J, Schmied J, Lehmann MJ, Hedtke B, Grimm B (2014) GluTR2 complements a hema1 mutant lacking glutamyl-tRNA reductase 1, but is differently regulated at the post-translational level. Plant Cell Physiol **55:** 645-657

Bals T, Dünschede B, Funke S, Schünemann D (2010) Interplay between the cpSRP pathway components, the substrate LHCP and the translocase Alb3: an in vivo and in vitro study. FEBS letters **584 (19):** 4138-4144

Barkow SR, Levchenko I, Baker TA, Sauer RT (2009) Polypeptide translocation by the AAA+ ClpXP protease machine. Chemistry & biology **16:** 605-612

Berlett BS, Stadtman ER (1997) Protein oxidation in aging, disease, and oxidative stress. Journal of Biological Chemistry **272:** 20313-20316

Betterle N, Ballottari M, Zorzan S, de Bianchi S, Cazzaniga S, Dall'Osto L, Morosinotto T, Bassi R (2009) Light-induced dissociation of an antenna hetero-oligomer is needed for non-photochemical quenching induction. Journal of Biological Chemistry **284:** 15255-15266

Betti C, Vanhoutte I, Coutuer S, De Rycke R, Mishev K, Vuylsteke M, Aesaert S, Rombaut D, Gallardo R, De Smet F, Xu J, Van Lijsebettens M, Van Breusegem F, Inze D, Rousseau F, Schymkowitz J, Russinova E (2016) Sequence-Specific Protein Aggregation Generates Defined Protein Knockdowns in Plants. Plant Physiol **171:** 773-787

Bielczynski LW, Schansker G, Croce R (2016) Effect of light acclimation on the organization of photosystem II super-and sub-complexes in Arabidopsis thaliana. Frontiers in plant science **7:** 105

Boekema EJ, van Roon H, Calkoen F, Bassi R, Dekker JP (1999) Multiple types of association of photosystem II and its light-harvesting antenna in partially solubilized photosystem II membranes. Biochemistry **38:** 2233-2239

Bogorad L (1958) The enzymatic synthesis of porphyrins from porphobilinogen I. Uroporphyrin I. Journal of Biological Chemistry **233:** 501-509

Bollivar D, Braumann I, Berendt K, Gough SP, Hansson M (2014) The Y cf54 protein is part of the membrane component of M g-protoporphyrin IX monomethyl ester cyclase from barley (H ordeum vulgare L.). The FEBS journal **281:** 2377-2386

Bollivar DW, Beale SI (1996) The chlorophyll biosynthetic enzyme Mg-protoporphyrin IX monomethyl ester (oxidative) cyclase (characterization and partial purification from Chlamydomonas reinhardtii and Synechocystis sp. PCC 6803). Plant Physiology **112:** 105-114

Breitenbach J, Zhu C, Sandmann G (2001) Bleaching herbicide norflurazon inhibits phytoene desaturase by competition with the cofactors. Journal of Agricultural and Food Chemistry **49:** 5270-5272

Brzezowski P, Richter AS, Grimm B (2015) Regulation and function of tetrapyrrole biosynthesis in plants and algae. Biochim Biophys Acta **1847:** 968-985

Buchanan BB, Gruissem W, Jones RL, editors (2015) Biochemistry and molecular biology of plants. John wiley & sons

Buhr F, El Bakkouri M, Valdez O, Pollmann S, Lebedev N, Reinbothe S, Reinbothe C (2008) Photoprotective role of NADPH: protochlorophyllide oxidoreductase A. Proceedings of the National Academy of Sciences **105:** 12629-12634

Bukau B, Horwich AL (1998) The Hsp70 and Hsp60 chaperone machines. Cell **92:** 351-366

Camm EL, Green BR (2004) How the chlorophyll-proteins got their names. Photosynthesis research **80:** 189-196

Carija A, Navarro S, de Groot NS, Ventura S (2017) Protein aggregation into insoluble deposits protects from oxidative stress. Redox Biology **12:** 699-711

Chaudhury S, Lyskov S, Gray JJ (2010) PyRosetta: a script-based interface for implementing molecular modeling algorithms using Rosetta. Bioinformatics **26:** 689-691

Chen X, Pu H, Fang Y, Wang X, Zhao S, Lin Y, Zhang M, Dai H-E, Gong W, Liu L (2015) Crystal structure of the catalytic subunit of magnesium chelatase. Nature Plants **1:** 1-5

Chiti F, Dobson CM (2006) Protein misfolding, functional amyloid, and human disease. Annual review of biochemistry. **75:** 333-366

Clough SJ, Bent AF (1998) Floral dip: a simplified method for Agrobacterium-mediated transformation of Arabidopsis thaliana. The plant journal **16:** 735-743

Croce R, Morosinotto T, Castelletti S, Breton J, Bassi R (2002) The Lhca antenna complexes of higher plants photosystem I. Biochimica et Biophysica Acta (BBA)-Bioenergetics **1556:** 29-40

Czarnecki O, Grimm B (2012) Post-translational control of tetrapyrrole biosynthesis in plants, algae, and cyanobacteria. Journal of Experimental Botany **63:** 1675-1687

Czarnecki O, Hedtke B, Melzer M, Rothbart M, Richter A, Schröter Y, Pfannschmidt T, Grimm B (2011) An Arabidopsis GluTR binding protein mediates spatial separation of 5-aminolevulinic acid synthesis in chloroplasts. The Plant Cell **23:** 4476-4491

Del Vesco AP, Gasparino E, Grieser DO, Zancanela V, Voltolini DM, Khatlab AS, Guimarães SEF, Soares MAM, Neto ARO (2015) Effects of methionine supplementation on the expression of protein deposition-related genes in acute heat stress-exposed broilers. PLoS One **10 (2):** e0115821

DeLille J, Peterson EC, Johnson T, Moore M, Kight A, Henry R (2000) A novel precursor recognition element facilitates posttranslational binding to the signal recognition particle in chloroplasts. Proceedings of the National Academy of Sciences **97:** 1926-1931

DeVay JE, Stapleton JJ, Elmore CL (1991) Soil solarization. cRC Press

Dogra V, Kim C (2019) Chloroplast protein homeostasis is coupled with retrograde signaling. Plant signaling & behavior **14 (11):** 1656037

Doyle SM, Wickner S (2009) Hsp104 and ClpB: protein disaggregating machines. Trends in biochemical sciences **34:** 40-48

Dunschede B, Bals T, Funke S, Schunemann D (2011) Interaction studies between the chloroplast signal recognition particle subunit cpSRP43 and the full-length translocase Alb3 reveal a membrane-embedded binding region in Alb3 protein. Journal of Biological Chemistry **286 (40):** 35187-35195

Dünschede B, Trager C, Schroder CV, Ziehe D, Walter B, Funke S, Hofmann E, Schunemann D (2015) Chloroplast SRP54 Was Recruited for Posttranslational Protein Transport via Complex Formation with Chloroplast SRP43 during Land Plant Evolution. Journal of Biological Chemistry **290:** 13104-13114

Efeoglu B, Ekmekci Y C¸ ic¸ ek N (2009) Physiological responses of three maize cultivars to drought stress and recovery. South African journal of botany **75 (1):** 31-42

Eggink LL, LoBrutto R, Brune DC, Brusslan J, Yamasato A, Tanaka A, Hoober JK (2004) Synthesis of chlorophyll b: localization of chlorophyllide a oxygenase and discovery of a stable radical in the catalytic subunit. BMC Plant Biology **4:** 1-16

Falk S, Sinning I (2010) cpSRP43 is a novel chaperone specific for light-harvesting chlorophyll a,b-binding proteins. Journal of Biological Chemistry **285:** 21655-21661

Farmer DA, Brindley AA, Hitchcock A, Jackson PJ, Johnson B, Dickman MJ, Hunter CN, Reid JD, Adams NB (2019) The ChlD subunit links the motor and porphyrin binding subunits of magnesium chelatase. Biochemical Journal **476:** 1875-1887

Fellerer C, Schweiger R, Schöngruber K, Soll J, Schwenkert S (2011) Cytosolic HSP90 cochaperones HOP and FKBP interact with freshly synthesized chloroplast preproteins of Arabidopsis. Molecular plant **4:** 1133-1145

Fenton WA, Horwich AL (1997) GroEL-mediated protein folding. Protein science: a publication of the Protein Society **6 (4):** 743

Fernandez-Escamilla AM, Rousseau F, Schymkowitz J, Serrano L (2004) Prediction of sequence-dependent and mutational effects on the aggregation of peptides and proteins. Nature Biotechnolgy **22:** 1302-1306

Fink AL (1998) Protein aggregation: folding aggregates, inclusion bodies and amyloid. Folding and design **3 (1):** R9-R23

Fink AL (1999) Chaperone-mediated protein folding. Physiological reviews **79:** 425-449

Flores-Perez U, Jarvis P (2013) Molecular chaperone involvement in chloroplast protein import. Biochimica et Biophysica Acta (BBA)-Molecular Cell Research **1833:** 332-340

Floris D, Kuhlbrandt W (2021) Molecular landscape of etioplast inner membranes in higher plants. Nature Plants **7:** 514-523

Frain KM, Gangl D, Jones A, Zedler JA, Robinson C (2016) Protein translocation and thylakoid biogenesis in cyanobacteria. Biochimica et Biophysica Acta (BBA)-Bioenergetics **1857:** 266-273

Franklin A, Hoffman N (1993) Characterization of a chloroplast homologue of the 54-kDa subunit of the signal recognition particle. Journal of Biological Chemistry **268:** 22175-22180

Frydman J (2001) Folding of newly translated proteins in vivo: the role of molecular chaperones. Annual review of biochemistry **70:** 603-647

Gabruk M, Mysliwa-Kurdziel B (2015) Light-Dependent Protochlorophyllide Oxidoreductase: Phylogeny, Regulation, and Catalytic Properties. Biochemistry **54:** 5255-5262

Gadjieva R, Axelsson E, Olsson U, Hansson M (2005) Analysis of gun phenotype in barley magnesium chelatase and Mg-protoporphyrin IX monomethyl ester cyclase mutants. Plant Physiology and Biochemistry **43:** 901-908

Galka P, Santabarbara S, Khuong TTH, Degand H, Morsomme P, Jennings RC, Boekema EJ, Caffarri S (2012) Functional analyses of the plant photosystem I–light-harvesting complex II supercomplex reveal that light-harvesting complex II loosely bound to photosystem II is a very efficient antenna for photosystem I in state II. The Plant Cell **24:** 2963-2978

Goforth RL, Peterson EC, Yuan J, Moore MJ, Kight AD, Lohse MB, Sakon J, Henry RL (2004) Regulation of the GTPase cycle in post-translational signal recognition particle-based protein targeting involves cpSRP43. Journal of Biological Chemistry **279:** 43077-43084

Goldschmidt-Clermont M, Bassi R (2015) Sharing light between two photosystems: mechanism of state transitions. Current opinion in plant biology **25:** 71-78

Grimm B (1990) Primary structure of a key enzyme in plant tetrapyrrole synthesis: glutamate 1-semialdehyde aminotransferase. Proceedings of the National Academy of Sciences **87:** 4169-4173

Grimm B, Bull A, Welinder KG, Gough SP, Kannangara CG (1989) Purification and partial amino acid sequence of the glutamate 1-semialdehyde aminotransferase of barley and Synechococcus. Carlsberg research communications **54:** 67-79

Groves MR, Mant A, Kuhn A, Koch J, Dubel S, Robinson C, Sinning I (2001) Functional characterization of recombinant chloroplast signal recognition particle. Journal of Biological Chemistry **276 (30):** 27778-86

Guo R, Luo M, Weinstein JD (1998) Magnesium-chelatase from developing pea leaves: characterization of a soluble extract from chloroplasts and resolution into three required protein fractions. Plant Physiology **116:** 605-615

Ha JH, Lee HJ, Jung JH, Park CM (2017) Thermo-Induced Maintenance of Photo-oxidoreductases Underlies Plant Autotrophic Development. Developmental Cell **41 (2):** 170-179

Hartl FU (1996) Molecular chaperones in cellular protein folding. Nature **381:** 571-580

Havaux M (1993) Rapid photosynthetic adaptation to heat stress triggered in potato leaves by moderately elevated temperatures. Plant, Cell & Environment **16:** 461-467

Hedtke B, Alawady A, Chen S, Börnke F, Grimm B (2007) HEMA RNAi silencing reveals a control mechanism of ALA biosynthesis on Mg chelatase and Fe chelatase. Plant molecular biology **64:** 733-742

Hemantaranjan A, Bhanu AN, Singh MN, Yadav DK, Patel PK, Singh R, Katiyar D (2014) Heat stress responses and thermotolerance. Advances in Plants & Agriculture Research **1 (3):** 1-10

Henderson RC, Gao F, Jayanthi S, Kight A, Sharma P, Goforth RL, Heyes CD, Henry RL, Kumar TK (2016) Domain organization in the 54-kDa subunit of the chloroplast signal recognition particle. Biophysical journal **111 (6):** 1151-1162

Hennig M, Grimm B, Contestabile R, John RA, Jansonius JN (1997) Crystal structure of glutamate-1-semialdehyde aminomutase: an α2-dimeric vitamin B6-dependent enzyme with asymmetry in structure and active site reactivity. Proceedings of the National Academy of Sciences **94:** 4866-4871

Hess WR, Müller A, Nagy F, Börner T (1994) Ribosome-deficient plastids affect transcription of light-induced nuclear genes: genetic evidence for a plastid-derived signal. Molecular and General Genetics MGG **242:** 305-312

Hey D, Rothbart M, Herbst J, Wang P, Muller J, Wittmann D, Gruhl K, Grimm B (2017) LIL3, a Light-Harvesting Complex Protein, Links Terpenoid and Tetrapyrrole Biosynthesis in Arabidopsis thaliana. Plant Physiology **174:** 1037-1050

Holdermann I, Meyer NH, Round A, Wild K, Sattler M, Sinning I (2012) Chromodomains read the arginine code of post-translational targeting. Nature structural & molecular biology **19:** 260-263

Holtorf H, Reinbothe S, Reinbothe C, Bereza B, Apel K (1995) Two routes of chlorophyllide synthesis that are differentially regulated by light in barley (Hordeum vulgare L.). Proceedings of the National Academy of Sciences **92:** 3254-3258

Horn A, Hennig J, Ahmed YL, Stier G, Wild K, Sattler M, Sinning I (2015) Structural basis for cpSRP43 chromodomain selectivity and dynamics in Alb3 insertase interaction. Nature communications **6 (1):** 1-11

Hou Z, Pang X, Hedtke B, Grimm B (2021) In vivo functional analysis of the structural domains of FLUORESCENT (FLU). The Plant Journal **107(2):** 360-76

Hou Z, Yang Y, Hedtke B, Grimm B (2019) Fluorescence in blue light (FLU) is involved in inactivation and localization of glutamyl-tRNA reductase during light exposure. The Plant Journal **97:** 517-529

Hristou A, Gerlach I, Stolle DS, Neumann J, Bischoff A, Dunschede B, Nowaczyk MM, Zoschke R, Schunemann D (2019) Ribosome-Associated Chloroplast SRP54 Enables Efficient Cotranslational Membrane Insertion of Key Photosynthetic Proteins. The Plant Cell **31:** 2734-2750

Hsu W, Miller G (1970) Coproporphyrinogenase in tobacco (Nicotiana tabacum L.). Biochemical Journal **117:** 215-220

Hu JH, Chang JW, Xu T, Wang J, Wang X, Lin R, Duanmu D, Liu L (2021) Structural basis of bilin binding by the chlorophyll biosynthesis regulator GUN4. Protein Science **30:** 2083-2091

Hu S, Ding Y, Zhu C (2020) Sensitivity and Responses of Chloroplasts to Heat Stress in Plants. Frontiers in Plant Science **11:** 375

Huang Y-S, Li H-m (2009) Arabidopsis CHLI2 can substitute for CHLI1. Plant Physiology **150:** 636-645

Hutin C, Havaux M, Carde JP, Kloppstech K, Meiherhoff K, Hoffman N, Nussaume L (2002) Double mutation cpSRP43–/cpSRP54—is necessary to abolish the cpSRP pathway required for thylakoid targeting of the light-harvesting chlorophyll proteins. The Plant Journal **29 (5):** 531-543

Jackowski G, Kacprzak K, Jansson S (2001) Identification of Lhcb1/Lhcb2/Lhcb3 heterotrimers of the main light-harvesting chlorophyll a/b–protein complex of

Photosystem II (LHC II). Biochimica et Biophysica Acta (BBA)-Bioenergetics **1504:** 340-345

Jaru-Ampornpan P, Liang FC, Nisthal A, Nguyen TX, Wang P, Shen K, Mayo SL, Shan SO (2013) Mechanism of an ATP-independent protein disaggregase: II. distinct molecular interactions drive multiple steps during aggregate disassembly. Journal of Biological Chemistry **288:** 13431-13445

Jaru-Ampornpan P, Shen K, Lam VQ, Ali M, Doniach S, Jia TZ, Shan SO (2010) ATP-independent reversal of a membrane protein aggregate by a chloroplast SRP subunit. Nature structural & molecular biology **17:** 696-702

Jonas-Straube E, Hutin C, Hoffman NE, Schunemann D (2001) Functional analysis of the protein-interacting domains of chloroplast SRP43. Journal of Biological Chemistry **276:** 24654-24660

Joyard J, Ferro M, Masselon C, Seigneurin-Berny D, Salvi D, Garin J, Rolland N (2009) Chloroplast proteomics and the compartmentation of plastidial isoprenoid biosynthetic pathways. Molecular plant **2:** 1154-1180

Jungkunz I, Link K, Vogel F, Voll LM, Sonnewald S, Sonnewald U (2011) AtHsp70-15-deficient Arabidopsis plants are characterized by reduced growth, a constitutive cytosolic protein response and enhanced resistance to TuMV. The Plant Journal **66:** 983-995

Kauss D, Bischof S, Steiner S, Apel K, Meskauskiene R (2012) FLU, a negative feedback regulator of tetrapyrrole biosynthesis, is physically linked to the final steps of the Mg++-branch of this pathway. FEBS letters **586:** 211-216

Kawai-Yamada M, Nagano M, Kakimoto M, Uchimiya H (2014) Plastidic protein Cdf1 is essential in Arabidopsis embryogenesis. Planta **239:** 39-46

Kindgren P, Norén L, Lopez JdDB, Shaikhali J, Strand Å (2012) Interplay between Heat Shock Protein 90 and HY5 controls PhANG expression in response to the GUN5 plastid signal. Molecular Plant **5:** 901-913

Klimyuk VI, Persello-Cartieaux F, Havaux M, Contard-David P, Schuenemann D, Meiherhoff K, Gouet P, Jones JD, Hoffman NE, Nussaume L (1999) A chromodomain protein encoded by the Arabidopsis CAO gene is a plant-specific component of the chloroplast signal recognition particle pathway that is involved in LHCP targeting. The Plant Cell **11:** 87-99

Klostermann E, Droste Gen Helling I, Carde JP, Schünemann D (2002) The thylakoid membrane protein ALB3 associates with the cpSecY-translocase in Arabidopsis thaliana. Biochemical Journal **368 (3):** 777-781

Kobayashi K, Masuda T, Tajima N, Wada H, Sato N (2014) Molecular phylogeny and intricate evolutionary history of the three isofunctional enzymes involved in the oxidation of protoporphyrinogen IX. Genome biology and evolution **6:** 2141-2155

Koch M, Breithaupt C, Kiefersauer R, Freigang J, Huber R, Messerschmidt A (2004) Crystal structure of protoporphyrinogen IX oxidase: a key enzyme in haem and chlorophyll biosynthesis. The EMBO journal **23:** 1720-1728

Kogata N, Nishio K, Hirohashi T, Kikuchi S, Nakai M (1999) Involvement of a chloroplast homologue of the signal recognition particle receptor protein, FtsY, in protein targeting to thylakoids. FEBS letters **447 (2-3):** 329-333

Kotak S, Larkindale J, Lee U, von Koskull-Döring P, Vierling E, Scharf K-D (2007) Complexity of the heat stress response in plants. Current opinion in plant biology **10:** 310-316

Kouřil R, Wientjes E, Bultema JB, Croce R, Boekema EJ (2013) High-light vs. low-light: effect of light acclimation on photosystem II composition and organization in

Arabidopsis thaliana. Biochimica et Biophysica Acta (BBA)-Bioenergetics **1827:** 411-419

Koussevitzky S, Nott A, Mockler TC, Hong F, Sachetto-Martins G, Surpin M, Lim J, Mittler R, Chory J (2007) Signals from chloroplasts converge to regulate nuclear gene expression. Science **316:** 715-719

Kumar Tewari A, Charan Tripathy B (1998) Temperature-stress-induced impairment of chlorophyll biosynthetic reactions in cucumber and wheat. Plant physiology **117:** 851-858

Kumar V, Punetha A, Sundar D, Chaudhuri TK (2012) In silico engineering of aggregation-prone recombinant proteins for substrate recognition by the chaperonin GroEL. BMC Genomics **13 (7):** 1-9

Laible M, Boonrod K (2009) Homemade site directed mutagenesis of whole plasmids. Journal of Visualized Experiments **11(27):** e1135.

Larkin RM, Alonso JM, Ecker JR, Chory J (2003) GUN4, a regulator of chlorophyll synthesis and intracellular signaling. Science **299:** 902-906

Ledford HK, Niyogi KK (2005) Singlet oxygen and photo-oxidative stress management in plants and algae. Plant, Cell & Environment **28:** 1037-1045

Lee GJ, Roseman AM, Saibil HR, Vierling E (1997) A small heat shock protein stably binds heat-denatured model substrates and can maintain a substrate in a folding-competent state. The EMBO journal **16:** 659-671

Lee GJ, Vierling E (2000) A small heat shock protein cooperates with heat shock protein 70 systems to reactivate a heat-denatured protein. Plant Physiology **122:** 189-198

Lee HS, Choi I, Jeon Y, Ahn HK, Cho H, Kim J, Kim JH, Lee JM, Lee S, Bunting J, Seo DH, Lee T, Lee DH, Lee I, Oh MH, Kim TW, Belkhadir Y, Pai HS (2021) Chaperone-like protein DAY plays critical roles in photomorphogenesis. Nature Communications **12 (1):** 1-13

Lee J-Y, Lee H-S, Song J-Y, Jung YJ, Reinbothe S, Park Y-I, Lee SY, Pai H-S (2013) Cell growth defect factor1/CHAPERONE-LIKE PROTEIN OF POR1 plays a role in stabilization of light-dependent protochlorophyllide oxidoreductase in Nicotiana benthamiana and Arabidopsis. The Plant Cell **25:** 3944-3960

Lee JH, Schöffl F (1996) An Hsp70 antisense gene affects the expression of HSP70/HSC70, the regulation of HSF, and the acquisition of thermotolerance in transgenic Arabidopsis thaliana. Molecular and General Genetics MGG **252:** 11-19

Lermontova I, Grimm B (2006) Reduced activity of plastid protoporphyrinogen oxidase causes attenuated photodynamic damage during high-light compared to low-light exposure. The Plant Journal **48:** 499-510

Li X, Henry R, Yuan J, Cline K, Hoffman NE (1995) A chloroplast homologue of the signal recognition particle subunit SRP54 is involved in the posttranslational integration of a protein into thylakoid membranes. Proceedings of the National Academy of Sciences. **92 (9):** 3789-3793

LI Zy, LONG Rc, ZHANG Tj, YANG Qc, KANG Jm (2016) Research progress on plant heat shock protein. Biotechnology Bulletin. **32 (2):** 7

Li Z, Wakao S, Fischer BB, Niyogi KK (2009) Sensing and responding to excess light. Annual review of plant biology **60:** 239-260

Liang FC, Kroon G, McAvoy CZ, Chi C, Wright PE, Shan SO (2016) Conformational dynamics of a membrane protein chaperone enables spatially regulated substrate capture and release. Proceedings of the National Academy of Sciences **113:** E1615-1624

Liberek K, Lewandowska A, Ziętkiewicz S (2008) Chaperones in control of protein disaggregation. The EMBO journal **27:** 328-335

Lightenthaler H (1987) Chlorophylls and carotenoids: pigments of photosynthetic biomembranes. Methods in enzymology **148:** 350-382

Lin Y-P, Wu M-C, Charng Y-y (2016) Identification of a chlorophyll dephytylase involved in chlorophyll turnover in Arabidopsis. The Plant Cell **28:** 2974-2990

Liu F, Marquardt S, Lister C, Swiezewski S, Dean C (2010) Targeted 3′ processing of antisense transcripts triggers Arabidopsis FLC chromatin silencing. Science **327:** 94-97

Liu G-T, Ma L, Duan W, Wang B-C, Li J-H, Xu H-G, Yan X-Q, Yan B-F, Li S-H, Wang L-J (2014) Differential proteomic analysis of grapevine leaves by iTRAQ reveals responses to heat stress and subsequent recovery. BMC plant biology **14:** 1-17

Liu H, Li Q, Yang F, Zhu F, Sun Y, Tao Y, Lo C (2016) Differential Regulation of Protochlorophyllide Oxidoreductase Abundances by VIRESCENT 5A (OsV5A) and VIRESCENT 5B (OsV5B) in Rice Seedlings. Plant Cell Physiology **57:** 2392-2402

Liu Y, Kuhlman B (2006) RosettaDesign server for protein design. Nucleic acids research **34:** W235-W238

Liu Z, Yan H, Wang K, Kuang T, Zhang J, Gui L, An X, Chang W (2004) Crystal structure of spinach major light-harvesting complex at 2.72 Å resolution. Nature **428:** 287-292

Lohscheider JN, Rojas-Stütz MC, Rothbart M, Andersson U, Funck D, Mendgen K, Grimm B, Adamska I (2015) Altered levels of LIL 3 isoforms in Arabidopsis lead to disturbed pigment–protein assembly and chlorophyll synthesis, chlorotic phenotype and impaired photosynthetic performance. Plant, cell & environment **38:** 2115-2127

Lord-Fontaine S, Averill-Bates DA (2002) Heat shock inactivates cellular antioxidant defenses against hydrogen peroxide: protection by glucose. Free Radical Biology and Medicine **32:** 752-765

Macknight R, Bancroft I, Page T, Lister C, Schmidt R, Love K, Westphal L, Murphy G, Sherson S, Cobbett C (1997) FCA, a gene controlling flowering time in Arabidopsis, encodes a protein containing RNA-binding domains. Cell **89:** 737-745

Marklew CJ (2012) Structural and Functional Characterisation of Magnesium Protoporphyrin IX Chelatase from Thermosynechococcus elongatus. Doctoral dissertation, University of Sheffiel

Marquez UML, Sinnecker P (2007) 2.1 Chlorophylls: Properties, Biosynthesis. Food colorants: Chemical and functional properties**:** 24-25

Marty NJ (2009) The membrane-binding motif of the chloroplast signal recognition particle receptor (cpFtsY) regulates GTPase activity. Journal of Biological Chemistry **284 (22):** 14891-903

Masoudi-Sadaghiani F, Babak AM, Zardoshti MR, Hassan R-SM, Tavakoli A (2011) Response of proline, soluble sugars, photosynthetic pigments and antioxidant enzymes in potato (Solanum tuberosum L.) to different irrigation regimes in greenhouse condition. Australian Journal of Crop Science **5:** 55-60

Masuda T, Takamiya K-i (2004) Novel insights into the enzymology, regulation and physiological functions of light-dependent protochlorophyllide oxidoreductase in angiosperms. Photosynthesis Research **81:** 1-29

Mathur S, Agrawal D, Jajoo A (2014) Photosynthesis: response to high temperature stress. Journal of Photochemistry and Photobiology B: Biology **137:** 116-126

Mazor Y, Borovikova A, Nelson N (2015) The structure of plant photosystem I super-complex at 2.8 Å resolution. Elife **4:** e07433

Meguro M, Ito H, Takabayashi A, Tanaka R, Tanaka A (2011) Identification of the 7-hydroxymethyl chlorophyll a reductase of the chlorophyll cycle in Arabidopsis. The Plant Cell **23:** 3442-3453

Meric G, Robinson AS, Roberts CJ (2017) Driving forces for nonnative protein aggregation and approaches to predict aggregation-prone regions. Annual review of chemical and biomolecular engineering **8:** 139-159

Meskauskiene R, Nater M, Goslings D, Kessler F, op den Camp R, Apel K (2001) FLU: a negative regulator of chlorophyll biosynthesis in Arabidopsis thaliana. Proceedings of the national academy of sciences **98:** 12826-12831

Mishra RC, Grover A (2016) ClpB/Hsp100 proteins and heat stress tolerance in plants. Critical Reviews in Biotechnology **36:** 862-874

Mochizuki N, Brusslan JA, Larkin R, Nagatani A, Chory J (2001) Arabidopsis genomes uncoupled 5 (GUN5) mutant reveals the involvement of Mg-chelatase H subunit in plastid-to-nucleus signal transduction. Proceedings of the National Academy of sciences **98:** 2053-2058

Mogk A, Dougan D, Weibezahn J, Schlieker C, Turgay K, Bukau B (2004) Broad yet high substrate specificity: the challenge of AAA+ proteins. Journal of structural biology **146:** 90-98

Mogk A, Schlieker C, Friedrich KL, Schönfeld H-J, Vierling E, Bukau B (2003) Refolding of substrates bound to small Hsps relies on a disaggregation reaction mediated most efficiently by ClpB/DnaK. Journal of Biological Chemistry **278:** 31033-31042

Mohanty S, Grimm B, Tripathy BC (2006) Light and dark modulation of chlorophyll biosynthetic genes in response to temperature. Planta **224:** 692-699

Moore M, Harrison MS, Peterson EC, Henry R (2000) Chloroplast Oxa1p homolog albino3 is required for post-translational integration of the light harvesting chlorophyll-binding protein into thylakoid membranes. Journal of Biological Chemistry **275 (3):** 1529-1532

Mork-Jansson AE, Eichacker LA (2018) Characterization of chlorophyll binding to LIL3. PLoS One **13 (2):** e0192228

Nakayama M, Masuda T, Bando T, Yamagata H, Ohta H, Takamiya K-i (1998) Cloning and expression of the soybean chlH gene encoding a subunit of Mg-chelatase and localization of the Mg2+ concentration-dependent ChlH protein within the chloroplast. Plant and cell physiology **39:** 275-284

Nelson N, Junge W (2015) Structure and energy transfer in photosystems of oxygenic photosynthesis. Annual review of biochemistry **84:** 659-683

Neuwald AF, Aravind L, Spouge JL, Koonin EV (1999) AAA+: A class of chaperone-like ATPases associated with the assembly, operation, and disassembly of protein complexes. Genome research **9:** 27-43

Nguyen HC, Melo AA, Kruk J, Frost A, Gabruk M (2021) Photocatalytic LPOR forms helical lattices that shape membranes for chlorophyll synthesis. Nat Plants **7:** 437-444

Nilsson R, Brunner J, Hoffman NE, van Wijk KJ (1999) Interactions of ribosome nascent chain complexes of the chloroplast-encoded D1 thylakoid membrane protein with cpSRP54. The EMBO Journal **18:** 733-742

Nilsson R, van Wijk KJ (2002) Transient interaction of cpSRP54 with elongating nascent chains of the chloroplast-encoded D1 protein;'cpSRP54 caught in the act'. FEBS letters **524:** 127-133

Nishimura K, Asakura Y, Friso G, Kim J, Oh S-h, Rutschow H, Ponnala L, van Wijk KJ (2013) ClpS1 is a conserved substrate selector for the chloroplast Clp protease system in Arabidopsis. The Plant Cell **25:** 2276-2301

Nishimura K, van Wijk KJ (2015) Organization, function and substrates of the essential Clp protease system in plastids. Biochimica et Biophysica Acta (BBA)-Bioenergetics **1847:** 915-930

Niyogi KK, Björkman O, Grossman AR (1997) The roles of specific xanthophylls in photoprotection. Proceedings of the National Academy of Sciences **94:** 14162-14167

Nouri MZ, Moumeni A, Komatsu S (2015) Abiotic Stresses: Insight into Gene Regulation and Protein Expression in Photosynthetic Pathways of Plants. International journal of molecular sciences **16(9):** 20392-20416

O'Brien C, Blanco M, Costanzo J, Enterline M, Fernandez E, Robinson A, Roberts C (2016) Modulating non-native aggregation and electrostatic protein–protein interactions with computationally designed single-point mutations. Protein Engineering, Design and Selection **29:** 231-243

Oborník M, Green BR (2005) Mosaic origin of the heme biosynthesis pathway in photosynthetic eukaryotes. Molecular biology and evolution **22:** 2343-2353

Oñate-Sánchez L, Vicente-Carbajosa J (2008) DNA-free RNA isolation protocols for Arabidopsis thaliana, including seeds and siliques. BMC research notes **1:** 1-7

Ono K, Hibino T, Kohinata T, Suzuki S, Tanaka Y, Nakamura T, Takabe T (2001) Overexpression of DnaK from a halotolerant cyanobacterium Aphanothece halophytica enhances the high-temperatue tolerance of tobacco during germination and early growth. Plant Science **160:** 455-461

Ouyang M, Li X, Ma J, Chi W, Xiao J, Zou M, Chen F, Lu C, Zhang L (2011) LTD is a protein required for sorting light-harvesting chlorophyll-binding proteins to the chloroplast SRP pathway. Nature communications **2 (1):** 1-11

Packer JC, Howe CJ (1996) The cyanobacterial genome contains a single copy of the ffh gene encoding a homologue of the 54 kDa subunit of signal recognition particle. Plant molecular biology **30:** 659-665

Pan X, Cao P, Su X, Liu Z, Li M (2020) Structural analysis and comparison of light-harvesting complexes I and II. Biochimica et Biophysica Acta (BBA)-Bioenergetics **1861(4):** 148038

Pan X, Ma J, Su X, Cao P, Chang W, Liu Z, Zhang X, Li M (2018) Structure of the maize photosystem I supercomplex with light-harvesting complexes I and II. Science **360:** 1109-1113

Peter E, Grimm B (2009) GUN4 is required for posttranslational control of plant tetrapyrrole biosynthesis. Molecular Plant **2:** 1198-1210

Pfaffl MW (2001) A new mathematical model for relative quantification in real-time RT–PCR. Nucleic acids research **29:** e45-e45

Pilgrim ML, Va KJ, Parry DH, Sy DA, Hoffman NE (1998) Expression of a dominant negative form of cpSRP54 inhibits chloroplast biogenesis in Arabidopsis. The Plant Journal **13:** 177-186

Piskozub M, Króliczewska B, Króliczewski J (2015) Ribosome nascent chain complexes of the chloroplast-encoded cytochrome b6 thylakoid membrane protein interact with cpSRP54 but not with cpSecY. Journal of bioenergetics and biomembranes **47:** 265-278

Pulido P, Leister D (2018) Novel DNAJ-related proteins in Arabidopsis thaliana. New Phytologist **217:** 480-490

Qbadou S, Becker T, Mirus O, Tews I, Soll J, Schleiff E (2006) The molecular chaperone Hsp90 delivers precursor proteins to the chloroplast import receptor Toc64. The EMBO journal **25:** 1836-1847

Qian P, Marklew CJ, Viney J, Davison PA, Brindley AA, Söderberg C, Al-Karadaghi S, Bullough PA, Grossmann JG, Hunter CN (2012) Structure of the cyanobacterial magnesium chelatase H subunit determined by single particle reconstruction and small-angle X-ray scattering. Journal of Biological Chemistry **287:** 4946-4956

Qin X, Suga M, Kuang T, Shen J-R (2015) Structural basis for energy transfer pathways in the plant PSI-LHCI supercomplex. Science **348:** 989-995

Reid J, Hunter C (2002) Current understanding of the function of magnesium chelatase. Biochemical Society Transactions **30:** 643-645

Reinbothe C, El Bakkouri M, Buhr F, Muraki N, Nomata J, Kurisu G, Fujita Y, Reinbothe S (2010) Chlorophyll biosynthesis: spotlight on protochlorophyllide reduction. Trends in plant science **15(11):** 614-624

Reinbothe S, Reinbothe C, Apel K, Lebedev N (1996) Evolution of chlorophyll biosynthesis—the challenge to survive photooxidation. Cell **86:** 703-705

Reumers J, Maurer-Stroh S, Schymkowitz J, Rousseau F (2009) Protein sequences encode safeguards against aggregation. Human mutation **30 (3):** 431-437

Richardson JS, Richardson DC (2002) Natural β-sheet proteins use negative design to avoid edge-to-edge aggregation. Proceedings of the National Academy of Sciences **99:** 2754-2759

Richter A, Peter E, Pors Y, Lorenzen S, Grimm B, Czarnecki O (2010) Rapid dark repression of 5-aminolevulinic acid synthesis in green barley leaves. Plant Cell Physiol **51:** 670-681

Richter AS, Banse C, Grimm B (2019) The GluTR-binding protein is the heme-binding factor for feedback control of glutamyl-tRNA reductase. Elife **8:** e46300

Richter AS, Hochheuser C, Fufezan C, Heinze L, Kuhnert F, Grimm B (2016) Phosphorylation of GENOMES UNCOUPLED 4 Alters Stimulation of Mg Chelatase Activity in Angiosperms. Plant Physiology **172:** 1578-1595

Richter AS, Wang P, Grimm B (2016) Arabidopsis Mg-Protoporphyrin IX Methyltransferase Activity and Redox Regulation Depend on Conserved Cysteines. Plant Cell Physiology **57:** 519-527

Richter CV, Bals T, Schunemann D (2010) Component interactions, regulation and mechanisms of chloroplast signal recognition particle-dependent protein transport. European journal of cell biology **89 (12):** 965-973

Roberts CJ (2014) Therapeutic protein aggregation: mechanisms, design, and control. Trends in biotechnology **32:** 372-380

Roberts CJ, Das TK, Sahin E (2011) Predicting solution aggregation rates for therapeutic proteins: approaches and challenges. International journal of pharmaceutics **418:** 318-333

Rosenblad MA, Samuelsson T (2004) Identification of chloroplast signal recognition particle RNA genes. Plant and cell physiology **45:** 1633-1639

Rousseau F, Serrano L, Schymkowitz JW (2006) How evolutionary pressure against protein aggregation shaped chaperone specificity. Journal of molecular biology **355 (5):** 1037-1047

Ruban AV, Johnson MP, Duffy CD (2012) The photoprotective molecular switch in the photosystem II antenna. Biochimica et Biophysica Acta (BBA)-Bioenergetics **1817:** 167-181

Ruckle ME, DeMarco SM, Larkin RM (2007) Plastid signals remodel light signaling networks and are essential for efficient chloroplast biogenesis in Arabidopsis. The Plant Cell **19:** 3944-3960

Runge S, Frick G, Apel K, Sperling U, Armstrong G (1995) Identification of NADPH: protochlorophyllide oxidoreductase A and B: a branched pathway for light-dependent chlorophyll in Arabidopsis thaliana. Plant Physiology **108:** 1505-1517

Rzeznicka K, Walker CJ, Westergren T, Kannangara CG, von Wettstein D, Merchant S, Gough SP, Hansson M (2005) Xantha-l encodes a membrane subunit of the aerobic Mg-protoporphyrin IX monomethyl ester cyclase involved in chlorophyll biosynthesis. Proceedings of the National Academy of Sciences **102:** 5886-5891

Sahin E, Jordan JL, Spatara ML, Naranjo A, Costanzo JA, Weiss IV WF, Robinson AS, Fernandez EJ, Roberts CJ (2011) Computational design and biophysical characterization of aggregation-resistant point mutations for γD crystallin illustrate a

balance of conformational stability and intrinsic aggregation propensity. Biochemistry **50:** 628-639

Santana MA, Tan F-C, Smith AG (2002) Molecular characterisation of coproporphyrinogen oxidase from Glycine max and Arabidopsis thaliana. Plant Physiology and Biochemistry **40:** 289-298

Schirmer EC, Glover JR, Singer MA, Lindquist S (1996) HSP100/Clp proteins: a common mechanism explains diverse functions. Trends in biochemical sciences **21:** 289-296

Schmied J, Hedtke B, Grimm B (2011) Overexpression of HEMA1 encoding glutamyl-tRNA reductase. Journal of plant physiology **168:** 1372-1379

Schmied J, Hou Z, Hedtke B, Grimm B (2018) Controlled Partitioning of Glutamyl-tRNA Reductase in Stroma- and Membrane-Associated Fractions Affects the Synthesis of 5-Aminolevulinic Acid. Plant Cell Physiology **59:** 2204-2213

Schramm F, Larkindale J, Kiehlmann E, Ganguli A, Englich G, Vierling E, Von Koskull-Döring P (2008) A cascade of transcription factor DREB2A and heat stress transcription factor HsfA3 regulates the heat stress response of Arabidopsis. The Plant Journal **53:** 264-274

Schroda M, Mühlhaus T (2009) A 'foldosome'in the chloroplast? Plant signaling & behavior **4:** 301-303

Schünemann D (2004) Structure and function of the chloroplast signal recognition particle. Current genetics **44:** 295-304

Schünemann D, Gupta S, Persello-Cartieaux F, Klimyuk VI, Jones JDG, Nussaume L, Hoffman NE (1998) A novel signal recognition particle targets light-harvesting proteins to the thylakoid membranes. Proceedings of the National Academy of Sciences **95 (17):** 10312-1036

Schymkowitz J, Borg J, Stricher F, Nys R, Rousseau F, Serrano L (2005) The FoldX web server: an online force field. Nucleic acids research **33(suppl_2):** W382-388

Shepherd M, Reid JD, Hunter CN (2003) Purification and kinetic characterization of the magnesium protoporphyrin IX methyltransferase from Synechocystis PCC6803. Biochemical Journal **371 (2):** 351-360

Shimoda Y, Ito H, Tanaka A (2016) Arabidopsis STAY-GREEN, Mendel's green cotyledon gene, encodes magnesium-dechelatase. The Plant Cell **28:** 2147-2160

Siegel A, McAvoy CZ, Lam V, Liang F-C, Kroon G, Miaou E, Griffin P, Wright PE, Shan S-o (2020) A disorder-to-order transition activates an ATP-Independent Membrane Protein Chaperone. Journal of molecular biology **432 (24):** 166708

Sperling U, Van Cleve B, Frick G, Apel K, Armstrong GA (1997) Overexpression of light-dependent PORA or PORB in plants depleted of endogenous POR by far-red light enhances seedling survival in white light and protects against photooxidative damage. The Plant Journal **12:** 649-658

Stadtman ER (2006) Protein oxidation and aging. Free radical research **40 (12):** 1250-1258

Standfuss J, Terwisscha van Scheltinga AC, Lamborghini M, Kühlbrandt W (2005) Mechanisms of photoprotection and nonphotochemical quenching in pea light-harvesting complex at 2.5 Å resolution. The EMBO journal **24:** 919-928

Steinberg R, Knüpffer L, Origi A, Asti R, Koch H-G (2018) Co-translational protein targeting in bacteria. FEMS microbiology letters **365 (11):** fny095

Stengel KF, Holdermann I, Cain P, Robinson C, Wild K, Sinning I (2008) Structural basis for specific substrate recognition by the chloroplast signal recognition particle protein cpSRP43. Science **321:** 253-256

Su Q, Frick G, Armstrong G, Apel K (2001) POR C of Arabidopsis thaliana: a third light- and NADPH-dependent protochlorophyllide oxidoreductase that is differentially regulated by light. Plant molecular biology **47:** 805-813

Suga M, Qin X, Kuang T, Shen J-R (2016) Structure and energy transfer pathways of the plant photosystem I-LHCI supercomplex. Current Opinion in Structural Biology **39:** 46-53

Sung DY, Guy CL (2003) Physiological and molecular assessment of altered expression of Hsc70-1 in Arabidopsis. Evidence for pleiotropic consequences. Plant Physiology **132:** 979-987

Susek RE, Ausubel FM, Chory J (1993) Signal transduction mutants of Arabidopsis uncouple nuclear CAB and RBCS gene expression from chloroplast development. Cell **74:** 787-799

Taiz L, Zeiger E, Møller IM, Murphy A (2015) Plant physiology and development (No. Ed. 6). Sinauer Associates Incorporated.

Takahashi K, Takabayashi A, Tanaka A, Tanaka R (2014) Functional analysis of light-harvesting-like protein 3 (LIL3) and its light-harvesting chlorophyll-binding motif in Arabidopsis. Journal of biological chemistry **289:** 987-999

Tanaka A, Ito H, Tanaka R, Tanaka NK, Yoshida K, Okada K (1998) Chlorophyll a oxygenase (CAO) is involved in chlorophyll b formation from chlorophyll a. Proceedings of the National Academy of Sciences **95:** 12719-12723

Tanaka R, Rothbart M, Oka S, Takabayashi A, Takahashi K, Shibata M, Myouga F, Motohashi R, Shinozaki K, Grimm B, Tanaka A (2010) LIL3, a light-harvesting-like protein, plays an essential role in chlorophyll and tocopherol biosynthesis. Proceedings of the National Academy of Sciences **107:** 16721-16725

Terry MJ, Kendrick RE (1999) Feedback inhibition of chlorophyll synthesis in the phytochrome chromophore-deficient aurea and yellow-green-2 mutants of tomato. Plant Physiology **119:** 143-152

Tomoyasu T, Mogk A, Langen H, Goloubinoff P, Bukau B (2001) Genetic dissection of the roles of chaperones and proteases in protein folding and degradation in the Escherichia coli cytosol. Molecular microbiology **40:** 397-413

Träger C, Rosenblad MA, Ziehe D, Garcia-Petit C, Schrader L, Kock K, Vera Richter C, Klinkert B, Narberhaus F, Herrmann C (2012) Evolution from the prokaryotic to the higher plant chloroplast signal recognition particle: the signal recognition particle RNA is conserved in plastids of a wide range of photosynthetic organisms. The Plant cell **24:** 4819-4836

Tu CJ, Peterson EC, Henry R, Hoffman NE (2000) The L18 domain of light-harvesting chlorophyll proteins binds to chloroplast signal recognition particle 43. Journal of Biological Chemistry **275:** 13187-13190

Tu CJ, Schuenemann D, Hoffman NE (1999) Chloroplast FtsY, chloroplast signal recognition particle, and GTP are required to reconstitute the soluble phase of light-harvesting chlorophyll protein transport into thylakoid membranes. Journal of Biological Chemistry **274 (38):** 27219-27224

Tzvetkova-Chevolleau T, Hutin C, Noël LD, Goforth R, Carde J-P, Caffarri S, Sinning I, Groves M, Teulon J-M, Hoffman NE (2007) Canonical signal recognition particle components can be bypassed for posttranslational protein targeting in chloroplasts. The Plant Cell **19:** 1635-1648

Uversky VN, Fink AL (2004) Conformational constraints for amyloid fibrillation: the importance of being unfolded. Biochimica et Biophysica Acta (BBA)-Proteins and Proteomics **1698:** 131-153

Verdecia MA, Larkin RM, Ferrer J-L, Riek R, Chory J, Noel JP (2005) Structure of the Mg-chelatase cofactor GUN4 reveals a novel hand-shaped fold for porphyrin binding. PLoS biology **3 (5):** e151

von Koskull-Döring P, Scharf K-D, Nover L (2007) The diversity of plant heat stress transcription factors. Trends in plant science **12:** 452-457

Vothknecht UC, Kannangara CG, Von Wettstein D (1996) Expression of catalytically active barley glutamyl tRNAGlu reductase in Escherichia coli as a fusion protein with glutathione S-transferase. Proceedings of the National Academy of Sciences **93:** 9287-9291

Vothknecht UC, Kannangara CG, von Wettstein D (1998) Barley glutamyl tRNAGlu reductase: mutations affecting haem inhibition and enzyme activity. Phytochemistry **47:** 513-519

Wang L, Ma H, Song L, Shu Y, Gu W (2012) Comparative proteomics analysis reveals the mechanism of pre-harvest seed deterioration of soybean under high temperature and humidity stress. Journal of Proteomics **75:** 2109-2127

Wang P, Grimm B (2021) Connecting Chlorophyll Metabolism with Accumulation of the Photosynthetic Apparatus. Trends in plant science **26:** 484-495

Wang P, Liang FC, Wittmann D, Siegel A, Shan SO, Grimm B (2018) Chloroplast SRP43 acts as a chaperone for glutamyl-tRNA reductase, the rate-limiting enzyme in tetrapyrrole biosynthesis. Proceedings of the National Academy of Sciences **115:** E3588-E3596

Wang P, Richter AS, Kleeberg JRW, Geimer S, Grimm B (2020) Post-translational coordination of chlorophyll biosynthesis and breakdown by BCMs maintains chlorophyll homeostasis during leaf development. Nature communications **11(1):** 1-17

Wang P, Wan C, Xu Z, Wang P, Wang W, Sun C, Ma X, Xiao Y, Zhu J, Gao X (2013) One divinyl reductase reduces the 8-vinyl groups in various intermediates of chlorophyll biosynthesis in a given higher plant species, but the isozyme differs between species. Plant physiology **161:** 521-534

Wang QL, Chen JH, He NY, Guo FQ (2018) Metabolic Reprogramming in Chloroplasts under Heat Stress in Plants. International journal of molecular sciences **19 (3):** 849

Wang W, Vinocur B, Shoseyov O, Altman A (2004) Role of plant heat-shock proteins and molecular chaperones in the abiotic stress response. Trends in Plant Science **9:** 244-252

Wei X, Su X, Cao P, Liu X, Chang W, Li M, Zhang X, Liu Z (2016) Structure of spinach photosystem II–LHCII supercomplex at 3.2 Å resolution. Nature **534:** 69-74

Weiss IV WF, Young TM, Roberts CJ (2009) Principles, approaches, and challenges for predicting protein aggregation rates and shelf life. Journal of pharmaceutical sciences **98:** 1246-1277

Wild K, Bange G, Motiejunas D, Kribelbauer J, Hendricks A, Segnitz B, Wade RC, Sinning I (2016) Structural basis for conserved regulation and adaptation of the signal recognition particle targeting complex. Journal of molecular biology **428 (14):** 2880-2897.

Willmund F, Schroda M (2005) HEAT SHOCK PROTEIN 90C is a bona fide Hsp90 that interacts with plastidic HSP70B in Chlamydomonas reinhardtii. Plant physiology **138:** 2310-2322

Wise R, Olson A, Schrader S, Sharkey T (2004) Electron transport is the functional limitation of photosynthesis in field-grown Pima cotton plants at high temperature. Plant, Cell & Environment **27:** 717-724

Wittmann D, Klove S, Wang P, Grimm B (2018) Towards Initial Indications for a Thiol-Based Redox Control of Arabidopsis 5-Aminolevulinic Acid Dehydratase. Antioxidants **7(11):** 152

Woodson JD, Chory J (2008) Coordination of gene expression between organellar and nuclear genomes. Nature Reviews Genetics **9(5):** 383-395

Wu G-Z, Bock R (2021) GUN control in retrograde signaling: How GENOMES UNCOUPLED proteins adjust nuclear gene expression to plastid biogenesis. The Plant Cell **33:** 457-474

Xiong J, Bauer CE (2002) Complex evolution of photosynthesis. Annual review of plant biology **53:** 503-521

Young JC, Moarefi I, Hartl FU (2001) Hsp90: a specialized but essential protein-folding tool. The Journal of cell biology **154(2):** 267

Zhang C, Zhang B, Mu B, Zheng X, Zhao F, Lan W, Fu A, Luan S (2020) A Thylakoid Membrane Protein Functions Synergistically with GUN5 in Chlorophyll Biosynthesis. Plant Commun **1(5):** 100094

Zhang F, Tang W, Hedtke B, Zhong L, Liu L, Peng L, Lu C, Grimm B, Lin R (2014) Tetrapyrrole biosynthetic enzyme protoporphyrinogen IX oxidase 1 is required for plastid RNA editing. Proceedings of the National Academy of Sciences **111:** 2023-2028

Zhang M, Zhang F, Fang Y, Chen X, Chen Y, Zhang W, Dai H-E, Lin R, Liu L (2015) The non-canonical tetratricopeptide repeat (TPR) domain of fluorescent (FLU) mediates complex formation with glutamyl-tRNA reductase. Journal of Biological Chemistry **290:** 17559-17565

Zhang S, Heyes DJ, Feng L, Sun W, Johannissen LO, Liu H, Levy CW, Li X, Yang J, Yu X, Lin M, Hardman SJO, Hoeven R, Sakuma M, Hay S, Leys D, Rao Z, Zhou A, Cheng Q, Scrutton NS (2019) Structural basis for enzymatic photocatalysis in chlorophyll biosynthesis. Nature **574:** 722-725

Zhao A, Fang Y, Chen X, Zhao S, Dong W, Lin Y, Gong W, Liu L (2014) Crystal structure of Arabidopsis glutamyl-tRNA reductase in complex with its stimulator protein. Proceedings of the National Academy of Sciences **111:** 6630-6635

Zhao A, Han F (2018) Crystal structure of Arabidopsis thaliana glutamyl-tRNA(Glu) reductase in complex with NADPH and glutamyl-tRNA(Glu) reductase binding protein. Photosynthesis Research **137:** 443-452

Zhichang Z, Wanrong Z, Jinping Y, Jianjun Z, Xufeng LZL, Yang Y (2010) Over-expression of Arabidopsis DnaJ (Hsp40) contributes to NaCl-stress tolerance. African Journal of Biotechnology **9:** 972-978

Zhou S, Sawicki A, Willows RD, Luo M (2012) C-terminal residues of oryza sativa GUN4 are required for the activation of the ChlH subunit of magnesium chelatase in chlorophyll synthesis. FEBS Letter **586(3):** 205-210

Zhuravleva A, Clerico EM, Gierasch LM (2012) An interdomain energetic tug-of-war creates the allosterically active state in Hsp70 molecular chaperones. Cell **151(6):** 1296-1307

Ziehe D, Dunschede B, Schunemann D (2018) Molecular mechanism of SRP-dependent light-harvesting protein transport to the thylakoid membrane in plants. Photosynthesis Research **138(3):** 303-313

Ziehe D, Dünschede B, Schünemann D (2017) From bacteria to chloroplasts: evolution of the chloroplast SRP system. Biological chemistry **398(5-6):** 653-661

Appendix I-Primer List

Fw is the forward primer from 5'->3' and Rev is the reverse primer from 3'->5'.

Table I List of primers used in this study

Name	Sequences	Purpose
SAND- Fw	AACTCTATGCAGCATTTGATCCACT	
SAND- Rev	TGATTGCATATCTTTATCGCCATC	
GluTR-Fw	TTGCTGCCAACAAAGAAGAC	
GluTR-Rev	CCGTCTCCAATGAATCCCTC	
CHLH-Fw	CTGGTCGTGACCCTAGAACAG	qRT-PCR
CHLH-Rev	GATTGCCAGCTTCTTCTCTG	
GUN4-Fw	TGATGGTAGATTCGGATACAGC	
GUN4-Rev	CAAGAAGCTTCATCCACTCAAC	
cpSRP43-FW	CTGCACATGGCGGCTGGTT	
cpSRP43- Rev	CGTCTTTGCCTTTCCCTCGTT	
cpSRP54-FW	GCTTCAGATAGATAAAGGCATG	qRT-PCR
cpSRP54- Rev	GCACCACCTCTTGAATCACC	
pGL1-cpSRP43-FW	TCTAGAATGCAAAAGGTCTTCTTGG	
pGL1-cpSRP43- Rev	CCCGGGTCACTTGTCATCATCGTCCTTGTAGT CTTCATTCATTGG	Plant transformation
pGL1-cpSRP43ΔCD3-FW	TCTAGAATGCAAAAGGTCTTCTTGG	
pGL1-cpSRP43ΔCD3-Rev	CCCGGGTCACTTGTCATCATCGTCCTTGTAGT CAGCGTACTCCAG	

cpSRP43ΔCD1-FW	CATCATCATCGTACGCTAGAAAAGCCG	Intermediate primers for cloning of truncated cpSRP43
cpSRP43ΔCD1- Rev	TCGGCTTTTCTAGCGTACGATGATGATG	
cpSRP43ΔAnk-FW	CCCTGGTGGACGGCACAAGTGTTCGAGTAC	
cpSRP43ΔAnk- Rev	GTACTCGAACACTTGTGCCGTCCACCAGG	
cpSRP43ΔCD2-FW	CAAGTGTTCGAGTACGTAGCGGAGAGTGT	
cpSRP43ΔCD2- Rev	GTACTCGAACACTTGTCCTTCCAGG	
pDonor-cpSRP43-FW	CAAAAAAGCAGGCTGAATGCAAAAGGTCTTC TT	BiFC constructs
pDonor-cpSRP43- Rev	CAAGAAAGCTGGGTGTTCATTCATTGGTTGTT GT	
pDonor-GUN4-FW	CAAAAAAGCAGGCTGAATGATGGCGACCA CAAAC	
pDonor-GUN4- Rev	CAAGAAAGCTGGGTG GAAGCTGTAATTTGTTTT	
pET28a-cpSRP43-FW	GACATATGGCCGCCGTACAAAG	Heterologous protein expression constructs
pET28a-cpSRP43- Rev	GCCTCGAGAGCGTACTCCAGCCCAT	
pET28a-GluTR-Fw	ATCATATGGCTTCTTCTGATTCTGC	
pET28a-GluTR- Rev	CTGAATTCTTACTTCTGTTGTTGTT	
HEMA1_seq_Fw	TCAGATCCTTGCACAGGTGA	For analyses of transgenic lines *HEMA1ΔAPR1*, *HEMA1ΔAPR2*, *HEMA1ΔAPR1/2*
HEMA1_seq_Rev	TTGGAGACGTGACAGCAAAAT	
HEMA1_seq_Rev2	TCTCCTCACGGATAGCTGAAA	
TDNA_Fw	CTGGCGTAATAGCGAAGAGG	
HEMA1_Rev3	TAGGTTTACCCGCCAATATATCC	

pJAHemA1-Fw-LO	AAGGCGCGCCATGGCGGTTTCAAGTGCTTTCG	
pJAHemA1-Rev-LO	CTCCTGCAGGTTACTTCTGTTGTTGTTCCGCC	
pJAHemA1V99P-Fw-LO	GAAGCAGTATTGTTCCGATTGGACTTAGTATT CACAC	
pJAHemA1V99P-Rev-LO	GTGTGAATACTAAGTCCAATCGGAACAATAC TGCTTC	
pJAHemA1V151P-Fw-LO	CCGTATGGAGATTTATCCTTTAGCTTTATCTC	For generation of transgenic lines *HEMA1(V99P/V151P), HEMA1(V99T/V151T)*
pJAHemA1V151P-Rev	GAGATAAAGCTAAAGGATAAATCTCC	
pJAHemA1V99T-Fw-LO	GAAGCAGTATTGTTACGATTGGACTTAGTATT CACAC	
pJAHemA1V99T-Rev-LO	GTGTGAATACTAAGTCCAATCGTAACAATACT GCTTC	
pJAHemA1V151T-Rev	GAGATAAAGCTAAAGTATAAATCTCC	
pJAHemA1V151T-Fw-LO	CCGTATGGAGATTTATACTTTAGCTTTATCTC	
pGL1-43SBD-Fw	TCTAGAATGCAAAAGGTCTTCTTGG	For chaos complementation line *cpSRP43(SBD)-OX*
pGL1-43SBD-Rev	CCCGGGTCACTTGTCATCATCGTCCTTGTAGT CGTACTCGAACACTTG	
pJAHemA1V99T-Fw-LO	GAAGCAGTATTGTTACGATTGGACTTAGTATT CACAC	
pJAHemA1V99T-Rev-LO	GTGTGAATACTAAGTCCAATCGTAACAATACT GCTTC	For expression of recombinant protein GluTR (V99T/V151T)
pJAHemA1V151T-Rev	GAGATAAAGCTAAAGTATAAATCTCC	
pJAHemA1V151T-Fw-LO	CCGTATGGAGATTTATACTTTAGCTTTATCTC	

Appendix II-HPLC Methods

Analyses:		Violaxanthin, Neoxanthin, Antheraxanthin, Lutein, Zeaxanthin, Chl a, Chl b, beta-carotin	
name of method:		Pigment 4A	HPLC: 4
standard:		10 pmol	
column:		Prontosil C30 250x4,6 mm 3µm	
detector and wavelength:		DAD: 440 nm	
mobile phase:		A. 90% acetonitrile (ACN) 10% H_2O 0,1% Triethylamin	
		B. 100% ethylacetat	
thermostated column comp. :		35°C	
flow rate:		1ml/ min	
length of method:		28 min	
injection:		1 - 90 µl	
run timetable:	time/min	A	B
	0	100	0
	1	70	30
	23	0	100
	24	0	100
	24.1 - 28	100	0

Analyses:		Protoporphyrin IX	
method:		Proto IX_06B	HPLC: 3
standard:		1 pmol	
column:		Agilent poroshell 120 - C18	
detector and wavelength:		FLD: Ex. 405 nm/ Em. 637 nm	
mobile phase:		B. 10% 1M ammoniumacetat pH 5.2, 90% methanol	
		D. 100% ethylacetat	
thermostated column comp.:		20°C	
flow rate:		0.5ml/min	
length of method:		12 min	
injection:		1 - 20µl	
run timetable:	time/min	%B	%D
	4	90	10
	4.1	100	0
	8	100	0
	8.1 - 12	90	10

Analyses:		Mg-Protoporphyrin IX, Mg-Protoporphyrin IX momomethylester	
method:		porph02B	HPLC: 3
standard:		1 pmol	both
column:		Agilent-Poroshell 120-C18	
detector and wavelength:		FLD: Ex. 420 nm/ Em. 600 nm	
mobile phase:		B. 10% 1M ammoniumacetat pH 5.2 90% methanol	
		D. 100% ethylacetat	
thermostated column comp.:		20°C	
flow rate:		0.450 ml/min	
length of method:		17 min	
injection:		1 - 20µl	
run timetable:	time/min	%B	%D
	5	100	0
	5.1	70	30
	9	70	30
	9.1 - 17	100	0

Analyses:	Chlorophyllid Protochlorophyllid		
method:	Pchlide_ HPLC3	auf HPLC: 3	
standard:	10 pmol		
column:	Waters Nova Pak C18 3,9x150mm		
detector and wavelength:	Chlide:	DAD: 430 nm	
	Pchlide:	FLD: Ex.435 nm/ Em. 644 nm	
mobile phase:	A. 20% 1M Ammoniumacetat pH 7,0 + 80% Methanol		
	B. 100 % Methanol		
thermostated column comp.:	20°C		
flow rate:	1ml/min		
length of method:	18 min		
injection:	1 bis 20µl		
run timetable:	time / min	% A	% B
	0	100	0
	5	50	50
	7	0	100
	12	0	100
	13.1 - 18	100	0

Analyses:		Heme	
method:		H3A1_B	HPLC: 5
standard:		10 pmol	
column:		Poroshell 120 EC C18 2,7µm	
detector and wavelength:		DAD: 398 nm	
mobile phase:		A1. Wasser pH 3,2 (with acetic acid)	
		B1. 100% Methanol	
thermostated column compartment:		30°C	
flow rate:		0.8 ml/min	
length of method:		11 min	
injection:		1 - 20 µl	
run timetable:	time/min	A1	B1
	4	30	70
	4.1	0	100
	8	0	100
	8.1 - 11	30	70

Appendix III-Sequence analyses of the APRs in GluTR, CHLH, GUN4 and PORB

The transipeptides are labelled in red and APRs are labelled in blue. The transpeptides were predicated by the algorithm TargetP-2.0 (https://services.healthtech.dtu.dk/service.php?TargetP).

GluTR

MAVSSAFVGCPKLETLLNHHNLSPSSSSSSSVSQTPLGLNGVRVLPKNNRTRRGLIQK
ARCELSASSDSASNAASISALEQLKNSAADRYTKERSSIVVIGLSIHTAPVEMREKLAIP
EAEWPRAIAELCGLNHIEEAAVLSTCNRMEIYVLALSQHRGVKEVTEWMSKTSGIPV
SEICQHRFLLYNKDATQHIFEVSAGLDSLVLGEGQILAQVKQVVKVGQGVNGFGRNI
SGLFKHAITVGKRVRTETNIASGAVSVSSAAVELALMKLPQSSNVSARMCVIGAGKM
GKLVIKHLMAKGCTKVVVVNRSEERVSAIREEMPGIEIIYRPLDEMLACASEADVVFT
STASETPLFLKEHVENLPQASPEVGGLRHFVDISVPRNVGSCVGEVETARVYNVDDL
KEVVAANKEDRMRKAMEAQTIITEESTQFEAWRDSLETVPTIKKLRAYAERIRVAEL
EKCMSKMGDDINKKTTRAVDDLSRGIVNRFLHGPMQHLRCDGSDSRTLSETLENMH
ALNRMYGLEKDILEEKLKAMAEQQQK

CHLH

MASLVYSPFTLSTSKAEHLSSLTNSTKHSFLRKKHRSTKPAKSFFKVKSAVSGNGLFT
QTNPEVRRIVPIKRDNVPTVKIVYVVLEAQYQSSLSEAVQSLNKTSRFASYEVVGYLV
EELRDKNTYNNFCEDLKDANIFIGSLIFVEELAIKVKDAVEKERDRMDAVLVFPSMPE
VMRLNKLGSFSMSQLGQSKSPFFQLFKRKKQGSAGFADSMLKLVRTLPKVLKYLPSD
KAQDARLYILSLQFWLGGSPDNLQNFVKMISGSYVPALKGVKIEYSDPVLFLDTGIW
HPLAPTMYDDVKEYWNWYDTRRDTNDSLKRKDATVVGLVLQRSHIVTGDDSHYVA
VIMELEARGAKVVPIFAGGLDFSGPVEKYFVDPVSKQPIVNSAVSLTGFALVGGPARQ
DHPRAIEALKKLDVPYLVAVPLVFQTTEEWLNSTLGLHPIQVALQVALPELDGAMEPI
VFAGRDPRTGKSHALHKRVEQLCIRAIRWGELKRKTKAEKKLAITVFSFPPDKGNVG
TAAYLNVFASIFSVLRDLKRDGYNVEGLPENAETLIEEIIHDKEAQFSSPNLNVAYKM
GVREYQDLTPYANALEENWGKPPGNLNSDGENLLVYGKAYGNVFIGVQPTFGYEGD
PMRLLFSKSASPHHGFAAYYSYVEKIFKADAVLHFGTHGSLEFMPGKQVGMSDACFP
DSLIGNIPNVYYYAANNPSEATIAKRRSYANTISYLTPPAENAGLYKGLKQLSELISSY
QSLKDTGRGPQIVSSIISTAKQCNLDKDVDLPDEGLELSPKDRDSVVGKVYSKIMEIES
RLLPCGLHVIGEPPSAMEAVATLVNIAALDRPEDEISALPSILAECVGREIEDVYRGSD
KGILSDVELLKEITDASRGAVSAFVEKTTNSKGQVVDVSDKLTSLLGFGINEPWVEYL
SNTKFYRANRDKLRTVFGFLGECLKLVVMDNELGSLMQALEGKYVEPGPGGDPIRN
PKVLPTGKNIHALDPQAIPTTAAMASAKIVVERLVERQKLENEGKYPETIALVLWGT
DNIKTYGESLGQVLWMIGVRPIADTFGRVNRVEPVSLEELGRPRIDVVVNCSGVFRDL
FINQMNLLDRAIKMVAELDEPVEQNFVRKHALEQAEALGIDIREAATRVFSNASGSYS

ANISLAVENSSWNDEKQLQDMYLSRKSFAFDSDAPGAGMAEKKQVFEMALSTAEVT
FQNLDSSEISLTDVSHYFDSDPTNLVQSLRKDKKKPSSYIADTTTANAQVRTLSETVR
LDARTKLLNPKWYEGMMSSGYEGVREIEKRLSNTVGWSATSGQVDNWVYEEANST
FIQDEEMLNRLMNTNPNSFRKMLQTFLEANGRGYWDTSAENIEKLKELYSQVEDKIE
GIDR

GUN4

MATTNSLHHHHHSSPSYTHHRNNLHCQSHFGPTSLSLKQPTSAATFSLICSASSTSSST
TAVSAVSTTNASATTAETATIFDVLENHLVNQNFRQADEETRRLLIQISGEAAVKRGY
VFFSEVKTISPEDLQAIDNLWIKHSDGRFGYSVQRKIWLKVKKDFTRFFVKVEWMKL
LDTEVVQYNYRAFPDEFKWELNDETPLGHLPLTNALRGTQLLKCVLSHPAFATADD
NSGETEDELNRGVAVAKEQAGVGADKRVFKTNYSF

PORB

MALQAASLVSSAFSVRKDAKLNASSSSFKDSSLFGASITDQIKSEHGSSSLRFKREQSL
RNLAIRAQTAATSSPTVTKSVDGKKTLRKGNVVVTGASSGLGLATAKALAETGKWN
VIMACRDFLKAERAAKSVGMPKDSYTVMHLDLASLDSVRQFVDNFRRTETPLDVLV
CNAAVYFPTAKEPTYSAEGFELSVATNHLGHFLLARLLLDDLKKSDYPSKRLIIVGSIT
GNTNTLAGNVPPKANLGDLRGLAGGLNGLNSSAMIDGGDFDGAKAYKDSKVCNML
TMQEFHRRFHEETGVTFASLYPGCIASTGLFREHIPLFRALFPPFQKYITKGYVSETESG
KRLAQVVSDPSLTKSGVYWSWNNASASFENQLSEEASDVEKARKVWEISEKLVGLA

Publications

Shuiling Ji, Alex Siegel, Shu-ou Shan, Bernhard Grimm & Peng Wang (2021) Chloroplast SRP43 autonomously protects chlorophyll biosynthesis proteins against heat shock. Nature Plants 7: 1420-1432.

Peng Wang, **Shuiling Ji**, Bernhard Grimm (2022) Post-translational regulation of metabolic checkpoints in plant tetrapyrrole biosynthesis. Journal of Experimental Botany.

Jiarui Yuan, Tingting Ma, **Shuiling Ji**, Boris Hedtke, Bernhard Grimm, Rongcheng Lin (2022) Two chloroplast-localized MORF proteins act as chaperones to maintain tetrapyrrole biosynthesis. New Phytologist.

Manuscripts in prearation:

Shuiling Ji, Peng Wang, Bernhard Grimm. Chloroplast SRP components act as chaperones for protochlorophyllide oxidoreductase B (PORB), the light-dependent enzyme in tetrapyrrole biosynthesis.

Shuiling Ji, Peng Wang, Bernhard Grimm. Functioanl analysis of the Aggregation-Prone Region (APR) in glutamyl-tRNA reductase, the rate-limiting enzyme in tetrapyrrole biosynthesis.

Acknowledgment

This work would not have been possible without the help of many people. Most importantly, I would like to thank my supervisor, Prof. Dr. Bernhard Grimm, for offering me a valuable opportunity to carry out this doctoral project in the Plant Physiology Group. He gave me excellent supervision in project selection, experimental design, and discussion of results, conceptual advances, and writing, revision of this thesis. His diligence, wisdom, tireless pursuit, and passion for scientific research impressed me so much, and it will positively influence my future academic career.

Special thanks to Dr. Peng Wang for his careful guidance of the whole project, especially in the experimental design and discussion of results. His keen insight and pioneering thinking have played a vital role in developing the entire project.

I would like to thank Prof. Dr. Andreas Richter for carefully guiding me to learn and master various experimental skills when I joined the group, which laid a good foundation for the successful development of my doctoral project.

Many thanks to Dr. Boris Hedtke for his comprehensive support in the daily operation of the lab and to Kersten Träder and Alexandra Hackel for their excellent organization of the laboratory stuff, who provided the best working conditions for everyone. Thanks to Heidemarie Schneider for the superb work on the HPLC analyses and PD Dr. Christina Kühn for teaching me how to use confocal microscopy.

Sincere thanks to Dr. Tingting Fan and Dr. Zhiwei Hou, who have graduated, for giving me a lot of care and help in my life and work when I first came to Berlin. I would like to thank Xiaoqing Pang, Bingxiao Wen, Yunshu Wang, and Yao-Pin Lin. We often discuss the progress of each project and exchange our ideas and comments together. Thanks to Steffanie Brembach, Dr. Pawel Brzezowski, Daniel Wittmann, Patrick Schall, Lena Rolling, Neha Sinha, Andrea Carolina Chiappe Pulido and other members in the group who have ever helped me. I would also like to thank my friends in Berlin: their company has never made me feel lonely.

I would like to thank the reviewers for the time they took to evaluate this dissertation.

Thanks to my collaborators from Cal-Tech, Prof. Shu-Ou Shan and Dr. Signel Alex for exchanging good ideas for this study. I am very grateful to the China Scholarship Council for the financial support for my study.

Finally, I would like to express my heartfelt thanks to my wife, Tian Luo, my parents, and my family. My PhD study would never have been possible without their selfless care, understanding, and support. I would also like to apologize to my wife and daughter, Nianyi Ji. I have missed a lot of precious time accompanying them while studying abroad. My daughter was born when I started my PhD, and therefore, this dissertation is dedicated to them.

Selbständigkeitserklärung

Hiermit erkläre ich, die Dissertation selbstständig und nur unter Verwendung der angegebenen Hilfen und Hilfsmittel angefertigt zu haben. Ich habe mich anderwärts nicht um einen Doktorgrad beworben und besitze keinen entsprechenden Doktorgrad. Ich erkläre, dass ich die Dissertation oder Teile davon nicht bereits bei einer anderen wissenschaftlichen Einrichtung eingereicht habe und dass sie dort weder angenommen noch abgelehnt wurde.

Shuiling Ji

Berlin, April 2022